University of Massachusetts Amherst
ScholarWorks@UMass Amherst

Doctoral Dissertations | Dissertations and Theses

9-1-2021

MULTISCALE INVESTIGATION OF THIXOTROPY IN SOFT CLAYS

Jing Peng
University of Massachusetts Amherst

Follow this and additional works at: https://scholarworks.umass.edu/dissertations_2

 Part of the Geotechnical Engineering Commons

Recommended Citation

Peng, Jing, "MULTISCALE INVESTIGATION OF THIXOTROPY IN SOFT CLAYS" (2021). *Doctoral Dissertations*. 2300.
https://doi.org/10.7275/24517400 https://scholarworks.umass.edu/dissertations_2/2300

This Open Access Dissertation is brought to you for free and open access by the Dissertations and Theses at ScholarWorks@UMass Amherst. It has been accepted for inclusion in Doctoral Dissertations by an authorized administrator of ScholarWorks@UMass Amherst. For more information, please contact scholarworks@library.umass.edu.

MULTISCALE INVESTIGATION OF THIXOTROPY IN SOFT CLAYS

A Dissertation Presented

by

JING PENG

Submitted to the Graduate School of the
University of Massachusetts Amherst in partial fulfillment
of the requirements for the degree of

DOCTOR OF PHILOSOPHY

September 2021

Civil and Environmental Engineering

© Copyright by Jing Peng 2021

All Rights Reserved

MULTISCALE INVESTIGATION OF THIXOTROPY IN SOFT CLAYS

A Dissertation Presented

by

JING PENG

Approved as to style and content by:

_____
Dr. Guoping Zhang, Co-Chair

_____
Dr. Don J. DeGroot, Co-Chair

_____
Dr. H. Henning Winter, Member

_____

John E. Tobiason, Department Head
Civil and Environmental Engineering Department

DEDICATION

To my parents

ACKNOWLEDGMENTS

First, I would like to express my sincere thanks to my advisor, Dr. Guoping Zhang, and my co-advisor, Dr. Don DeGroot, for their continuous support, guidance, and help along the journey. Their insightful feedback inspired me to grow as a researcher who thinks critically, which will continue to affect me in the future. I would also like to extend my thanks to my committee member, Dr. H. Henning Winter, for providing thoughts and suggestions.

This research was funded by the National Science Foundation (NSF). Additional support from the Charles Perrell Scholarship is also gratefully acknowledged.

Then, I would like to thank Dr. Ren from Advanced Photon Source (APS) at Argonne National Laboratory (ANL) for scheduling beamline time for the 2DXRD experiments; Dr. Settens from MIT for assistance with 1DXRD tests; and Mr. Raboin from UMass, for the arrangement with critical point drying experiments.

I would also like to acknowledge my past and present fellow students for their assistance and advice: Dr. Yongkang Wu, Dr. Dongfang Wang, Yucheng Li, Shreeya Pandey, Dr. Pamela Judge, Dr. William Lukas, and Dr. Yibing Deng. I treasure your friendship, and it has been a pleasure working with all of you. A special thanks to Yiming Cao for his help with some of the macroscale experiments.

Finally, I would like to thank my parents, Anfu and Zuxia, for their endless love and support during the tough times. Last but not least, my husband, Dr. Shengmin Luo, for his encouragement and considerations from the first day of my Ph.D. journey. I could not have completed the work presented in this dissertation without their love, inspiration, and patience.

ABSTRACT

MULTISCALE INVESTIGATION OF THIXOTROPY IN SOFT CLAYS

September 2021

JING PENG, B.Eng., WUHAN UNIVERSITY OF TECHNOLOGY

M.S., ZHEJIANG UNIVERSITY

Ph.D., UNIVERSITY OF MASSACHUSETTS AMHERST

Directed by: Professors Guoping Zhang and Don DeGroot

Fine-grained clay particles of <2 μm in size are ubiquitous in soils and sedimentary rocks. Due to their platy shape, high aspect ratio, and surface charges, clay particles play a dominant role in controlling the mechanical properties of those fine-grained geomaterials such as soft clays and shales. In physics and engineering, some materials show that the strength and stiffness increases with time even if the boundary conditions remain unchanged (e.g., no change in pressure, temperature, or composition), and such a phenomenon is called thixotropy. It is generally agreed that the principle of thixotropy of wet clays is complex. For a closed, isothermal physical system (such as a wet clay without changes in pressure, temperature, volume, or composition), any change in macroscopic mechanical properties with time (e.g., stiffness and strength) must stem from certain internal processes occurring within the system.

Both the macroscale mechanical and microscale structural mechanisms of thixotropic hardening of soft clays were uncovered through multiscale experimental investigations to better understand the underlying mechanisms of thixotropy and develop connections between quantitative time-dependent clay fabric evolution and macroscale thixotropic process. Macroscale laboratory experiments, including bender element and

undrained shear strength testing, were applied to obtain mechanical properties (e.g., stiffness and strength) during thixotropy. Owing to the small sizes (e.g., <2 μm) of the clay particles, it is challenging to quantify non-destructively the clay texture evolution with time. Fortunately, both conventional one-dimensional X-ray diffraction (1DXRD) and advancement in two-dimensional synchrotron X-ray diffraction (2DXRD) has provided a tangible and powerful approach to determine the clay particle orientation for such geomaterials as wet soils and shales. A better, systematic understanding of the thixotropic behavior of soft clays can hence be expectedly achieved through directly quantitative clays' microfabric evolution (e.g., particle rearrangement, reorientation, and reaggregation) with time.

In the final phase of this study, to further understand the influences of physical and chemical factors on the thixotropic behavior of wet clays, clay specimens with different mineralogy cured at different temperatures (e.g., 4, 24, 44, 84 ºC), various salinities (e.g., 0, 0.017, 0.034, 0.068 g/g NaCl as pore fluid concentration), and different initial water contents relative to liquid limit (e.g., 0.8*LL*, 1.0*LL*, 1.2*LL*) were also studied following methods developed in the first phase. In general, all studied soft clays possess thixotropic hardening behavior, which is affected by the porewater salinity, temperature, and initial water content, and their interplay in controlling the thixotropy is rather complex. The temporal evolution of the microfabric of soft clays is complex, including reorientation from the high shearing-induced parallel orientation, hydrogen bond, or other interparticle force-induced aggregation to form face-to-face associated particle groups, further flocculation of aggregates, and continuous formation of thicker aggregates. Different clay minerals may exhibit different degrees of thixotropic hardening rate and magnitude, and the salinity and

temperature at the maximum of the hardening rate and magnitude are also affected by the clay mineralogy. These findings here can have significant impacts on a series of engineering practices and problems, including offshore applications, such as floating offshore wind turbine and oil and gas platform, geothermal structure, and pile installation, which involve clays, especially soft clays.

TABLE OF CONTENTS

Page

LIST OF TABLES

Page

LIST OF FIGURES

Page

CHAPTER 1

INTRODUCTION

1.1 Background

Large-strain shearing of clays during sampling, in situ testing, and infrastructure installation often results in a significant loss of their initial intact undrained shear resistance. Depending on the sensitivity of clay, the loss of undrained shear strength after complete remolding can vary from very little for heavily over-consolidated, low-sensitivity clays to near-complete for high-sensitivity, quick clays (Moretto, 1948; Skempton and Northey, 1952). However, it has long been observed in the geotechnical practices that the disturbed soils, especially clays and clayey silts, can gradually gain recovery in the shear strength with time, even though the composition and volume of the soils remain constant during the entire process (Mitchell, 1960; Zhang et al., 2013; Zhang et al., 2017). This phenomenon has also been observed for other materials such as clay suspensions, crude oils, paints, and coatings (Arnold and Goodeve, 1940; Chang et al., 1999; Gamble, 1936; Ma et al., 2018; Turner and Rodewald, 1949). Such a stiffness hardening process is called thixotropy, a term that was first invented by Herbert Freundlich in 1927 to originally describe the sol-gel transitions in colloidal suspensions. An appropriate and widely accepted definition of thixotropy for soils was given in Mitchell and Soga (2005): "Thixotropy is an isothermal, reversible, time-dependent process occurring under conditions of constant composition and volume whereby a material stiffens while at rest and softens or liquefies upon remolding".

In geotechnical engineering, the thixotropic hardening in shear strength of soils following remolding and disturbance can be influential. For example, the undrained shear strength (s_u) of clay along a driven pile or around a suction anchor may decrease after

installation because of the mechanical disturbance. However, since the thixotropic effect can result in an increase to 100% or more than remolded strength (Mitchell, 1960), it is still possible to rely on the s_u determined from the laboratory experiments by using the intact sample (i.e., prior to the disturbance). The finite element analysis of clays with different plasticity indexes showed that the amount of strength gain for the disturbed soil near a suction anchor and the required time for such thixotropic hardening following installation is controlled by the way in which the anchor is penetrated (Andersen and Jostad, 2004, 2002). To understand the mechanisms behind this time-dependent soil behavior, some research was carried out to study the influences of various factors (e.g., water content, plasticity index, activity, and clay mineralogy) on the thixotropic hardening process of the clayey soils. Yang and Andersen (2016) found that liquidity index and water content show the best correlation with thixotropy strength ratio (s_u after t-days recovery divided by the remolded s_{ur}), which is the higher water content and liquidity index, the higher the thixotropic strength ratio. Similar experimental results can also be found in other studies (Lunne and Andersen, 2007; Seng and Tanaka, 2012).

Early explanation or proposed mechanisms, including particle-level microstructural changes, pore pressure redistribution, and interparticle force redistribution, can be found in the literature. One commonly accepted explanation is the microstructural changes towards a more flocculated structure. The structure is no longer in equilibrium with the surroundings immediately after the removal of the externally applied energy from remolding or compaction. A tendency toward flocculation of particles and particle groups, and reorganization of the water–cation structure to a lower energy state, will be achieved if the interparticle force of attraction is somewhat in excess of repulsion (Mitchell, 1960;

Mitchell and Soga, 2005). Another new finding is the reorientation and rearrangement of the particles to achieve homogenization of flaws or weak links, which is the contribution to the thixotropic behavior (Zhang et al., 2013a). For a closed, isothermal physical system (such as a wet clay without a change in pressure, temperature, volume, or composition), any change in macroscopic mechanical properties with time (e.g., stiffness and strength) must stem from certain internal processes occurring within the system. The purpose of this dissertation is to fill the gap and produce a comprehensive investigation on soil thixotropy for the broader geotechnical profession since not much research work has been carried out in the geotechnical field to better understand this aspect of fundamental soil behavior. Furthermore, early interpretation of proposed mechanisms was qualitative and sometimes speculative.

The primary objectives of this dissertation were to elucidate the linkage between the microscale microstructural processes (e.g., texture/fabric evolution) and the macroscale mechanical properties (e.g., stiffness and strength), and to investigate the effects of temperature and porewater salinity on thixotropic hardening of soft clays, which have been rarely studied according to the literature. Correspondingly, both pure clays and natural clays, with different clay mineralogy and soil compositions, were studied to provide a better understanding of the role of different clay minerals with varying surface chemistry in thixotropic hardening.

1.2 Research Objectives

The overall goal of this research was to develop a basic understanding of the microstructural and macromechanical mechanisms of thixotropy of soft clays, which can

help expand the knowledge base about this time-dependent soil behavior. Specific research objectives were as follows:

- Obtain macroscale thixotropic hardening behavior of soft clays via mechanical testing. Collect mechanical properties, including strength and stiffness at different curing times.
- Characterize thixotropy-governed microscale soil fabric evolution. Gather the microstructural change of a polycrystalline material during the thixotropic hardening process.
- Understand the effects of some physical and chemical factors (e.g., temperature, porewater salinity, initial water content) on thixotropy since clay is a complicated material and the properties are affected by a group of factors.

1.3 Dissertation Organization

This dissertation consists of seven chapters, and a brief outline of each chapter is given below:

(1) Chapter 1 (current chapter) is an introduction to this research, including the background, research objectives, and dissertation organization.

(2) Chapter 2 summarizes a comprehensive review of the history and concept of thixotropy. Fundamental principles of XRD are discussed and serve as a prerequisite for later advanced two-dimensional X-ray diffraction (2DXRD). A general review of the advanced 2DXRD technique is given to provide the necessary experimental background knowledge for this dissertation research to conduct the microscale experiments.

(3) Chapter 3 presents an experimental program that measured the macroscopic thixotropic behavior of four soft remolded clays. In this work, both the temporal evolution in the undrained shear strength s_u and small-strain shear modulus G_{max} were measured. The evolution of rigidity index I_R (= G_{max}/s_u) during thixotropic hardening was also investigated. The five-parameter modified Burgers model can best describe and fit all experimental s_u and G_{max} data, indicating that multiple mechanisms contribute to the dissimilar rates of thixotropic hardening at different stages.

(4) Chapter 4 presents results from an experimental program that measured the thixotropy-governed temporal evolution of microfabric in two soft clays. Two fabric-related indexes, orientation index (*OI*) and texture index (*TI*), were obtained to quantitively characterize the microfabric change. Multiple mechanisms of thixotropy unraveled by combining the microscale experiments with the macroscale experiments in the previous chapter are discussed. The combined results and findings presented in Chapter 3 and this chapter are given in a paper submitted to the *Journal of Geotechnical and Geoenvironmental Engineering* that is primarily focused on the 1D XRD results and a second paper submitted to *Applied Clay Science* that is primarily focused on the 2D XRD results

(5) Chapter 5 uses the previously developed multiscale experimental program to study the influence of porewater salinity on the thixotropic behavior of a variety of soft clays. The underlying mechanisms and factors that contribute to the different thixotropic behavior of clays with different porewater salinity were

also examined. This paper has been prepared for submission to the *Journal of Geotechnical and Geoenvironmental Engineering*.

(6) Chapter 6 presents the macroscopic investigation of thixotropic behavior of soft clays under the influence of both temperature and initial water content. Factors that contribute to the various extent of thixotropic hardening with different temperatures and initial water contents were examined, and applications are discussed.

(7) Chapter 7 is a concluding chapter that summarizes the significant findings of this dissertation research and provides recommendations for future study on the thixotropic behavior of soft clays as well as other geomaterials.

CHAPTER 2

LITERATURE REVIEW

2.1 Introduction

This section includes a summary of the literature review that was conducted for this dissertation. First, the literature review begins with a general introduction of the history and concept of thixotropy. Second, the fundamental principles of XRD are reviewed and serve as a prerequisite for presentation of the advanced two-dimensional X-ray diffraction (2DXRD) technique which was used in this dissertation to conduct the micro-scale experiments. This chapter presents aspects of thixotropy for which there is insufficient fundamental knowledge and provided a rationale of the work presented in this dissertation.

2.2 Thixotropy

2.2.1 Introduction

Thixotropy is one of the oldest rheological phenomena in colloid science. The term thixotropy, which is a combination of two Greek words, was introduced by Freundlich and Peterfi (Freundlich and Rawitzer, 1927; Peterfi, 1927). The origin of this phenomenon was discovered by Schalek and Szegvari in the lab in 1923. They studied iron oxide aqueous dispersions and found that the gel can be completely transformed to liquid through gentle shaking. The liquid can also be solidified to gel, with no distinguishable difference from the origin gel, after an amount of time. This reversible process can be repeated several times without any visible changes in the system. Some researchers began to use the time required to solidify in this kind of transition to quantify the effect since such a phenomenon of gel-sol transitions was subsequently discovered in an increasing number of materials,

including oil products (Chang et al., 1999; Petrellis and Flumerfelt, 1973), greases and waxes (Kassem et al., 1970; Mas and Magnin, 1994), paints and coatings (Basta et al., 1998; Gamble, 1936), food products (Berland and Launay, 1995; Coussot and Gaulard, 2005; Wei et al., 2015), and dispersions of clay minerals (e.g., drilling muds) (Astbury and Moore, 1970; Pignon et al., 1998; Toorman, 1997). However, the mechanisms underlying thixotropy are complicated and still poorly understood, even though the phenomenon is common in both natural and industrial systems.

The following sections present a literature review on thixotropy, including the concept, research development, and important applications. Some previous comprehensive reviews of thixotropy include Mewis (1979), Barnes (1997), Mewis and Wagner (2009).

2.2.2 Origins and Definition

In geotechnical engineering, researchers started considering the importance of thixotropy when clay sensitivity was discovered and studied and multiple research teams worked on the topic (e.g., Jacobsson and Pusch, 1972; Mitchell, 1960; Nalezny and Li, 1967; Seed and Chan, 1959; Skempton and Northey, 1952), even though the first work on this topic is unclear. Boswell (1948) carried out a preliminary examination of a representative series of unconsolidated rocks and discovered thixotropic behavior for all the sediments excepting coarse clean sands and gravels and consider various factors including grain-size, grading, mineralogical composition and the presence of electrolytes. Skempton and Northey (1952) presented results on the recovery of the strength of some undisturbed clays after remolding, which showed only a small fraction of the undisturbed strength is regained. The sensitivity of the tested clays was not completely caused by

thixotropy since the tested clays were only partially thixotropic materials, compared to a purely thixotropic material for which the original strength can ultimately be completely regained after remolding (Figure 2.1). Similar discovery and discussion were reported by Rosenqvist (1953), Osterman (1963), Liebling and Kerr (1965), Lessard and Mitchell (1985).

In the scientific community (e.g., chemistry, colloidal science, rheology), there is a general agreement that thixotropy is defined as: the continuous decrease of viscosity with time when flow is applied to a sample that has been previously at rest and the subsequent recovery of viscosity in time when the flow is discontinued (Mewis and Wagner, 2009). Other definitions proposed by different researchers (Coussot et al., 2002; de Souza Mendes and Thompson, 2012; Goodeve, 1939; Larson and Wei, 2019) are generally similar with all being based on viscosity. The process is described as a time-dependent decrease of the viscosity, which is induced by flow, and it reverses if the flow is decreased or arrested. Therefore, the viscosity of a fluid, which is a measurement of its resistance to gradual deformation by shear stress or tensile stress, is an important parameter to describe this kind of phenomena in these fields.

However, this kind of definition is not appropriate to describe the thixotropic behavior of soils. Soil consists of solids and pore spaces, which are filled with gases and water. The amount of water is usually lower than that which can turn the soil into a suspension. A more appropriate definition for soils is given by Mitchell and Soga (2005) as: “Thixotropy is an isothermal, reversible, time-dependent process occurring under conditions of constant composition and volume whereby a material stiffens while at rest and softens or liquefies upon remolding.”

2.2.3 Thixotropy Research Progress and Proposed Mechanisms

Much thixotropic work over the past 50 years was conducted on the sol-gel transition according to rheology and colloidal fields (Abend and Lagaly, 2000; Joshi et al., 2008; Labanda and Llorens, 2008; Wang et al., 1994). Neumann and Sansom (1970) utilized optical and rheological methods to study the gel formation and flocculation of aqueous dispersions of synthetic hectorite-like clay. Weymann (Mercer and Weymann, 1974; Ross et al., 1973; Weymann et al., 1973) worked on the thixotropic behavior of bentonite-water suspensions and developed a model to predict the mechanical behavior of the suspension. Optic transmission experiments were further quantitatively applied to confirm his work.

Newly developed techniques, including light, neutron, and X-ray scattering, have been utilized to understand the underlying mechanisms of the thixotropic process. There are two general mechanisms in particle dispersions derived to explain this kind of gel-sol transition or behavior. The first one stems from the interparticle attractions or adhesion. The particles form aggregations inside the suspensions due to the attractions or adhesion between each other. Such gels are commonly formed by aggregated mineral particles. The second one stems from interparticle repulsion which keeps particles from moving since there is no free space around each particle. Ionic analysis of the aqueous phase, static light, small-angle neutron scattering, rheological experiments, and centrifugation were employed to study the mechanisms of the fluid-gel and gel-fluid transitions of laponite dispersions in water (Martin et al., 2002). The results showed that the particles form aggregations due to the edge-to-face attractions, and the healing time needed to finish the transition from fluid to gel is much longer with weaker the edge-to-face attractions.

In geotechnical/soil engineering, early research work was focused on measuring the thixotropy regain or thixotropic strength ratio of undisturbed clays after remolding. The thixotropic strength ratio of a remolded clay was defined as a ratio of the strength of the clay after a period of aging over its remolded strength. Thixotropic regain of some typical undisturbed clays after remolding and three clay minerals of which the water contents equal to their liquid limit (*LL*), are presented in Figure 2.2. The results indicate that kaolin exhibits almost no thixotropy, illite shows a small effect of thixotropy, while the bentonite shows a remarkable regain at very short time intervals, and it is not possible to suggest an upper limit for this material since the strength continued to increase throughout the experiment (Skempton and Northey, 1952). Primary efforts were also made observing the structure of clay to explain some of the clay properties (Casagrande, 1932; Lambe, 1953; Pusch, 1966, 1962). Mitchell (1960) provided one possible explanation of thixotropic effects in soils with the assumption that the internal energy and stress conditions in a thixotropic soil immediately after remolding are not in equilibrium conditions. Macroscale thixotropic phenomena are associated with the particle-level microstructure changes toward a lower energy state. Most of the early published contributions have been summarized in a thesis conducted by Arnold (1967). Two distinct stages, a rapid micro-particle link-bond reformation, and a slower, time-dependent diffusion stage, were discovered and confirmed for the thixotropic regain process from investigations conducted on Wyoming bentonite by Arnold (1967). Pusch (1968) described a technique for investigating clay microstructure based on acrylate embedding and microtome sectioning, small specimens of undisturbed clay were treated with different chemicals to be hard enough to be sliced in a microtome. Later, transmission electron microscope (TEM) and

nuclear spin echo technique were adopted by Jacobsson and Pusch (1972) to study particle rearrangement and reordering of water phases during the strength recovery of remolded natural marine and sensitive clays and showed that the increase in strength with time was connected with flocculation after dispersion by remolding. Microstructural changes were also observed from electron micrographs of ultrathin sections of Rollsbo clay during the thixotropic hardening process. Representative research afterward was conducted on microstructural changes associated with thixotropic phenomena in clayey soils through scanning electron microscopy (SEM) images by Osipov et al. (1984). The study indicated that the soil microstructure was not ruptured but more homogenous during the shear process, and it rapidly restored to its initial state after the termination of the vibration or shear. The reductions in cohesion at contacts contribute to a decrease in strength in the system.

It is obvious that these general explanations or interpretations of soil thixotropy mechanisms are limited to the available techniques used in earlier studies and lagged behind other research communities (e.g., physics, colloidal science). However, it is surprising that not too many studies were conducted afterward in the geotechnical community about the underlying mechanisms of such thixotropic behavior in clays or other soils. As explained by Mitchell and Soga (2005), sedimentation, remolding, and compaction result in specific soil structures compatible with these processes. The structure is no longer in equilibrium with the external surroundings immediately after the removal of the externally applied energy from remolding or compaction. A tendency toward flocculation of particles and particle groups, reorganization of the water–cation structure to a lower energy state, will be achieved if the interparticle force of attraction is somewhat

in excess of repulsion. Seng and Tanaka (2012) conducted a study on thixotropic hardening and behavior of very soft clays under low consolidation pressure, which showed that the increment in shear modulus developed in the thixotropic process appears to be noticeably higher than that in the secondary consolidation process. Díaz-Rodríguez and Santamarina (1999) proposed several potential contributors to the phenomenon of thixotropy, including interparticle contact creep, interparticle force redistribution, nonuniform pore pressure distribution in saturated and partially saturated soils, alteration in ionic distribution and mobility, the ensuing changes in interparticle forces, and the mobility of the finer fraction in the soil mass, after a study on the thixotropy behavior of Mexico city soils. Zhang et al. (2013) conducted a novel micro/nano compression study on saltwater clay flocs and concluded that the rearrangement of structural flaws towards greater uniformity is another factor contributing to the thixotropic behavior of the flocs, which has nearly zero effective stress or self-weight. The revealed mechanism is similar to one of the mechanisms proposed by Díaz-Rodríguez and Santamarina (1999) involving the homogenization of nonuniform pore pressure distribution. In essence, the remolded soil always aims to achieve a uniform distribution of energy within the enclosed system, being either structural disturbance, porewater pressure, and interparticle forces.

Zhang et al. (2017) utilized unconfined compression (UC), pocket penetrometer (PP) tests, SEM imaging, and mercury intrusion porosimetry (MIP) to investigate the thixotropic behavior of one Chinese clay and the microstructural changes and pore size distribution during the hardening process. Figure 2.3 presents SEM images that show the changes in the microstructure during thixotropy. The initial microstructure of undisturbed clay exhibited an open flocculated structure, and it was damaged after disturbance. Pore

size changes and volume distribution (Figure 2.4 and Figure 2.5) of the tested clay during thixotropic hardening can be observed in two stages. In the early stage of the process, the micropores decreased first and followed by the relative increase in mesopores and micropores. In the later stage, the mesopores increased with a decrease in the micropores and the macropores. Therefore, the strength loss is caused by the disturbance, resulting from the microstructure changes from the initial structure to the dispersed structure. On the other hand, the regain in strength during thixotropy results from the previously dispersed structure to the newly established flocculated structure. These changes may be accompanied by the homogenization of the pore size distribution. The unbalanced interparticle attraction and repulsion forces contribute to microscale particle movement, which leads to the homogenization of pore size distribution. It can also be explained differently. The process of thixotropy is a reflection of energy minimization: any systems of mixtures tend to transition to a status of minimal energy. The energy equilibrium in the initial state of the remolded sample is disturbed and non-uniform, and it finally transformed into a new energy balance. This new restabilization requires particle movement, including both the soil particles, water, and ions (Zhang et al., 2017). Other researchers argue that energy minimization is not the reason since a physically enclosed system holds constant total energy. The major reason is energy homogenization within the system, or the energy equilibrium and homogenization among different locations/parts within the enclosed soil system, just like thermal energy or hydraulic energy transport via conduction. One example of such a mechanism governing the thixotropy proved by Zhang et al. (2013) is the homogenization of flaws or weak links.

To date, some research has been carried out to study the influences of various factors (e.g., water content, plasticity index, activity, temperature, and clay mineralogy) on the thixotropic hardening process of clayey soils since the thixotropic strength recovery was discovered to be influenced by them. Jeong et al. (2015) conducted experimental studies of the rheological behavior on both clay-rich and clay-poor soils with a focus on the effect of mineralogy and grain size. Yang and Andersen (2016) found that liquidity index and water content show the best correlation with thixotropy strength ratio (s_u after t-days recovery divided by the remolded s_{ur}), which is the higher water content and liquidity index, the higher the thixotropic strength ratio. Similar experimental results can also be found in other studies (Lunne and Andersen, 2007; Seng and Tanaka, 2012). However, controversial results on the effect of water content were obtained by others. For example, Shahriar et al. (2018) argue that clays at a water content of 0.75 times its liquid limit exhibit the optimal thixotropic hardening or best thixotropic gain in strength, which is contrary to the conclusions drawn above.

2.2.4 Importance and Applications

A series of important engineering practices and problems, including pile and suction caisson setup in clays, drilling muds, sampling and sample storage-relate strengthening, quick clays, sensitive clays, consolidation of very soft clays (e.g., dredged soils), relate to thixotropy. A better understanding of this fundamental soil behavior will have significant impacts on those problems. For instance, bentonite-water suspension, which is known as drilling mud, is wildly used for construction. The degree of thixotropy of these suspensions, despite intensive pre-shearing, depends on the bentonite used, the

bentonite concentration, and the presence and amount of salt (Kelessidis, 2008). The thixotropy of drilling mud should be promoted or suppressed depends on specific circumstances. Another example that thixotropy should be minimized is for undisturbed sample storage. When collecting undisturbed thin-walled tube samples of soft clays there is a zone of intense shearing at the interface of the soil sample and the tube inner wall (e.g., Baligh et al., 1987). If the sample is quickly extruded thereafter it is likely that little additional shear-induced damage will occur to the sample. However, if the sample is stored for days or weeks after collection, water content redistribution and thixotropic hardening will occur at the soil-tube interface and any subsequent extraction can cause additional strain-induced sample disturbance. For this reason, (Ladd and DeGroot, 2003) recommend that tube samples of soft clays should be cut and debonded for extracting samples that will be used for 1-D consolidation and consolidated shear tests.

As mentioned above, some engineering problems involved with soft clays, including the pile and suction caisson setup and construction of wind farm foundations, should consider the influence of thixotropy of the constructed soils (Abu-Farsakh et al., 2015a; Jeanjean, 2006; Zakeri et al., 2014). For instance, the "set-up" effect as the subsequence of suction caisson installation refers to the changes of caisson capacity. Once the suction caisson has penetrated to its target depth in the seabed, excess pore pressure around the caisson will gradually dissipate, and the strength of surrounding soil may also recover with time due to thixotropy, both of which will result in a change of vertical pullout capacity of the suction caisson (Guo et al., 2014). Finite element analysis for clays with different plasticities showed that the amount of strength gain for the disturbed soil along

the suction anchor and the required time for such thixotropic hardening after installation are controlled by the how the anchor is penetrated (Andersen and Jostad, 2004, 2002).

Since soil thixotropy plays an important role in many engineering practices and problems, a better understanding of the underlying mechanism generates significant practical impacts on geotechnical engineering, particularly the design and construction involving soft clays.

2.3 Fundamental Principles of X-Ray Diffraction

2.3.1 Introduction

X-rays are electromagnetic radiation, which has a wavelength in the range of 0.01-100 Å and energies varying from 120 eV to 120 keV. According to the energy level, X-rays are classified as soft and hard X-rays (Malmgren et al., 2013; Philippe et al., 2012; Popmintchev et al., 2009). Hard X-rays are known as an imaging tool to gather information inside of an object, owing to their high energy and hence the power of penetration through the studied object. For instance, crystal structures can be determined by X-ray crystallography with the help of the hard X-ray (Davis et al., 1995; Lanzirotti et al., 2010; Rack et al., 2008). When an incident monochromatic X-ray beam hits a sample, scattered X-rays with the same wavelength as the incident beam generated besides X-ray absorption and other phenomena. The distribution of the scattered X-rays in space is a function of the distribution of the electrons within the sample. Therefore, the intensities and spatial distributions of the scattered X-rays, which form a distinct diffraction pattern, is a reflection of the atomic structure of the sample.

Many existing theories and equations can be used to explain and describe the relationship between the diffraction pattern and the structure of a material. Bragg's law is an easy way to describe the X-ray diffraction from a crystal. The following section presents the background and derivation of Bragg's law.

2.3.2 Bragg Condition and Derivation

Lawrence Bragg and his father William Henry Bragg discovered Bragg diffraction in 1913. They found some surprising patterns of reflected X-rays, which were produced by some crystalline solids. At certain X-ray wavelengths and incident angles, these crystals produced intense peaks or reflected radiation. A model regarding crystals as a set of discrete parallel planes separated by a constant parameter d was invented to explain the result by Lawrence Bragg (Figure 2.6). Bragg peak would produce if the incident X-ray radiation and their reflections off the various planes interfered constructively, and interference is constructive when the phase shift is a multiple of 2π. Lawrence Bragg first presented this condition as Bragg's law, which is discussed and explained later in this section. Braggs' law seems simple, but it indicates that real particles at the atomic scale exist and provides a powerful tool to study crystals by using X-ray and neutron diffraction (Brown et al., 1977; Nishiyama et al., 2002; Svergun et al., 1998). In 1915, Lawrence Bragg and his father were awarded the Nobel Prize in physics for their discoveries in the analysis of crystal structure utilizing X-rays.

There is a relationship between the angle at which X-rays must fall on the parallel planes of atoms in a crystal to achieve Bragg peak due to constructive interference. The

relationship of the wavelength of the X-rays, the distance between the crystal planes, and the incident angle can be expressed as:

$$\sin\theta = n\lambda/2d \tag{2.1}$$

where θ is the angle between the incident or the reflected beam and the crystal plane; λ is the X-ray wavelength; d is the spacing between crystal planes; n is an integer, called the order of reflection.

The above equation can be easily derived. Consider the crystal lattice plan arrangement of a crystal exhibit in the Figure 2.7. The path difference between the two diffracted X-rays (ABC and A'B'C') can be written based on the geometrical relationship. Constructive interference will happen if the path difference is equal to a value which is an integer of the wavelength.

On the one hand, a known incident X-ray, including wavelength and angle, can help identify the crystal structure of an unknown crystal (Harris et al., 1994; Pecharsky and Zavalij, 2009; Poojary and Clearfield, 1997). Harris et al. (1994) developed and applied a method employing a Monte Carlo algorithm for unknown crystal structure determination from powder diffraction data. On the other hand, analyzing a crystal with known *d*-spacing will satisfy Braggs' law only at a specific wavelength and incident angle. It can be used to quantify elements within a sample because every element produces X-rays at a fixed wavelength (Jaswal et al., 2019; O'Day et al., 2004; Twining et al., 2003).

2.3.3 Diffraction Pattern

As mentioned above, XRD can provide information on crystalline materials with long periodicity atomic arrangements. Meanwhile, atomic arrangements of materials with

short-range order or no order at all (e.g., gases, liquids, and amorphous solids) can also be provided. A material may have either one of the atomic arrangement types or a mixture of them. Figure 2.8 shows a schematic comparison of diffraction patterns from a few representative materials with different types, including crystal, liquid or amorphous solid, monatomic gas, amorphous solid with crystals, and mixtures. Detailed information and introduction about the differences between these diffraction patterns can be found in He (2009a). The diffraction pattern from crystals is emphasized here, which has many sharp reflections corresponding to various crystal planes satisfying Bragg law. The diffraction pattern from crystals can also be called a powder diffraction pattern since the diffraction should be obtained from polycrystalline materials or powder materials to satisfy the Bragg condition at all crystal planes. The peaks at low 2θ angles are diffracted from crystals with larger d-spacing and vice versa at high 2θ angles (He, 2009a).

2.4 Two-dimensional X-Ray Diffraction Techniques

2.4.1 Introduction

With the development of advanced techniques, researchers are able to conduct more detailed studies on more complex problems. 2DXRD is an ideal, widely used, and nondestructive technique for different kinds of analysis of various materials, such as metals, polymers, and rocks (Bontempi et al., 2008; Collins et al., 2015; Kanitpanyacharoen et al., 2011; Rodriguez-Navarro et al., 2012; Speziale et al., 2006; Widjonarko, 2016). An area detector, compared to a point detector for conventional 1DXRD, is used for 2DXRD. The difference between the XRD and 2DXRD is not only the detector used in the system. In addition to 2D detector technology, a completely new concept and theory are necessarily

constructed for the new system to process and interpret the data collected. To ensure the 2D data can also be used for conventional applications, the new theory should be consistent with the conventional theory.

The following sections presents a literature review on this advanced technique, including the diffraction patterns, experimental system, major components, and applications. Some previous comprehensive reviews of this topic are also presented by He (2003, 2009a), Engler and Randle (2010).

2.4.2 Diffraction Pattern Measured by Area Detector

Bob B. He introduced different diffraction patterns from single crystal and polycrystalline samples, which is shown in the Figure 2.9. As the names suggest, a single crystal is only one crystal or grain, while polycrystalline or multi-crystalline materials consist of many crystallites of varying size and orientation. The following paragraph will discuss diffraction patterns from polycrystalline materials since polycrystalline materials were the focus of the soil studied in this research.

Polycrystalline materials can be single-phase or multiphase. Crystallites in single-phase polycrystalline materials have the same crystal structure but different orientations. For multiphase polycrystalline materials, composited crystallites also can have different crystal structures. The actual distribution of the diffraction from a sample is in 3D space. With the incident X-ray beam, the diffracted beams form a series of diffraction cones in (Figure 2.9(c)) 3D space due to the randomly oriented crystals in polycrystalline materials. Each diffraction cone is the diffraction generated from the same family of crystalline planes. Diffraction frame is the cross-section of the detecting plane and the diffraction cones,

which is the data collected with a detector from the X-ray diffraction test for a specimen. Figure 2.9(d) is a diffraction frame collected from corundum powder with an area detector. The XRD with an area detector is called 2DXRD due to the collected data from the diffraction pattern is a two-dimensional image-like diffraction frame.

2.4.3 The 2DXRD System and Major Components

A typical 2DXRD system consists of five major components, including an X-ray source, X-ray optics, goniometer and sample stages, sample alignment and monitor, and an area detector. Figure 2.10 shows a schematic sketch by He et al. (2000) that shows the five major components in a typical 2DXRD system. X-ray tubes, rotating anodes, and synchrotrons are three common devices that are used to generate X-rays. Different laboratories or systems have their designed X-ray sources for producing X-rays at specific energies and intensities. X-ray optics are used to manipulate the X-rays generated from the X-ray source to a required condition for later research work, including wavelength, monochromatic beam, and beam focus size. Common optics include focusing optics, collimating optics, and crystal optics, are manufactured and developed for different techniques (e.g., X-ray fluorescence, small-angle X-ray scattering, X-ray microscopy). As the name suggests, the sample stage is used to locate a tested specimen. A goniometer can be used to measure an angle or place the specimen at a precise angular position, which helps form the geometric relationship of the incident beam, specimen, and detector. Sample alignment and monitor assists users to position the specimen in the instrument center and check the position and state of the specimen before and during the test. There are various kinds of area detectors with the development of new techniques. Area detector records the

scattering X-rays from a sample while displaces and saves the diffraction pattern into a two-dimensional frame.

Each of the components mentioned above may have some differences due to the different applications and manufacturers. Besides the five basic components, other accessories can also be equipped within the system to meet the needs of different research purposes. For instance, low-temperature and high-temperature stages can be used to study the influence of the environment. A computer controls the whole system, and software can help with instrument control, data acquisition, and data analysis.

2.4.4 Comparison between One and Two-dimensional XRD

Figure 2.11 is a schematic from He (2009b) that shows X-ray diffraction from a powder (polycrystalline) sample. Only two diffraction cones, including one forward and one backward cone, were plotted for simplicity to explain the difference between the conventional and two-dimensional XRD. A point detector or a one-dimensional position sensitive detector (PSD) is used in conventional diffractometer for conventional diffraction measurement. Both of them are confined within the diffractometer plane and move along the detection circle shown in the figure. Therefore, the diffraction information in the perpendicular direction to the diffractometer plane is not considered in conventional measurements. However, diffraction data can still be measured with additional sample rotations with longer data acquisition time. With a 2D detector, the measurements are not only limited to the diffractometer plane. On the contrary, the whole or a large portion of the diffraction rings can be measured simultaneously, depending on the detector's size and position (He et al., 2000). Figure 2.12 presents typical diffraction patterns measured with

a 2D detector, compared to conventional point detector and PSD. The point detector can collect the diffraction pattern in a range of 2theta by moving the detector within the plane, while PSD can collect the diffraction pattern in a range of 2theta simultaneously. But either of them can collect information in the direction perpendicular to the diffractometer plane.

2.4.5 Applications

In a 2DXRD test, a crystalline sample interacts with an incident beam and then generates many diffracted beams for different crystallographic planes based on Bragg's Law. The diffracted beams are recorded by an area detector, and the distribution of the diffracted X-ray intensity on the detector is converted to an image-like diffraction frame. Then, the integrated diffraction spectrum is used to perform different kinds of analysis based on the needs of the utilizer (e.g., phase identification, texture analysis, stress measurement) (Almer et al., 2003; Helming and Preckwinkel, 2005; Ramirez-Rico et al., 2016; Tang et al., 2001). The following section will only introduce phase identification (phase ID) and texture measurements since those are the methods used in this dissertation.

In physical chemistry, a phase is characterized by having a relatively uniform chemical composition and physical properties. As mentioned before, a material or a sample can contain only one single-phase or multi-phase. With the help of XRD, phases of a material or sample can be individually determined by examining the diffraction pattern. After integration of the interested region of a Debye-ring from a sample, the spectrum can be used to compare with a list of standard diffraction patterns of known materials by using software or a database to do the phase ID or quantitative phase analysis of the unknown material or sample. The most comprehensive database is the powder diffraction file (PDF)

updated annually by International Centre for Diffraction Data (ICDD). The diffraction patterns of unknown materials can be used to search and match with the database, which gives a rapid sense of the tested material. It also helps a new user in this field or researchers who lack a background in physics or chemicals. Dubrovinsky et al. (1997) presented a study designed to minimize the difficulties encountered in earlier experiments under extreme conditions on transformations of phases of silica at various pressures. Figure 2.13 shows diffraction patterns collected using a charge-coupled device (CCD) area detector of quartz during the transformation at high pressure after heating. Different phases can be easily identified from the results. Lange et al. (2010) utilized both conventional XRD and other non-destructive analytical methods to characterize the geosynthetic clay liner bentonite. The two-dimensional General Area Diffraction Detector System (GADDS) images proved to be particularly advantageous in differentiating between the microcrystalline clay, which appeared as homogenous Debye rings, and the 'spotty' or 'grainy' appearance of primary, more coarsely crystalline, accessory minerals (Lange et al., 2010). Figure 2.14 demonstrates each identified phase analyzed in corresponding software with the reference ICDD database after the integrations of the GADDS images.

In material science, texture refers to the orientation distribution of all the crystallites in a polycrystalline sample. Fabric, which has a similar meaning as texture, is used in geology and soil science as well as geotechnical engineering. The material is said to have no texture if the orientation distribution of crystallites in this material or sample is completely random, and the material shows isotropic properties. Conversely, anisotropy is directly related to the preferred orientation of crystallites in a material. A material or a sample showing anisotropic properties has certain texture. The texture of a sample can be

described as strong, moderate, and weak, depending on the percentage of crystallites having the preferred orientation. Almost all the engineered materials show texture, whether it is strong or weak, and texture significantly affects the material properties. Therefore, it has been broadly studied in different fields, and its analysis developed with new advanced techniques. Texture analysis by using 2DXRD is significantly faster than the conventional measurement with a point X-ray detector. In the former, the texture data can be simultaneously collected by an area detector for multiple poles and directions. Pole figures can be measured at very fine steps, even for materials with sharp texture, because of the high speed for data collection. The new technique and analysis have been applied to study a variety of materials, including geomaterials (e.g., rocks, shales), biomaterials (e.g., fetal bone, dinosaur tendon, and salmon scale), electrical thin films, and metals (Engler and Randle, 2010; Helming and Preckwinkel, 2005; Kanitpanyacharoen et al., 2011; Wenk et al., 2010; Wenk and Grigull, 2003). Diffraction images obtained by area detectors can immediately show if there is a preferred orientation within the materials, which is shown in Figure 2.15.

In 2005, a Rietveld method was used by Lonardelli et al. (2005) to conduct an interesting texture analysis on two biological samples, including an ossified pachycephalosaurid dinosaur tendon and an Atlantic salmon scale, by using monochromatic synchrotron X-rays. Figure 2.16 gives the two-dimensional synchrotron diffraction images that show a strong intensity variation for the dinosaur tendon and a lesser one for the salmon scale, which is an indication of different degrees of the texture of the two materials. The image data were input into the software MAUD (Materials Analysis Using Diffraction) for texture analysis, and brief Rietveld processing procedures were

provided. The pole figures calculated from the orientation distribution, shown in Figure 2.17, are further evidence that the texture of the dinosaur tendon is stronger than the salmon scale. The comparison of the results with optical observations is also consistent. A similar but more complicated analysis was conducted on three deeply buried Qusaiba shales since the samples are multiphase materials. The variation of intensity with Debye rings, as shown in Figure 2.18, is an indication of the preferred orientation of different phases. For example, kaolinite, illite-smectite, illite-mica, and chlorite show strong preferred orientation with (001) pole figure, but quartz (101) shows a lack of preferred orientation since the uniform intensity along the ring (Kanitpanyacharoen et al., 2011). Further Rietveld refinement was conducted, and the simulation works well. Figure 2.19 presents the difference between the calculated and experimental diffraction spectra that is negligible, and the variation of the intensity of each phase also can obviously be observed from the simulation patterns. The final results can help calculate the elastic properties of the shale matrix. Similar studies can also be found in Wenk et al. (2010, 2014).

In summary, geotechnical research on thixotropy in clays and other soils lags behind the counterpart for suspensions, gels, and other non-Newtonian fluids performed by colloid scientists. No recent comprehensive review articles on thixotropy are available in the geotechnical literature and the understanding of this topic remains fragmental due to the knowledge gap developed after the 1960s. This research utilizes the latest advanced analytical techniques to probe the microfabric evolution of soft clays accompanying thixotropic process. Moreover, it makes the pilot effort to investigate the effects of both temperature and porewater salinity on thixotropic hardening, which has been rarely studied according to the literature.

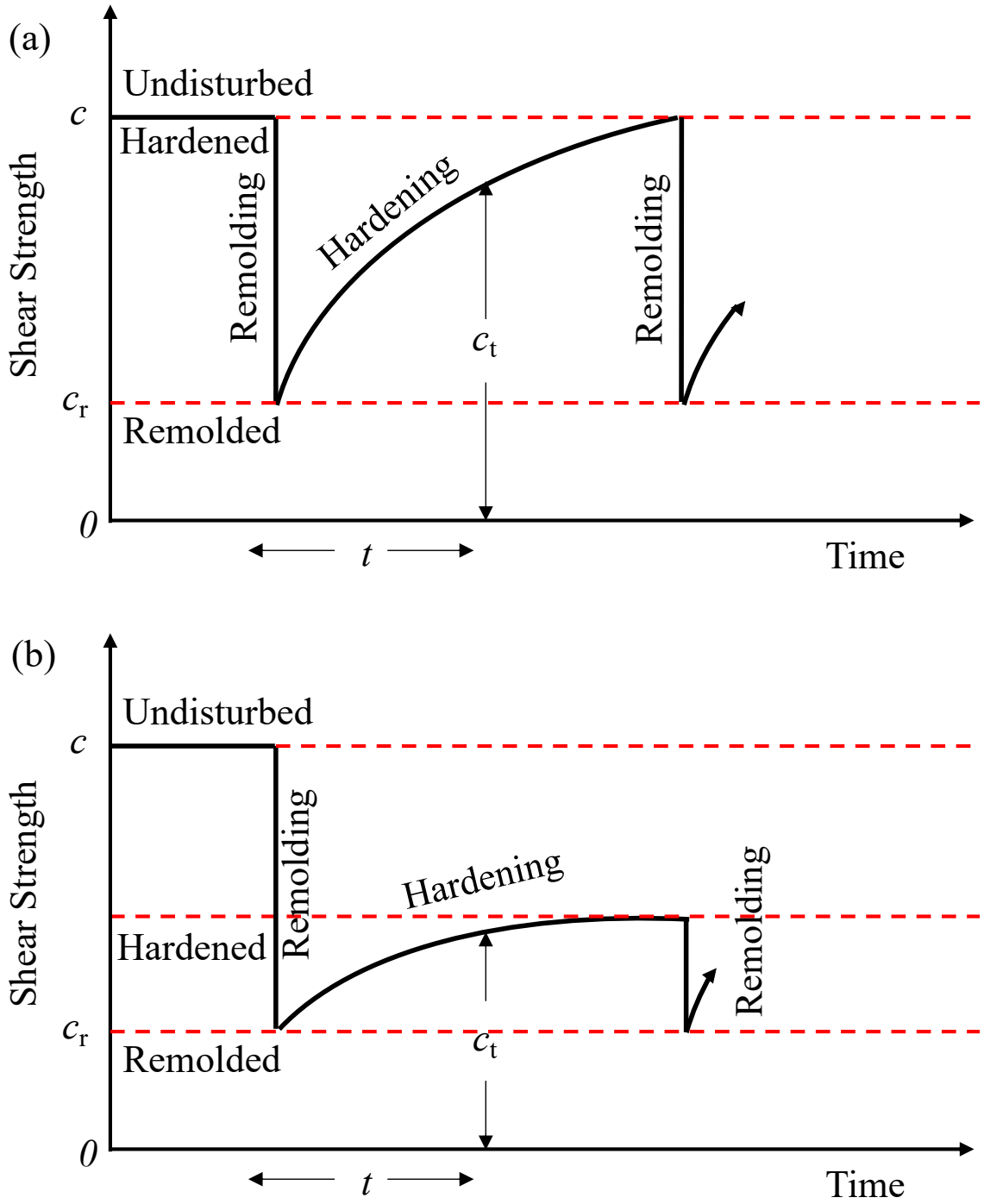

Figure 2.1 Characteristics of thixotropic materials (modified from Skempton and Northey, 1952): (a) purely thixotropic material and (b) partially thixotropic material.

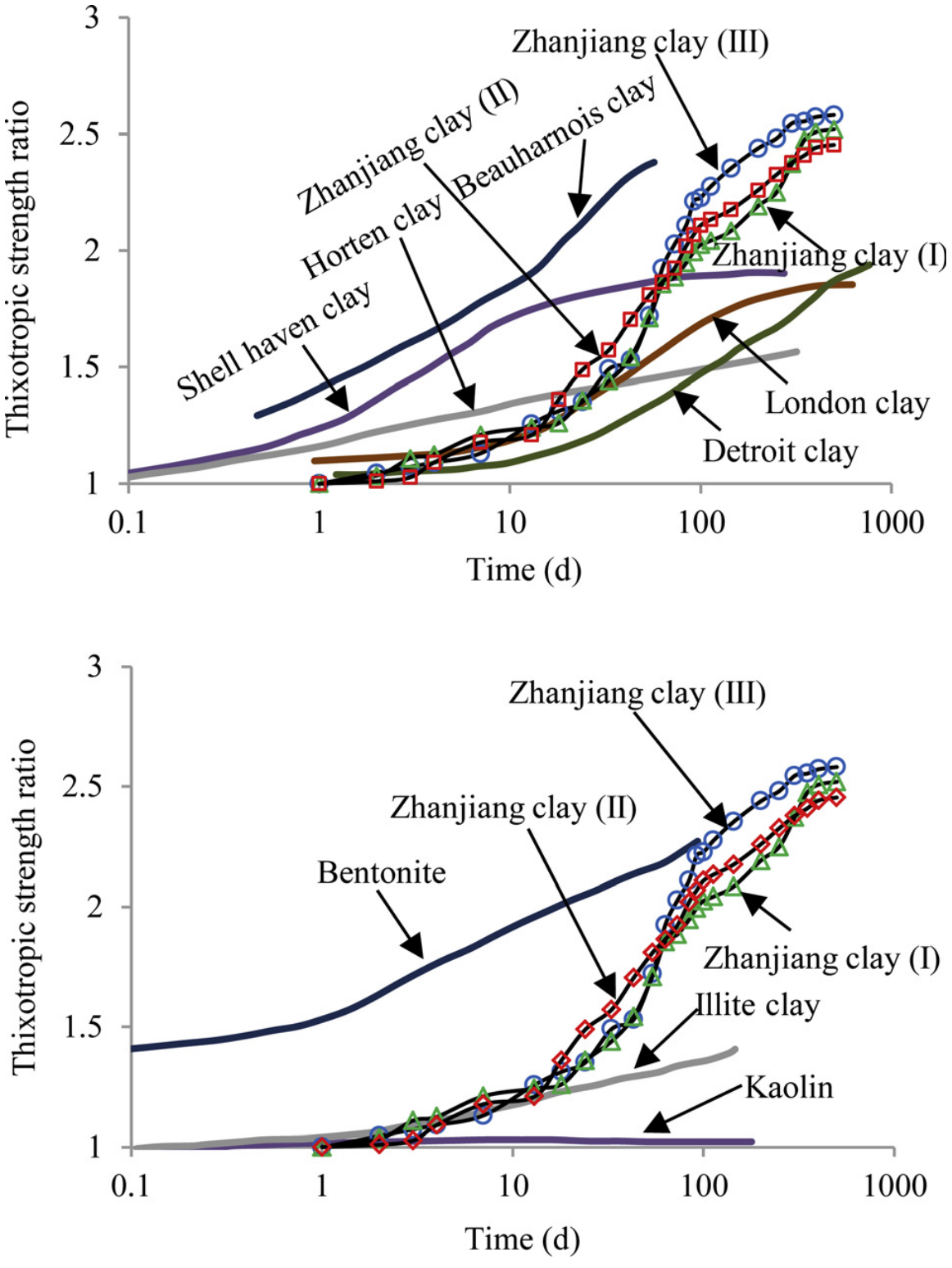

Figure 2.2 Thixotropic regain in some typical clays and clay minerals (Zhang et al., 2017).

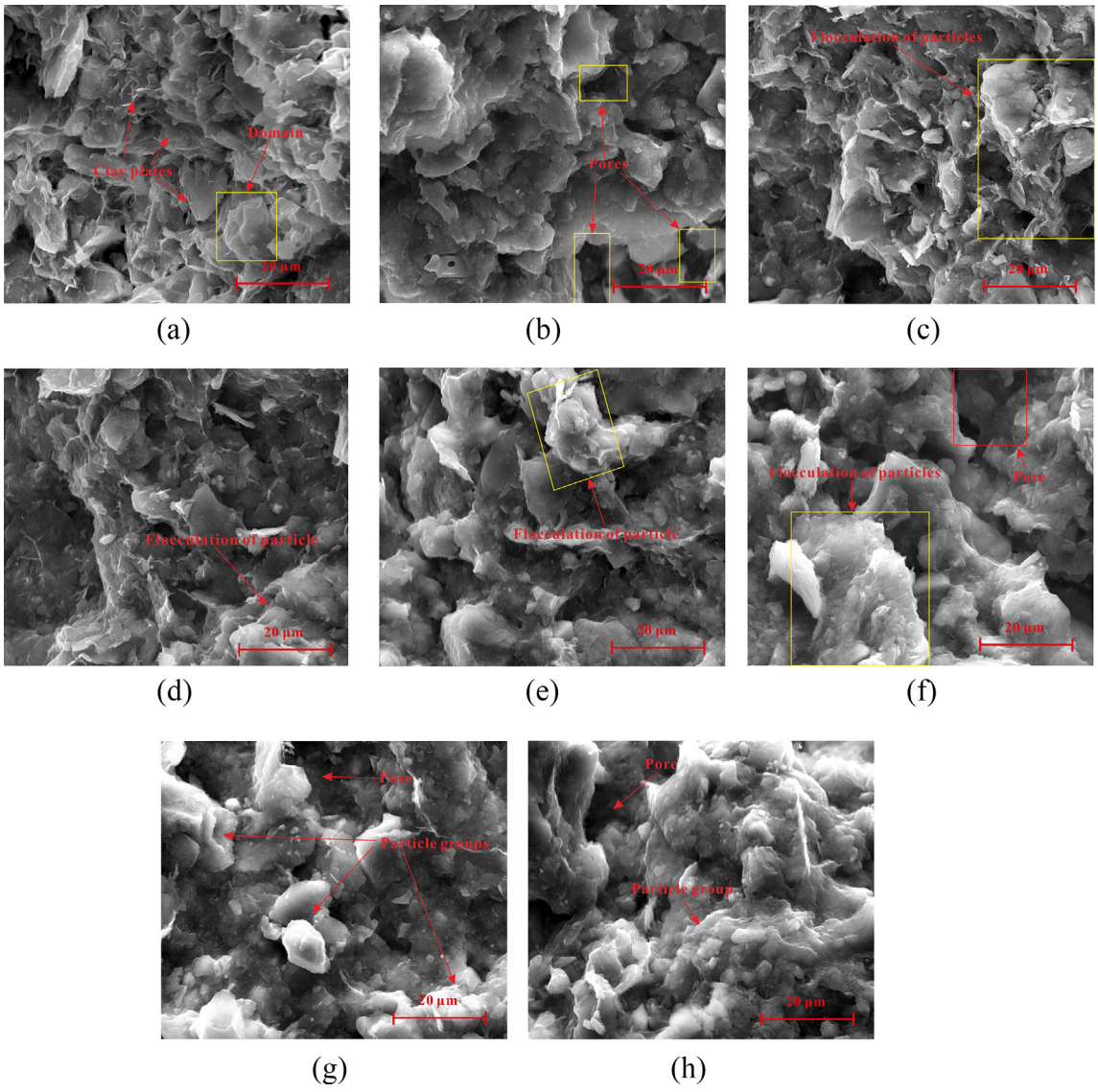

Figure 2.3 SEM images: (a) natural Zhanjiang clay and remolded clay at different thixotropic times; (b) 1 d; (c) 3 d; (d) 7 d; (e) 30 d; (f) 100 d; (g) 300 d; (h) 500 d (Zhang et al., 2017).

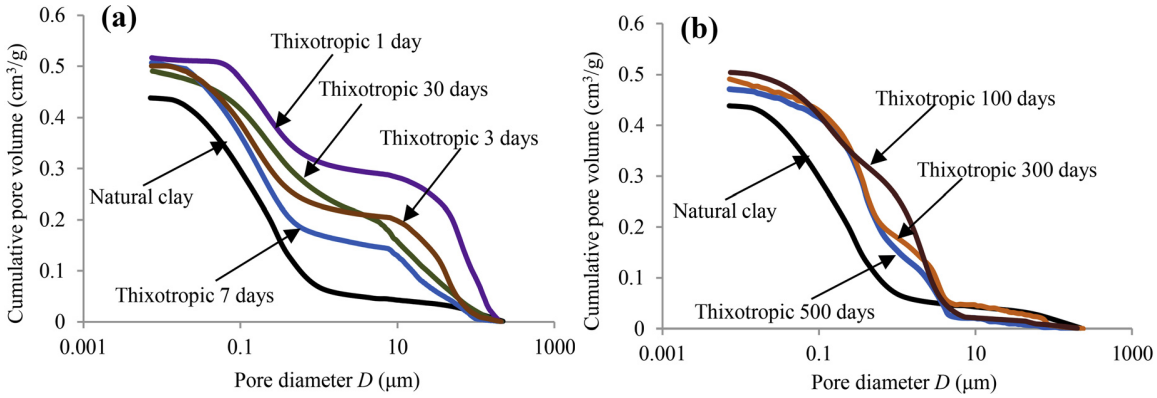

Figure 2.4 Pore size distribution curves of natural Zhanjiang clay and remolded clay at different thixotropic times: (a) 1, 3, 7, and 30 d; (b) 100, 300, and 500 d (Zhang et al., 2017).

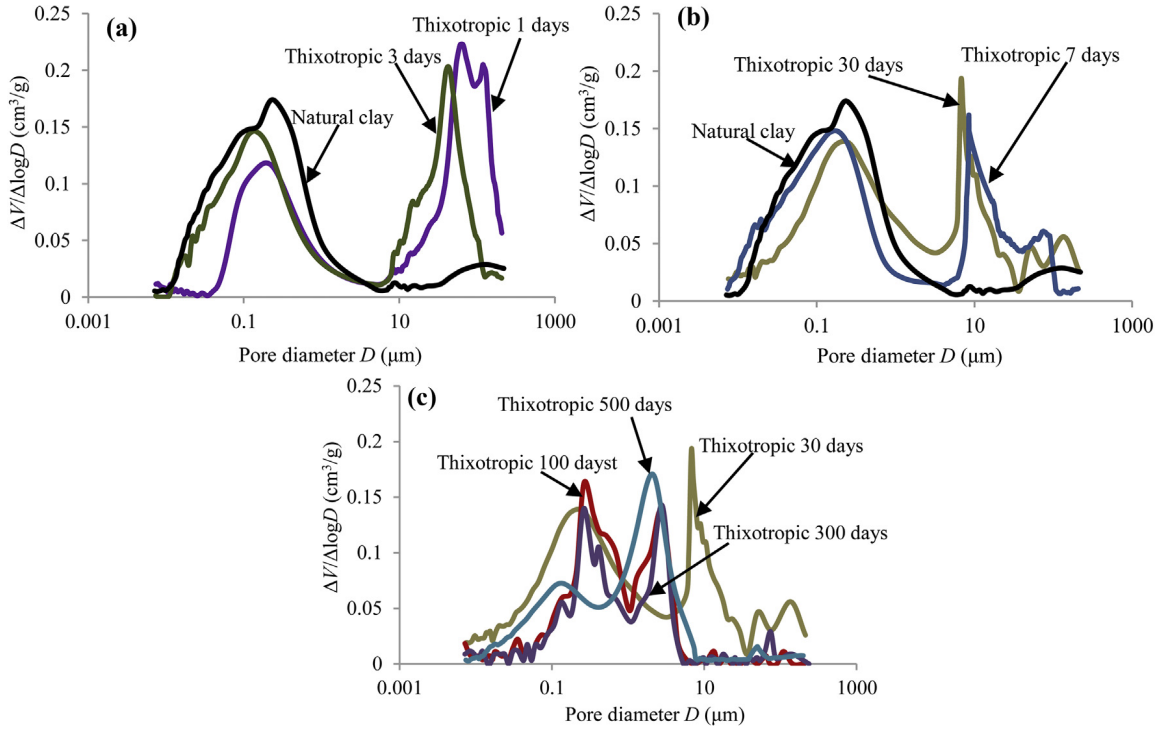

Figure 2.5 Cumulative pore volume curves of natural Zhanjiang clay and remolded clay at the different thixotropic times: (a) 1 and 3 d; (b) 7 and 30 d; (c) 30, 100, 300, and 500 d (Zhang et al., 2017).

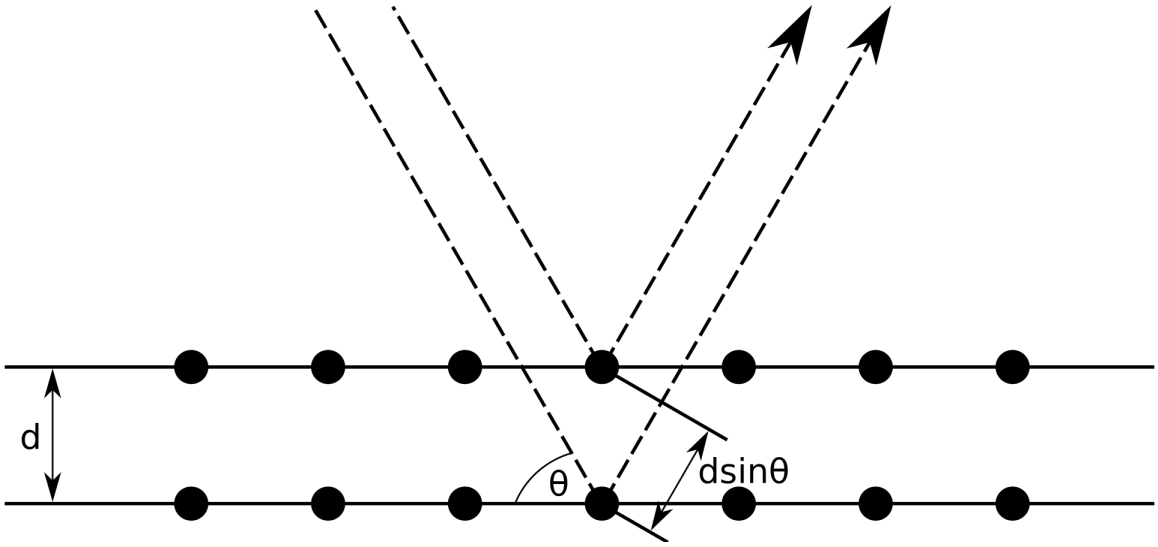

Figure 2.6 Bragg diffraction.

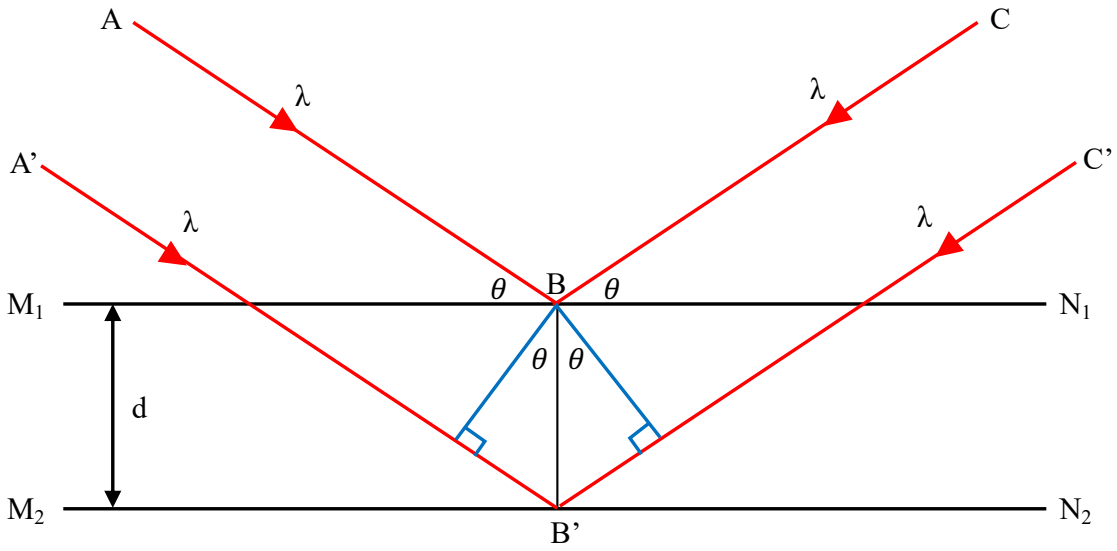

Figure 2.7 Principle of X-ray diffraction analysis.

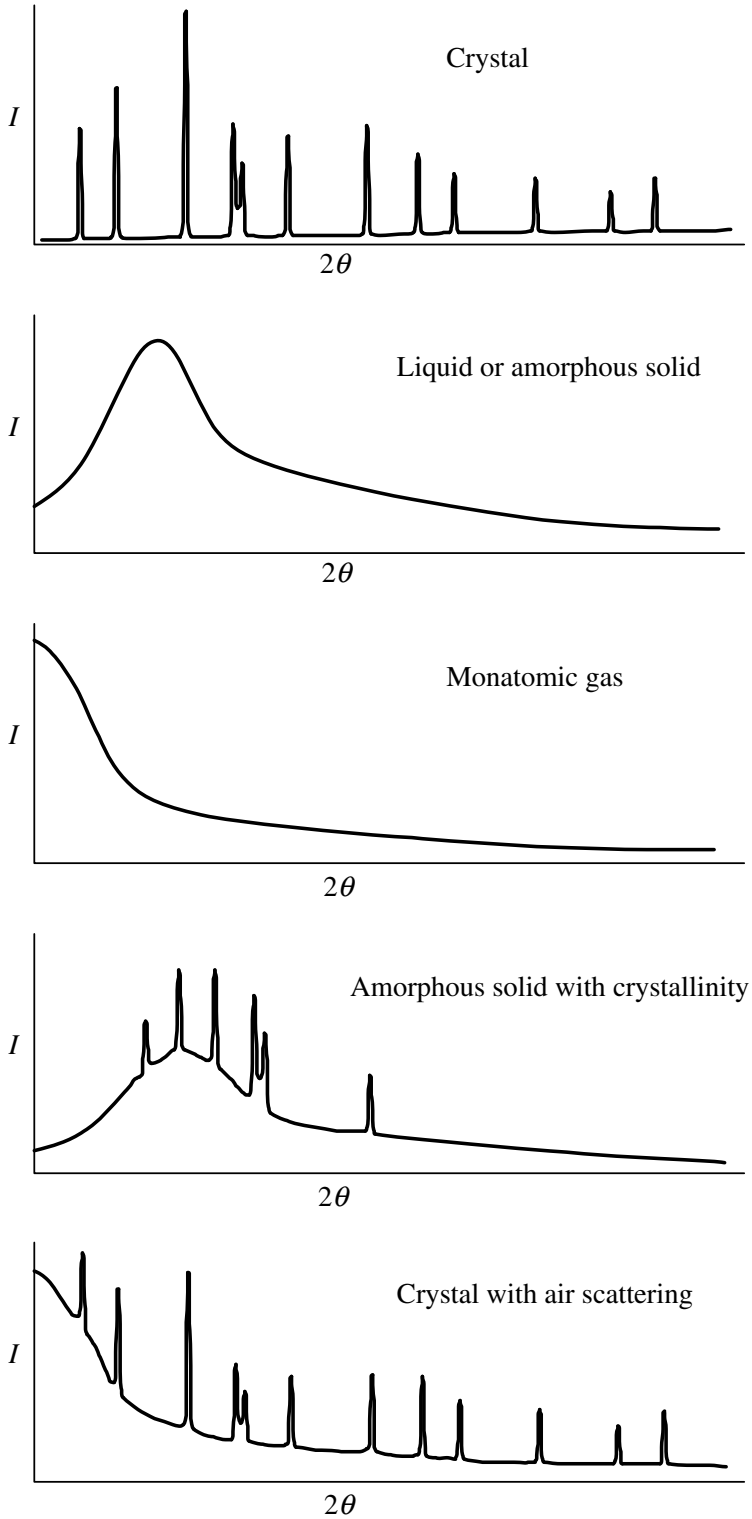

Figure 2.8 Diffraction patterns from crystalline solids, liquids, amorphous solids, and monatomic gases as well as their mixtures (He, 2009a).

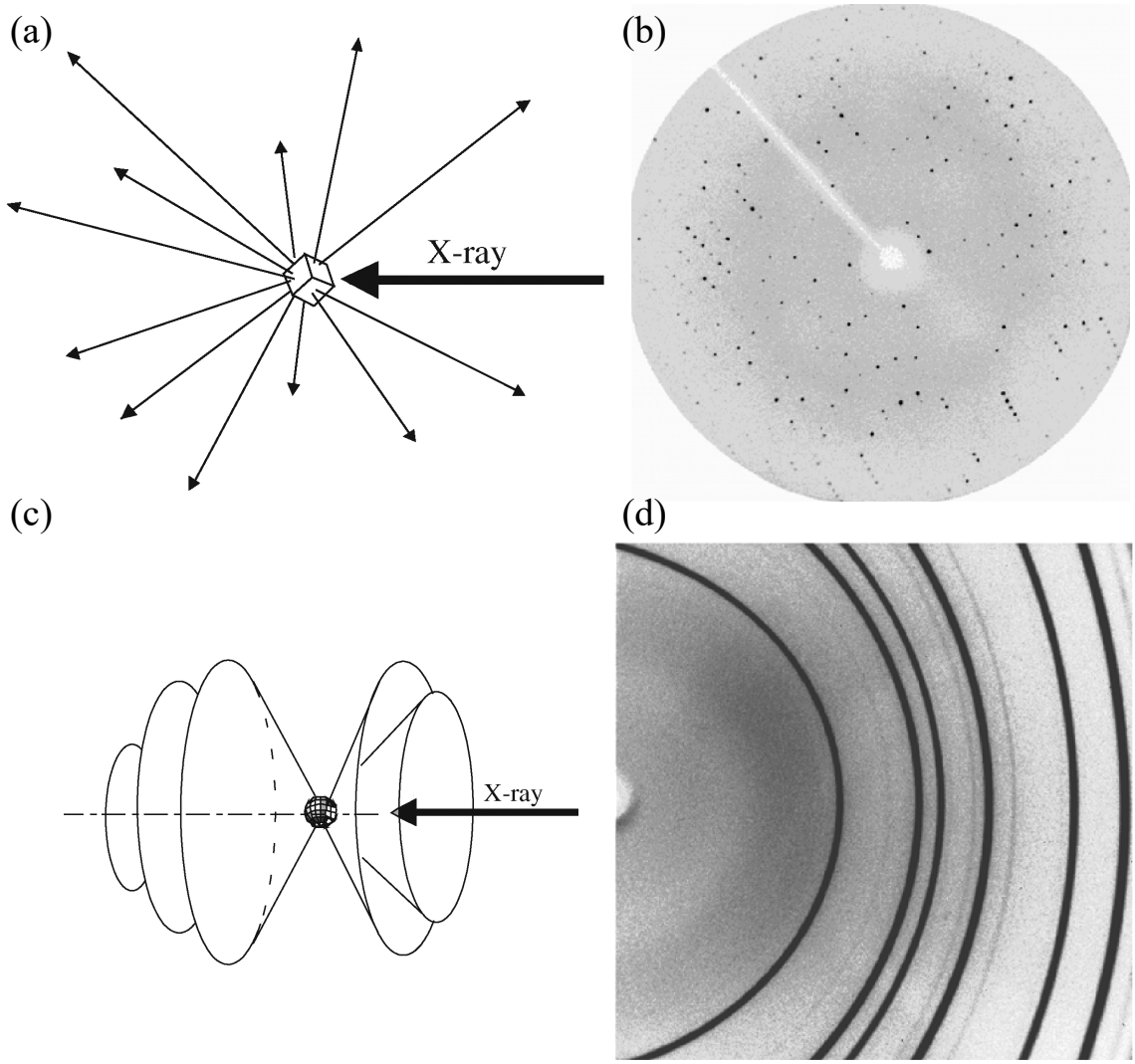

Figure 2.9 The patterns of diffracted X-rays: (a) from a single crystal; (b) diffraction frame from a lysozyme protein single crystal; (c) diffraction cones from a polycrystalline sample; (d) a diffraction frame from corundum powder (He, 2009a).

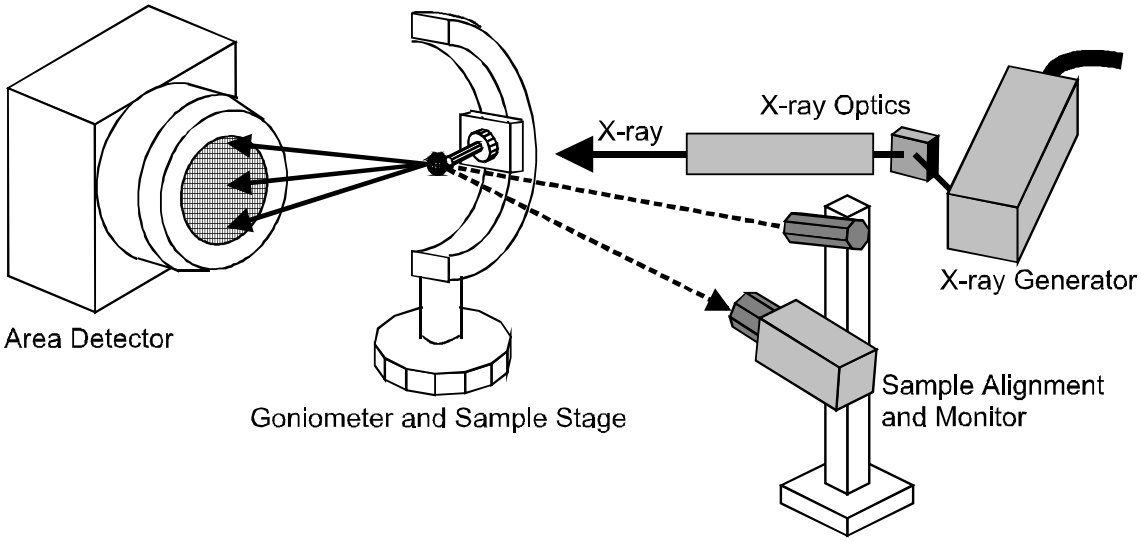

Figure 2.10 Five major components in an 2DXRD system (He et al., 2000).

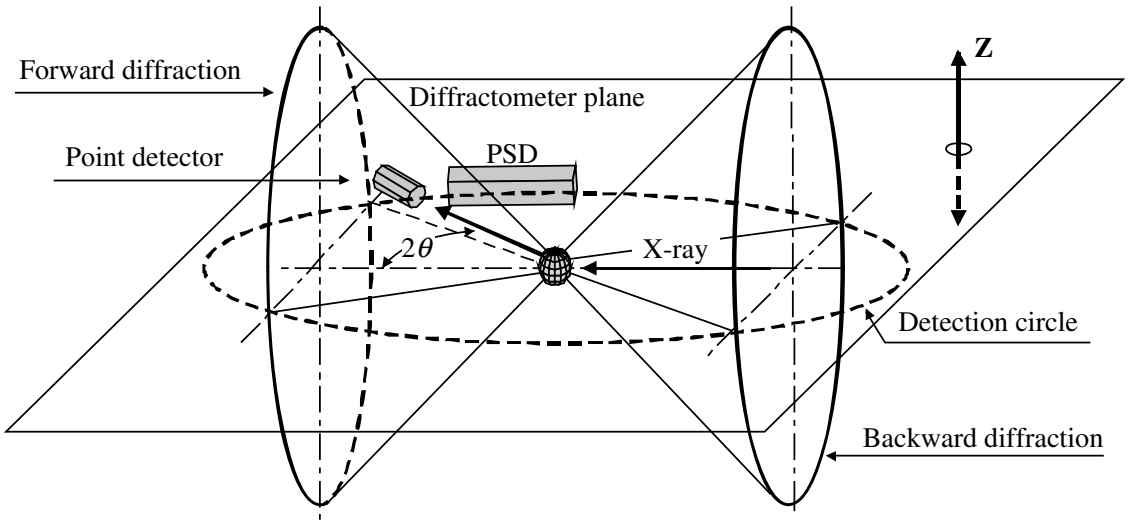

Figure 2.11 Diffraction patterns in 3D space from a powder sample and the diffractometer plane (He, 2009b).

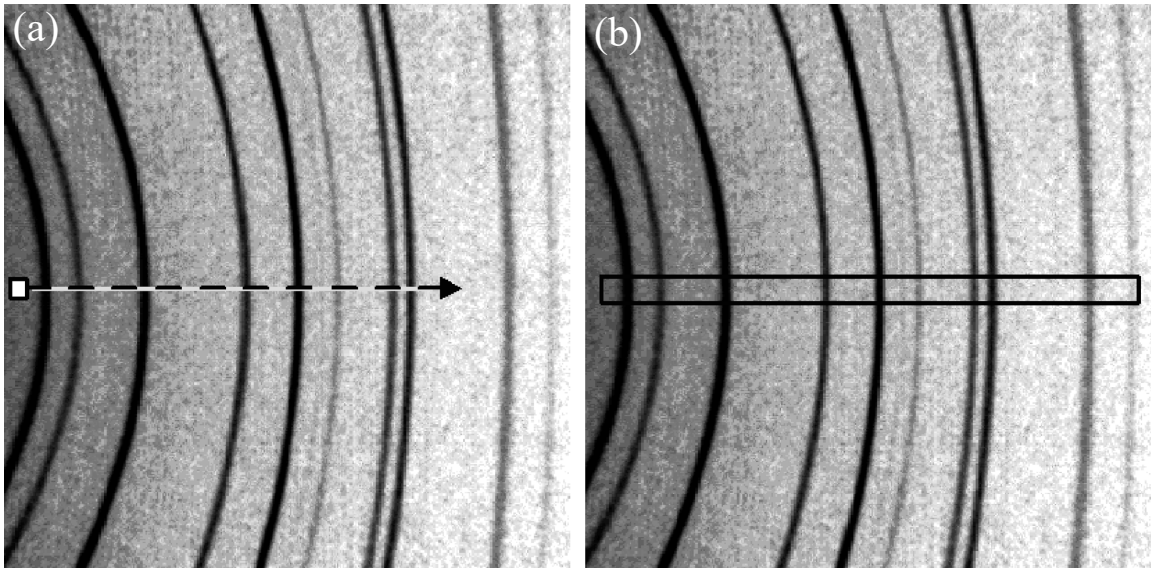

Figure 2.12 Coverage comparison: point, line, and area detectors (He, 2009b).

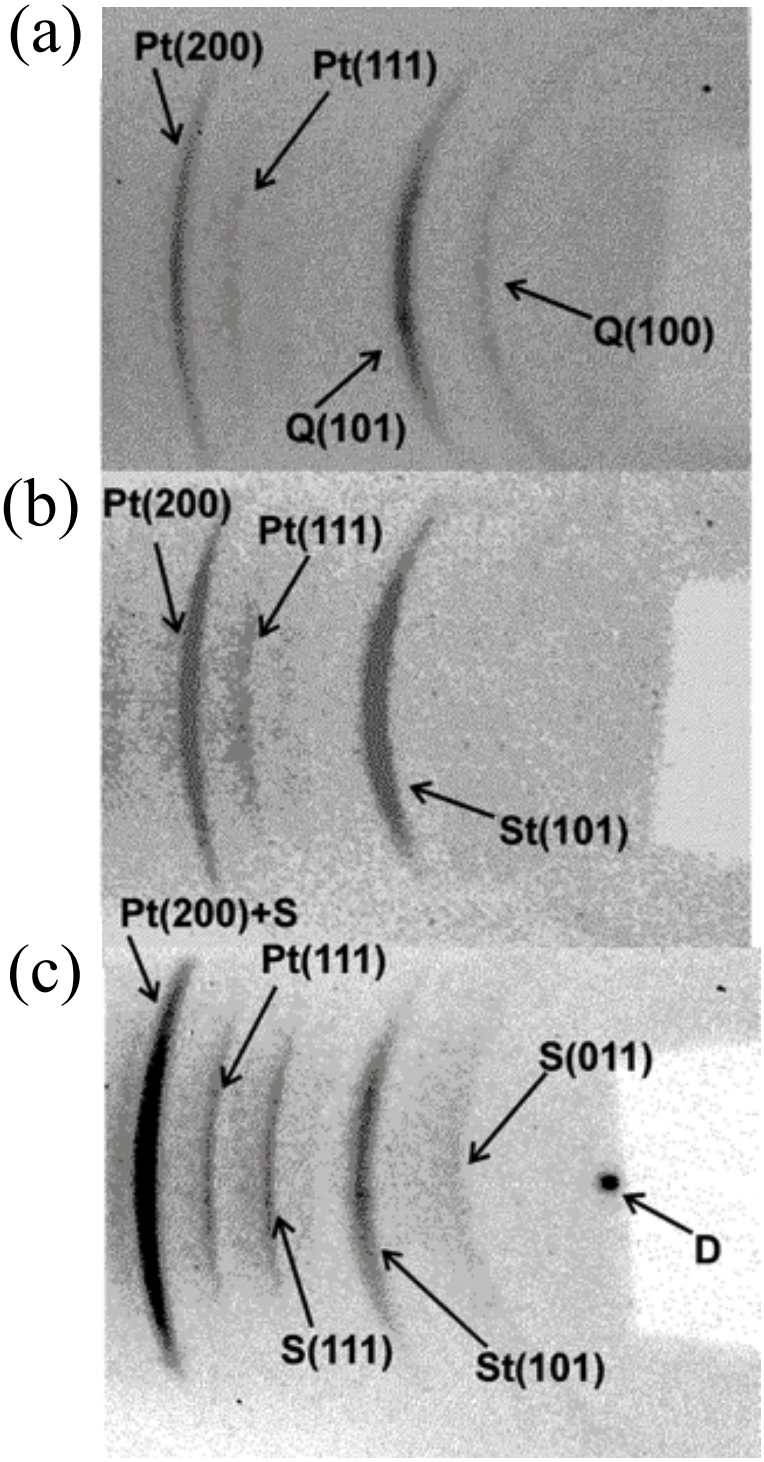

Figure 2.13 Examples of diffraction patterns collected during the transformation: (a) quartz at 45(±5) GPa before heating; (b) same sample after heating at 2,350(±150) K; (c) same sample after pressurizing at 68(±5) GPa and heating at 2,450(±150) K (Dubrovinsky et al., 1997).

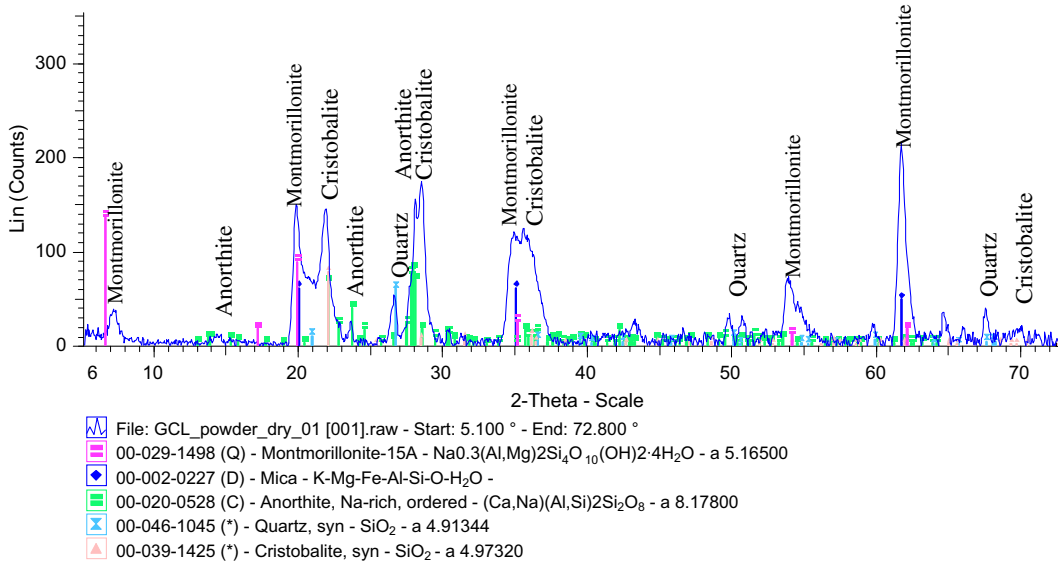

Figure 2.14 Integration of 2D GADDS image: 1D intensity versus 2θ plot with major peaks are labeled (Lange et al., 2010).

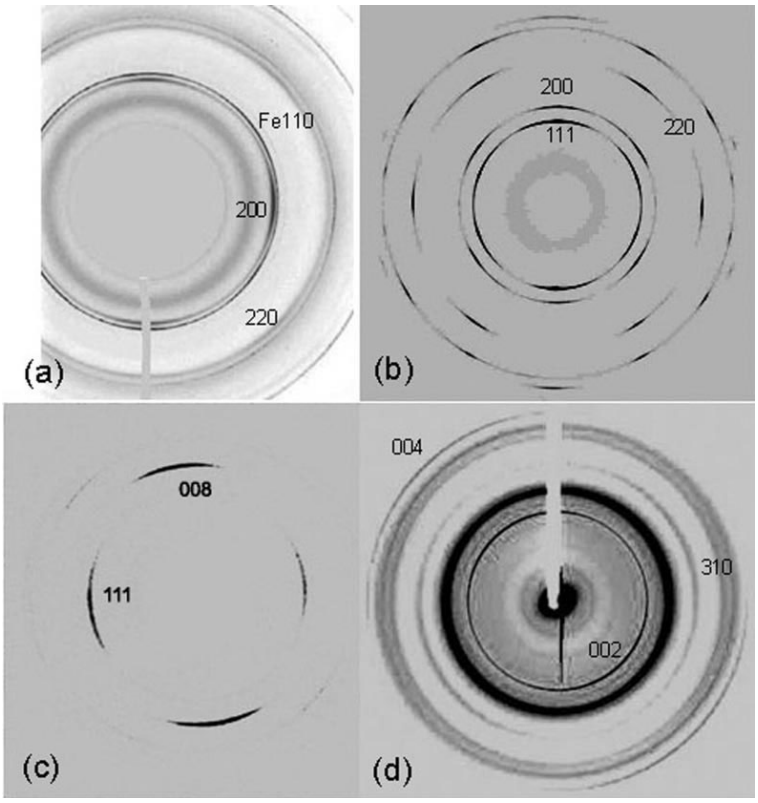

Figure 2.15 Diffraction images illustrating preferred orientation: (a) periclase (MgO); (b) gold wire; (c) fiber-reinforced γ-polypropylene; (d) fetal bone (Wenk and Grigull, 2003).

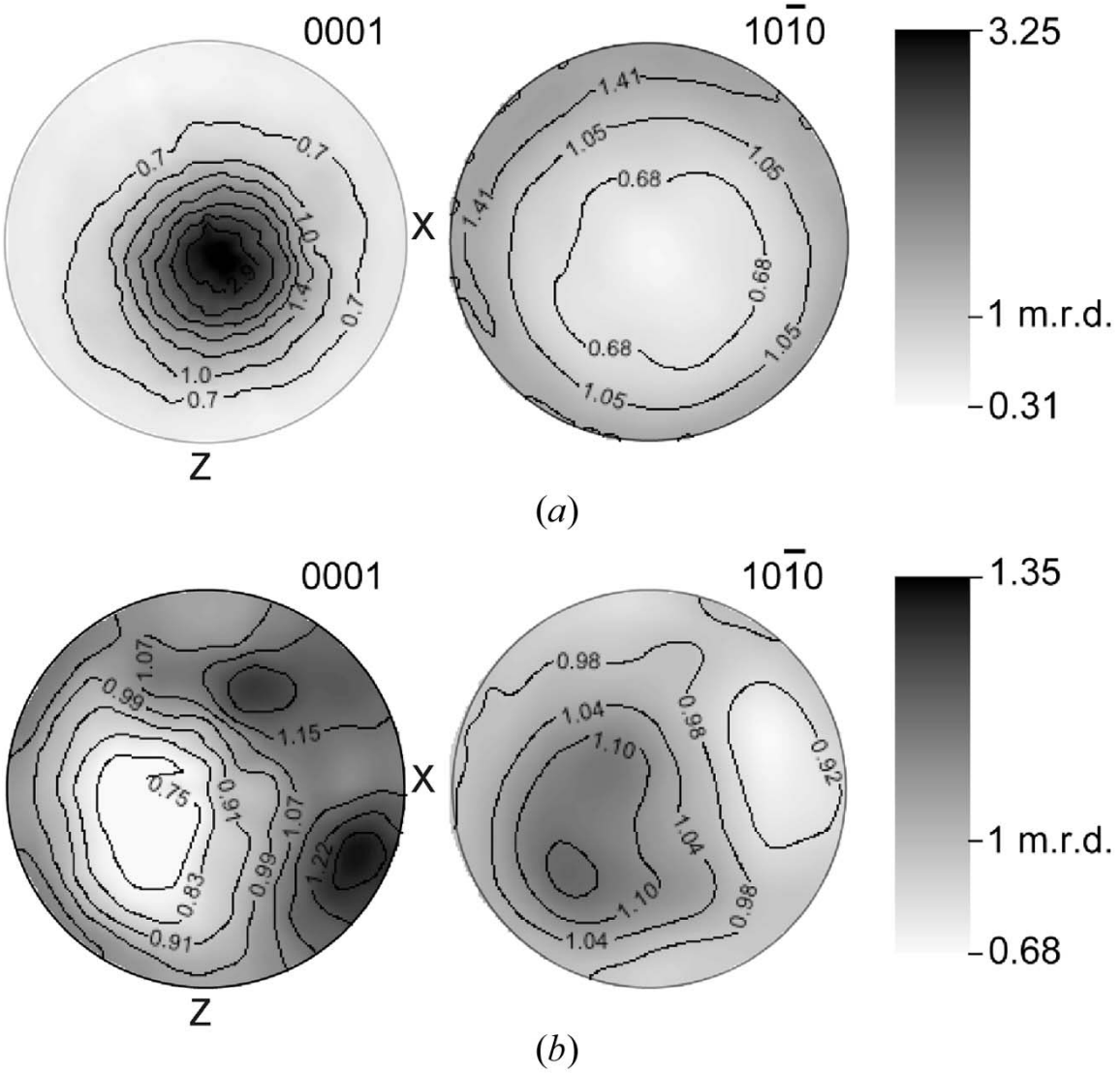

Figure 2.16 Pole figures (equal area projection): (a) dinosaur tendon; (b) salmon scale (Lonardelli et al., 2005).

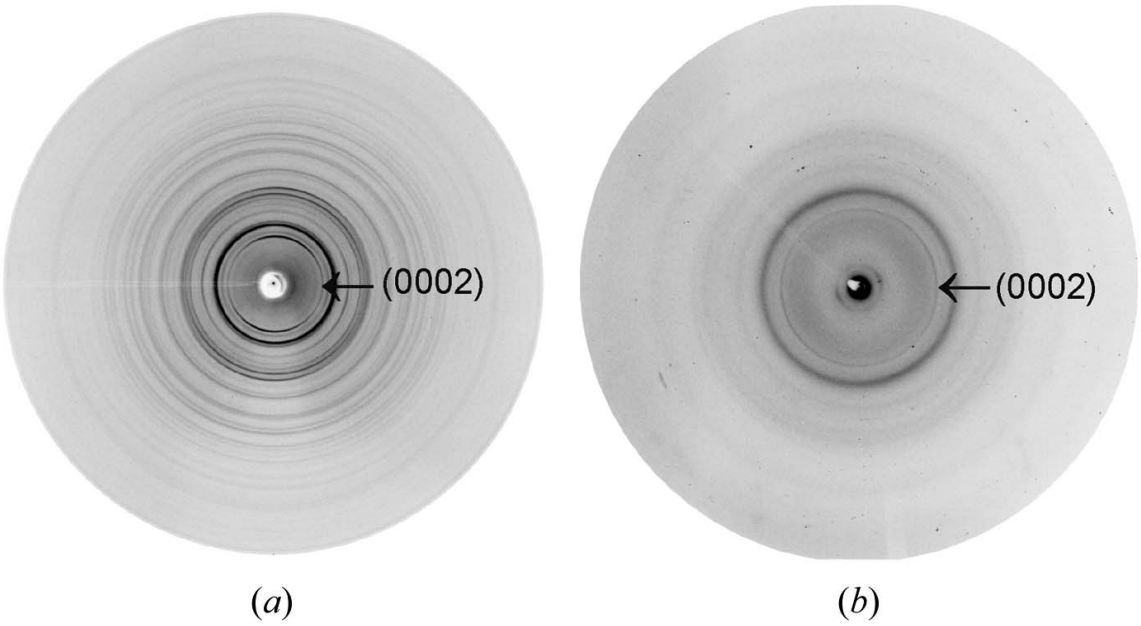

Figure 2.17 Two-dimensional synchrotron diffraction images: (a) dinosaur tendon recorded using an image plate; (b) salmon scale recorded using a CCD camera (Lonardelli et al., 2005).

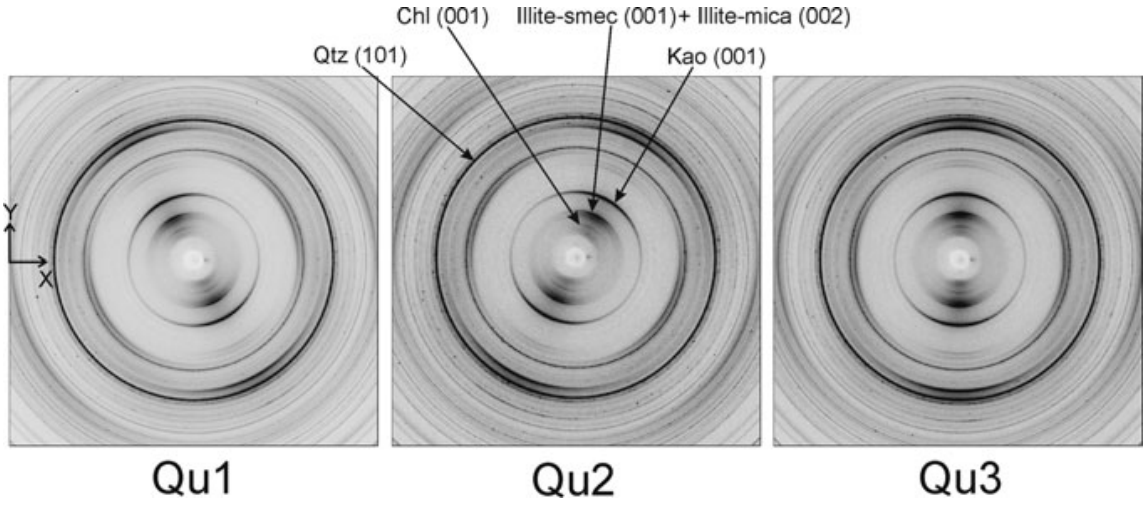

Figure 2.18 Diffraction images showing variation of intensity along Debye rings of the three shale samples (Kanitpanyacharoen et al., 2011).

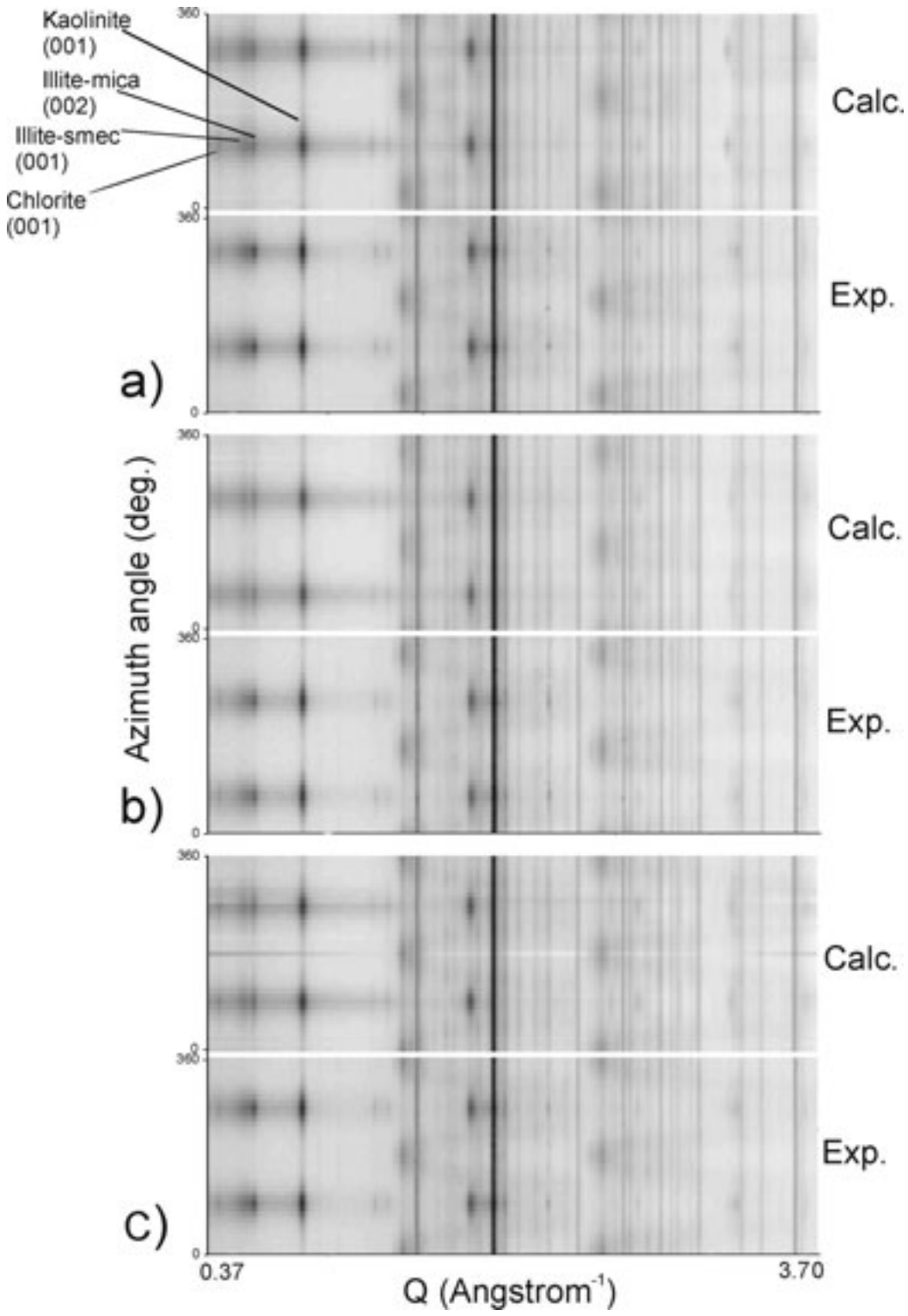

Figure 2.19 Map 2D plots of a stack of calculated (top) and experimental (bottom) diffraction spectra: (a) Qu1; (b) Qu2; (c) Qu3 samples (Kanitpanyacharoen et al., 2011).

CHAPTER 3

MACROSCOPIC THIXOTROPIC BEHAVIOR OF SOFT CLAYS

This paper presents results from an experimental program that measured the macroscopic thixotropic behavior of four soft remolded clays, including two naturally occurring, illite-rich, soft marine clays with moderate salinities and two manufactured, highly purified clays that contain mainly kaolinite and smectite, respectively. Measurements were conducted at various thixotropic curing times ranging from 1.0 hour to 847 days. The temporal evolution in the undrained shear strength s_u was measured using fall cone (FC) while companion specimens were also prepared and mounted in a bender element jig for measurement of temporal changes in small-strain shear modulus G_{max} from shear wave velocity V_{vh}. The bender element specimens allowed for much greater frequency of repeated data collection since the measurement was nondestructive and only one specimen was needed per clay for the full curing period. Furthermore, the combination of measurements provided data at each curing period for the rigidity index I_R taken as the ratio of the small-strain shear modulus G_{max} to s_u. Results show that both the s_u and G_{max} of all four clays exhibit a two-stage, time-dependent increase with drastically different rates, a much higher rate at the initial 4-10 days and a lower one for prolonged time. The three-unit modified Burgers model can best describe and fit all experimental s_u and G_{max} data, indicating that multiple mechanisms contribute to the dissimilar rates of thixotropic hardening at different stages. Moreover, the evolution of rigidity index during thixotropic hardening suggests that the I_R could be treated approximately as a constant in typical engineering practice for the studied clays. These data shed light on analyzing the behavior

of offshore infrastructure and in situ tools that remold soft clays during installation such as pipelines, embedment anchors, and full-flow penetrometers.

3.1 Introduction

Thixotropy, which was first introduced and defined by Freundlich and Peterfi (Freundlich and Rawitzer, 1927; Peterfi, 1927), is one of the oldest rheological phenomena in colloid science. The term is a combination of two Greek words, *thixis* (i.e., shaking or mixing) and *trepo* (i.e., turning or changing) (Mewis and Wagner, 2009). A colloid gel can be completely transformed into a liquid through gentle shaking, and the liquid can also be solidified reversely to gel, which has no distinguishable difference from the original one. Therefore, the phenomenon, thixotropy, describes a reversible process of sol to gel transition that can be repeated several times without any visible changes in the colloidal system. Later on, such a phenomenon of sol to gel transitions was also discovered in an increasing number of fine-grained or colloidal materials, including dispersions of clay minerals (e.g., drilling muds) (Astbury and Moore, 1970; Pignon et al., 1998; Toorman, 1997), oil products (Chang et al., 1999; Petrellis and Flumerfelt, 1973), greases and waxes (Kassem et al., 1970; Mas and Magnin, 1994), paints and coatings (Basta et al., 1998; Gamble, 1936), and food products (Berland and Launay, 1995; Coussot and Gaulard, 2005; Wei et al., 2015), among others. In soil and geotechnical engineering, researchers started to consider the importance of thixotropy when the clay sensitivity was discovered and studied. A lot of pioneers (Jacobsson and Pusch, 1972; Mitchell, 1960; Nalezny and Li, 1967; Seed and Chan, 1959; Skempton and Northey, 1952) have worked in this field of thixotropy. A more appropriate definition of thixotropy specifically formulated for soils is

given by Mitchell and Soga (2005): “Thixotropy is an isothermal, reversible, time-dependent process occurring under conditions of constant composition and volume whereby a material stiffens while at rest and softens or liquefies upon remolding.”

Most of the previous effort to study thixotropy in soils and geotechnical engineering focused on measuring the thixotropic regain or thixotropic strength ratio (i.e., the ratio of the undrained shear strength s_u after a given period of recovery to the initial, fully remolded s_{ur}) of remolded clays (Mitchell, 1960; Shahriar et al., 2018), and the ratio of recovered strength to the intact counterpart was also studied when undisturbed soil samples were available (Skempton and Northey, 1952; Zhang et al., 2017). A variety of factors can influence the thixotropic process, usually accompanied by the hardening and stiffening of the considered systems such as clays, including water content, plasticity index, activity, temperature, and composition such as mineralogy, among others. Jeong et al. (2015) conducted experimental studies comparing the rheological behavior of both clay-rich and clay-poor soils, with a particular focus on the effects of soil mineralogy and particle size. Yang and Andersen (2016) found that the liquidity index and water content show the best correlation with the thixotropic strength ratio, i.e., the higher the water content and liquidity index, the higher the thixotropic strength ratio. Similar experimental results have also been reported in other studies (Lunne and Andersen, 2007; Seng and Tanaka, 2012). However, controversial results on the effect of water content have also been found by other researchers. For example, Shahriar et al. (2018) argued that clays at a water content 25% lower than its liquid limit exhibit the optimal thixotropic hardening or best thixotropic gain in strength, which is directly contrary to the conclusions drawn by others.

The rigidity index (I_R), as proposed by Vesic (1972), is defined as the ratio of the shear modulus (G) to s_u and is a soil property frequently used as an indicator of clay stiffness. In offshore practice it is used for several applications including estimating the coefficient of consolidation from piezocone dissipation tests (Teh and Houlsby, 1991), post installation consolidation of piles (Randolph et al., 2005), modeling of piezocone partial drainage conditions during penetration (DeJong and Randolph, 2012), and interpretation of full-flow penetrometer behavior (Low et al., 2010). The I_R of intact clays can be estimated from in situ tests such as the seismic piezocone (e.g., Krage et al., 2014) either alone or in combination with advanced laboratory test data such as anisotropically consolidated triaxial compression (CAUC) tests conducted on high-quality samples. In the absence of such measurements, empirical correlations have been developed including that of (Keaveny and Mitchell, 1986) and further developed by (Mayne, 2007), which uses plasticity index and overconsolidation ratio to estimate I_R.

However, there is little to no data available on how I_R may differ for intact clays versus remolded clays and how I_R potentially evolves during thixotropic hardening. To this end the objective of the study presented in this paper was to investigate the thixotropic behavior of fully remolded soft clays and the evolution of I_R during thixotropic hardening. The small-strain shear modulus (G_{max}) and s_u of the tested clay samples were measured using bender elements (BEs) for G_{max} and the FC for s_u. The paper describes the test soils and measurement methods and a presentation and interpretation of the measured data.

3.2 Materials and Methods

3.2.1 Materials

Totally four different soft clays were studied, including Prestige, PureGold Gel, Boston Blue Clay (BBC), and Onsøy. First, to minimize sample variability and reduce the complexity of analysis, two commercially available purified clays, Prestige, a highly pure kaolinite clay, and PureGold Gel, a relatively pure Na-Montmorillonite clay with other secondary clay minerals and impurities, were obtained from the Unimin Corporation (New Canaan, Connecticut, USA) and CETCO (Arlington Heights, Illinois, USA), respectively. Second, two naturally occurring clays were also studied, including BBC, a glacial marine clay recovered from Boston, Massachusetts, and Onsøy, a sensitive marine clay collected at the Norwegian Geotechnical Institute's (NGI) test site located in south-eastern Norway. Index, physical, and chemical testing were performed on these four samples: liquid limit (*LL*) was measured by the ISO fall cone method (ISO 17892-12 (2018)), and all other indices such as plastic limit (*PL*), silt fraction, and clay fraction (CF) were determined by following the relevant ASTM standard methods (ASTM, 2020). Natural porewater salinity was defined by the ratio of the mass of soluble salts to the mass of saltwater (i.e., the solution but not the solvent) (Burt, 2014).

The mineralogical compositions of these four clays were further determined by X-ray powder diffraction (XRPD) that usually requires dry powdery samples with particle sizes of 5 to 20 μm (Środoń et al., 2001). The two natural clays, BBC and Onsøy, were wet in their original, natural state, so they were first air-dried and lightly crushed with a percussion mortar and rubber tipped pestle to pass all materials through a 0.4 mm sieve, followed by wet-grinding of approximate 3.0 g of the crushed material with 7.0 mL 2-

propanol (C_3H_8O) in a McCrone micronizing mill (The McCrone Group, Westmont, IL, USA) for 10 min, resulting in particles of < 4 μm in size upon drying (Luo et al., 2020). This step was not required for the other two relatively pure clay samples, Prestige and PureGold Gel, and hence the as-received materials as dry powders were directly used for XRPD without further processing. Each dry powder sample was thoroughly and homogeneously mixed with 10 wt.% zincite (ZnO) serving as an internal standard for quantitative XRPD analysis. The powder mixture was then mounted into the sample holder via a razor-tamped surface (RTS) method to achieve highly random orientation of the platy clay particles (Zhang et al., 2003). The diffraction patterns of all specimens were collected in a PANalytical X'Pert PRO X-ray diffractometer (Almelo, Netherlands) using CuKα radiation with a wavelength λ = 1.5418 Å generated at 45 kV and 40 mA, a continuous scan range of 2º–64º 2θ, and a scan speed of 1º 2θ/min, where 2θ is the diffraction angle. The acquired patterns were then analyzed both qualitatively and quantitatively using Profex, an open-source program integrated with Rietveld refinement (Döbelin and Kleeberg, 2015).

3.2.2 Fall Cone Testing

Temporal evolution of the undrained shear strength s_u of the soft clay specimens during thixotropic hardening was assessed using fall cone (FC) testing by following the ISO 17892-6 standard method (2017). Each clay sample, being either dry or wet, was first thoroughly mixed with the carefully calculated amount of deionized (*DI*) water to achieve a consistency at or near its *LL*, followed by overnight curing for temperature and moisture equilibrium in a sealed plastic bag stored in a temperature-controlled chamber set at 24 °C. Prior to the commence of actual hardening process, the equilibrated sample was thoroughly

mixed and remolded again, and such a state served as the starting point of thixotropy or zero time.

Experimental assessment of thixotropic hardening of clays involves multiple measurements of shear strength and stiffness. Therefore, each thoroughly remolded clay was carefully filled into a series (e.g., usually 8 to 10 jars) of jars (Fisher Scientific, Inc., Hampton, NH) with an inner diameter and height of 45 and 44 mm respectively, and special caution was taken to minimize the entrapment of air during filling and to ensure the specimen surface smooth and flush with the rim of the jar using a straight edge. To maintain constant water content during the entire hardening process, each jar was tightly sealed by placing a layer of Parafilm (Sigma Aldrich, St. Louis, MO) on the clay surface and then the native cap with its inner surface coated by a thin layer of vacuum grease, and all sealed jars were stored underwater in a temperature-controlled water bath set at 24 °C. Such a series of carefully prepared specimens enabled multiple s_u measurements by following a pre-designed temporal curing schedule of up to 142 days (e.g., 0, 1, 2, …, 64, 128, 142 days). At each specific hardening or curing time, one jar from each studied clay was retrieved from the water bath, and three to five FC measurements were performed at different locations of the specimen surface to avoid mutual interference using a 60° and 60 g cone (ISO 2017). These multiple measurements of cone penetrations were averaged, and the s_u was computed as:

$$s_u = c\frac{mg}{i^2} \tag{3.1}$$

where c is a constant determined by the tip angle of the cone and 0.27 is used for a 60° cone; m is the mass of the cone (i.e., 60 g); g is the gravitational acceleration (i.e., 9.81 m/s^2); i is the averaged cone penetration into the specimen surface (in mm).

For quality control, after the above measurements, each tested specimen was again fully remolded and examined to ensure that the fully remolded undrained shear strength s_{ur} was equal to that at time $t = 0$ or the commencement of thixotropic hardening. Additionally, the final water content of the cured specimen was also measured at the end of all these measurements, and then compared with that at $t = 0$. If the final water content deviated from the initial one by 2%, then all results and measurements from that specific jar were discarded, and a new specimen was prepared, and all measurements repeated. If the initial and final water contents were close to each other, with a difference of < 2%, then the difference was used to adjust the undrained shear strength.

3.2.3 Bender Element Measurements

Non-destructive bender elements (BEs) testing was used to determine the small-strain shear modulus G_{max} of the studied clays so that the temporal development of G_{max} was assessed on the same specimen to eliminate the possible errors from the variability of different specimens. A small part of the above wet samples prepared for the FC measurements was filled into an acrylic cylinder of 63 and 100 mm in inner diameter and height, respectively. Such a customer-built cylinder was machined with the interior lips to accommodate top and bottom platens (Figure 3.1). Each of the platens contained a central bender element that was either directly epoxied into the platen (Landon et al., 2007) or housed in a stainless steel mounting disc that was epoxied into the platen (Salazar and Coffman, 2014). Parallel and series-poled piezoelectric ceramic elements that were electronically grounded and waterproofed using epoxy were inserted into the clay during specimen preparation and were used as transmitter and receiver, respectively. Before

assembly, the calibration time was first determined for the system delay by running the test at zero tip-to-tip distance (i.e., two BEs are in direct contact), and the orientation of platens was also determined to ensure positive wave polarization between the transmitter and receiver. Three layers of barriers, including vacuum grease, Parafilm, and electrical tape, were applied to the end platen connections to make an air-tight seal for maintaining a constant water content for an extremely prolonged period of time. Once assembled, a constant temperature of 24 °C was also maintained in a temperature-controlled chamber for all specimens undergoing the thixotropic hardening process.

The transmitting signal was generated by a Wavetek model 29 10 MHz Direct Digital Synthesis (DDS) Function Generator (WAVETEK, Paris, France), which was used to excite the transmitting BE with a single sine wave of ±10 V in amplitude triggered at a 10 Hz delay. The excitation frequency was selected such that the frequency of the received signal nominally matched that of the excitation wave (e.g., ASTM 2020) and, for the studied specimens, it ranged from 0.85 to 2.0 kHz. The transmitted and received signals were both recorded using a Model 5242B Pico PC-based oscilloscope (Pico Technology, TX, USA) with a variable 12 bit or 16 bit resolution and PicoScope 6 signal analysis software. The initial strong received traces were averaged over time, and a 30 kHz low-pass filter was applied using PicoScope 6 to eliminate high frequency noise, which did not change the received signal to an extent that could measurably alter the travel time of the shear waves.

The shear wave velocity v_{vh} (where the subscript *vh* denotes vertical propagation and horizontal polarization) was derived from the transmitting and receiving signals as follows (Landon et al., 2007):

$$v_{vh} = \frac{L_{tt}}{\Delta t - t_c} \tag{3.2}$$

where L_{tt} is the tip-to-tip distance between the two bender elements; Δt is the shear wave travel time that is estimated using the first zero crossover method (ASTM, 2020; Yamashita et al., 2009); t_c is the calibration time. There is often a slightly negative deviation in the received wave prior to the arrival of the wave due to near field effects. The first zero crossover is hence determined by fitting a horizontal line to the pre-deviation received wave and extending that line until it first intersects with the post-deviation received wave.

The G_{max} was then computed based on the theory of elasticity:

$$G_{max} = \rho_t v_{vh}^2 \tag{3.3}$$

where ρ_t is the total density of the specimen.

Since BEs simply measure the shear wave velocity within the specimen and are usually considered as a non-destructive technique (Sas et al., 2014), only one specimen was needed for each studied clay and multiple measurements were obtained from the same specimen along the entire prolonged thixotropic hardening process.

3.3 Results and Discussion

3.3.1 Soil Classification and Mineralogical Compositions

Table 3.1 summarizes some basic physical and index properties of the four studied clays. Based on the Unified Soil Classification System (USCS) (ASTM, 2020), the four studied clay samples are classified into two categories: Prestige and BBC are low-plasticity clays (CL), while the other two, PureGold Gel and Onsøy, are high-plasticity ones (CH). While the Prestige has the lowest activity, the PureGold Gel has a very high one due to its

high fraction of Na-montmorillonite, as discussed later. These four clays all contain a certain fraction of silt-sized particles (i.e., from 2 to 75 μm in size). Finally, the two processed samples have a very low salinity, while the natural counterparts have relatively higher salinities, especially Onsøy.

Table 3.2 compares the mineralogical compositions of the four clays obtained by quantitative 1DXRD analysis. Prestige and PureGold Gel are two commercial clays that have been purified, so their major compositions are kaolinite and montmorillonite, respectively, with only small amounts of impurities therein. On the contrary, these two naturally occurring clays consist of complex, multiple mineral phases, including a variety of clay minerals, such as illite, kaolinite, chlorite, and biotite, and other nonclay phases as minor fractions. Due to their marine origin or initial settling in a seawater environment, they contain a higher fraction of illite. The mineralogical compositions of these four clays agree with their USCS classification and activity: PureGold Gel and Onsøy contain high fractions of Na-montmorillonite and illite, respectively, and hence they belong to CH with a relatively higher activity.

3.3.2 Macroscopic Strength and Stiffness Measurements

Figure 3.2 shows the temporal evolution of s_u of the four clays measured by the FC at different thixotropic hardening times, with the initial fully remolded undrained shear strength s_{u0} defined as the s_u at time $t = 0$ day ranging from 1.1 to 1.8 kPa for the four tested clays. Overall, all the clays exhibit thixotropic hardening to various extents, and generally have an initial fast increase in s_u at the first few days, followed by a slower increase in s_u with time that tends to level off at prolonged curing durations, especially for the two

naturally occurring clays, BBC and Onsøy. Since different specimens have different s_{u0} values (i.e., the starting point for the thixotropic process), their normalized thixotropic strength ratios (TSR), s_u/s_{u0}, are also plotted in Figure 3.2b, which shows that all specimens have a thixotropic strength ratio of at least 2.2 at $t = \sim 64$ days. Additionally, the two natural clays show a higher tendency of thixotropic hardening than the two manufactured counterparts, and BBC can achieve a thixotropic strength ratio of ~5.0 after 150 days of curing. On another hand, the two processed clays, Prestige and PureGold Gel, exhibit the lowest thixotropic strength ratio, which is consistent with the findings from previous research (Skempton and Northey, 1952). In the extra prolonged durations (e.g., when t > 70 days), PureGold Gel has the lowest thixotropic strength ratio, although it has the highest activity. This clay also has the highest *LL* of 394%. Such a difference in the thixotropic strength ratios among these four clays indicates that the mineralogy as well as chemical compositions (e.g., salinity) may all contribute to the thixotropic hardening behavior, and the effect of porewater chemistry warrants further investigations.

As part of the quality control, Figure 3.3 show the water content measurements of all FC specimens. Statistics of all specimens' water contents measured after all FC measurements are summarized in Table 3.3. The small coefficient of variation (COV) values for all four samples indicate that the measured water contents have very little variation, verifying that these specimens did not experience noticeable alterations in water content during the thixotropic curing period.

Figure 3.4a and Figure 3.4b present G_{max} measured by BE testing and normalized G_{max} with reference to that, G_{max0}, obtained at $t = 0$ day (i.e., thixotropic shear modulus ratio G_{max}/G_{max0}) for the four specimens at different thixotropic curing times, respectively.

Similar to the s_u behavior (Figure 3.2), both G_{max} and G_{max}/G_{max0} also exhibit a two-stage, time-dependent thixotropic stiffening process for all four clays: the shapes of these two sets of curves are very similar, especially the locations of the apparent transition points during the first few days. The G_{max}/G_{max0} determined at t = 64 days ranges from 2.5 to 4.9 for all the specimens, showing similar thixotropic shear modulus ratios and thixotropic undrained shear strength ratios after two months of curing. Although the BE measurements for Prestige are only available for up to 64 days, it is interesting to note that the thixotropic stiffening process for the other three specimens continues even after more than ~2.3 years. Similarly, the thixotropic stiffening behavior is different for the two natural clays with a higher tendency for thixotropic stiffening compared to the two manufactured clays. This is hypothesized to be due to the more complex mineral composition and higher salinity (Figure 3.4).

3.3.3 Thixotropy Model Fitting

Several time-dependent creep, thixotropic, or rheological models were reviewed and the modified Burgers' five parameter model (Barnes, 2000) was found to best fit the experimental measurements:

$$M = c_1 + c_2(1-\exp(-c_3 t)) + c_4(1-\exp(-c_5 t)) \tag{3.4}$$

where c_1 to c_5 are the optimized fitting parameters that reflect the mechanical and viscoelastic properties of the considered thixotropic materials; t is the thixotropic curing time; M is a specific mechanical property (e.g., s_u, s_u/s_{u0}, G_{max}, or G_{max}/G_{max0}) measured at a specific curing time t. The dashed lines in Figure 3.2, Figure 3.4 and Table 3.4 represent the best fit form of Equation (3.4) to the s_u and G_{max} data.

In fact, this complex model is usually used to describe the viscoelastic behavior of a material, especially for creep and stress relaxation, and it consists of three mechanical units in series, including a purely elastic spring and two viscoelastic Kelvin-Voigt units, the latter consisting of a purely viscous damper (i.e., a dashpot) and purely elastic spring connected in parallel (Figure 3.5). All five parameters in the equation are related to the springs' constants or dampers' viscosities. The Kelvin-Voigt unit is one of the simplest representations of a viscoelastic material. In general, the more complicated the internal structure of a viscoelastic material, the more non-linear the viscoelastic behavior and the more viscoelastic components (i.e., the Kelvin-Voigt unit) should have for better describing its viscoelastic behavior (Lin, 2020). The modified Burgers' model, when used to describe thixotropy, which is a reversible, time-dependent process, includes three mechanical components: immediate elastic response and two delayed elastic responses with different retardation times. For viscoelastic materials, the elastic behavior occurs with a certain time of delay, when compared to an ideal elastic material. The retardation time is used to describe the delay of the elasticity. As shown in Figure 3.5b, the three terms in the modified Burgers' model essentially describe the time-independent (i.e., purely elastic) response at time of zero, the temporal rapid increase in the mechanical property at the initial phase over a very short time, and the temporal slow increase in the mechanical property at the later phase over a prolonged time, respectively.

In Equation (3.4), the first parameter c_1 refers to the first component, which is the mechanical property (i.e., undrained shear strength or stiffness) at the beginning of the thixotropic process. The values of c_1 shown in Table 3.4 also confirm it. All c_1 values for the undrained shear strength are around 1.08 to 1.86 kPa since all the clay specimens were

prepared at their *LL*, while the c_1 for G_{max} decreases with increasing *PI*. Parameters c_3 and c_5 from the latter two viscoelastic components (Equation (3.4) & Figure 3.5a) are the reciprocal of the two different retardation times, which are basically an indication of the degree of viscosity of the clays and hence govern the degree of rigidity (or fluidity) of it. If these two parameters are very high (i.e., the retardation times are very small), the material can be classified as a highly elastic solid, and behaves like a highly stiff or rigid body. However, when these parameters are very small (e.g., $c_5 = 2.61\times10^{-5}$ for Prestige, Table 3.4), the viscous property of the material suppresses its elastic counterpart, and the material behaves like a fluid and its mechanical response (i.e., strength gain) can occur over a highly prolonged period. For example, corresponding to the very small c_5 (Table 3.4), the s_u of Prestige continuously increases even after a long curing time (Figure 3.2). Moreover, the retardation time is affected by the clays' salinity, and it decreases with increasing salt concentration (Joshi et al., 2008). The fitting parameters also confirm this (Table 3.4): the two natural clays with higher natural salinities, especially Onsøy, have lower retardation times or much higher c_3 and c_5 values when compared to the two manufactured clays. Because at higher porewater salinities, the thickness of the electrical double layer on the clay particles' surface is suppressed, and hence the particles can move closer, thus forming stronger contacts and resulting in higher degree of rigidity or stiffness. The sum of the two parameters c_2 and c_4 indicates the ultimate gain of strength or stiffness at the end of thixotropic process at an infinity time. There are three unreasonable values (i.e., c_4 for the G_{max} of BBC, c_4 for the s_u and s_u/s_{u0} of Prestige, Table 3.4) among the sixteen sets of fitting parameters, which indicates the retardation times at ~100 years. This may result from the high viscosity of the clay specimen (i.e., Prestige) itself, as well as the limited data points

for the extremely prolonged thixotropic process (i.e., the s_u of the Prestige continuously increases even after a long time, Figure 3.2).

3.3.4 Rigidity Index

Another mechanical property of soils frequently used as an indicator of stiffness or shear modulus is the rigidity index I_R, defined as the ratio of the shear modulus G to undrained shear strength s_u (Vesic, 1972). Figure 3.6a shows the relationship between the G_{max} and s_u measured at the same curing time, and a near linear relationship for the two mechanical properties can be observed for each clay, suggesting that the I_R (i.e., the slope of the linear regression line) of each clay could be treated approximately as a constant during thixotropic hardening in typical engineering practice. Similar findings from other different clays are also discussed in Peng et al. (2020). The I_R decreases with increasing PI (Table 3.1), which is consistent with prior published findings (Keaveny and Mitchell, 1986; Krage et al., 2014; Mayne, 2007). The two naturally occurring clays show a higher I_R, because of their significantly higher porewater salinity, while the PureGold Gel has the lowest I_R. For the same clay mineral, with increasing ionic strength of the porewater, the thickness of the electrical double layer (EDL) decreases, which results in a tendency for more mineral to mineral contact (i.e., a flocculated structure) and hence a greater resistance to interparticle shearing, a manifestation of the increased I_R.

Additionally, since both G_{max} and s_u can also be determined based on the modified Burgers models, the I_R can be nearly continuously recalculated based on the fitted analytical model equations. As such, the model-derived I_R is plotted in Figure 3.6a for comparison, as well as in Figure 3.6b to show its variation with time. As such, the model-

derived I_R varies slightly during thixotropic hardening: for all four clays, it decreases rapidly over a very short period at the beginning, but then increases slowly over a prolonged duration. In fact, the temporal change in the I_R also validates that different microscopic physical mechanisms dominate thixotropic hardening at different stages, which is further discussed in the next chapter.

3.4 Conclusions

Macroscopic experimentation was conducted to investigate the thixotropic behavior of four soft clays, including two natural marine clays, BBC and Onsøy, and two manufactured clays, Prestige and PureGold Gel. Based on the above results and findings, the following major conclusions can be drawn:

- Thixotropic hardening is observed in all four soft clays, and the two natural clays show a higher regain in thixotropic hardening than the two manufactured counterparts, most likely due to their higher porewater salinity and different and more diverse clay mineralogy.
- Both the strength s_u and stiffness G_{max} regain a twofold increase at least with 150 days of curing, and the BBC can increase the strength s_u by 5 times for prolonged thixotropic hardening.
- For all four soft clays, the rigidity index I_R generally decreases with increasing *PI*. Its rapid decrease at the initial thixotropic stage with a following slow increase over a prolonged period suggests that different thixotropic mechanisms dominate at the two different aging stages.

- Mineralogy and porewater chemistry of clays can impact the macroscopic thixotropic hardening behavior.

3.5 Acknowledgments

This work was supported by the National Science Foundation (NSF) under Award CMMI 1640306. Partial support was also received from the Charles F. Perrell Scholarship. The author wants to thank Yiming Cao, a graduate student in the same group as the author from UMass Amherst, who helped with the experiments.

3.6 Declarations of Interest

None.

Table 3.1 Index properties and classification of the four studied clays

Index properties		Sample			
		Manufactured		Natural	
		Prestige	PureGold Gel	BBC	Onsøy
Silt Fraction (%)		37	11	44	31
Clay Fraction (%)		63	89	56	69
Atterberg Limits	*LL* (%)	45	394	48	67
	PL (%)	20	27	20	24
	PI (%)	24	367	28	43
A		0.38	4.12	0.50	0.62
USCS classification		CL	CH	CL	CH
Density ρ_t (Mg/m^3)		1.67	1.13	1.78	1.59
Natural salinity (g/g)		0.001	0.003	0.010	0.028

Note: ρ_t is bulk density of clay prepared at its *LL*, A is Activity = *PI*/clay fraction, CF = % < 2 μm, Silt fraction % between 2 and 75 μm

Table 3.2 Mineralogical compositions of the four studied clays

Minerals	Ideal chemical formula	Percentage (wt.%)			
		Prestige	PureGold Gel	BBC	Onsøy
Kaolinite	$Al_2Si_2O_5(OH)_4$	97.4		8.1	
Illite	$KAl_2(AlSi_3)O_{10}(OH)_2$		14.9	27.0	39.4
Montmorillonite*	$Na_{0.75}Si_8[Mg_{0.75}Al_{3.25}]O_{20}(OH)_4 \cdot nH_2O$		60.6		
Anatase	TiO_2	2.6			
Quartz	SiO_2		14.7	20.6	18.4
Albite	$NaAlSi_3O_8$			13.4	12.9
Biotite	$K(Mg,Fe)_3(AlSi_3O_{10})\ (F,OH)_2$			19.5	16.5
Orthoclase	$KAlSi_3O_8$			4.7	
Chlorite	$Mg_5Al(AlSi_4)O_{10}(OH)_8$			3.6	11.1
Hornblende	$Ca_2(Mg,Fe,Al)_5(Al,Si)_8O_{22}(OH)_2$			3.1	1.7
Ettringite	$Ca_6Al_2(SO_4)_3(OH)_{12} \cdot 26H_2O$		4.7		
Calcite	$CaCO_3$		1.7		
Nordstrandite	$Al(OH)_3$		3.4		

Note: * Teich-McGoldrick et al. (2015)

Table 3.3 Water content statistics of all clay specimens during the FC testing

Sample	Number of observations	Average (wt.%)	Standard deviation (wt.%)	Coefficient of variation (%)
BBC	10	45	0.35	0.78
Onsøy	8	66	0.50	0.76
PureGold Gel	9	417	3.79	0.91
Prestige	10	43	0.47	1.09

Table 3.4 Summary of the fitting parameters for the modified Burgers model

Sample	Property	c_1	c_2	c_3	c_4	c_5	R^2
BBC	s_u (kPa)	1.40	2.49	1.93	3.03	$2.42\text{x}10^{-2}$	0.99
	s_u/s_{u0}	1.00	1.79	1.93	2.167	$2.42\text{x}10^{-2}$	0.99
	G_{max} (MPa)	0.97	1.12	0.15	304.94	$4.00\text{x}10^{-5}$	1.00
	G_{max}/G_{max0}	1.00	2.18	0.61	14.58	$1.73\text{x}10^{-3}$	1.00
Onsøy	s_u (kPa)	1.08	1.32	5.99	1.71	$6.94\text{x}10^{-2}$	0.98
	s_u/s_{u0}	1.00	1.21	6.99	1.59	$6.97\text{x}10^{-2}$	0.99
	G_{max} (MPa)	0.34	0.43	0.56	7.05	$1.42\text{x}10^{-3}$	1.00
	G_{max}/G_{max0}	1.00	1.65	0.74	23.98	$1.46\text{x}10^{-3}$	1.00
PureGold Gel	s_u (kPa)	1.86	1.85	0.64	1.40	$9.90\text{x}10^{-3}$	0.99
	s_u/s_{u0}	1.00	1.02	0.65	0.76	$1.00\text{x}10^{-2}$	0.99
	G_{max} (MPa)	0.11	0.11	0.07	0.49	$1.29\text{x}10^{-3}$	1.00
	G_{max}/G_{max0}	1.00	1.41	0.11	5.49	$1.42\text{x}10^{-3}$	1.00
Prestige	s_u (kPa)	1.48	1.11	0.74	529.24	$2.61\text{x}10^{-5}$	0.99
	s_u/s_{u0}	1.00	0.76	0.74	427.18	$2.19\text{x}10^{-5}$	0.99
	G_{max} (MPa)	0.31	0.11	0.54	0.44	$2.30\text{x}10^{-2}$	1.00
	G_{max}/G_{max0}	1.00	0.36	0.85	1.43	$2.70\text{x}10^{-2}$	1.00

Note: R^2 = coefficient of determination

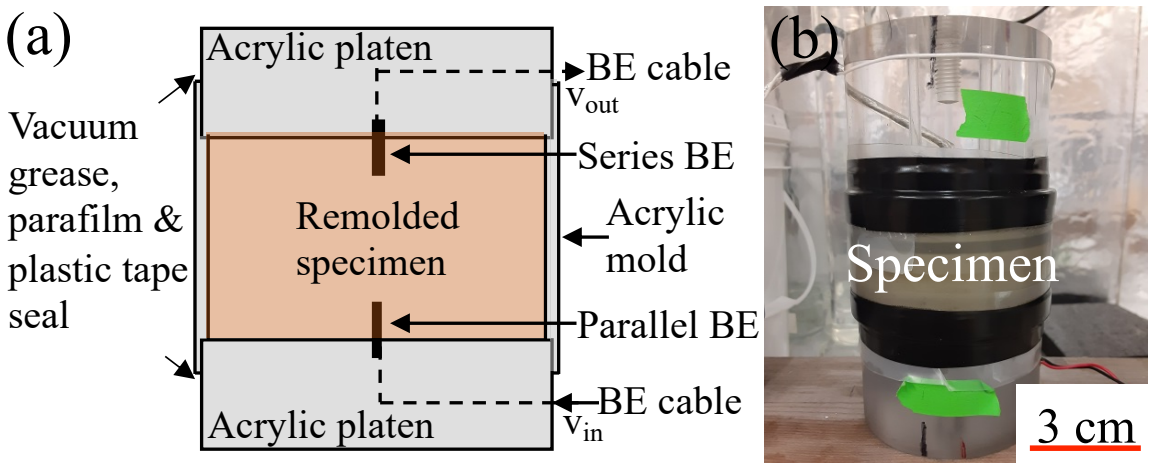

Figure 3.1 Setup for G_{max} measurements: (a) schematic showing the bender element (BE) platens; (b) picture of the setup.

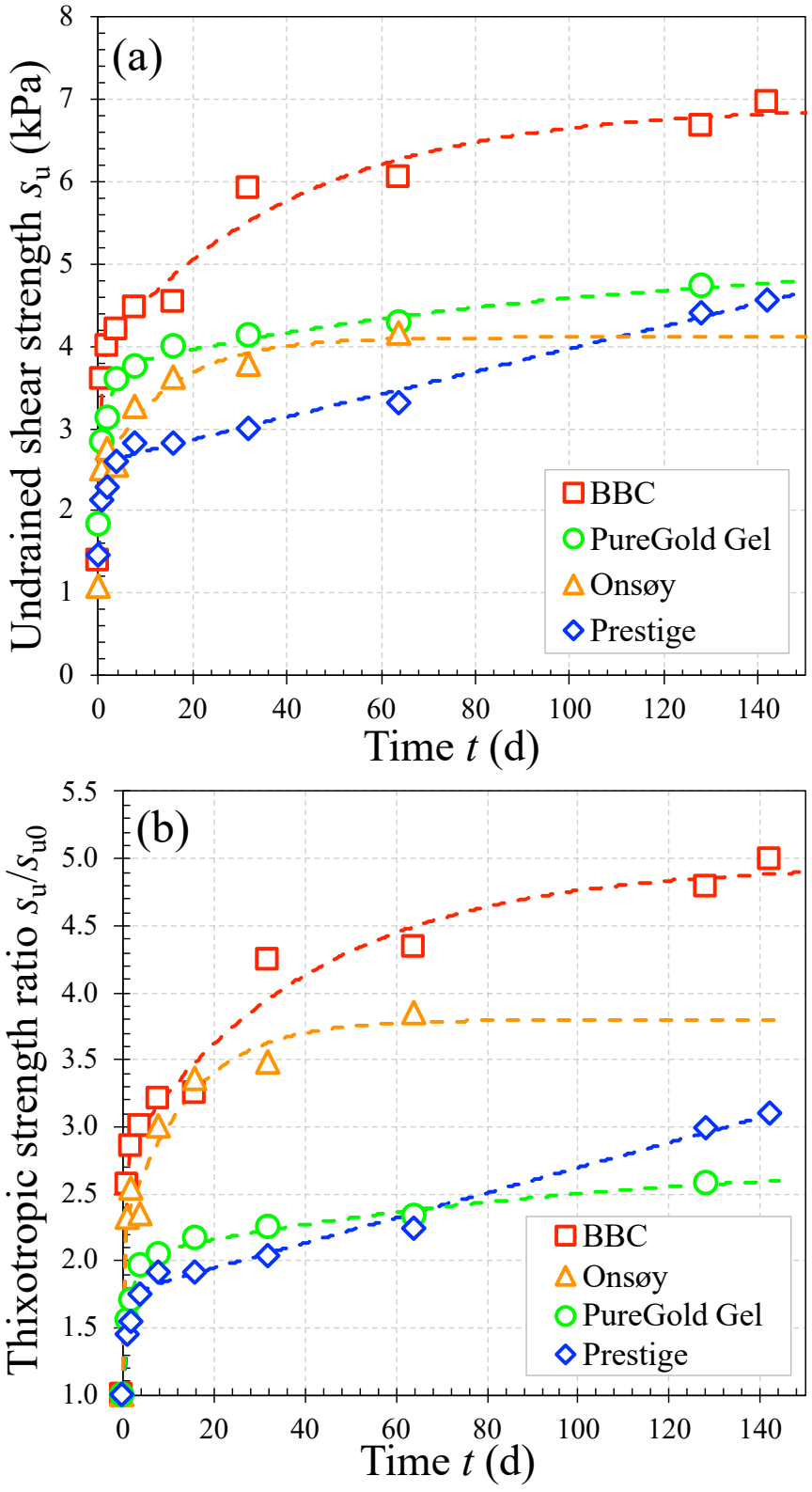

Figure 3.2 Thixotropic evolution of undrained shear strength: (a) s_u vs. time; (b) TSR vs. time.

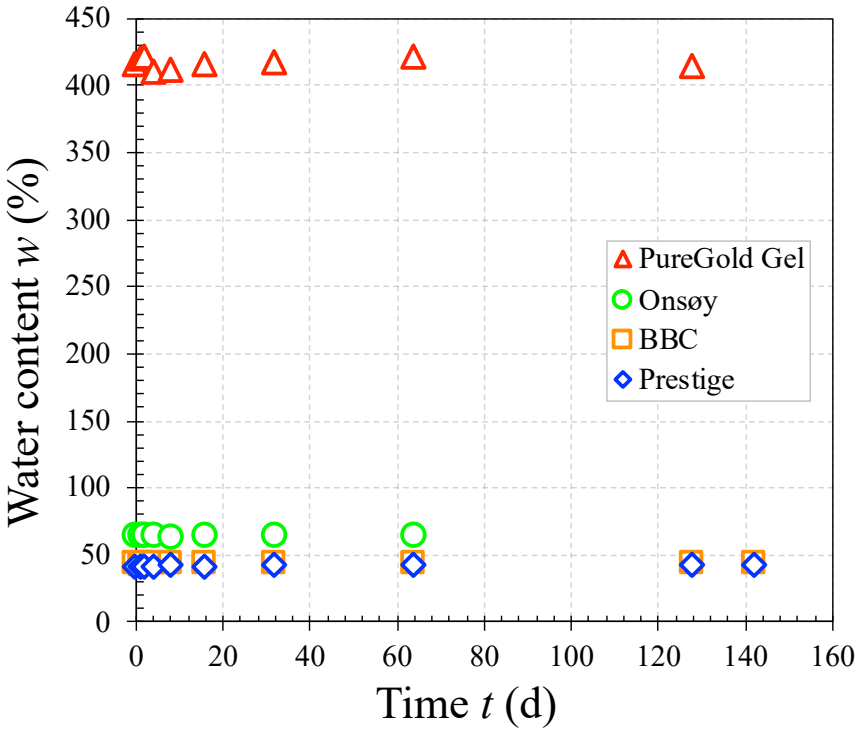

Figure 3.3 Water content measurements of all FC specimens during thixotropy.

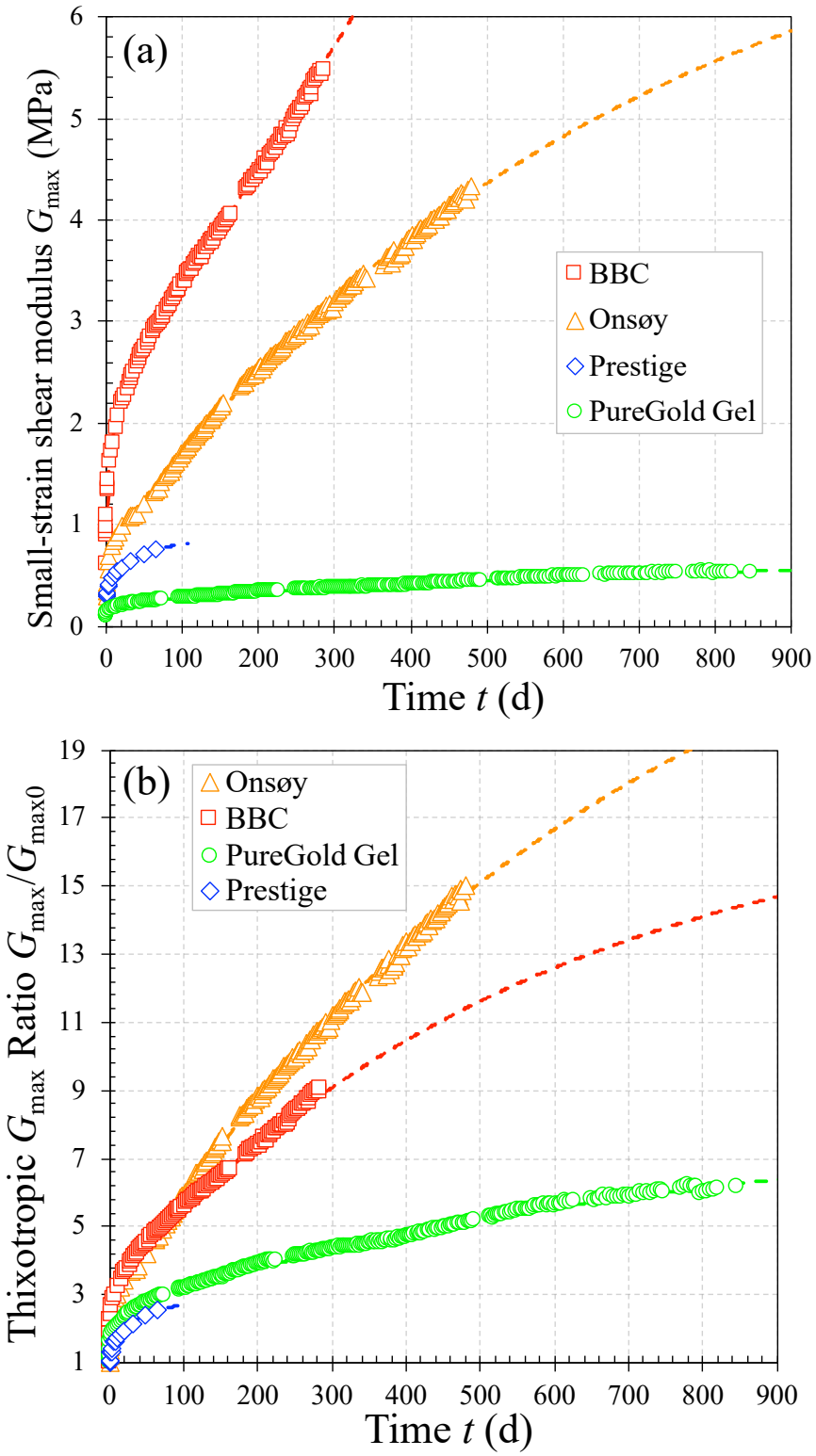

Figure 3.4 Thixotropic evolution of shear modulus: (a) G_{max} vs. time; (b) G_{max}/G_{max0} vs. time.

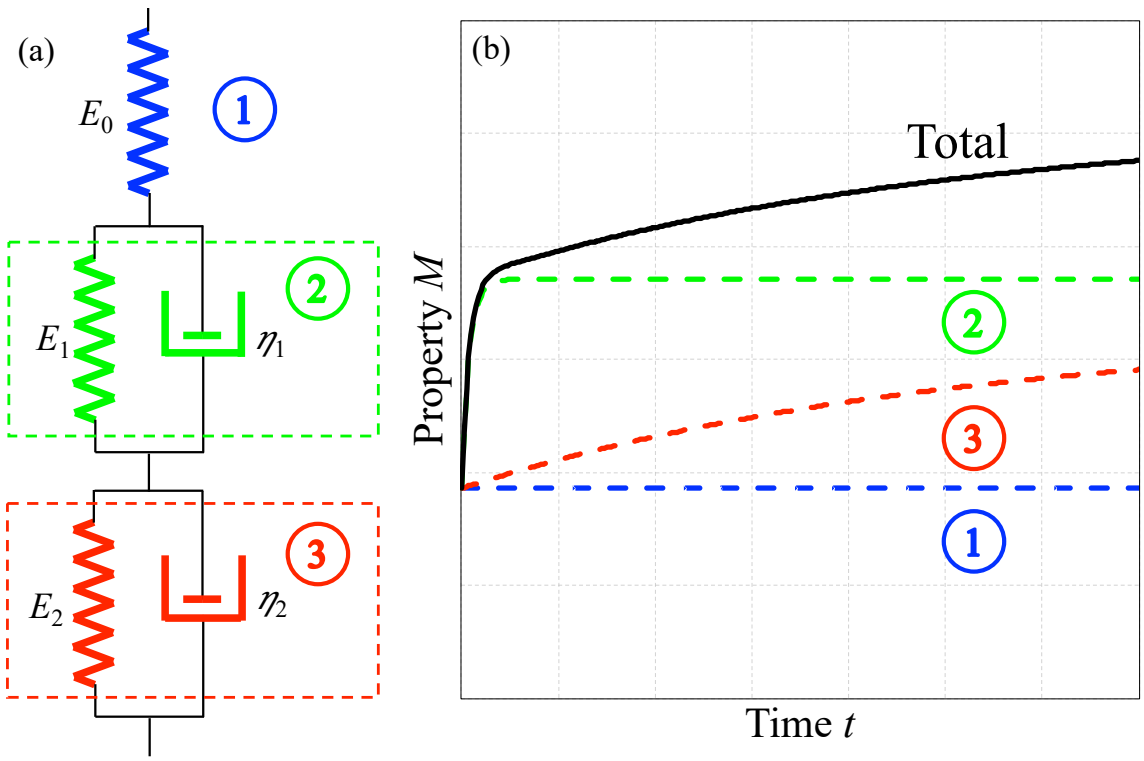

Figure 3.5 The modified Burgers extended rheology model: (a) mechanical representation; (b) behavior representation (note: the three mechanical components in (a) correspond to the three property curves in (b)).

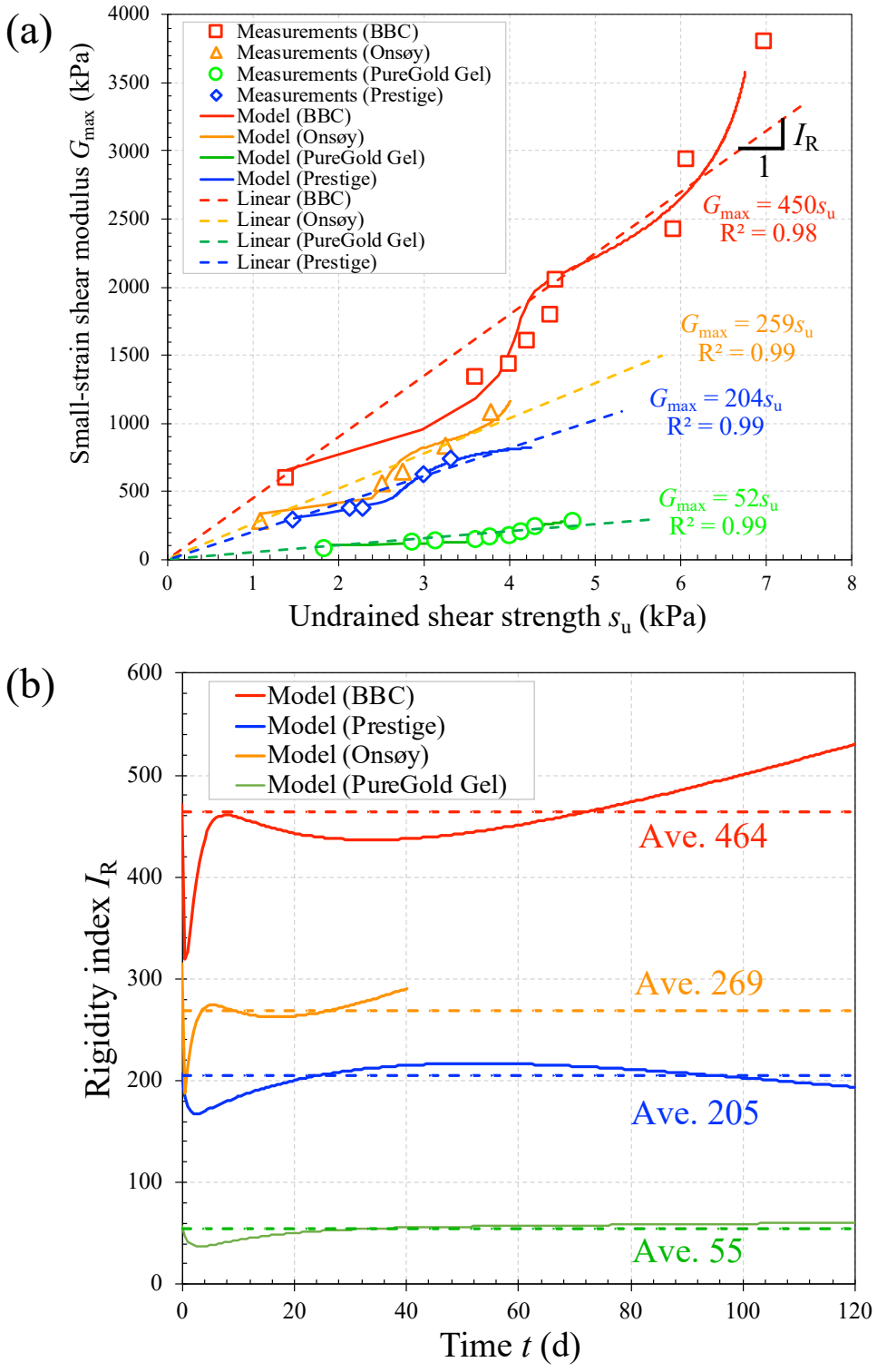

Figure 3.6 Relationship between G_{max} and s_u at different thixotropic curing times: (a) definition of the rigidity index (I_R) and the linear regression to determine the I_R; (b) the evolution of I_R with time based on the modified Burgers model of thixotropy.

CHAPTER 4

MULTIPLE MECHANISMS OF THIXOTROPY IN SOFT CLAYS UNRAVELED BY MICROSCALE EXPERIMENTATION

Thixotropy-governed temporal evolution of microfabric in two soft clays, including a naturally occurring, illite-rich, marine clay and a manufactured, highly purified, kaolin clay, was probed quantitatively by both one-dimensional X-ray diffraction (1DXRD) and 2DXRD for curing of up to 125 days. Results show that the two fabric-related indexes, orientation index (*OI*) and texture index (*TI*) obtained by 1DXRD and 2DXRD respectively, continuously evolve nonmonotonically but consistently during the thixotropic hardening process for the two clays at their respective liquid limits. Due to the initial large-strain remolding, both clays start with a fabric with more parallel particle orientation, followed by reorientation and flocculation with more face-to-edge association. With increasing time, the *OI* varied from 23.1 to 36.6 and from 3.8 to 4.5, while their *TI* ranged from1.004 to 1.008 and 1.010 to 1.029 for the kaolinitic and illitic clays, respectively. Moreover, the consistency between the *OI* and *TI* for both clays indicates that both experimental methods are applicable to characterizing the temporal microfabric changes during thixotropic hardening. These fabric data may result from various microscale particle rearrangements, likely including clay particle reorientation, aggregation, and flocculation, which in turn are controlled by interparticle forces. The advantages and disadvantages of the two methods and pertinent sample preparation techniques are also discussed, which can shed light on similar studies involving soft clays, especially for the time-dependent behavior. Combing the macroscopic results from the previous chapter, a transition in the hardening rate actually manifests that different thixotropic mechanisms play dominant roles at different

stages: the initial one is controlled by fabric aging, including particle rearrangements (e.g., reorientation, aggregation, and flocculation) and homogenization of defects and disturbance, and the later one by contact aging, responsible for the long-term continuous increase in the G_{max}.

4.1 Introduction

In physics and engineering, many materials, such as colloids, polymer solutions, and clayey soils, among others, exhibit a temporal increase in strength and stiffness even if the boundary remains constant (e.g., no change in pressure, temperature, or composition), a phenomenon termed "thixotropy" (Barnes, 1997; Mewis, 1979; Mewis and Wagner, 2009). In soils, the clay particles play a dominant role in controlling their physico-chemical and mechanical properties, especially in soft clays and shales, because of their platy shape, high aspect ratio, and permanent negative surface charges (Berthonneau et al., 2017; Seng and Tanaka, 2012). For an enclosed isothermal physical system (e.g., a wet soft clay) that receives no external input (e.g., no change in pressure, temperature, volume, or composition), a temporal increase in its macro-mechanical properties (e.g., stiffness and strength) must stem from certain microscopic internal processes occurring at the particle level, such as particle rearrangements.

It is generally agreed that the mechanisms of thixotropy in clays or cohesive soils are diverse and complex. Some pioneering efforts were made to examine the internal structural changes in clays, in an attempt to explain some macroscopically observed clay behavior (Casagrande, 1932; Lambe, 1953; Pusch, 1966, 1962). In fact, viable interpretations and mechanisms for this macroscopic phenomenon have been proposed to

associate thixotropy with microscopic, particle-level structural changes (Arnold, 1967; Jacobsson and Pusch, 1972; Osipov et al., 1984; Pusch, 1968), but most of these explanations or interpretations are generally conceptual or hypothesized owing to the limitations of available experimental techniques for studying the temporal evolution of clay microstructure. Understanding and knowledge of clay thixotropy are behind other scientific communities (e.g., physics, colloidal science). More recently, a limited number of studies (Díaz-Rodríguez and Santamarina, 1999; Seng and Tanaka, 2012; Zhang et al., 2013; Zhang et al., 2017) have been conducted thereafter in the geotechnical community to further uncover the underlying mechanisms of thixotropy in soft clays, yet most of these work is mainly based on indirect measurements (e.g., mechanical behavior, Weibull modulus) or qualitative observations (e.g., electron microscopy) of the microstructural evolution of clays during the thixotropic process. Direct, quantitative measurements of microstructure, particularly the temporal changes, of clays and other cohesive soils are seldomly reported in the literature.

However, prior understanding of thixotropy-related microstructural changes is more or less speculative, hypothetical, or qualitative in nature. Direct, quantitative measurements of microstructure, particularly its temporal evolution, of wet clays and other cohesive soils are rarely reported in the literature. Owing to the small size of colloidal clay crystals, it is challenging to quantify non-destructively a clay's temporal microstructure evolution. Fortunately, both conventional one-dimensional X-ray diffraction (1DXRD) and advanced 2DXRD are viable, powerful approaches to quantify clay particles' orientation. In fact, the former has been widely used in clay-related studies, part of which has been conducted on dry clay powders to investigate preferred orientation in powder mounts

induced by sample preparation methods (Dohrmann et al., 2009; Mitchell and Soga, 2005; Zhang et al., 2003). Similarly, 2DXRD has also been used for quantitative analyses (e.g., texture or fabric, stress/strain measurements) of various materials, such as metals, polymers, and rocks (Bontempi et al., 2008; Collins et al., 2015; Kanitpanyacharoen et al., 2011; Rodriguez-Navarro et al., 2012; Speziale et al., 2006; Widjonarko, 2016). Detailed introduction to the scientific principles of 2DXRD is well documented in the literature (He, 2009c, 2003; He et al., 2000). For instance, 2DXRD has been successfully applied to probe the texture and hence anisotropy of shales (Kanitpanyacharoen et al., 2011; Lonardelli et al., 2005; Wenk et al., 2014, 2010). However, quantifying the texture or fabric of wet clays and its evolution over a long time is challenging, especially for naturally occurring clays with complicated mineralogy and porewater chemistry.

This paper presents an experimental study, probably the first of its kind, of the microfabric changes of two soft clays during thixotropic hardening, and provides quantitative evidence to reveal the temporal microfabric evolution. Since soil structure consists of fabric and non-frictional interparticle forces (Mitchell and Soga, 2005), the term "fabric", part of soil structure, is used hereafter to focus on the texture (i.e., particle arrangement and association) of clays, but exclude the interparticle forces that cannot be assessed via nondestructive XRD. Both 1DXRD and 2DXRD were utilized to directly quantify the clays' microfabric evolution (e.g., particle rearrangement, reorientation, and reaggregation) with time, and assessment and comparison of the results and applicability of the two methods are also discussed. Since soil thixotropy plays an important role in many engineering practices, a better, systematic understanding of its underlying mechanisms can generate significant practical impacts to the geotechnical design and

construction. Therefore, the overall objective of the experimental study was to quantify and assess the temporal evolution of microfabric of soft clays during thixotropic hardening and hence to unravel the underlying fundamental thixotropic mechanisms contributing to the macroscopic hardening process. Meanwhile, practical guidance is also provided on choosing an appropriate method for fabric characterization of soft clays, especially when time-dependent behavior is of interest. The developed techniques can expectedly be used to study other long-standing issues in the soil mechanics discipline, such as particle reorientation in the shear band and the dependence of anisotropy upon particle orientation.

4.2 Materials and Methods

4.2.1 Materials

Two different clays, Prestige and BBC, described in detail in Chapter 3 (section: 3.2.1), were studied. The detailed experimental method of mineralogical compositions of these two clays determined from X-ray powder diffraction (XRPD) was also explained in Chapter 3.2.1.

Each sample was prepared at a water content near its respective *LL*, followed by overnight curing in a temperature-controlled chamber set at 24 °C for temperature and moisture equilibrium. The equilibrated sample was again thoroughly mixed prior to preparation of individual specimens for thixotropy testing.

4.2.2 1DXRD

Only one specimen of each clay was prepared for the non-destructive 1DXRD analysis, since thixotropy describes the time-dependent hardening under a constant

condition, and the same specimen can be re-examined at different curing times. A novel sample preparation method was developed to completely prevent drying or water loss of the wet clay, using the so-called "back-loading" method, which minimized the effect of final surface-leveling process on the clay fabric (i.e., as required in the "front-loading" method) and hence better revealed the inherent, thixotropy-induced fabric evolution. A 7.5 μm thick Kapton or polyimide sheet (Chemplex Industries, Inc., FL, USA), which was transparent to X-rays or yielded no detectable XRD reflections, was first attached onto the front side (i.e., the side accepting incident X-ray beam) to cover the empty window of the specimen holder, which was then turned over to expose the back side (Figure 4.1), followed by back-loading the thoroughly remolded wet clay into the specimen window (Figure 4.1). After the surface of the clay specimen was leveled flush with the holder's back surface (i.e., to avoid any gap or air entrapment), a piece of glass cut out of a regular microscopy slide was immediately placed to cover the surface of wet clay contained inside the window. To maintain a constant water content during thixotropic process, the perimeters of both the Kapton sheet and glass cover were all tightly sealed by epoxy resin. During the preparation, the initial water content of each clay sample was measured by oven-drying a small representative portion at 105-110 °C), and the mass of the wet clay contained in the sample holder obtained. Then the specimens were stored for curing in a chamber with a nearly 99% relative humidity (RH). XRD scans were repeated on each specimen retrieved intermittently from the chamber at different curing times (e.g., 0, 1, 7, …, 28, 62, 120 days), and upon completion the specimen was immediately returned into the humidity chamber for curing. The same X-ray diffractometer and configurations described in Chapter 3.2.1 for quantitative XRPD was used to collect the 1DXRD patterns. Any reduction in the total

mass of each specimen measured after each XRD scan relates to the loss of water. The true water content of each specimen at the moment of the experiment was calculated and used as quality control.

Whether and how the clay microfabric of the specimen changes during thixotropic hardening can be characterized by the evolution and alteration of orientation of platy clay particles, which can be quantified by the orientation index, *OI* (Brindley and Kurtossy, 1961; Zhang et al., 2003):

$$OI = \frac{Intensity\ of\ \ a\ suitable\ basal\ reflection, I_{00l}}{Intensity\ of\ \ non-basal, prism\ reflection, I_{060}} \tag{4.1}$$

where l = 1 or 2; I is the intensity of a reflection on the collected XRD pattern. In addition to the prism plane (060), the ratio of I_{002}/I_{020} can also be used as *OI*.

In this study, a reflection's intensity was calculated by the peak area enclosed under the reflection of the corresponding crystalline plane, and the background profile of a diffraction pattern for Prestige was determined based on that developed for kaolinite (Zhang et al., 2003). Specifically, the background for the (020) plane reflection needed to be determined separately to consider the stacking disorder of the 1:1 layers of kaolinite (i.e., resulting in an unsymmetric diffusive reflection for the (020) plane). Also, due to the diffusive (020) reflection, the background for (002) reflection was also determined manually. For BBC containing multiple minerals, the *OI* was determined based on the reflections from illite, after the intensity of the overlapped reflections from the biotite mica (Table 3.2) was subtracted based on the relative percentages of illite and biotite. A commercial program, HighScore Plus (Malvern Panalytical, Netherlands), with embedded International Centre for Diffraction Data (ICDD) database, was used to identify the 2θ positions of all major reflections.

4.2.3 2DXRD

Generally, low-energy X-rays generated in the small-scale laboratory 1DXRD instruments can only penetrate the surficial layer of ~ 200 μm in thickness (i.e., corresponding to 63% attenuation of incident beam intensity) of typical aluminosilicate materials. However, clay particle movements, including rearrangement, aggregation, and rotation, in the surface layer (e.g., which is in the contact with the Kapton sheet) may be constrained or affected by the interfacial interactions (e.g., friction, surface forces) between the wet clay specimen and Kapton sheet. As such, the thixotropic microfabric changes measured via 1DXRD from the very shallow surficial layer of the soft clay specimen may not be representative of the entire specimen. Therefore, high-energy synchrotron-based 2DXRD was also conducted in the Beamline 11-ID-C of the Advanced Photon Source (APS) at Argonne National Laboratory (ANL).

Preparation of wet specimens for thixotropic hardening followed the same procedures used in the FC testing, but the critical point-dried specimens were used for 2DXRD, due to the limited access and the difficulty in scheduling the experiments with the APS at the desired times. Wet clay samples were first filled into a series of duplicate porous cylindrical pots (EMS 800A, Electron Microscopy Sciences, Hatfield, PA, USA) with dimensions of 8 × 10 mm in inner diameter × inner height. Upon completion of filling, these pots were immediately stored for thixotropic hardening in a 99% RH chamber to different curing durations (e.g., 0, 1, 2, 4, 7, 9, 12 days). The same method for water content measurements during 1DXRD was used here to check the water content of each 2DXRD specimen. At the end of a specific curing time, one duplicate pot covered with a lid was

transferred to a Balzers CPD030 critical point dryer (Leica Microsystems, Milton Keynes, Watford, UK) to remove the pore water of the wet specimens.

The Critical point drying (CPD) method is known to be ideal for drying small-volume, very delicate hydrated samples while preserving their original microstructures, and the latter plays a vital role in the subsequent analysis of clay particle orientations in the thixotropically hardened samples (Zhang et al., 2004a). A typical CPD process generally consisted of two steps: pore fluid replacement and evaporation of the replacing fluid. In the former, the wet specimen hosted inside the porous pot was gradually submerged into a pressure chamber filled with acetone, an intermediate replacing fluid with a weak polarity and a low surface tension, at a cooling temperature of 10 °C and an elevated pressure of 5000 kPa. This step resulted in the replacement of polar pore water and hence was also called dehydration step. After dehydration, liquid carbon dioxide (CO_2) that is miscible with acetone was then flowed into the chamber to fully flush away the acetone (i.e., the intermediate dehydrating fluid). Once completed, the temperature and pressure inside the chamber were raised to 31 °C and 7380 kPa (i.e., the critical drying point), respectively, at which the liquid CO_2 evaporated, and the specimen became completely dried at the end of evaporation and could not undergo further fabric changes.

The porous pots with dried specimens were embedded in epoxy, followed by cutting off both the top lid and bottom of the pot, resulting in a 4 mm thick disk that contained the CPD-processed clay specimen in its center. The hardened epoxy helped preserve and protect the delicate, dry clay specimens still hosted inside the porous pot after the top lid and bottom of the pot were removed by cutting. As a result, a dry clay disk with preserved fabric inside a porous ring that was protected by the outside hardened epoxy was

prepared, with its two end surfaces exposed for 2DXRD scans (Figure 4.2). It was expected that little epoxy permeated into the pore space of the dried clay due to its high viscosity and fast setting. However, even if the epoxy permeated partially or completely into pores of the clay, it would not interfere with the 2DXRD measurements since the epoxy is amorphous.

The high-energy (i.e., 105.7 keV) synchrotron XRD experiments allowed the diffraction patterns to be collected in a transmission geometry (i.e., the diffracted X-rays passed through the entire specimen, which was 4 mm thick in this study) (Liu et al., 2018). Each specimen disk was mounted on the goniometer, and the exposed top surface was penetrated perpendicularly by a monochromatic synchrotron X-ray beam with a wavelength of 0.1173 Å and a beam size of 0.5 × 0.5 mm. The transmitted diffracted Debye rings were recorded by a high-resolution imaging plate with 2480 × 2480 pixels at a sample to detector distance of 1.8 m calibrated by the standard CeO_2 powder. Each specimen was scanned nine times at pre-defined specified locations with a center-to-center spacing of 1.0 mm to increase the overall specimen coverage (Figure 4.2).

Fabric analysis was performed on the collected 2DXRD patterns using the MAUD (Materials Analysis Using Diffraction) software (He et al., 2000; O'Brien et al., 1987; Van Houtte, 1980). Each diffraction image was first divided into multiple azimuthal sectors with an equal apex angle of 5°, and integration of the intensity was conducted on individual arcs within each sector to obtain one spectrum, resulting in a total of 72 spectra for each 2D diffraction image. These spectra were loaded into the MAUD for Rietveld refinement (e.g., background parameters, scale factors for intensities, unit cell parameters for peak positions, etc.) to simulate the experimental diffraction data (Lutterotti et al., 2014; Toby,

2006; Wenk et al., 2014), followed by refinements of texture related parameters (Wenk et al., 2010) for fabric analysis to determine the orientation distribution functions (ODF) and pole figures, which were the stereographic projection of the normal of all crystalline planes with respect to the sample coordinates (Helming and Preckwinkel, 2005; O'Brien et al., 1987; Wenk and Grigull, 2003), and the plane parallel to the top and bottom flat surfaces of the clay disk (Figure 4.2) was selected as the projection plane in this study. Finally, texture index (*TI*) (Engler and Randle, 2010; Matthies et al., 1988; Ramirez-Rico et al., 2016) for the studied whole specimen was then calculated using MTEX, a free MATLAB toolbox. The *TI* of an ODF denoted as *f* is defined as:

$$TI = \int f(g)^2 \, dg \tag{5.2}$$

where *g* is the orientation that is normally identified using three Euler angles. The ODF was estimated from pole figures, and its estimation f_{est} in MTEX was based upon the modified least squares estimator:

$$f_{est} = \arg\min \sum_{i=1}^{N} \sum_{j=1}^{N_i} \frac{\left| \alpha_i Rf\left(h_i, r_{ij} - I_{ij}\right) \right|^2}{I_{ij}} \tag{5.3}$$

where argmin is the argument of the minimum, α_i are the unknown normalized coefficients, h_i the lattice planes, r_{ij} the specimen directions, I_{ij} the reflection intensity, and *R* the Radon transform. A precise description of the estimator and the algorithm can be found in Hielscher and Schaeben (2008).

Further microfabric imaging and observation were performed on selected CPD-prepared Prestige specimens (e.g., after curing for 6 days) in a high-resolution Magellan 400 XHR scanning electron microscope (FEI Company, Hillsboro, OR, USA) operated at a 5 kV beam voltage and 13 pA beam current. No conductive coating was applied to the

examined specimen since the electron beam was generated at a very low voltage and current.

4.3 Analysis of Results

4.3.1 1DXRD Analysis

For 1DXRD, the diffraction patterns were collected from the same Prestige and BBC specimens while they continuously cured for up to 125 days during. To ensure result accuracy (i.e., the change in the clay's microfabric was not caused by drying but by the internal particle-to-particle interactions within the clay), the weight or water content of each specimen was re-checked prior to each XRD scan, and no detectable water loss was observed even after ~125 days of curing and storage. In fact, all water contents measured after each XRD scan have an average, standard deviation, and coefficient of variation of 45 wt.%, 0.17 wt.%, and 0.38% for Prestige and 45 wt.%, 0.16 wt.%, and 0.35% for BBC, respectively. Figure 4.3 shows all XRD patterns of the same Prestige and BBC specimen obtained at different curing times, with the background already removed from the original diffraction patterns.

The orientation index (*OI*) for each pattern was calculated in terms of the peak area of the (002) and (020) reflections for Prestige specimen. Similarly, *OI* for each pattern was calculated based on the peak area of the (002) and (040) reflections for illite in the BBC are shown in Figure 4.4a. The magnitude of the *OI* pertains to the degree of preferred orientation of clay particles, with a higher value indicating more individual clay particles are face-to-face associated and vice versa. The results (Figure 4.4 and Table 4.1) indicate

that the particle orientation within both Prestige and BBC specimens continuously evolves in a complex pattern during the thixotropic hardening process.

4.3.2 2DXRD Analysis

Similarly, as sample quality control, the water contents of the clay specimens prepared for 2DXRD testing were also measured after thixotropic curing but before the CPD, and results show very little variation. As such, the clay specimens inside the porous pots did not undergo compositional changes (i.e., loss of the porewater). As the examples for illustration, diffraction images collected from the 0 day specimen are shown in Figure 4.5. Each diffraction image consists of a series of concentric Debye rings, each of which is the projection of a diffraction cone produced by the scattered X-rays at a specific 2θ angle. As such, the outward radial direction represents the increase in the diffraction 2θ angle. In addition, whether or not preferred orientation of particles, especially platy clay minerals, exists within the specimen can be observed directly but qualitatively from the diffraction image, because the variation in the intensity (e.g., brightness) of the X-rays along the ring or even a broken ring manifests the dominant orientation direction of the particles (Kanitpanyacharoen et al., 2011; Wenk and Grigull, 2003). In other words, a specimen with perfectly randomly oriented particles generates uniform rings with the same intensity (e.g., brightness) for each ring. For instance, Figure 4.5d shows a 2D diffraction image with all uniform rings obtained from the standard CeO_2 powder with randomly oriented crystallites. However, the inner four to five rings on the diffraction images collected from the tested Prestige specimen (e.g., Figure 4.5c) exhibit obvious intensity variations (darker vs. lighter color). Simple visual examination of the 2DXRD images provided limited qualitative

information on the orientation of clay particles, and further data processing was still necessary to obtain quantitative results.

Since the pole figure illustrates the orientation of crystalline planes enclosed within the specimen volume excited by the incident X-ray beam, and kaolinite is a platy-shaped clay mineral, Figure 4.6 presents 9 example pole figures of (001) basal plane obtained from the nine different scanned locations (Figure 4.2) on the 0 day-cured specimen. The orientation of clay particles is relatively random at the center of the specimen, while distinct features of preferred orientation with identifiable patterns dependent on the scanned locations can be observed on the pole figures closer to the edge of the specimen. A single representative pole figure averaged over the 9 scanned locations (Figure 4.2) was needed for subsequent assessment of the temporal microfabric evolution. In fact, during initial injection of the thoroughly remolded soft clay, which could almost flow freely under gravity at their *LL*, into the porous cylindrical pods, an axisymmetric fabric should be expected. Therefore, it is more appropriate to conduct the spatial averaging in a polar coordinate system (i.e., r, α, where r is the radial distance and α is the clockwise azimuthal angle) of different scanned locations, especially for those obtained from the edge locations (i.e., Points 6-9). As such, the 9 scanned locations were assigned to three sub-groups, which are Center (Point 1), Middle (Points 2-5), and Edge (Points 6-9) based on their radii (i.e., distance to the center of the specimen) in the polar coordinate system. As shown in Figure 4.2, $\alpha = 0$ was desired in this study, so the pole figures obtained from all other six locations (i.e., Points 3-5 and 7-9) with non-zero alpha angles were rotated by the corresponding degrees and directions (counterclockwise for a positive number and clockwise for negative number). The new pole figures after rotation were presented in Figure 4.7a. Once the

rotation was finished, the pole figures within the same sub-group were averaged and the results are presented in Figure 4.7b. It can be observed that the average pole figure of the (001) crystal plane from the "Edge" subgroup has a very strong preferred orientation such that the normal of the basal planes is almost parallel to the top and bottom surfaces of the specimen disk. Although the CPD is generally known as a drying method that does not alter the microstructure of the specimen, the edge effect might be still profound in the tested clay, considering the high pressure used for water replacement as well as the platy shape of the clay particles. As a result, the final representative pole figure for the whole specimen was obtained by averaging the two pole figures from the Center and Middle locations, but the third one corresponding to the Edge subgroup was discarded (Figure 4.7b).

The above data reduction process was repeated for all other specimens that experienced different thixotropic curing times before CPD drying and 2DXRD measurement. Figure 4.8 shows these averaged pole figures obtained from specimens that were cured for up to 12 days. Such a temporal series of pore figures provides a direct visualization of how the microstructure evolved with time during thixotropic hardening. Obviously, the clay particles continuously change their orientation throughout the entire thixotropic hardening process, similar to the observation found in 1DXRD. The preferred parallel orientation of clay particles caused by the initial mixing gradually changes with curing time towards a more random orientation, even if the boundary conditions remain unchanged and the entire system is closed. Noteworthy is that representative pole figures of many other crystal planes (e.g., (001), $(0\bar{1}1)$, (100), $(\bar{1}\bar{1}1)$, etc.) can also be obtained independently by following the same procedure. For each specimen, a 3D orientation distribution function (i.e., ODF) was derived according to the pole figures of eight different

crystal planes since kaolinite has a triclinic crystal structure (He et al., 2002; Van Houtte, 1980). For BBC, due to its complex mineralogical composition, only four major phases, including illite, biotite, quartz, and kaolinite, were included in the Rietveld simulations to reduce the computational time and difficulty. Similarly, all of the above data processing steps were repeated for all 2DXRD measurements from the BBC specimens. Figure 4.10 gives some collected diffraction images, while Figure 4.10 to Figure 4.12 show example pole figures of the (002) basal plane of illite on the 0 day-cured specimen, and the final results (Figure 4.12) are the average of all scanned 9 locations.

Once the ODF of individual specimens was determined, an integrated quantitative parameter for evaluating the 3D orientation of clay particles *TI* was then calculated, and the results are also summarized together with *OI* in Table 4.1. Texture refers to the distribution of crystallographic orientations of a polycrystalline material. Depending on the degree of the preferred orientation, a material is referred to as having a strong, moderate, or weak texture (He, 2009d), and can even be classified as no texture if all crystallites are perfectly randomly oriented (i.e., $TI = 1.0$). Therefore, the calculated *TIs* (i.e., from 1.004 to 1.008 and 1.010 to 1.029 for the Prestige and BBC respectively) indicate that the specimens appear to have a weak texture without strong ordered parallel orientation throughout the entire volume, and the possible reasons for small *TI*s are discussed later.

4.3.3 Microstructural Evolution and Comparison of Two Fabric Indexes

Both the two fabric indexes indicate continuous temporal changes in fabric (e.g., particle rearrangement) for the two studied clays during the thixotropic process, most likely resulting from the interparticle interactions. Although the interparticle forces cannot be

investigated by nondestructive and nonintrusive techniques, they are responsible for the evolution of soil fabric that can be probed by the nondestructive techniques such as XRD. Soil fabric refers to the structural or textural arrangements of particles, particle groups, and pores in a soil. The fabric of most fine-grained clays are typically formed by complex particle units of micro- to milli-meter (or even greater) scales, which consist of multi-particle aggregates, flocs, and pores, but not so much fully dispersed individual clay particles (unless in some processed clays with added chemical dispersants and mechanical energy for dispersion, Zhang et al., 2005, 2004, 2013b). Large-strain remolding and shearing can move the clay system away from the equilibrium corresponding to the minimum free energy state (Figure 4.13). According to the EDL (e.g., the Derjaguin-Landau-Verwey-Overbeek (DLVO)) theory, the interactions between two clay particles are dominated by the net force between the van der Waals (vdW) attractions and EDL repulsion. External input of energy (e.g., remolding, shearing) can break up the equilibrium of forces established previously over a long period, and the system's free energy moves away from the minimum. However, once the external input is absent, the unbalanced attraction versus repulsion forces tend to move the system back to the minimum. Detailed information of mechanisms proposed for fabric evolution can be found in Peng et al. (2021b).

Figure 4.14 gives an exemplified schematic illustration of the microfabric changes (Prestige was used as an example for the following illustration). In general, the initially completely remolded specimen at t = 0 day has a relatively higher *OI* value, because the excessive large-strain remolding (e.g., continuously mixing with a spatula or knife, stirring, etc.) has sheared the clay with a lot of internal shearing failure planes where the clay

particles orient in a face-to-face association (e.g., like those observed in a shear band on a failure plane). The decrease in the *OI* in the first few days of curing demonstrates a tendency in microstructural change towards a more flocculated structure (i.e., face-to-edge association). This also indicates that the initially parallel-oriented clay particles induced by large-strain shearing tend to transform into a more random orientation. In the second stage (i.e., t = 10–20 days for Prestige) of curing, a significant increase in the *OI* occurs, indicating that particle aggregation, which is defined as the formation of face-to-face associated thicker particle groups, also termed as "flocculi" (Zhang et al., 2013b), becomes the dominant microstructural changes that even counteract the previous particle flocculation process.

Kaolinite is known to tend to form booklet-like aggregates where individual particles are associated with face-to-face association, and the temporal increase in the *OI* obtained by the 1DXRD also confirms this commonly observed phenomenon. The underlying mechanisms for the formation of such aggregates are the crystal structure and surface properties of the kaolinite mineral. The 1:1 type kaolinite crystal consists of two different basal planes: while an O-based plane is at the tetrahedral sheet of the 1:1 layer, an OH-based basal plane is at the octahedral sheet. If the kaolinite without a high negative surface charge has little soluble salts, which is the case for the studied Prestige, and hence little cations on its two basal surfaces, the two different basal planes tend to attract each other via hydrogen bonding. Aggregates formed by relatively strongly bonded parallel clay particles act somewhat like individual bulky grains or particulate units, inducing the increase in both macroscopic strength and stiffness through relatively coarser bulky grains and possibly also interparticle frictional and attractive forces.

In the third stage, the *OI* decreases again, indicating that the clay aggregates within the specimen are converting further to a more random distribution. The difference between the third and first stages is probably that, while individual particles are becoming randomly oriented, it is the aggregates that become more randomly oriented in the third stage. Finally, after ~60 days of curing, the *OI* increases again, suggesting that higher-level, even coarser aggregation is again the dominant process, which may result in even thicker kaolinite booklets or super-particles of even greater size. An illite crystal consists of two symmetrical siloxane basal planes with negative surface charges, and hence no hydrogen bonding can develop between two adjacent illite particles. However, the BBC contains significant amounts of soluble salts that provides cations adsorbed onto the illite surface. As such, different from kaolinite, the major interparticle forces responsible for the temporal fabric evolution are primarily the Coulomb forces (including cation bridging) and secondarily van der Waals attraction. Nevertheless, the overall pattern of the temporal *OI* evolution for the two clays is similar. Finally, since BBC contains a non-negligible fraction of anhedral quartz and other non-platy minerals, its absolute *OI* values are generally much smaller than those of Prestige.

Further microfabric observation and imaging performed on the Prestige specimens, as shown in Figure 4.15, indicate the formation of such complex clay fabric, including the formation of clay aggregates, further flocculation of clay aggregates, and then the formation of thicker aggregates within the flocculates during thixotropy. Due to the nonsymmetrical basal surfaces of kaolinite crystals, aggregates can readily form in the clay (Figure 4.15a, 15b, and 15d). For highly dispersed kaolinite particles, flocculation of primary individual particles and thinner aggregates also takes place (Figure 4.15a and 15c).

Although the proposed conceptual fabric evolution (Figure 4.14) seems to occur sequentially, it is likely to observe all different forms of microfabric in a clay sample cured to a specific time, as shown in Figure 4.15.

Figure 4.14 also plots and compares the temporal evolution of the two fabric indexes, *OI* and *TI*. Although the considered curing time was much shorter for the *TI*, the trend of its temporal change was similar to that of the *OI*, which further self-validated the results from the two methods. In general, the *TI* values were much smaller than those of the *OI*. The *OI* defined in this study is also called peak ratio previously (Martin, 1966; Mitchell and Soga, 2005). According to the literature, for kaolinite with completely random orientation (e.g., air-dry powder), the *OI* was about 2.0. However, it could reach up to ~200 for high parallel orientation achieved from dispersed kaolinite slurry slowly dried on a glass slide (Martin, 1966). Moreover, based on the XRD patterns of oriented clay thin films that showed no reflections of the kaolinite's (020) plane, the *OI* could be nearly infinity (Zhang, 2002). Therefore, it may not be appropriate to compare the absolute values of *OI* versus *TI*, but their relative changes or trends.

The small *TI* values might result from two possible reasons. Raw clays could possess complex fabric consisting of different clay particle assemblages at different size levels (Figure 4.16a). At the smallest level, individual particles may form a dispersed or flocculated fabric. However, clay particles tend to form higher-level face-to-face associated aggregates, which can again form dispersed-and-aggregated and flocculated-and-aggregated fabric. If a natural soft cohesive soil also contains sand and silt particles, then their presence may interfere with the fabric. An aggregated-and-flocculated particle assemblage has two-level particle orientations: at the smaller level, individual clay particles

form an aggregate with high parallel orientation (but only at the local small scale). At the larger level, the aggregates flocculate to form the "aggregated-and-flocculated" fabric that consists of randomly oriented aggregates. As such, the overall *TI* for this large particle assemblage is small. The second reason is that the local particle orientation, induced by initial shearing, at different locations throughout the entire specimen volume may not be the same. As shown schematically in Figure 4.16b, although three of the four locations had very high parallel-oriented local fabric, the overall fabric, upon averaging, tended to become a random orientation, or a small *TI*. On the other hand, such heterogeneous local fabric could also be one possible reason for the nonmonotonic evolution of the *OI* and *TI*. Moreover, due to the different mineralogical (e.g., kaolinite vs. illite), physical (e.g., particle size), and chemical (e.g., salinity) properties between the Prestige and BBC, fabric evolution started earlier in the BBC than Prestige, but much larger-sized, face-to-face-associated aggregates can form in the Prestige because the non-symmetrical basal surfaces (i.e., the siloxane vs. hydroxyl planes) of kaolinite crystals tend to attract to each other via hydrogen bonds. Tan et al. (2017) conducted a study of evaluating the particle sizes of four source clay minerals in aqueous suspensions, including processed kaolinite and illite, and found that the particle size distributions of all four clay minerals exhibited multimodal lognormal distributions with local maxima representing <2 μm primary clay particles, 10-20 μm flocculi, and sometimes 50-500 μm microflocs. Similar findings can also be found in Shein et al. (2019), which showed the formation of kaolinite microaggregates with a diameter of 50 to 500 μm.

In summary, both the *TI* and *OI* suggested continuous microfabric evolution in the two soft clays during the entire thixotropic process. Different microscopic movements of

individual clay particles take place, including reorientation, flocculation, and aggregation. These conceptual particle movements or fabric changes may occur sequentially or simultaneously throughout the entire process, and compete with each other for the dominant role at different stages. Finally, the results suggest that the combined effects of these particle-level movements eventually transform the clay fabric into a more flocculated state with thicker clay aggregates consisting of the face-to-face associated individual particles, and such a microfabric may possess the lowest free energy of the considered clay system. Further noteworthy is that this conceptual interpretation of fabric evolution is just one possible, but not the only definitive, mechanism supporting the measurements.

4.4 Discussion

4.4.1 Comparison between Different Experimental Methods

Although both microfabric characterization methods, 1DXRD and 2DXRD, can provide quantitative index values for the degree of preferred orientation of clay particles, each has its own advantages and disadvantages. The 2DXRD favors the collection of a large quantity of data from multiple crystalline planes meanwhile at a rate that is a few orders of magnitude faster than the conventional 1DXRD that only relies on data from a few crystalline planes. The high-energy synchrotron X-rays used in the 2DXRD also enable greater penetration (i.e., usually transmission) through a material, which improves the measurement range and yields more accurate and representative results due to the large sample volume irradiated by the X-ray beam. Another unique advantage of the 2DXRD is that particle arrangements relative to the sample orientation can also be determined, and the reorientation of constituent clay particles can be directly visualized. As a result, more

effort (e.g., time) is required to process and interpret the collected data because a more sophisticated instrument system is used to collect the massive experimental data, when compared with the conventional 1DXRD. Additionally, there are more concerns and difficulties in preparing wet clays samples that require the control and prevention of water loss, whereas it is much easier to prepare and deal with dry samples. However, when wet clays must be used, especially for the temporal evolution of time-dependent behavior, it is more difficult to accurately determine the microfabric, since problems could also arise from either the preservation of the water content if wet specimens are prepared, or the prevention or minimization of microstructure disturbance during dehydration and drying if dry specimens are required. For the latter, appropriate drying methods such as CPD and freeze-drying, which can preserve the original microstructure, become essential for the study of long-term evolution of soil fabric. There are still ongoing debates about whether or not the original microstructure can be truly preserved even by different advanced, mature drying techniques. Findings have been reported on the artifact of previously observed honeycomb microstructure of clay minerals caused by freeze-drying (Deirieh et al., 2018; Ye et al., 2019). Therefore, the CPD method, instead of freeze-drying, was adopted for sample preparation in this study.

When compared to 2DXRD, the best benefits offered by the conventional 1DXRD are its wide availability and simplicity. Both the sample preparation and instrumental operation (including data processing) are well established in the literature. XRD instruments are widely available in many academic and commercial materials characterization laboratories, and the powder diffraction databases, the excellent resources for mineral identification and quantification, are often available with the software for data

analysis. However, since the penetration depth of the low-energy X-rays generated in the 1DXRD instrument is relatively small (e.g., about 200 μm for typical aluminosilicates) when compared to the thickness (e.g., a few millimeters) of the entire specimen, the collected 1DXRD data are averaged over a small irradiated volume. As a result, the soil fabric near the specimen surface is specifically favored by the 1DXRD. Moreover, to maintain a constant moisture of wet clays for a prolonged period, the front surface of the specimen has to be covered by a thin Kapton sheet that may be soft and flexible. As such, any disturbance to the cover sheet could potentially propagate to the underlying clay and hence may cause errors in the XRD measurements, even if the specimen is carefully handled and stored during thixotropic curing. In addition, the Kapton sheet as a cover may also induce the so-called "boundary effect": the displacement and rotation of clay particles that are in direct contact with or near the Kapton sheet can be restricted to certain extent by the sheet due to friction or other microscale forces, affecting the behavior of thixotropic hardening of the surficial clay layers that are significant for the 1DXRD measurements. Finally, the Kapton sheet cover can also absorb to certain extent the intensity of both the incident and diffracted X-rays, further reducing the specimen volume irradiated by the incident X-rays and reducing the intensity of the diffracted X-rays.

Nevertheless, if specimens can be well prepared with extra caution and care, as demonstrated in this study, both 1DXRD and 2DXRD can be used to quantify the fabric and its evolution in soft clays, and yield consistent results. The quantitative temporal fabric evolution data obtained in this study provide direct experimental evidence to support prior hypotheses on soil thixotropy: upon resting, a remolded clay can increase in strength and stiffness with time even without receiving any external energy or input. Such

phenomenological strengthening and stiffening stem from internal microscopic processes, and soil microfabric evolution is definitely one of these particle-level mechanisms responsible for thixotropy.

4.4.2 Multiple Mechanisms of Thixotropy

In this section, multiple mechanisms of thixotropy in soft clay are summarized and discussed based on the multiscale experimental results (this chapter and study presented in Chapter 3) as well as some former findings from the literature, for a better understanding of clay thixotropy, a fundamental time-dependent soil behavior. As mentioned previously, the microscale experiments including 1DXRD and 2DXRD uncover that the thixotropic hardening of soft clays results, at least partially, from the microstructural evolution, mainly particle rearrangement such as particle reorientation, aggregation, and flocculation, which continuously occurs during the entire thixotropic hardening process. For kaolinite minerals with fewer surface charges and two dissimilar basal planes (i.e., one O plane, while the other OH plane), hydrogen bonds between the O and OH planes tend to cause kaolinite particles to form face-to-face associated aggregates. For other minerals such as illite and smectite, similar phenomenon may take place resulting from other interparticle forces, such as van der Waals attraction, Coulomb attraction, and cation bridging, but not so much hydrogen bonding. In fact, the BBC has a relatively higher natural salinity.

Of the aforementioned different modes of microscale particle movement, aggregation tends to increase parallel orientation resulting from face-to-face association, while flocculation usually induces more random orientation due to face-to-edge association (Mitchell and Soga, 2005). Based on the 1DXRD and 2DXRD results, each of them

becomes dominant one at different stages. In the first stage, the microfabric starts to transform, most likely via rotation or reorientation, from a dispersed (i.e., resulting from large-strain shearing and remolding) to a flocculated one, and both the orientation index and texture index decrease. The second stage is dominated by the particle aggregation. The particles tend to attract to each other to form face-to-face association because of the predominant hydrogen bond, van der Waals attraction, Coulomb attraction, and cation bridging, among others (O'Brien, 1971; Zhang et al., 2013b). As such, more aggregates or domains (a term mainly used to describe the smectite tactoids) are then formed, and hence orientation index and texture index increase. In the later stages, clay aggregates become more face-to-edge associated (i.e., flocculated) fabric until a more aggregated-and-flocculated microstructure is formed, resulting from the long-term particle rearrangement that eventually moves the enclosed clay system toward the minimal energy.

However, the thixotropy mechanisms are not limited to the particle rearrangement (i.e., aggregation and flocculation). Zhang et al. (2013) conducted a novel micro/nano compression study on saltwater clay flocs that have nearly zero effective stress or self-weight, and they concluded that the rearrangement of structural flaws (e.g., induced by remolding or shearing) towards a greater uniformity is another microscale mechanism contributing to the macroscopic thixotropic behavior. In addition, another different study, based on the quantitative pore size distribution of soft clays, also concluded that homogenization of pore size distribution takes place during the thixotropic process (Zhang et al., 2017). Similar mechanisms were also proposed by Díaz-Rodríguez and Santamarina (1999) involving the homogenization of nonuniform pore pressure distribution during thixotropy. In essence, although these findings refer to different physical properties of soils,

a key concept common to these studies is that the enclosed clay system, without any external input or disturbance, tends to homogenize any prior disturbance that is distributed nonuniformly within the system. In fact, the remolded clay always aims to achieve a uniform distribution of energy within the enclosed system through structural rearrangement and redistribution of porewater pressure and interparticle forces. Since the clay during thixotropy is in a physically enclosed system that holds a constant total energy, it is reasonable to observe differences in local energy as well as energy homogenization and equilibrium at different locations within the enclosed soil system, just like transport of thermal energy, advection of hydraulic energy, or diffusion of chemical potential.

Finally, the third mechanism involves the time-dependent contact bond development and strengthening. In fact, such a microscopic mechanism has been hypothesized or postulated in prior literature, particularly for clays, other geomaterials, and colloids (Angelini et al., 2014; Meng et al., 2008; Roussel et al., 2012). However, partly due to the limitations of microscopic experimental techniques, direct evidences are not available until a very recent article describing an experimental study on the contact and macroscopic aging in colloidal suspensions (Bonacci et al., 2020). In this article, one of the major conclusions is that contact-controlled aging, consisting of progressive stiffening of the particle-to-particle contacts, governs the increase in the shear modulus of two colloid systems (e.g., aqueous dense silica and polymer latex suspensions) at moderate ionic strengths. Although the above findings are obtained from colloids, it is logical to conclude that microscopic contact aging can also occur in clays and hence contribute to the temporal evolution of both s_u and G_{max} of soft clays, which are of shear or frictional resistance in nature.

In summary, the above three microscopic mechanisms, including particle rearrangements, homogenization of physical disturbance, and contact aging, can be the major contributors to the macroscopic thixotropic hardening or stiffening of soft clays. While the former two are of structural evolution in nature, the latter is related to interparticle forces. In general, microfabric characterization techniques, such as the 1DXRD and 2DXRD used in this study, can quantify the microstructural evolution, but not the contact aging. Direct measurements of temporal evolution of interparticle forces are still challenging, although the aforementioned article (Bonacci et al., 2020) has successfully quantified the contact aging in isolated particle groups.

Further noteworthy is the linkage between the macroscopic thixotropic behavior and microscopic mechanisms. As shown in Figure 3.2 and Figure 3.4 as well as equation (3.4), the temporal thixotropic hardening consists of three components, of which the first is the instaneous, time-independent response. The transition in the hardening phenomenon (i.e., both the s_u and G_{max} curves exhibit two contrasting, dissimilar slopes) indicates that two different mechanisms control and contribute to the different rates of hardening during thixotropic process. According to Figure 3.4, the G_{max} still increases at a fast rate but not asymptotically to a constant even after two years of aging. This unusual phenomenon suggests that contact aging still plays a vital role at a prolonged duration. As concluded by Bonacci et al. (2020), contact stiffening, i.e., the growth of interparticle flexural rigidity, mainly contributes to the macroscopic shear modulus increase. Therefore, it is logical to conclude that fabric evolution or fabric aging mainly dominates the initial faster hardening, while contact aging plays the dominant role in the second phase, relatively slower hardening. However, both fabric aging and contact aging may occur simultaneously in a

thixotropic system. At certain times, one plays the primary role, while the other is secondary.

Temporal evolution of both microstructure and macroscopic s_u and G_{max} of both Prestige (Figure 4.17) and BBC (Figure 4.18) are compared. For Prestige, when the thixotropic curing time is < ~10 days, fabric aging plays the dominant role, and the mechanical properties increase dramatically. On the other hand, after ~10 days, fabric evolution tends to disappear, but contact aging starts to dominate the process, which is most likely due to the formation of thicker clay aggregates due to the hydrogen bonding-induced face-to-face association or contact. For BBC, the transition point is ahead of Prestige, and the Coulomb force via cation bridging dominates fabric and contact aging. The temporal evolution of model-derived I_R (Figure 3.6b) further validates the respective dominant roles of fabric aging versus contact aging at different stages: the initial fast decrease in I_R over a very short time indicates that the s_u increases much more rapidly than G_{max} (although both of them increases during this stage), while the slow increase in I_R at later prolonged time manifests the opposite (i.e., G_{max} increases more rapidly than s_u). Finally, the respective dominant roles of fabric aging versus contact aging can also be explained conceptually in a logical way: contact aging commences only after the particles come into real close contacts, and the latter requires particle movements such as reorientation and rearrangement. In other words, two particles that are apart or not in contact with each other may not develop real contact or contact aging.

4.5 Conclusions

In this study, both 1DXRD and 2DXRD were conducted to investigate the fabric evolution of two soft clays at their respective liquid limits during thixotropic hardening process, including a manufactured, relatively pure Prestige and a natural, multiphase BBC. Based on the above results and findings, the following major conclusions can be drawn:

- It is hypothesized that thixotropic hardening process in soft clays is controlled by three major mechanisms, including particle rearrangements, homogenization of disturbance, and contact aging, as reflected by the transition points in the macroscopic s_u and G_{max} hardening curves (Chapter 3). While structural aging appears to dominate the short-term thixotropic hardening, contact aging plays the primary role in the later stage, particularly for the continuous increase in shear modulus.
- It is interesting to observe that the G_{max} continuously increased (in Chapter 3) even when the measurement was taken after three years of curing, which also indicates the contact aging in addition to the structural aging and warrants further analysis on the preferred orientation by the microscopic experiments for a longer curing time.
- Continuous microfabric changes with time are observed for both the Prestige and BBC during the entire considered thixotropic curing duration, and the fundamental modes of fabric evolution are complex, including reorientation from the high shearing-induced parallel orientation, hydrogen bond-induced aggregation to form face-to-face associated particle groups, further flocculation of aggregates, and continuous formation of thicker aggregates. Both the *OI* and

TI from 1DXRD and 2DXRD respectively demonstrate these microfabric evolutions.

- Both 1DXRD and 2DXRD are viable techniques for quantitatively characterizing the temporal fabric evolution of wet clays, which provides direct and quantitative evidence for the fundamental microscopic mechanisms governing the thixotropic behavior of soft clays.
- Moreover, clay mineralogy and porewater chemistry, two factors that are not explicitly investigated in depth in this study, also show non-negligible influence on microfabric evolution, which warrants further investigation.

4.6 Acknowledgments

This work was supported by the National Science Foundation (NSF) under Award CMMI 1640306. Partial support was also received from the Charles F. Perrell Scholarship. The author greatly appreciates access to the beamline 11-ID-C at APS of Argonne National Laboratory and the technical help from Dr. Yang Ren. Thank Mr. Louis Raboin of the University of Massachusetts Amherst, for performing the critical point drying. The author also wants to thank Dr. Shengmin Luo for his help with the microscale experiments. This work also made use of the Shared Experimental Facilities (i.e., X-ray diffractometer) at MIT, supported in part by the NSF MRSEC Program under Award DMR1419807.

4.7 Declarations of Interest

None.

Table 4.1 Fabric indexes of the two studied clays during thixotropic process

Time (d)	*OI*		*TI*	
	Prestige	BBC	Prestige	BBC
0	23.3	3.8	1.005	1.024
1	25.1		1.008	
2		3.4	1.006	1.029
3				1.010
4			1.005	
6		4.5		1.024
7	22.4			
9			1.004	
10				1.022
12			1.005	
14		4.0		
16	36.6			
18				1.021
28	26.5	3.3		
62	23.1	2.8		
119	30.5			
125		3.0		

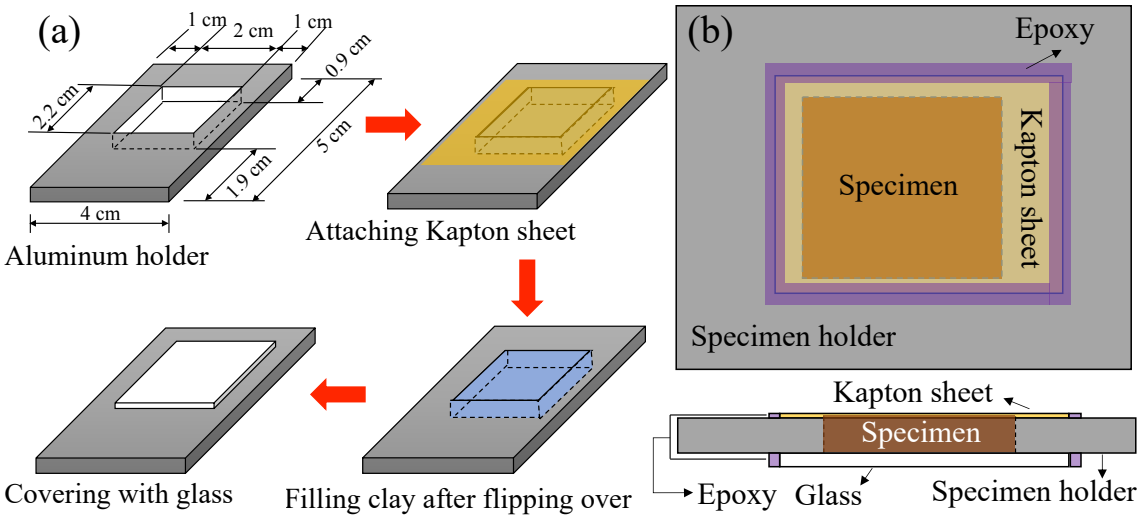

Figure 4.1 Sample preparation for *OI* measurements: (a) schematic showing back-loaded process; (b) a prepared clay specimen in the holder.

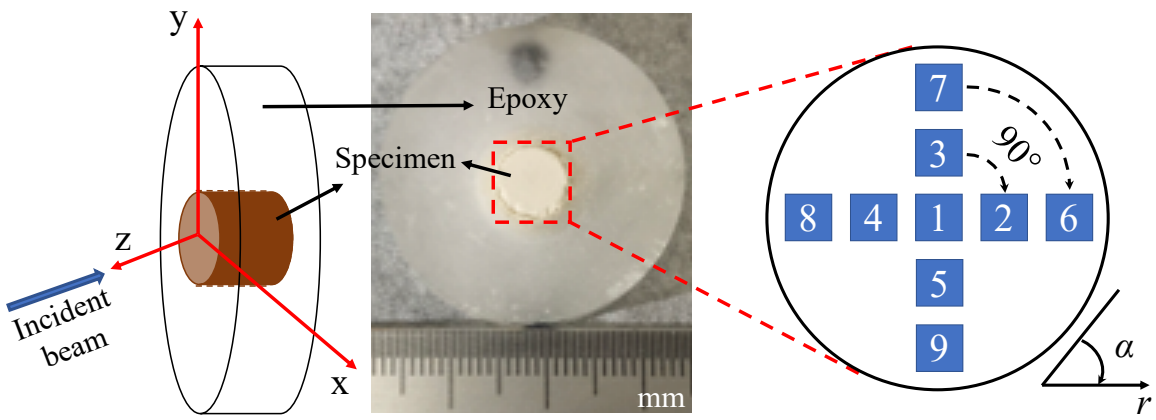

Figure 4.2 CPD-prepared specimen for 2DXRD: orientation configuration and scanned locations.

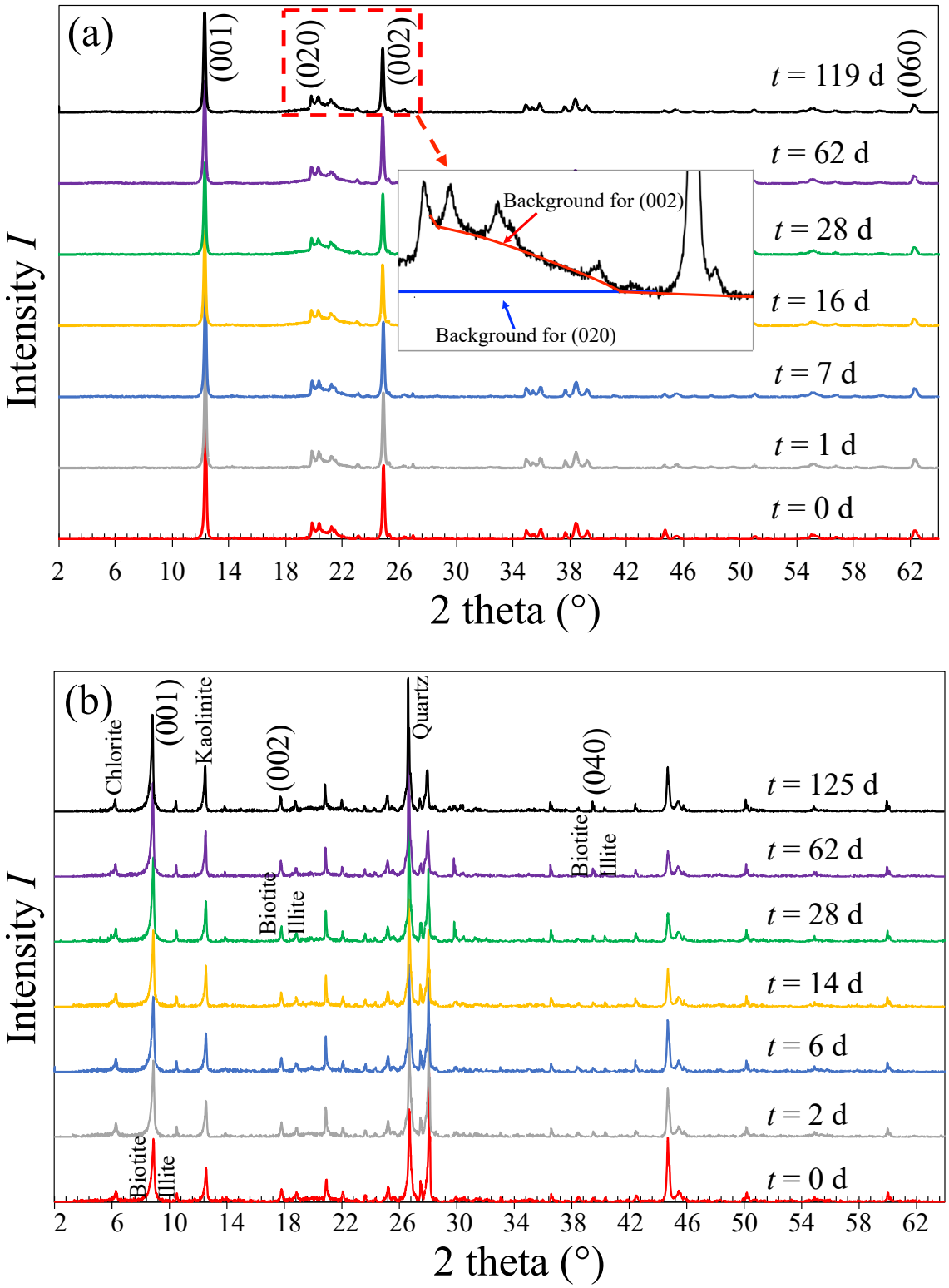

Figure 4.3 1DXRD patterns acquired at different curing times (BG stands for background): (a) Prestige; (b) BBC.

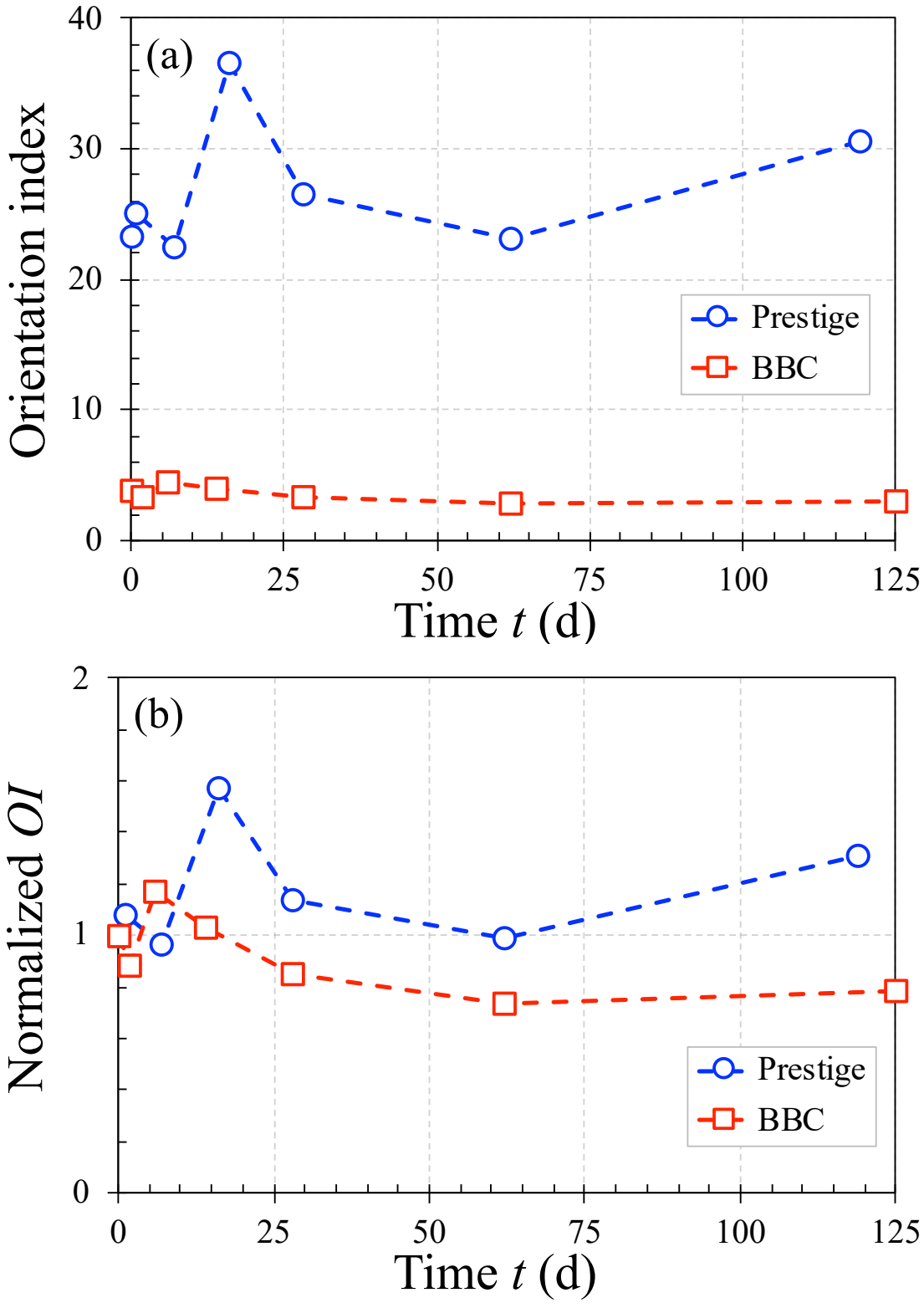

Figure 4.4 Relationship between the orientation index and time: (a) *OI*; (b) normalized *OI*.

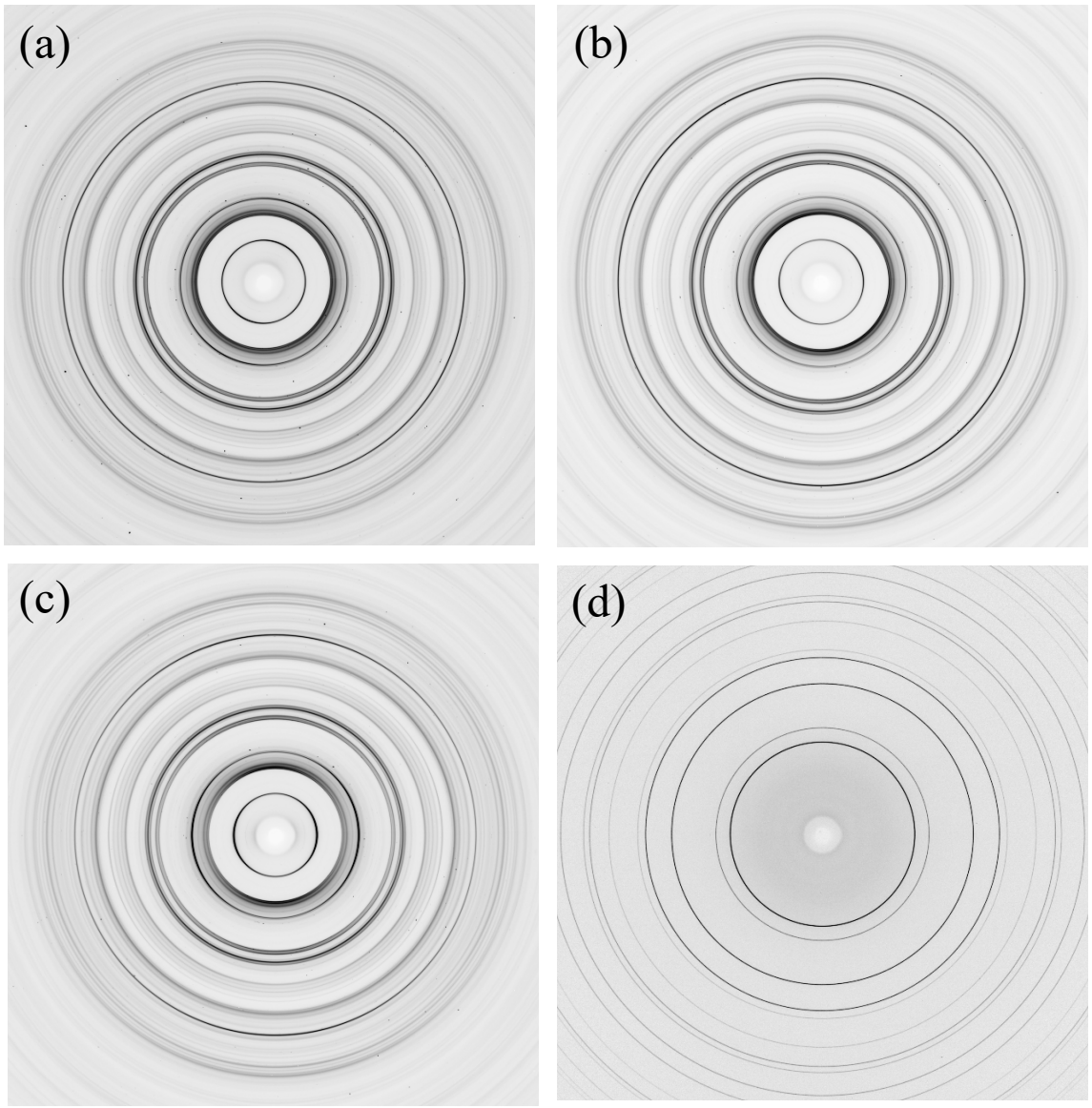

Figure 4.5 Example 2DXRD diffraction images with Debye rings measured from the 0 day-cured Prestige specimen: (a) location 1; (b) location 2; (c) location 6; (d) CeO_2 standard.

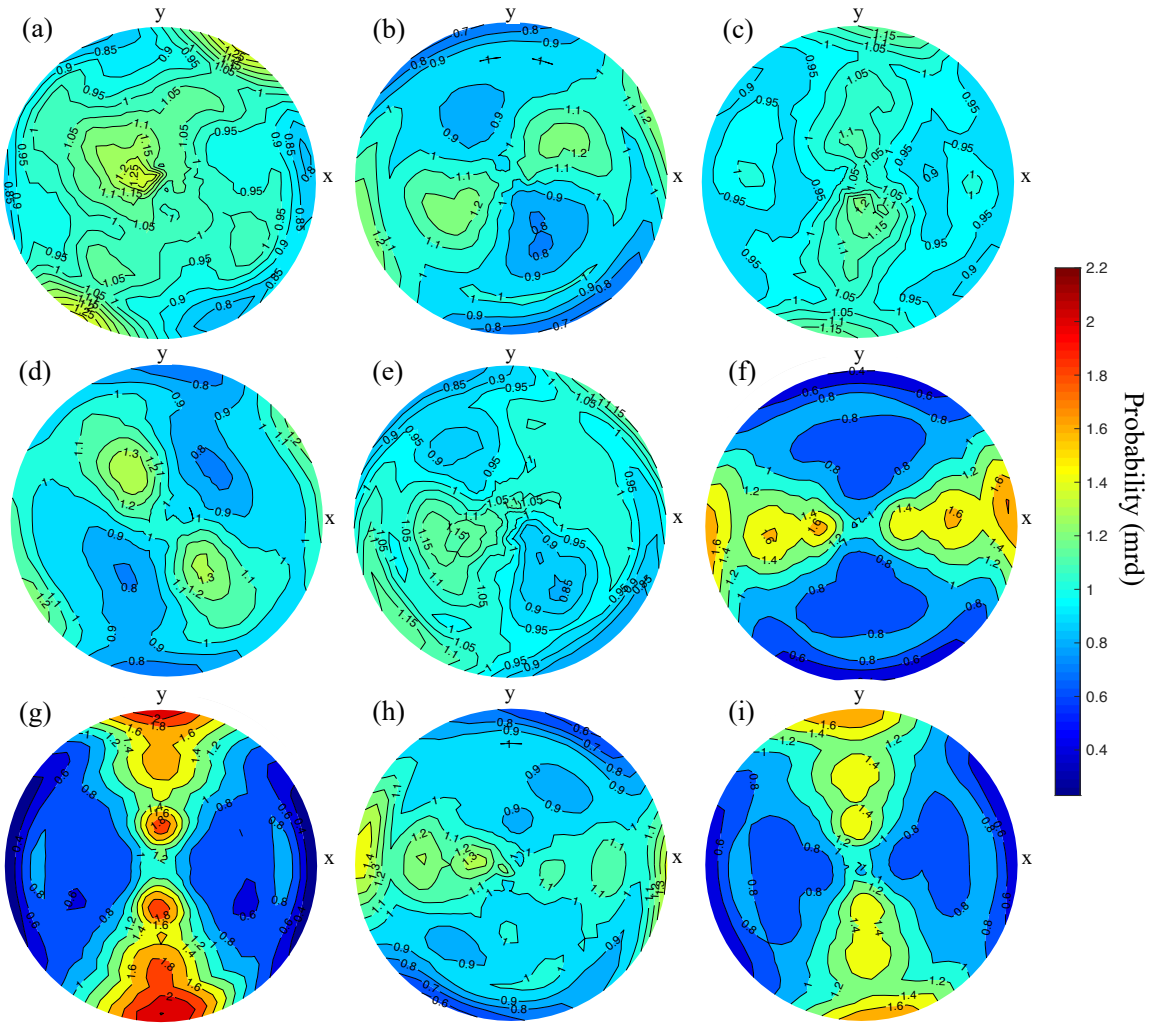

Figure 4.6 Pole figures of (001) basal plane for a Prestige specimen after 0 d curing for locations: (a) 1; (b) 2; (c) 3; (d) 4; (e) 5; (f) 6; (g) 7; (h) 8; (i) 9 (mrd: multiples of random density).

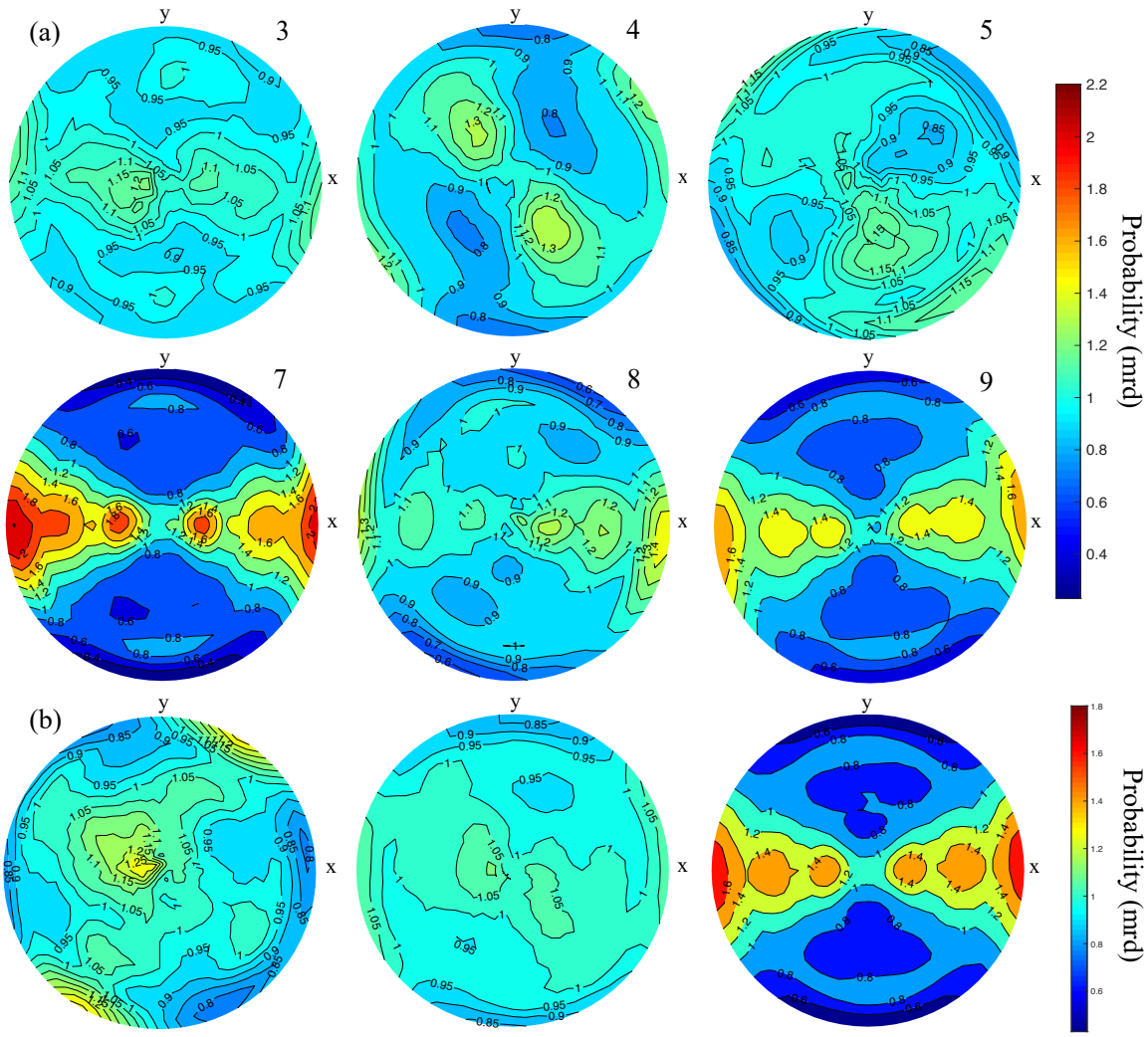

Figure 4.7 Data averaging for the (001) basal plane of a Prestige specimen after 0 d curing: (a) pole figures for locations 3 to 5 and 7 to 9 after rotation; (b) averaged pole figures for the Center, Middle, and Edge (from left to right) sub-groups of the scanned locations.

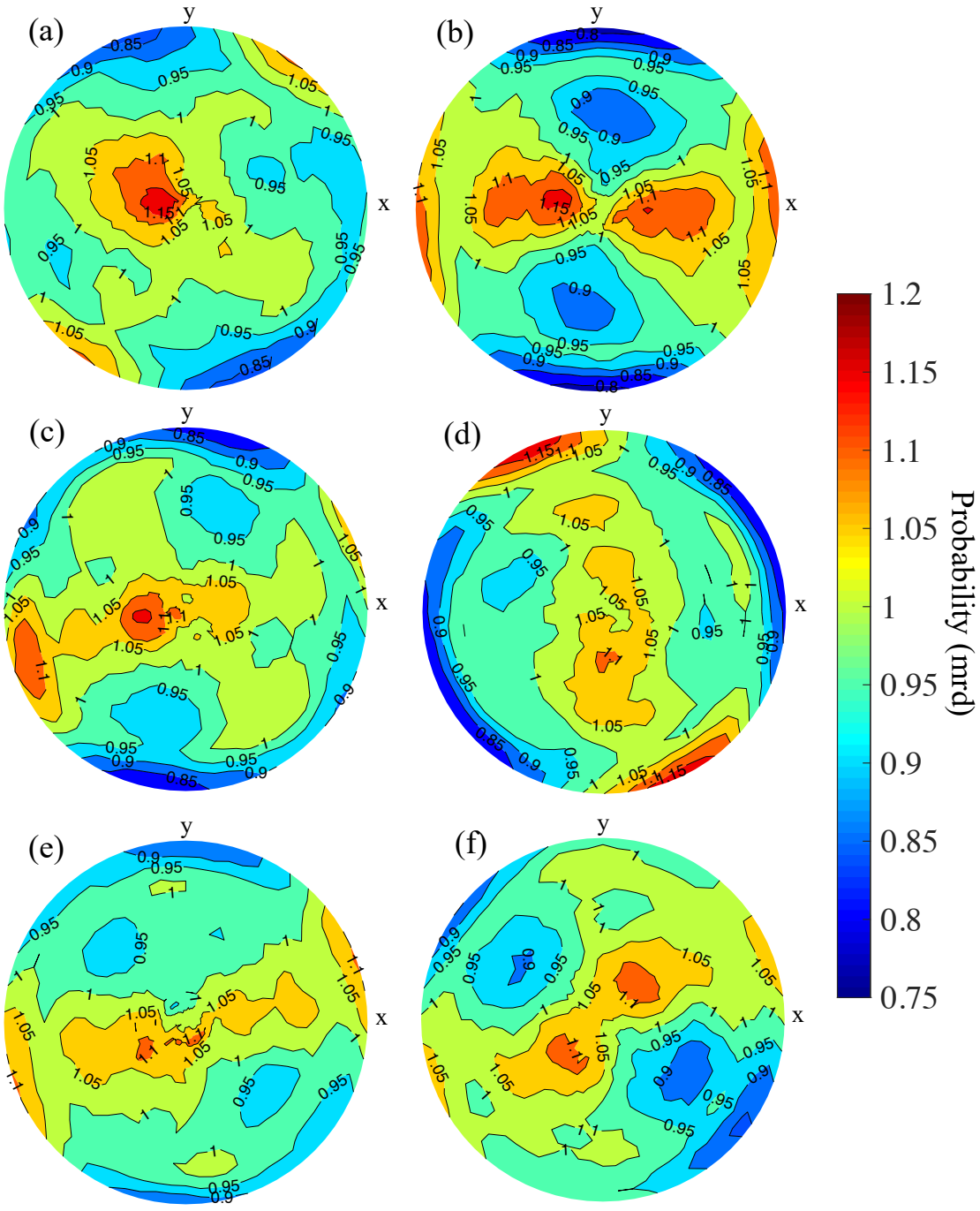

Figure 4.8 Pole figures of (001) basal plane of Prestige specimens at different thixotropic curing times: (a) 0 d; (b) 1 d; (c) 2 d; (d) 4 d; (e) 9 d; (f) 12 d.

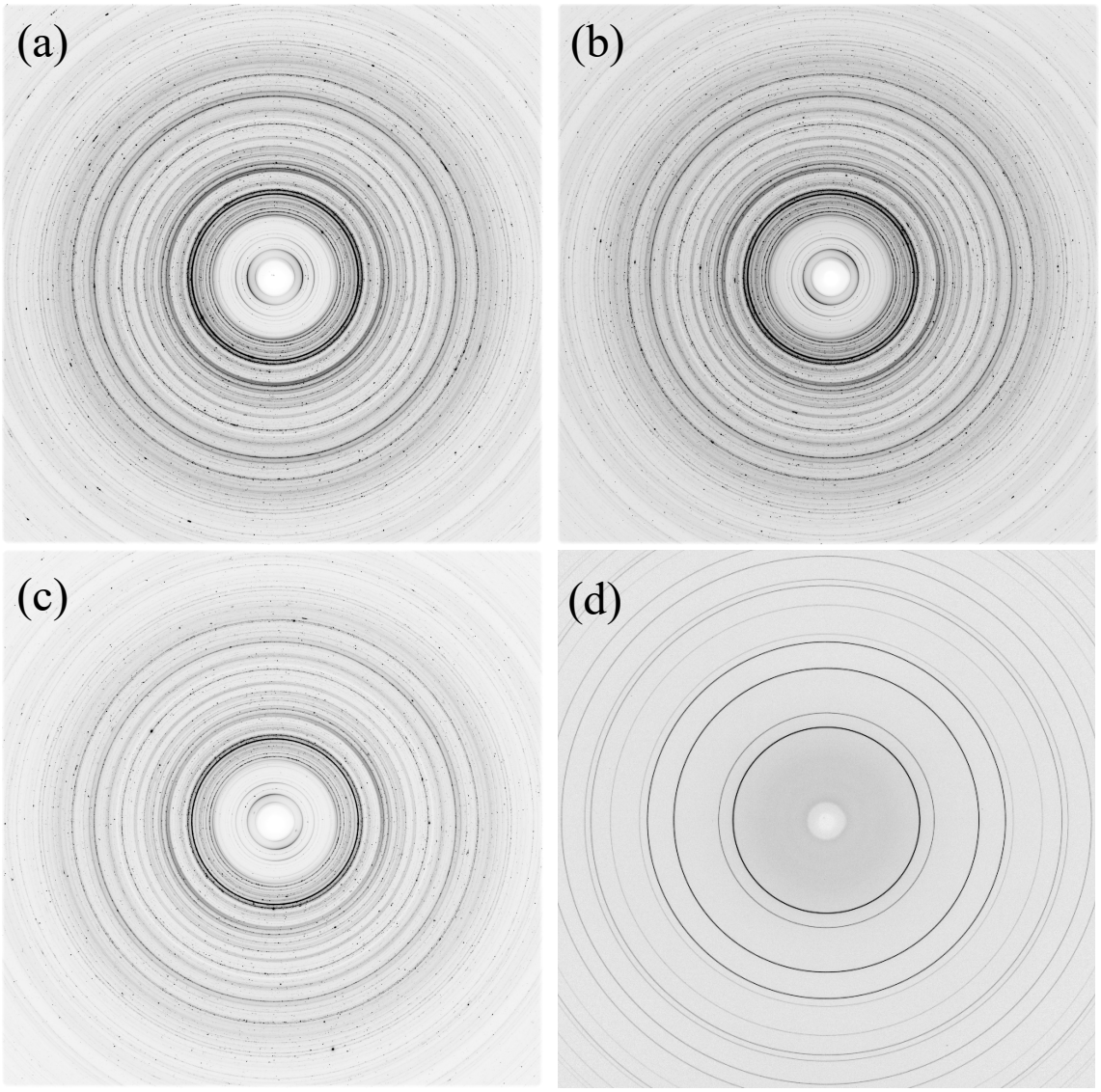

Figure 4.9 Example 2DXRD diffraction images with Debye rings measured from the 0 day-cured BBC specimen: (a) location 1; (b) location 3; (c) location 7; (d) CeO_2 standard.

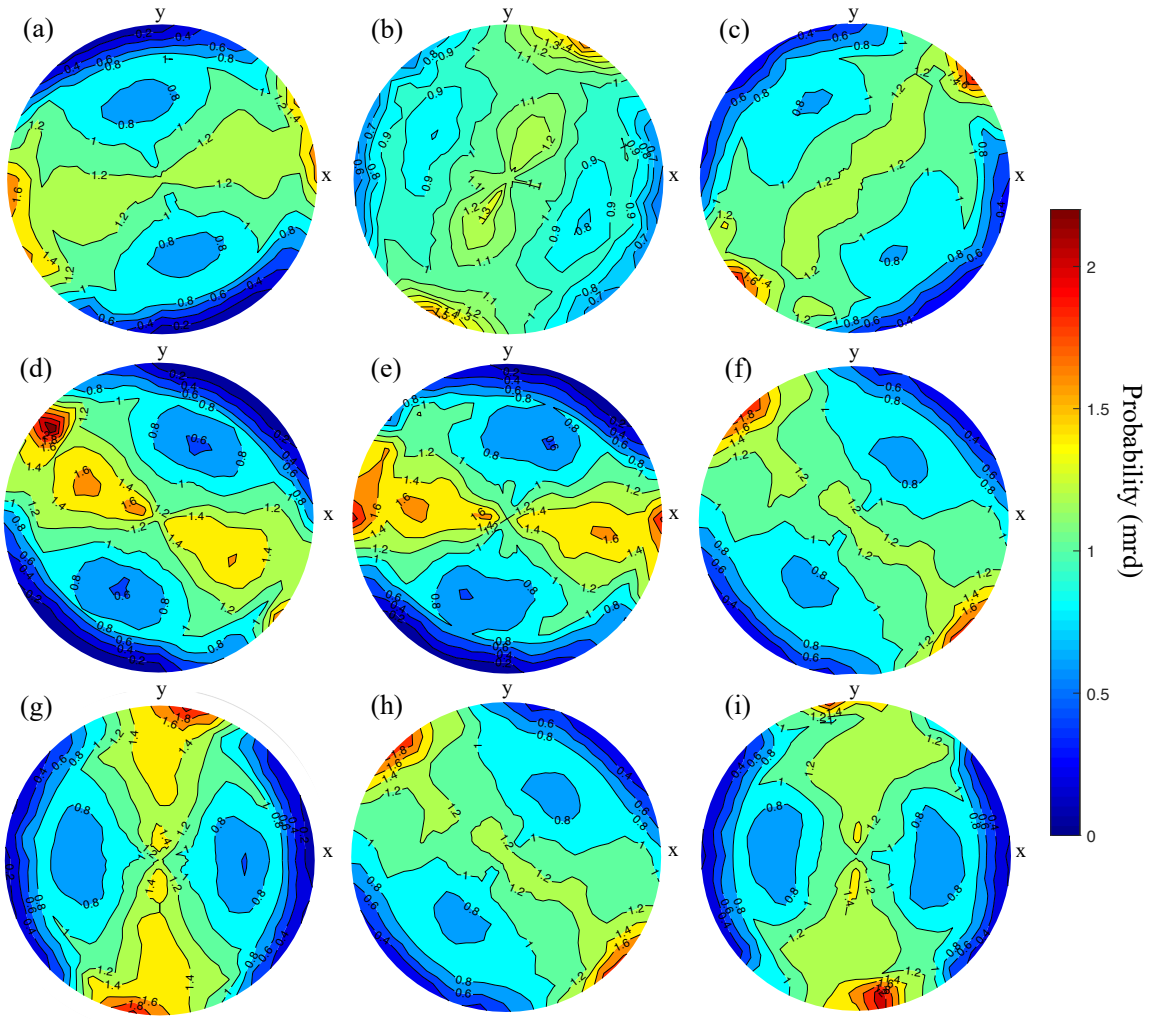

Figure 4.10 Pole figures of (002) basal plane of illite in the BBC specimen after 0 d curing at locations: (a) 1; (b) 2; (c) 3; (d) 4; (e) 5; (f) 6; (g) 7; (h) 8; (i) 9.

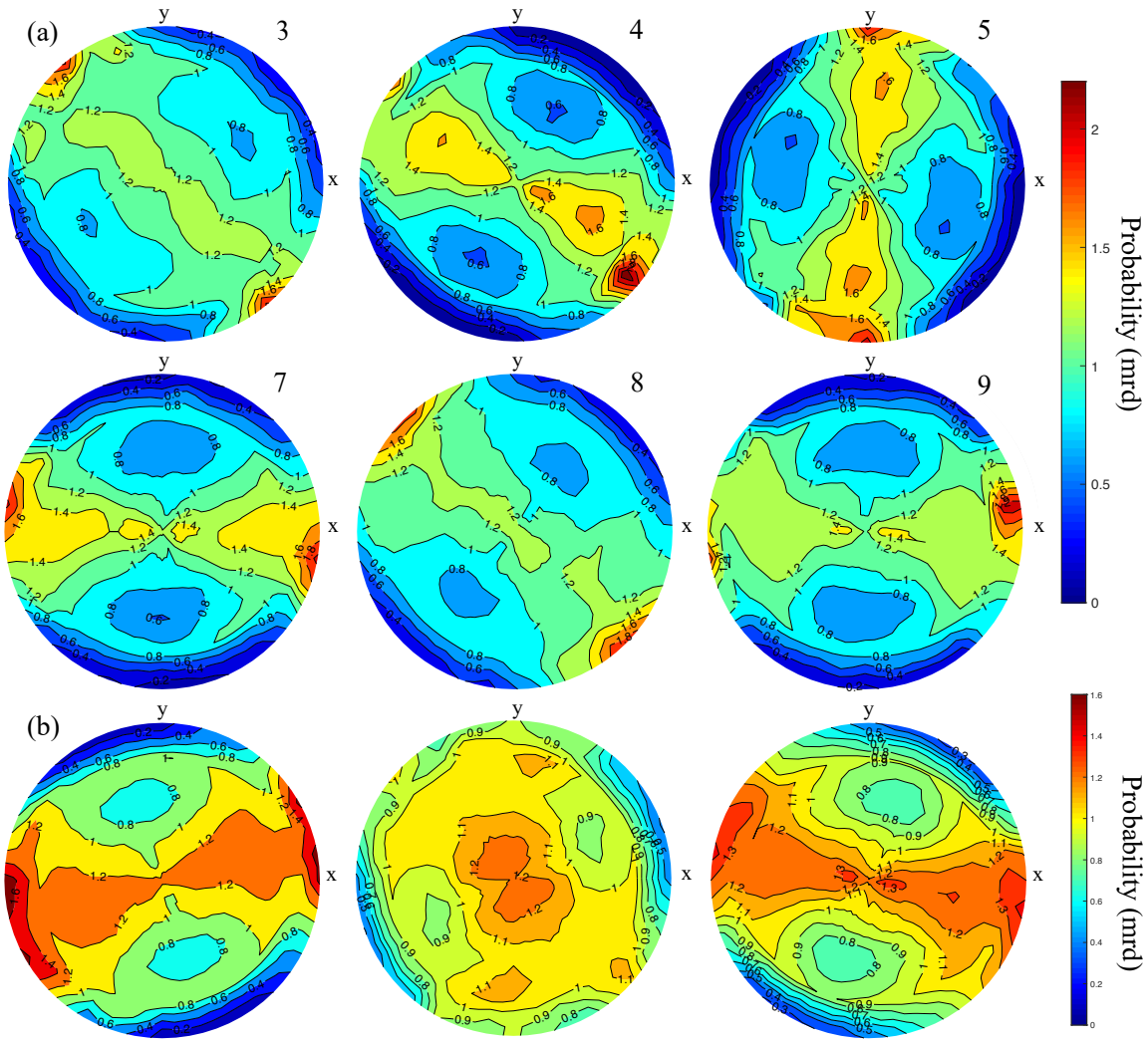

Figure 4.11 Data averaging procedure of (002) basal plane of illite in a BBC specimen after 0 d curing: (a) pole figures for locations 3 to 5 and 7 to 9 after rotation; (b) averaged pole figures for the Center, Middle, and Edge (from left to right) sub-groups of the scanned locations.

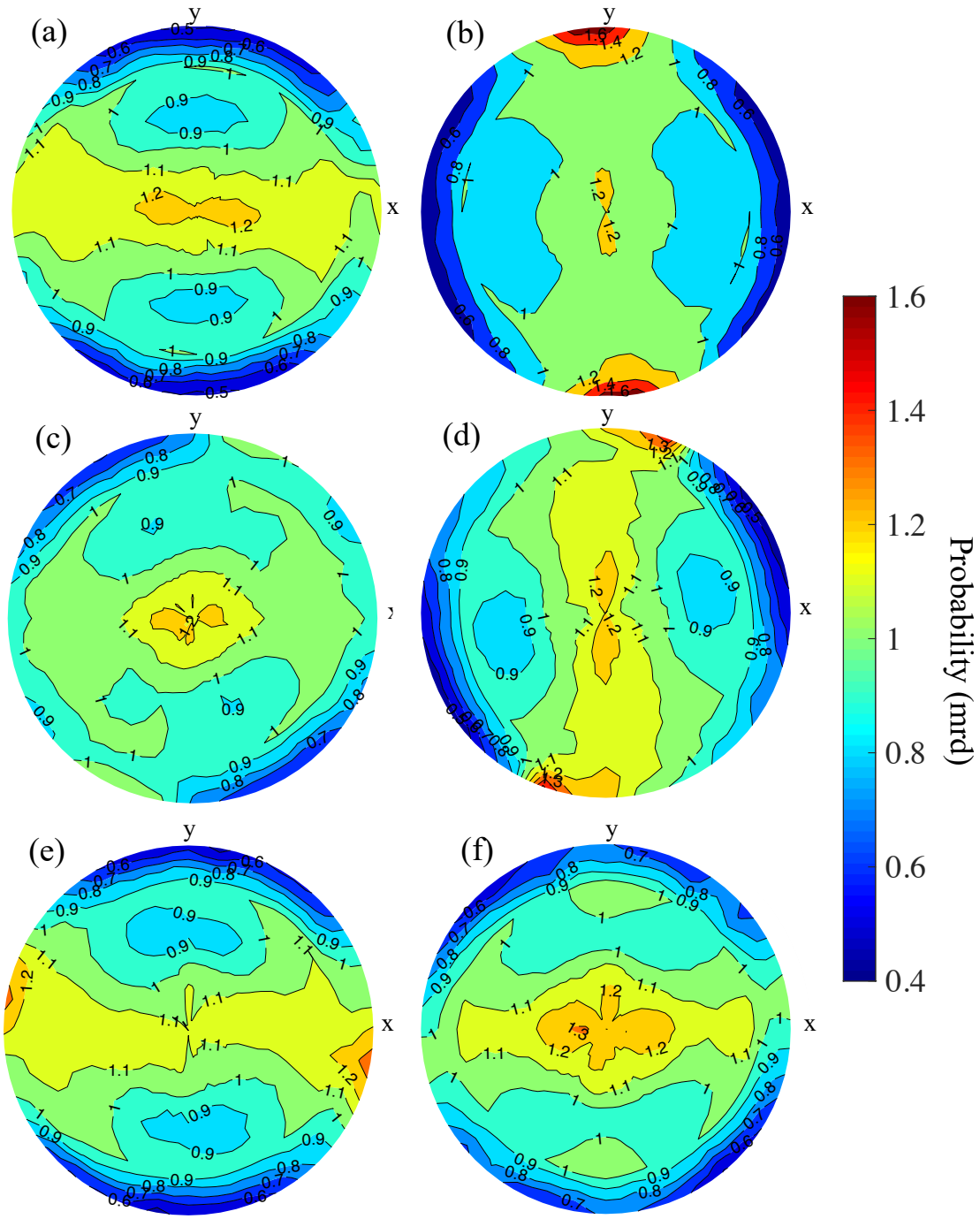

Figure 4.12 Pole figures of (002) basal plane of illite at different thixotropic curing times: (a) 0 d; (b) 2 d; (c) 3 d; (d) 6 d; (e) 10 d; (f) 18 d.

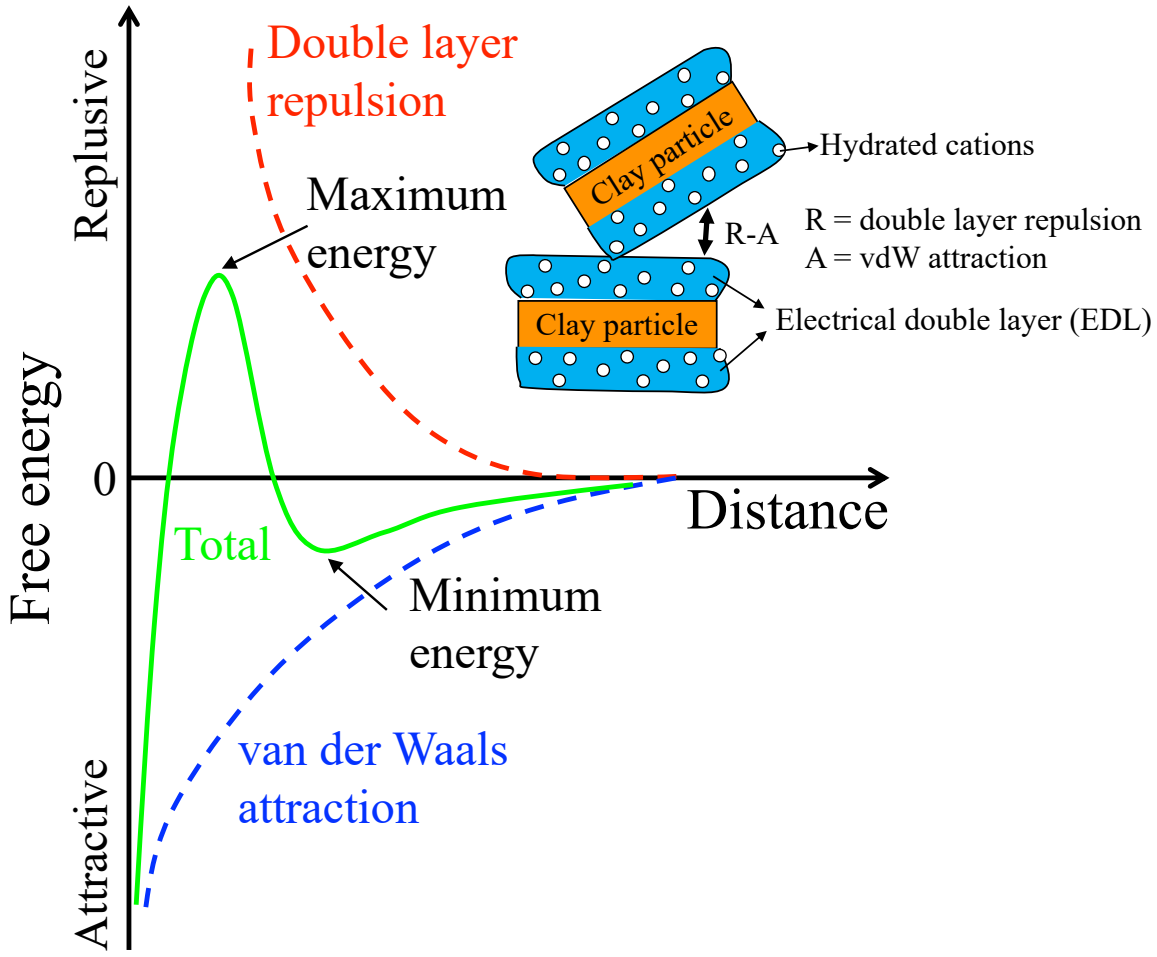

Figure 4.13 Interaction energy between two clay particles defined by the Derjaguin-Landau-Verwey-Overbeek (DLVO) theory.

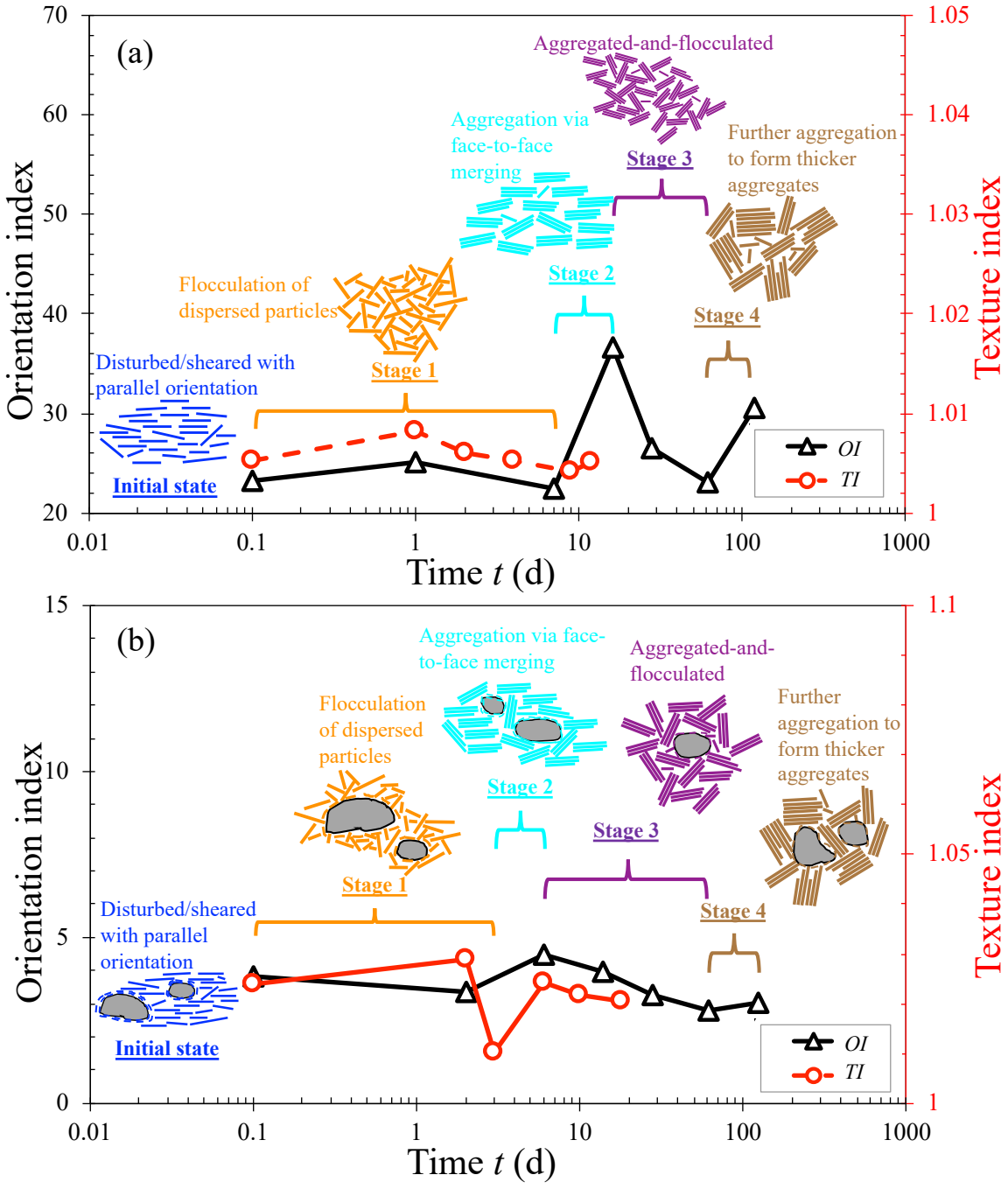

Figure 4.14 Comparison between the *OI* and *TI* and illustration of a possible interpretation of temporal microfabric evolution during thixotropy: (a) Prestige; (b) BBC (note: data at 0.1 d represents the measurement at zero time).

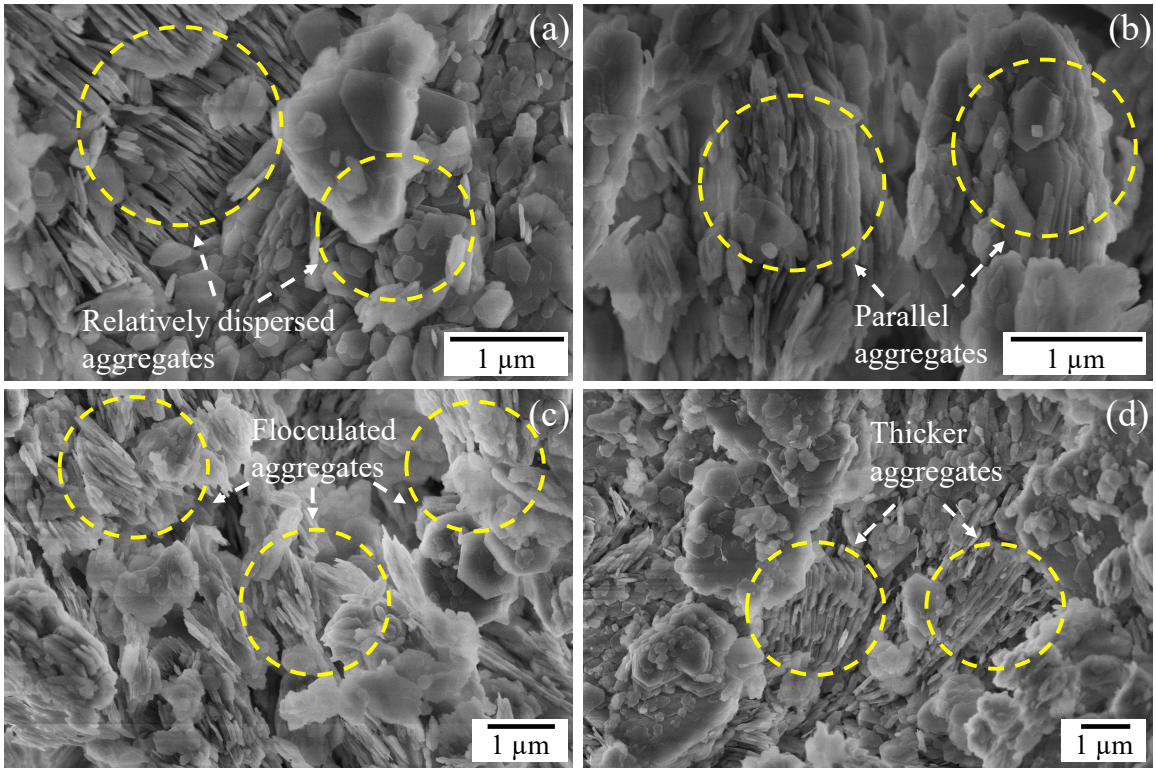

Figure 4.15 Selected SEM micrographs showing the complex fabric of the 6-day thixotropically cured Prestige specimen: (a) relatively dispersed aggregates; (b) clay particle aggregates with a parallel face-to-face configuration; (c) randomly orientated clay aggregates; (d) thicker aggregates.

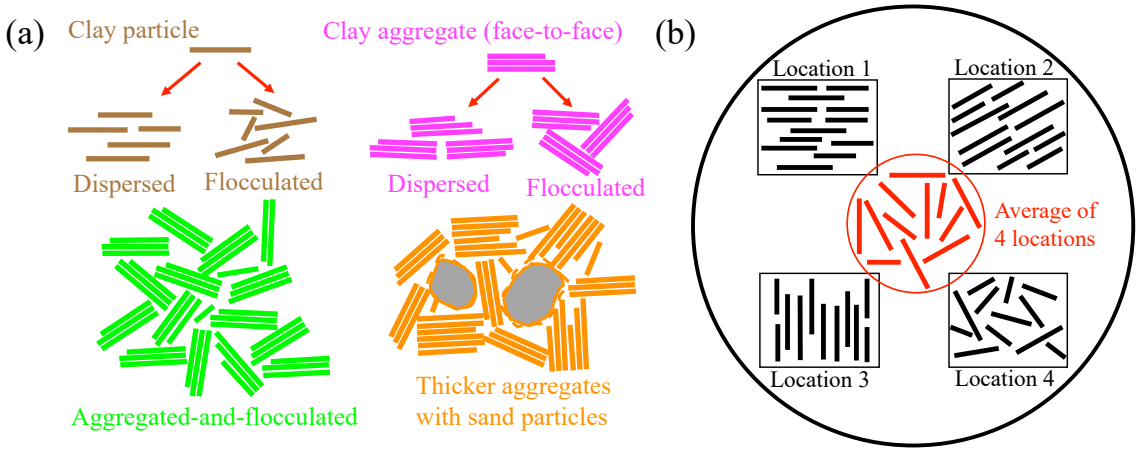

Figure 4.16 (a) schematic illustration of various microfabric patterns; (b) one possible reason for the small averaged *TI*.

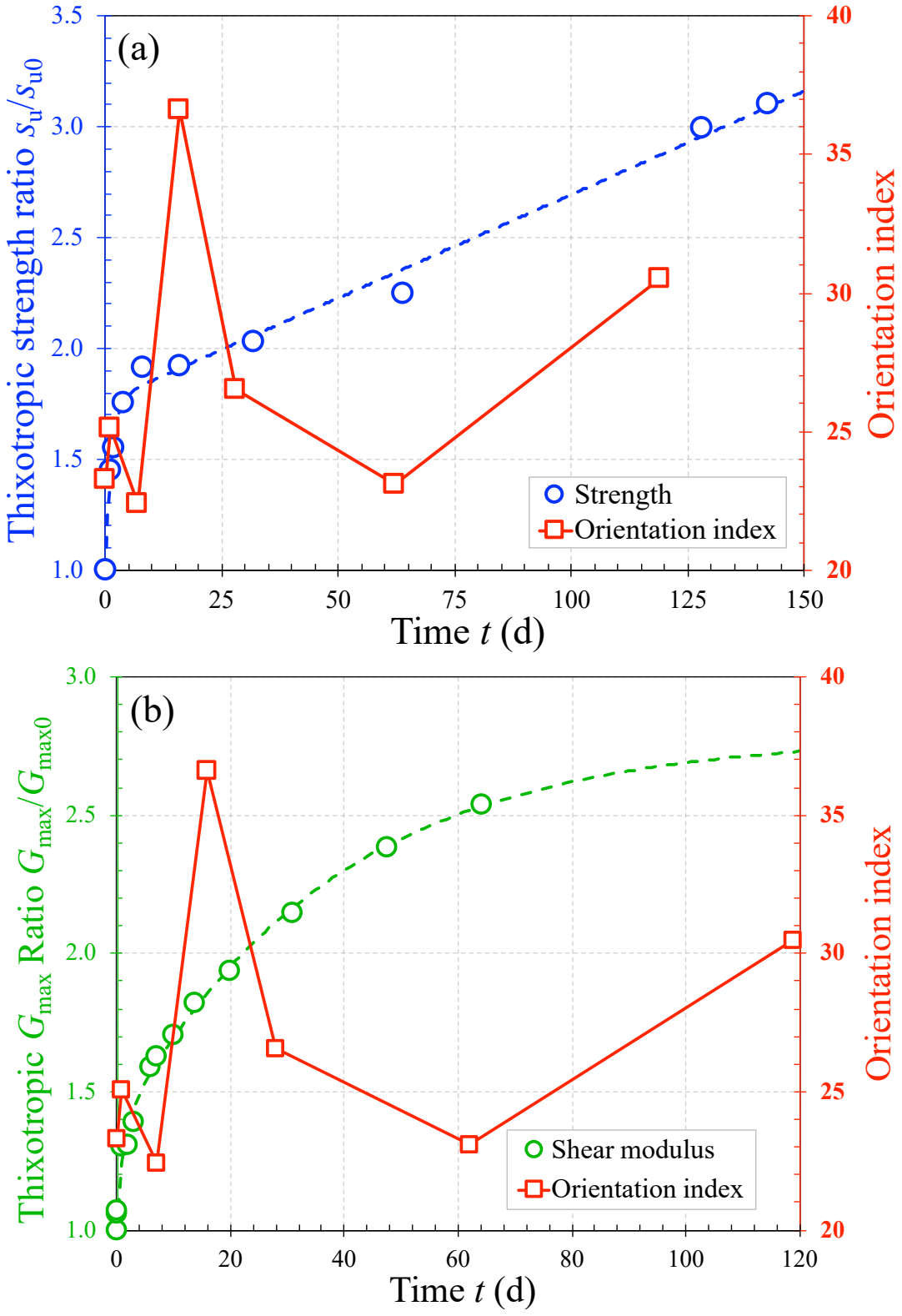

Figure 4.17 Comparison between the TSR and normalized G_{max} vs. *OI* of Prestige specimens: (a) TSR; (b) normalized G_{max}.

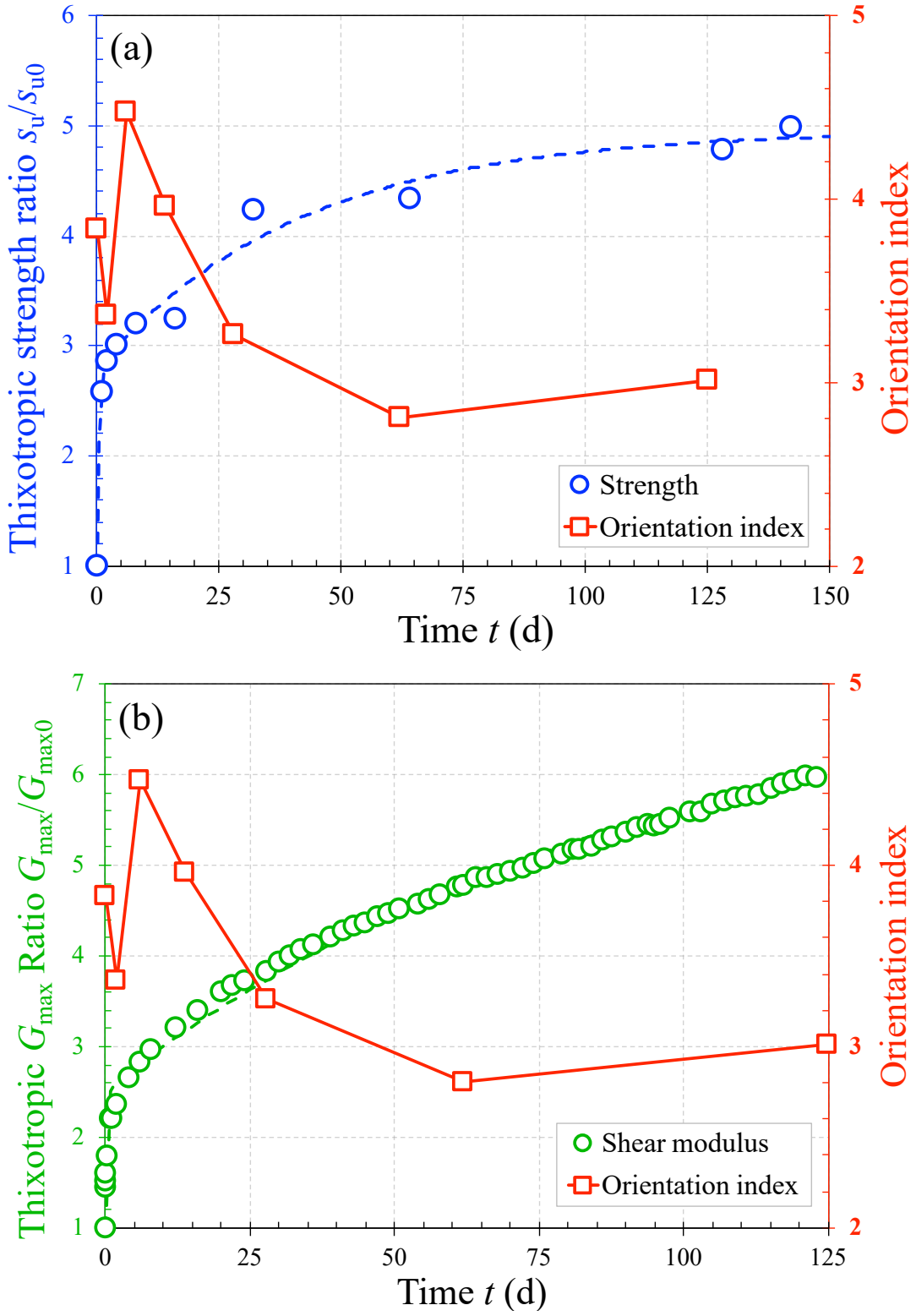

Figure 4.18 Comparison between the TSR and normalized G_{max} vs. *OI* of BBC specimens: (a) TSR; (b) normalized G_{max}.

CHAPTER 5

INFLUENCE OF POREWATER SALINITY ON THIXOTROPY OF SOFT CLAYS

This paper presents results from a multiscale experimental study on the influence of porewater salinity on the thixotropic behavior of two manufactured, relatively highly purified clays that contain mainly kaolin and smectite, respectively, and a naturally occurring, illite-rich, soft marine clay. The temporal evolution in the undrained shear strength s_u for each clay at four different target porewater salinities was assessed by fall cone testing, while microfabric changes were probed by one-dimensional X-ray diffraction. Results indicate the influence of clay mineralogy besides the porewater salinity on thixotropy. An optimum porewater salinity exists, varying from clay to clay, at which a soft clay may exhibit the highest thixotropic regain in strength. It results from a greater degree of microfabric changes. The increasing porewater salinity, which reduces the thickness of electrical double layer (EDL) on the external surfaces of the clay particles, advances the flocculation and improves the aggregation. However, the enhanced flocculated structure and stronger mineral contact result in lower thixotropic regain. Additionally, the increased water surface tension and viscosity result from increasing porewater salinity hinder the rearrangement (e.g., reorientation) or movement of the clay particles, which further weaken the microfabric of clay with a lower thixotropic gain.

5.1 Introduction

Most clays, except those which have been heavily over-consolidated, lose a proportion of their strength when remolded (Skempton and Northey, 1952), and the loss of intact undrained shear resistance often results from large-strain shearing of clays, like

sampling, in situ testing, and infrastructure installation. However, the strength or stiffness of either partially or fully remolded clays can gradually increase with time under conditions of constant composition and temperature (Mitchell, 1960; Seng and Tanaka, 2012; Zhang et al., 2017). It is one of the oldest documented rheological phenomena termed as "thixotropy" (Barnes, 1997; Larson and Wei, 2019; Mewis, 1979; Mewis and Wagner, 2009). In physics and engineering, many materials, such as clay suspensions, crude oils, paints, and coatings (Arnold and Goodeve, 1940; Chang et al., 1999; Gamble, 1936; Ma et al., 2018; Turner and Rodewald, 1949), exhibit thixotropic behavior. Thixotropy of soils is well described by Mitchell and Soga (2005) as an isothermal, reversible, time-dependent process occurring under conditions of constant composition and volume that it stiffens while at rest and softens or liquefies upon remolding.

In offshore geotechnical engineering practice, thixotropic hardening after soil remolding can be a significant consideration. For example, the installation of a driven pile or suction caisson will reduce the shear strength of the clay along the soil-structure interface to the remolded undrained shear strength (s_{ur}) (Andersen and Jostad, 2002). However, the shear strength of the clay along the interface after completion of installation will increase with time due to the combined effects of consolidation and thixotropy. For some clays, the regain in undrained shear strength (s_u) due to thixotropy alone can be greater than a factor of 2 (Peng et al., 2020; Yang and Andersen, 2016). A lot of soils in the near- and offshore environment are marine soft clays with saline water in the pore space and characterized as having a high water content, low strength, and high compressibility. Since clays are electrochemically very active, the presence of salt ions in the pore fluid has a significant impact on their geotechnical properties (van Olphen, 1963).

Numerous studies were conducted to investigate the effects of pore fluid salinity on engineering properties of clayey soils, including index properties, shear strength, compressibility, and sedimentation behavior (Gorakhki and Bareither, 2015; Jeong et al., 2012; van Paassen and Gareau, 2004; Yukselen-Aksoy et al., 2008). Pineda et al. (2013) highlighted the importance of how pore water salinity affects both clay compressibility and shear strength. The strength parameters of a soft clay studied showed a clear dependency on the pore fluid with a decreased in strength with a decrease in salt concentration. Di Maio (1996) summarized the behavior of bentonite specimens exposed to different types of salt solutions and concluded that specific chemical treatments might cause a lasting improvement of the mechanical properties of active clays. Since the concentration and compositions of ions in the pore fluid show significant impacts on the engineering properties of clays, it is reasonable to assume it also influences the thixotropic behavior of clays. (Zhang et al., 2013a) studied the thixotropism of micron-sized saltwater clay flocs but otherwise there is little data available on how salinity affects the thixotropic hardening of clays. The objective of the study presented in this paper was to investigate the influence of porewater salinity on thixotropic behavior of soft clays, and provide quantitative evidence to reveal the temporal microfabric evolution of clays at different salinities. The undrained shear strengths and microstructural evolution (e.g., rearrangement, reorientation, reaggregation) of each tested clay during thixotropic hardening were measured and quantified using fall cone (FC) and X-ray diffraction (XRD), respectively. Therefore, the overall objective of this experimental study was to quantitatively characterize the macroscopic thixotropic behavior and associated microstructure evolution of fully remolded soft clays at different porewater salinities through multiscale experimentation

and hence to have a better and systematic understanding of the influence of seawater on fundamental behavior of soft clays, which can generate significant practical impacts.

5.2 Materials and Methods

5.2.1 Materials

In this study, three soft clays with different mineralogy were studied, including Prestige, PureGold Gel, and Boston Blue Clay (BBC). Detailed determinations of index properties and mineralogical compositions of these clays are presented in Chapter 3.

5.2.2 Sample Preparation

Porewater salinity *r*, which has units of kg/kg (or g/g), is defined as the ratio of the mass of soluble salts to the mass of saltwater (i.e., the solution but not the solvent) (Burt, 2014). The definition is commonly used by geotechnical engineers. The natural porewater salinity of each clay was first determined by following the USDA Kellogg Soil Survey Laboratory Methods Manual (Burt, 2014). For each clay, 2 g of <2 mm air-dried powder was prepared and placed into a 15 mL tube (Fisher Scientific, Inc.) with 10 mL deionized (*DI*) water. The soil/water suspension was mixed and maintained at room temperature for 23 hours for equilibrium and better dissolution. Each specimen was then shaken for one hour at a speed of 100 oscillation min^{-1} by using Burrell Scientific Model 95 variable speed Wrist Action Shaker (Pittsburgh, PA). The suspension was then centrifuged for 20 minutes at 2000 rpm in a Champion F-33D Centrifuge (Ample Scientific, LLC, Norcross, GA, USA). 5 mL supernatant was extracted with a syringe assembled with a filter (Fisher Scientific, Inc.) since all three clays have high fine contents. Another 25 mL *DI* water was

added to dilute the supernatant, and the salinity of the dilution was determined using a Fisherbrand Traceable salinity meter (ISO 17025 Calibrated). The salt content of each clay can be determined since the mass of the salt and soil solids of the 2 g sample can be derived separately based on the measurements.

Different amounts of NaCl and *DI* water were added to the original clay to vary the porewater salinity. BBC was washed to bring the porewater salinity down to half of the natural salinity to prepare specimens at a lower salinity. The *LL* of each clay at four target porewater salinities were first determined, but the porewater salinity will change during the process as the soil dries. Therefore, clay samples for *LL* determinations were prepared at varying water contents with the same porewater salinity to compensate for this error. The water contents presented in this study were corrected since the salt content in the sample affects the measurements (Fugro, 2004).

5.2.3 Fall Cone Testing

The change of the undrained shear strength s_u of the soft clay specimens during thixotropic hardening was assessed using fall cone (FC) testing by following ISO 17892-6 (2017). For each clay, four batches of samples were first prepared by thoroughly mixing with different amounts of NaCl and *DI* water to achieve a consistency at or near its *LL* with target porewater salinity, followed by sealing in a plastic bag and storing in a temperature-controlled chamber set at 24 °C overnight for temperature and moisture equilibrium. The equilibrated samples were thoroughly mixed and remolded again, each of which was carefully filled into a series of jars as described in the Chapter 3 (section 3.2.2). All jars were stored underwater in a temperature-controlled water bath set at 24 °C to maintain a

constant water content during the entire hardening process. The series of carefully prepared specimens allowed multiple s_u measurements by following a pre-designed experimental schedule up to 142 days (e.g., 0, 1, 2, …, 64, 128, 142 days). The same method following Chapter 3 (section 3.2) was used to determine the s_u.

For quality control, after the fall cone measurement, each specimen was again fully remolded and tested again to ensure that the fully remolded undrained shear strength s_{ur} was equal to that measured at time $t = 0$. Moreover, the water content was also measured to compare with that at $t = 0$. If the final water content deviated from the initial one by 2%, then a new specimen was prepared, and all measurements were repeated. In addition to water content, the void ratio of each specimen was also determined.

5.2.4 Microstructural Characterization

Due to the limited access to the advanced analytical facilities, microstructure characterization was conducted only on Prestige and BBC. One-dimensional XRD (1DXRD), using the same X-ray diffractometer and configurations described in Chapter 4 (section 2.2) was utilized. The same customized aluminum sample holders and specimen preparation method was used to prepare specimens to probe microstructural evolution of each clay caused by thixotropy with different porewater salinities. Since the same specimen can be scanned at different curing times, only one specimen at each target porewater salinity was needed for the 1DXRD testing. All specimens were stored in a chamber with controlled relative humidity (RH) of nearly 99% to minimize possible water loss. Each specimen was retrieved from the chamber for XRD scanning at a particular thixotropic

hardening time and placed back for curing immediately upon completion of XRD measurements.

Orientation index (*OI*) can quantitatively describe the changes of the fabric of the specimen with platy clay particles during thixotropic hardening, which was explained in Chapter 4 (section 2.2). Meanwhile, other information, including reflection planes used to calculate the *OI*, method to determine the background profile, and identification of 2θ positions of all major reflections of kaolinite and illite, were also described in Chapter 4.

5.3 Analysis of Results

5.3.1 Soil Classification and Mineralogical Compositions

The results of the index properties of the three soft clays are listed in Table 3.1. The activity determinations of the three clays are consistent with what can be found in literature i.e., Montmorillonite has an activity > 1.0, illitic clays from 0.5-1.0, whereas kaolinites are from 0.3-0.5 (Casagrande, 1948; Mitchell and Soga, 2005). It can also be verified from the mineralogical compositions determined from XRPD as presented in Table 3.2. The major compositions of Prestige and PureGold Gel are kaolinite and montmorillonite, respectively. BBC, as a naturally occurring clay, contains more complex mineral phases, including a variety of clay minerals, such as illite, kaolinite, chlorite, and biotite, and other nonclay phases as minor fractions.

Four target porewater salinities (summarized in Table 5.1) were investigated for each clay. Figure 5.1 shows the determinations of Atterberg Limits (*AL*) for the three clays at different porewater salinities. PureGold Gel is porewater salinity-dependent, the *LL* of which dramatically decreases with increasing salinity. Comparing to PureGold Gel, *LL* of

Prestige and BBC are less sensitive to the pore fluid salinity, which slightly increases with increasing salinity. *PL* of all three clays shows little or no change with different salinities.

5.3.2 Undrained Shear Strength Measurements

Figure 5.2a to Figure 5.2c summarize the temporal evolution of s_u of the three clays at different thixotropic curing times up to more than 140 days. Generally, all the specimens show thixotropic hardening with a similar trend, except for the influence of porewater salinity as discussed in Section 5.4, a fast initial increase in s_u in the first few days, accompanied by a slower increase in s_u that tends to level off at prolonged curing durations. The initial fully remolded undrained shear strength s_{u0} is defined as the s_u at time $t = 0$ day (i.e., the starting point for the thixotropic process). It ranges from 1.3 to 1.5 kPa for Prestige, 1.8 to 2.2 kPa for PureGold Gel, and 1.4 to 1.8 kPa for BBC. To compensate for the difference of s_{u0} values, the normalized thixotropic strength ratios (TSR), s_u/s_{u0}, are also plotted in Figure 5.3d to Figure 5.3f. The TSR of Prestige ranges from 2.2 to 3.2 at $t = \sim$ 140 days, while PureGold Gel can reach the same range after ~50 days of curing. Additionally, BBC shows a much higher tendency of thixotropic hardening and can achieve a TSR ranging from 3.4 to 5.3 after 140 days of curing. The various extent of thixotropic hardening of each specimen was caused by the differences in porewater salinities and mineralogy.

Figure 5.3a shows that zero or very low salinity causes Prestige to have the fastest initial rate of thixotropic hardening (i.e., the strength increase rate is the fastest at the beginning of thixotropic process), but the overall trend of TSR is attenuated with increasing salinity for Prestige. BBC has a relatively high initial natural porewater salinity, the natural

salinity enables the BBC to exhibit the fastest rate of hardening, and the increasing salinity, in general, reduces the TSR (Figure 5.3b). For PureGold Gel, Figure 5.3f indicates that the highest rate of hardening and the highest TSR are at the intermediate salinity (0.017 g/g). An optimum porewater salinity exists, varying from clay to clay, at which a soft clay may exhibit the highest TSR and a lower TSR for other salinities below or above this critical value.

The dashed lines in Figure 5.2 and Figure 5.3 represent the best fit of s_u and TSR data for all the specimens using modified Burgers' five parameter model (Barnes, 2000). The two-part thixotropic behavior of all the specimens, including a rapid increase in s_u at the initial phase over a very short time and a slow increase in s_u later over a prolonged time, can be efficiently described by the model. The equation is expressed as $M = c_1 + c_2(1-\exp(-c_3 t)) + c_4(1-\exp(-c_5 t))$, and detailed fitting parameters c_1 to c_5 and the coefficient of determination R^2 are summarized in Table 5.2. Since the fitting parameters, c_3 and c_5, are indications of the degree of viscosity of the clays (Peng et al., 2021a), the results show they are greatly affected by both the clay mineralogy and porewater salinity. In general, low to moderate low porewater salinity (0-0.017 g/g) can improve the rigidity of BBC and PureGold Gel, whereas imposing the opposite effect on Prestige. Moderate low to moderate porewater salinity (0.017-0.034 g/g) tends to reduce the rigidity of BBC and PureGold Gel but increases it of Prestige. Moreover, moderate to high porewater salinity (0.034-0.068 g/g) can increase the rigidity of BBC but lower it of Prestige and PureGold Gel.

As part of the quality control, both the water contents measured after all FC measurements and void ratio computed from phase relationships for all specimens are

shown in Figure 5.4. The void ratio calculations indicate that all specimens were consistently prepared in this study. The water content measurements show little variation and verify that these specimens did not experience noticeable water loss during the thixotropic process.

5.3.3 Microstructural Evolution

Figure 5.5 and Figure 5.6 show the diffraction patterns without general backgrounds, which were collected from Prestige and BBC specimens at varying porewater salinities cured for up to 125 days. The *OI* values of each clay at four different porewater salinities are compared in Figure 5.7a and Figure 5.7b. To ensure the change in the fabric of each specimen was not caused by drying, the water content of each specimen was checked prior to each XRD scan. Statistics of all water content measurements listed in Table 5.3 indicate no detectable water loss during 125 days of curing and storage.

The magnitude of *OI* suggests the degree of preferred orientation of clay particles and decreasing *OI* represents the particle reorientation towards a more flocculated structure, while increasing *OI* represents the particle aggregation to form particle groups. A previous study conducted by the author summarized three microscopic thixotropisms contribute to the macroscopic hardening of soft clays and suggested that the soil fabric transformed into a more flocculated state with thicker clay aggregates during thixotropy (Peng et al., 2021a). Similar results can also be observed on these specimens except effects of different porewater salinities on the changes of the soil fabric. The continuous changes of *OI* of each salinity indicate the temporal fabric evolution during thixotropic hardening, including reorientation, aggregation, and flocculation. For Prestige, low and moderate porewater

salinity (e.g., 0 and 0.034 g/g) show similar patterns, and higher thixotropic gain in strength can be observed from FC, while for the other two higher salinities are similar to each other but with relatively lower thixotropic gain in strength. Since BBC contains a high fraction of non-clay minerals, the specimens show much smaller *OI* values than Prestige, and all patterns show comparable trends. In general, higher thixotropic gain in strength results from greater *OI* changes. The increasing porewater salinity, which reduce the thickness of electrical double layer (EDL) on the external surfaces of the clay particles, advances the flocculation and improves the aggregation.

5.4 Discussion and Practical Implications

Both fabric evolution and contact aging contribute and are responsible for the two stages of thixotropic hardening as discussed in Chapter 4 and Peng et al. (2021a). Fabric evolution plays a dominant role in the initial faster hardening, while contact aging dominates in the latter relatively slower hardening. The EDL thickness ($1/\kappa$) can be estimated according to Derjaguin-Landau-Verwey-Overbeek (DLVO) theory using the following equation (Mitchell and Soga, 2005):

$$1/\kappa = \sqrt{\varepsilon_0 DkT / 2n_0 e^2 \upsilon^2} \tag{5.1}$$

where ε_0 is the permittivity of vacuum, 8.8542×10^{-12} $C^2J^{-1}m^{-1}$; D is dielectric constant; k is Boltzmann constant, 1.381×10^{-23} JK^{-1}; T is absolute temperature, 297 K (24°C); n_0 is electrolyte concentration, e is electronic charge, 1.602×10^{-19} C; and υ is cation valence.

Since NaCl was added to alter porewater salinity, υ can be assumed as 1 (monovalent) for simplicity. BBC is a marine clay, while the dissolved salts in seawater are predominantly sodium (Na^-) and chloride (Cl^-) ions. Therefore, NaCl can be assumed

as the only type of salt to calculate n_0 for each specimen. The dielectric constant D, which decreases as the salinity increases, was first determined and plotted in Figure 5.8a. The EDL thickness of each clay at different salinity was then calculated and plotted in Figure 5.8b. Similar results can also be found in Tan et al. (2014). With increasing porewater salinity, the thickness of the EDL on the external surfaces of clay particles is suppressed, and hence the particles can move closer, thus forming stronger mineral contacts. The enhanced flocculated structure and stronger mineral contacts result in greater resistance to interparticle shearing hence a higher s_u in the beginning. However, it also makes the rearrangements of the clay particles (e.g., reorientation) more difficult to complete. Meanwhile, surface tension and viscosity of water are both affected by porewater salinity. The intermolecular bonds in the water strengthen after adding salt result in higher surface tension, which is the property of the surface of a liquid that allows it to resist an external force. Surface tension was reported to increase with increasing salt concentration (Bzdek et al., 2016; Ozdemir et al., 2009). The viscosity of water increases remarkably with salinity, and the flow resistance increases with decreasing viscosity (Goldsack and Franchetto, 1977; Lide, 2005). The higher viscosity and resistance hinder the reorientation or movement of the clay particles, which is one factor that further limits the rearrangement and movement of clay particles. Since the majority of gain in strength during thixotropy is the first stage of fast thixotropic hardening governed by fabric evolution, the TSR of each specimen at higher porewater salinity is less. Similarly, the slight increase in LL of both Prestige and BBC with increasing salinity also results from the flocculation. More water is needed to get the separation of clay particles with a more flocculated structure than a dispersed

structure to get the s_{ur} down to about 2 kPa (i.e., approximate value of s_{ur} at the liquid limit), hence higher *LL*.

However, the *LL* of PureGold Gel decreases with increasing salinity, which is contrary to the other two non-swelling clays, which is consistent with results in the literature (Jeong et al., 2012; Svensson and Hansen, 2013). Na-montmorillonite particles can exist as single 2:1 layers at low porewater salinity, and a greater amount of EDL water results from the greater external surface area (Zhang et al., 2004b). A significant reduction in the external surface area due to thicker particle formation and EDL thickness reduction caused by the increasing porewater salinity are the main reasons for the decrease in the *LL*. Meanwhile, the increasing porewater salinity shows little to no effect on *PL* of each clay since the EDL is not fully developed.

The effect of porewater salinity is very pronounced for PureGold Gel, and it shows the greatest TSR is achieved at an intermediate porewater salinity (e.g., 0.017 g/g), while the overall thixotropic gain in strength of Prestige decreases with increasing salinity. The TSR of BBC indicates that the behavior of BBC is kind of between Prestige and PureGold Gel. The results from XRPD show the different mineralogy compositions of Prestige, PureGold Gel, and BBC. Prestige mainly consists of kaolinite, while PureGold Gel mainly consists of Na-montmorillonite and a small amount of illite. BBC mainly contains illite and a small amount of kaolinite. Therefore, the thixotropic behavior of the Prestige and PureGold Gel are extremely different, while the BBC behaves somewhere between them. The average void ratio of specimens at each salinity plotted in Figure 5.9 show that the compressibility characteristics of Prestige and BBC are not significantly affected by salinity. PureGold Gel specimens have the highest void spaces because of the high water

content, and the void ratio decreases with increasing porewater salinity. The high water content acts as a lubricant, while the high void ratio provides more free space for the clay particles to move around to form a more flocculate structure for higher TSR. On the contrary, the void ratios of both Prestige and BBC are relatively low, and the change in void ratio with different porewater salinity is not evident. Montmorillonite has a higher activity and large EDL relative to the size of the particle, while the increasing porewater salinity does not have a significant influence on kaolinite because the size of the kaolinite particles is relatively large compared to its EDL.

For offshore geotechnical engineering practice, where the environment involves mostly marine soft clays with saline water in the pore space, the presence of salt ions in the pore fluid can fundamentally change the mechanical behavior of the soft clays. This study shows that the soft clays at different porewater salinity, when remolded at or near the liquid limit, can experience a significant increase in undrained shear strength over time at constant water content due to thixotropic hardening. For the artificial Prestige, PureGold Gel, and natural BBC studied in this work, s_u increased by a factor of 2 for all pore water salinities within 140 days, and TSR can reach 2 in one to two months for all clay specimens at a salinity of seawater (e.g., 0.034 g/g). Therefore, the soil behavior learned from this work can serve as guidance of the design of suction caissons for the anchoring of mooring lines for floating energy systems such as oil and gas platforms and wind turbines (e.g., Abu-Farsakh et al., 2015; Shen et al., 2008), which necessitate disturbance of the soft clays at seawater salinity during construction. There exists an optimum porewater salinity for each clay at which the highest TSR occurs. Hence, steps can be taken in-situ to manipulate clay's

natural salinity to its optimum, such that a higher shear capacity can be achieved to improve the construction.

Meanwhile, other than porewater salinity, mineralogy also plays a vital role in the thixotropic process based on this study. Illitic and montmorillonitic clays show relatively higher regain in s_u, especially in short term, while an extremely long time for thixotropic hardening is indicated for kaolinitic clay. They can be utilized for different engineering purposes. For example, the thixotropic behavior of bentonite that is widely used as drilling mud should be promoted in situations like maintaining the borehole stability and carrying cuttings out of the hole. However, in other situations like lubrication and storage, thixotropic hardening behavior should be suppressed. Different amounts of salt can help achieve either suppression or promotion of thixotropic behavior of the drilling mud based on the results from this work. Kelessidis (2008) also concluded that the strength and viscosity regain of a bentonite slurry depend on the types and concentration of swelling mineral smectites and the amount of salt.

5.5 Conclusions

In this study, fall cone for the s_u measurements and 1DXRD for microstructural characterization were conducted to investigate and understand the effect of porewater salinity on thixotropic behavior of three soft clays, including a natural marine clay, BBC, and two manufactured clays, Prestige and PureGold Gel, all prepared to their respective liquid limits prior to testing. The following major conclusions can be drawn:

- All clays at different porewater salinity exhibit thixotropic hardening to various extents, and an optimum porewater salinity exists, varying from clay to clay, at which a soft clay may exhibit the highest TSR.
- Each specimen shows a two-parts thixotropic behavior, including a rapid increase in s_u at the initial phase over a very short time and a slow increase in s_u later over a prolonged time.
- Higher thixotropic gain in strength results from greater *OI* changes. The increasing porewater salinity, which reduces the thickness of electrical double layer (EDL) on the external surfaces of the clay particles, advances the flocculation and improves the aggregation.
- The enhanced flocculated structure and stronger mineral contacts contribute to greater resistance to interparticle shearing hence a higher s_u in the beginning, but entangle the rearrangements of the clay particles (e.g., reorientation) in difficulty hence lower TSR. Additionally, surface tension and viscosity of water increase with increasing porewater salinity, which furthers hinder the rearrangement and movement of clay particles to lower TSR.
- The thixotropic behavior of the Prestige and PureGold Gel are extremely different, while the BBC behaves somewhere between them, indicating the effect of mineralogy besides the porewater salinity on thixotropic behavior of soft clays, which warrants further analysis.

5.6 Acknowledgments

This work was supported by the National Science Foundation (NSF) under Award CMMI 1640306. This work also made use of the Shared Experimental Facilities (i.e., X-ray diffractometer) at MIT, supported in part by the NSF MRSEC Program under Award DMR1419807. The author wants to thank Dr. Shengmin Luo, who graduated from UMass Amherst, for help with the microscale experiments.

5.7 Declarations of Interest

None.

Table 5.1 Summary of porewater salinities *r* (g/g) of prepared soil samples

Clay samples	Natural *r*	1	2	3	4
Prestige	0.001	0.001	0.017	0.034	0.068
BBC	0.010	0.005	0.010	0.034	0.068
PureGold Gel	0.003	0.003	0.017	0.034	0.068

Table 5.2 Summary of the fitting parameters for the modified Burgers model

Sample	Salinity r (g/g)	Property	c_1	c_2	c_3	c_4	c_5	R^2
BBC	0.005	s_u (kPa)	1.69	3.19	0.35	4.12	1.11×10^{-2}	0.99
		s_u/s_{u0}	1.00	2.13	0.39	2.63	1.22×10^{-2}	0.99
	0.010	s_u (kPa)	1.40	2.47	1.97	3.04	2.53×10^{-2}	0.99
		s_u/s_{u0}	1.00	1.77	1.96	2.18	2.53×10^{-2}	0.99
	0.034	s_u (kPa)	1.76	2.14	0.51	6.08	7.64×10^{-3}	1.00
		s_u/s_{u0}	1.00	1.24	0.52	3.51	7.71×10^{-3}	1.00
	0.068	s_u (kPa)	1.58	0.80	1.28	3.09	3.23×10^{-2}	1.00
		s_u/s_{u0}	1.00	0.49	1.54	1.95	3.19×10^{-2}	1.00
PureGold Gel	0.003	s_u (kPa)	1.90	1.82	0.61	2.18	4.78×10^{-3}	1.00
		s_u/s_{u0}	1.00	0.99	0.62	1.12	4.95×10^{-3}	1.00
	0.017	s_u (kPa)	1.83	3.01	1.38	3.97	9.90×10^{-3}	0.99
		s_u/s_{u0}	1.00	1.65	1.39	2.16	1.00×10^{-2}	1.00
	0.034	s_u (kPa)	2.20	2.16	0.85	331.57	3.72×10^{-5}	0.99
		s_u/s_{u0}	1.00	1.00	0.88	125.46	4.56×10^{-5}	0.99
	0.068	s_u (kPa)	2.17	1.58	0.63	1.57	2.18×10^{-2}	1.00
		s_u/s_{u0}	1.00	0.72	0.63	0.73	2.19×10^{-2}	1.00
Prestige	0.001	s_u (kPa)	1.40	1.11	0.73	533.53	2.59×10^{-5}	0.99
		s_u/s_{u0}	1.00	0.81	0.74	467.00	2.13×10^{-5}	0.99
	0.017	s_u (kPa)	1.41	0.47	0.54	472.32	2.36×10^{-5}	0.99
		s_u/s_{u0}	1.00	0.34	0.58	467.34	1.72×10^{-5}	0.99
	0.034	s_u (kPa)	1.31	0.56	0.52	2.35	1.04×10^{-2}	0.98
		s_u/s_{u0}	1.00	0.42	0.51	1.80	1.02×10^{-2}	0.98
	0.068	s_u (kPa)	1.45	0.44	0.13	238.27	3.56×10^{-5}	0.99
		s_u/s_{u0}	1.00	0.33	0.16	147.65	4.13×10^{-5}	0.99

Note: R^2 = coefficient of determination

Table 5.3 Water content statistics of all specimens during the 1DXRD testing

Specimens	Salinity *r* (g/g)	Average	Standard deviation	Coefficient of variation
BBC	0.005	44	0.24	0.56
	0.010	45	0.16	0.35
	0.034	48	0.74	1.55
	0.068	51	0.92	1.83
Prestige	0.001	45	0.17	0.38
	0.017	49	0.31	0.64
	0.034	47	1.16	2.47
	0.068	51	1.19	2.33

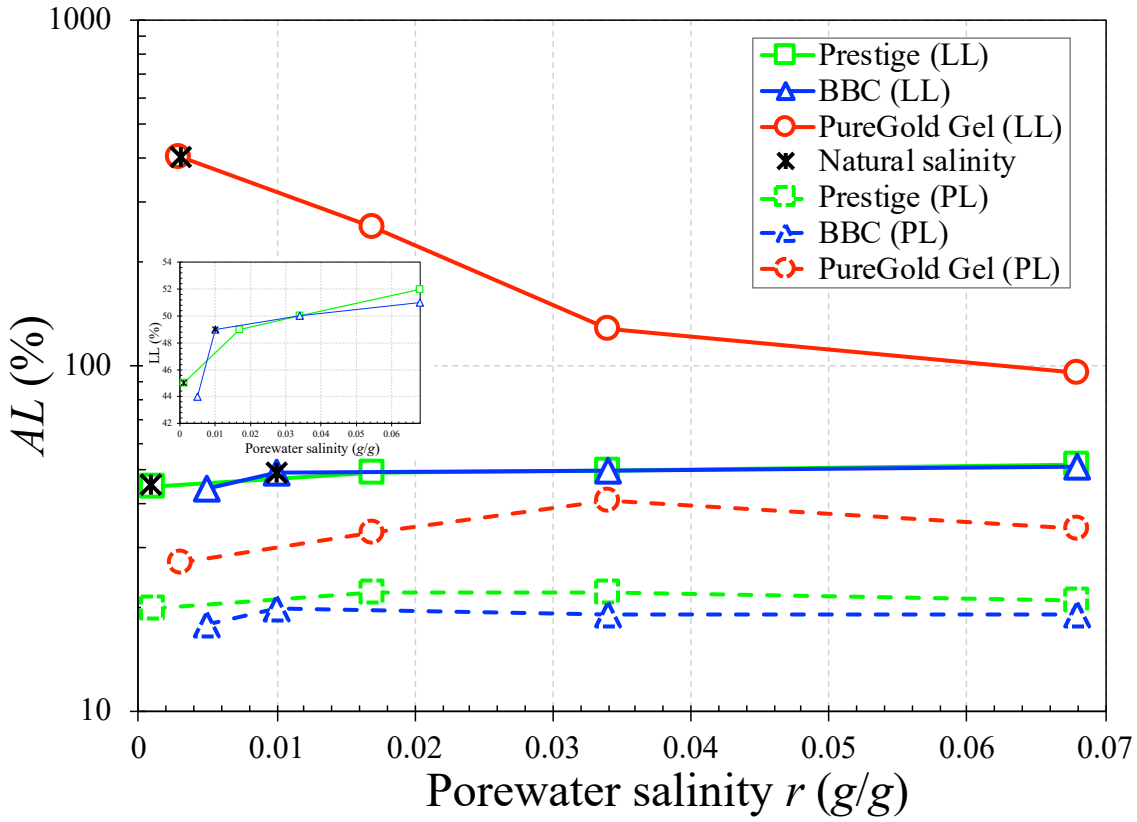

Figure 5.1 Atterberg Limits determinations of each clay at different porewater salinities.

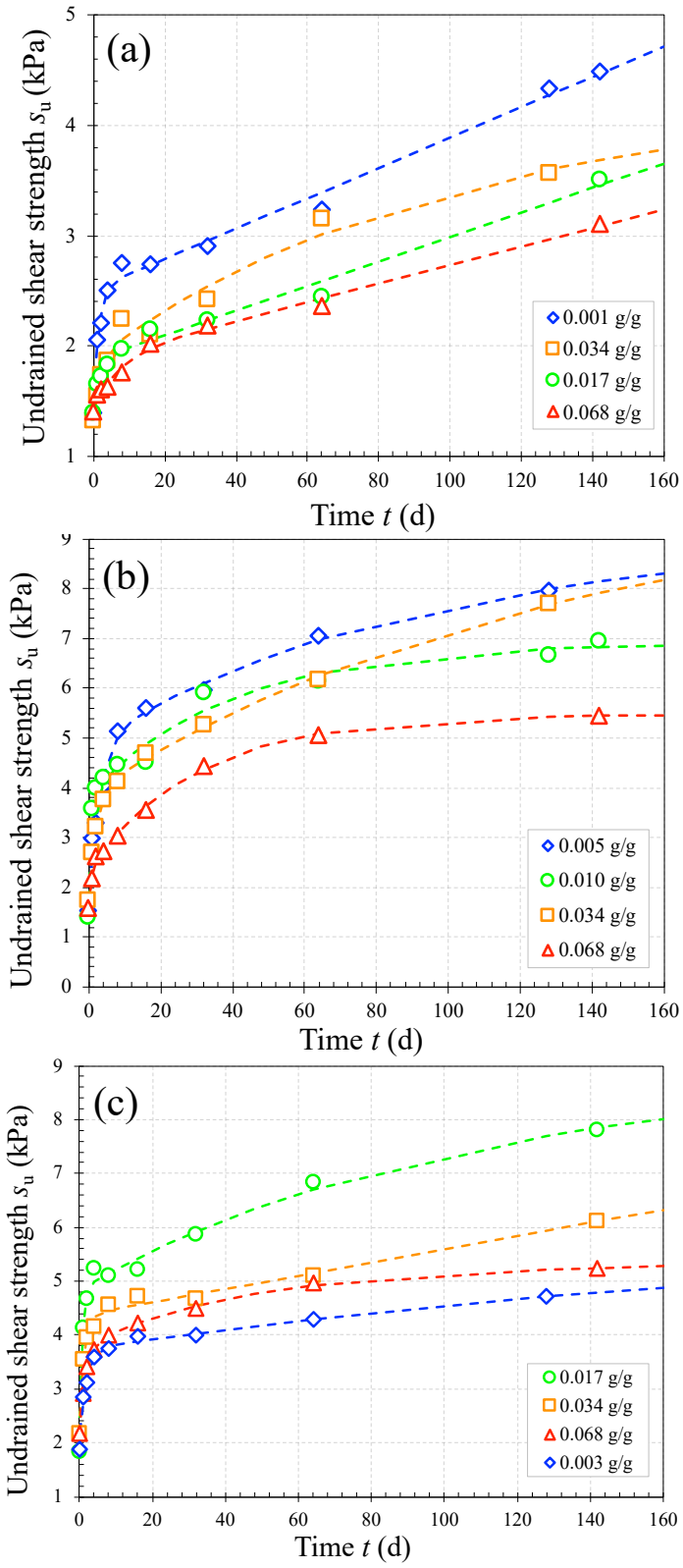

Figure 5.2 Thixotropic evolution of undrained shear strength: s_u vs. time of (a) Prestige; (b) BBC; (c) PureGold Gel.

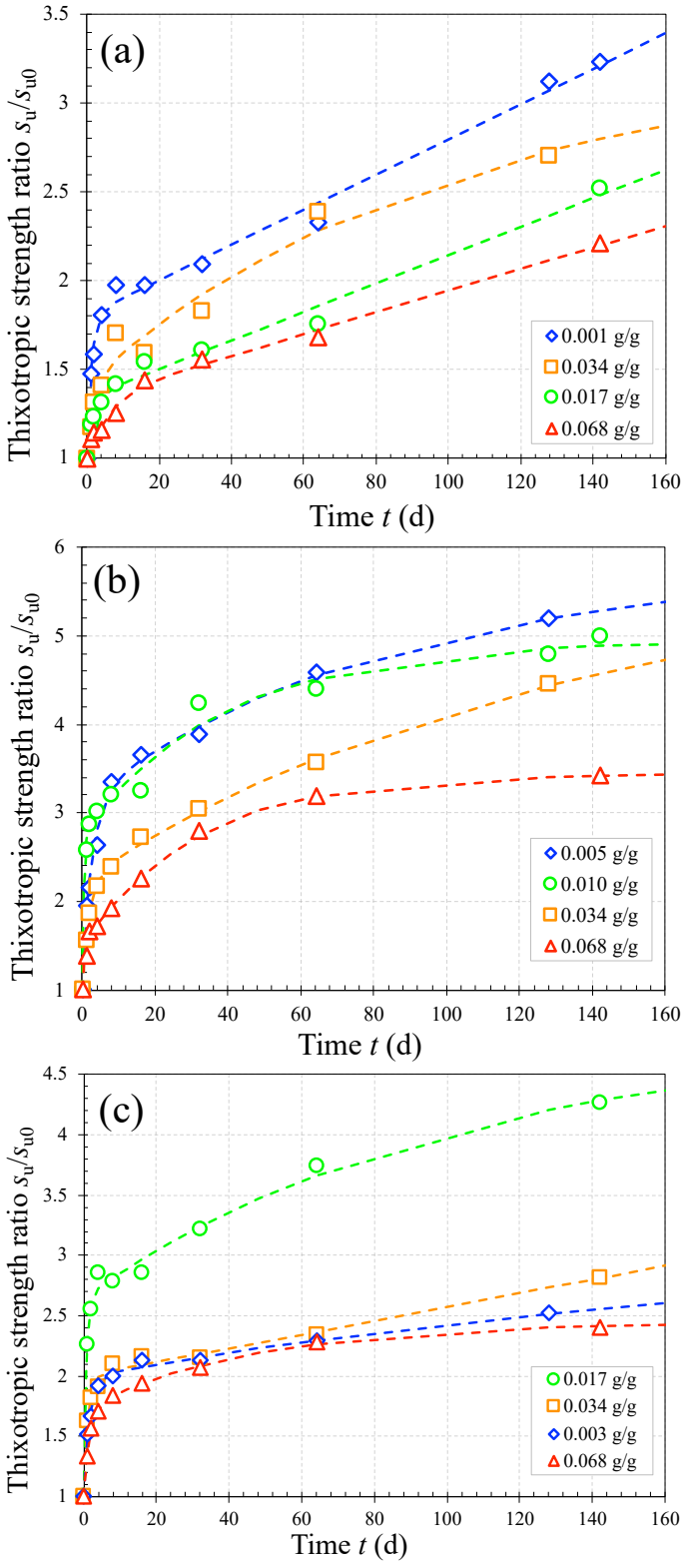

Figure 5.3 Thixotropic evolution of undrained shear strength: TSR vs. time of (a) Prestige; (b) BBC; (c) PureGold Gel.

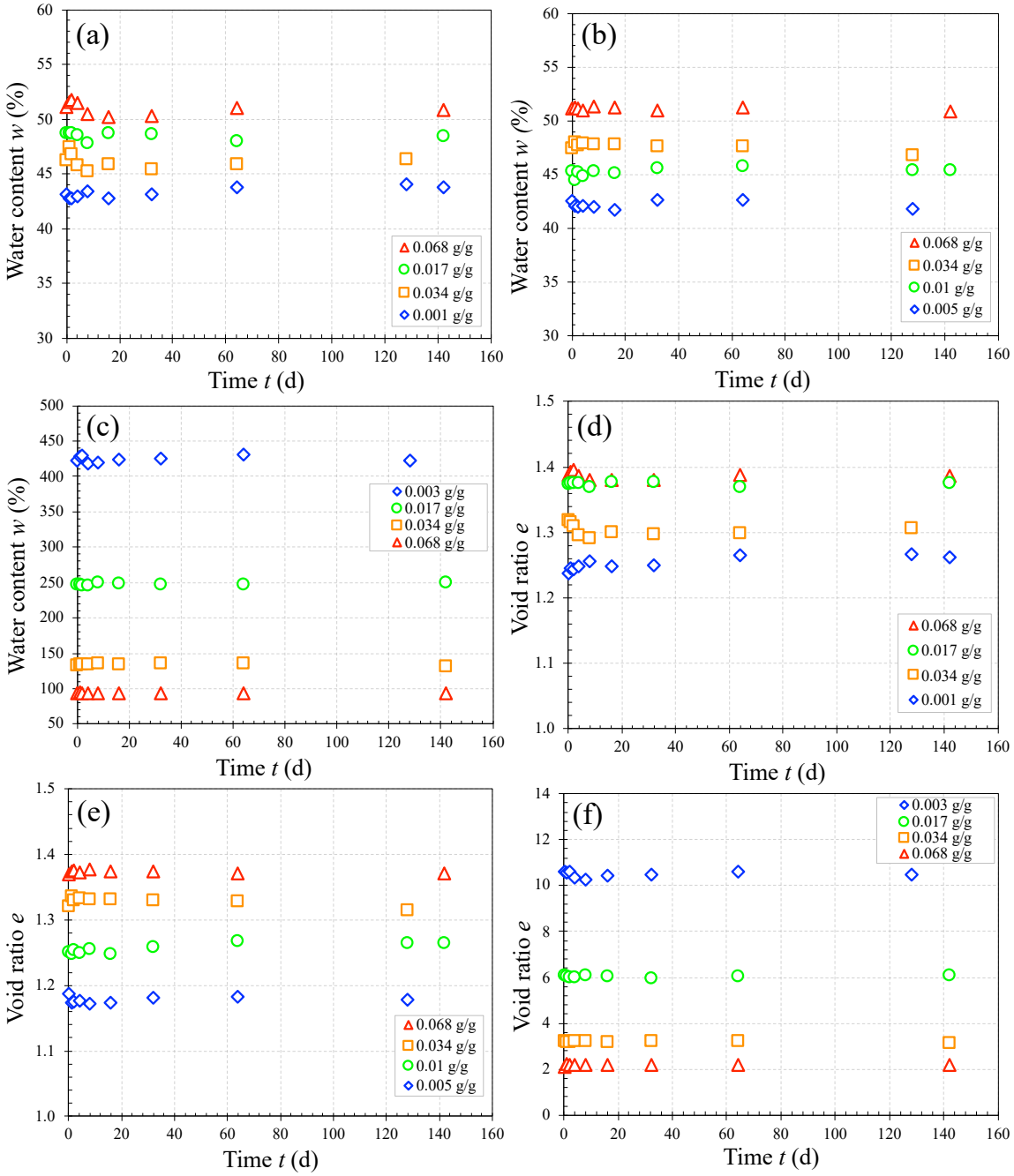

Figure 5.4 Quality control of all FC specimens: water content measurements of (a) Prestige; (b) BBC; (c) PureGold Gel; void ratio measurements of (d) Prestige; (e) BBC; (f) PureGold Gel.

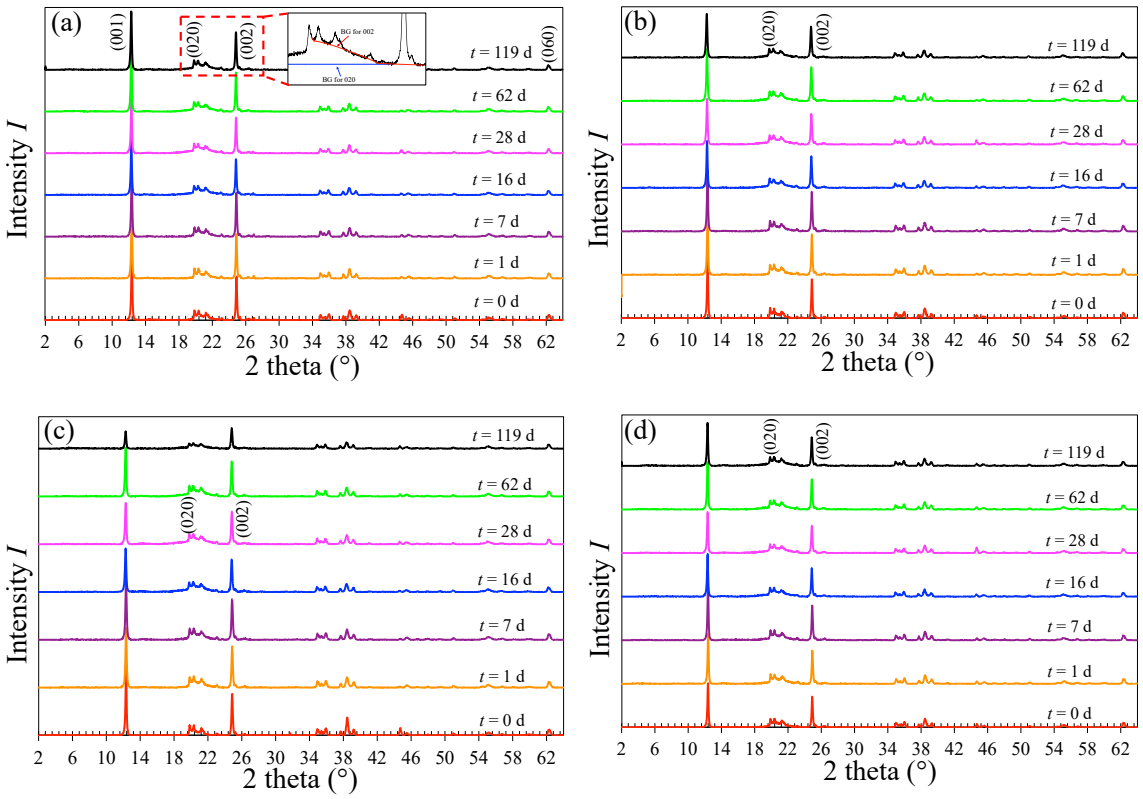

Figure 5.5 Diffraction patterns of Prestige at varying porewater salinities: (a) 0.001 g/g; (b) 0.017 g/g; (c) 0.034 g/g; (d) 0.068 g/g.

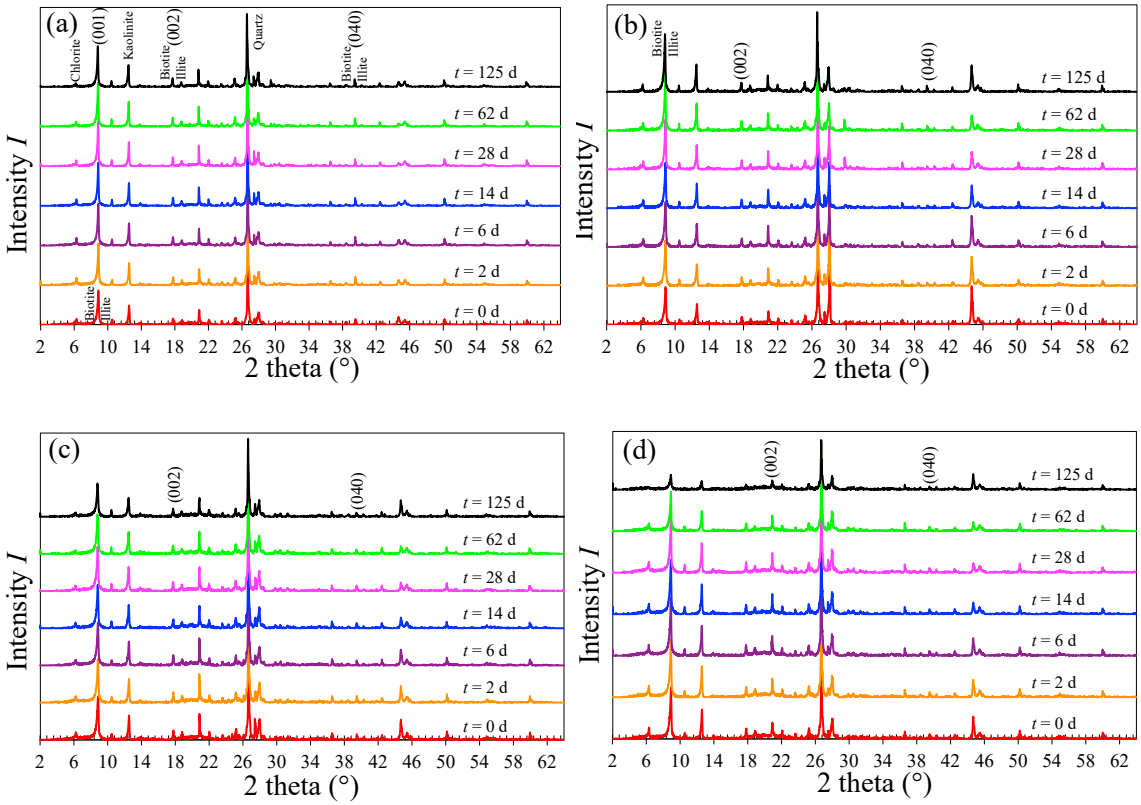

Figure 5.6 Diffraction patterns of BBC at varying porewater salinities: (a) 0.005 g/g; (b) 0.010 g/g; (c) 0.034 g/g; (d) 0.068 g/g.

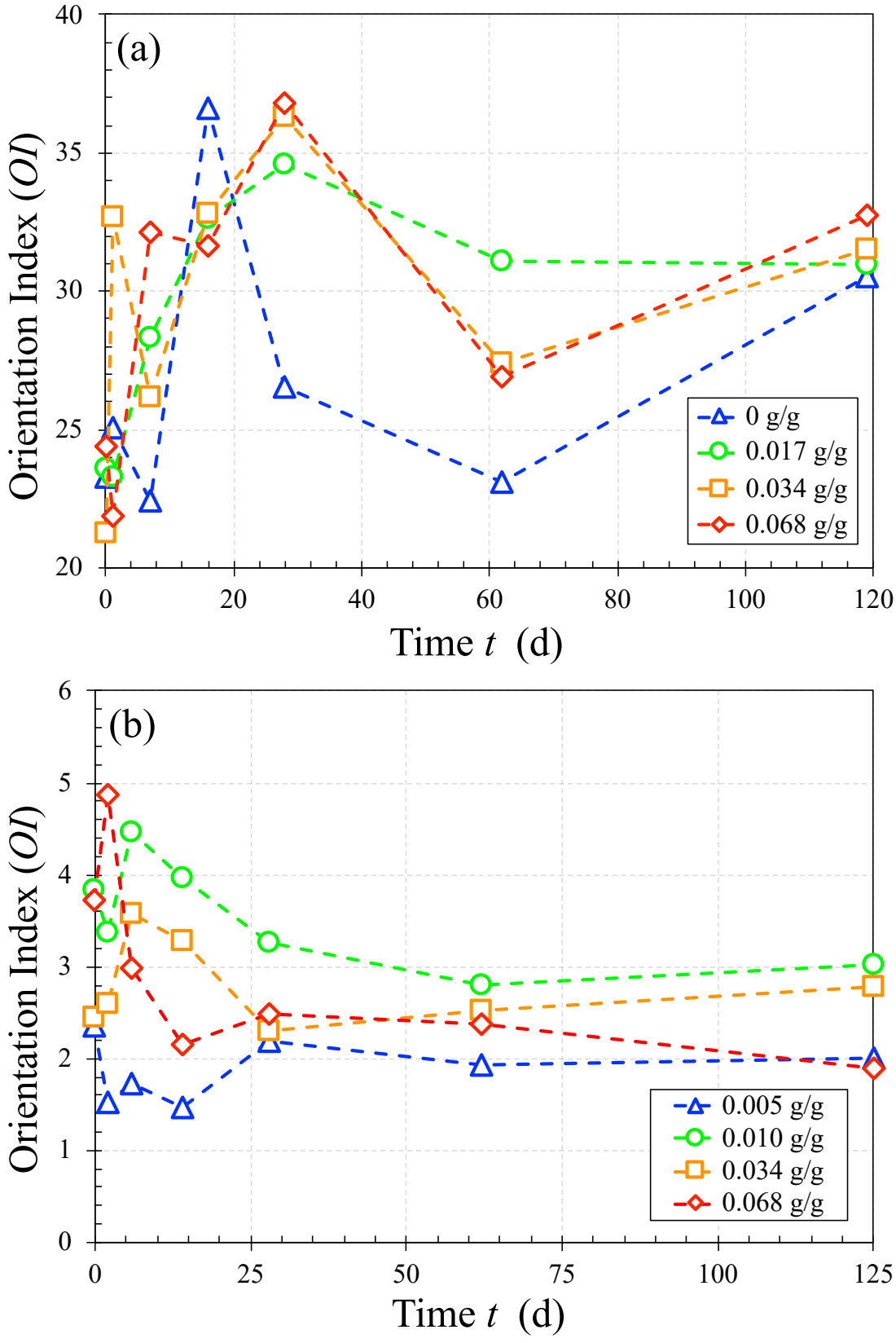

Figure 5.7 Orientation index (*OI*): (a) Prestige; (b) BBC.

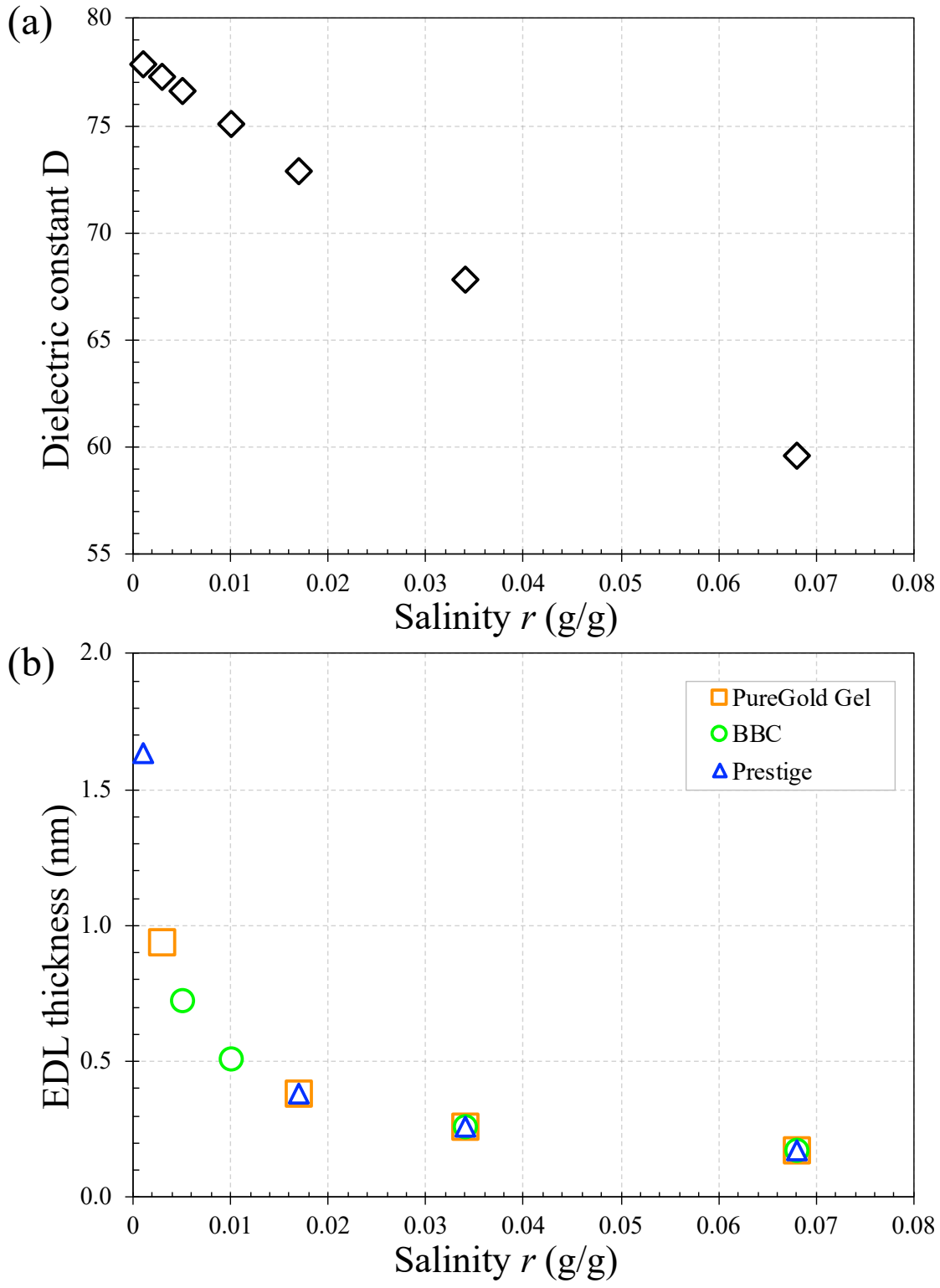

Figure 5.8 EDL thickness determinations of each specimen: (a) dielectric constant; (b) thickness.

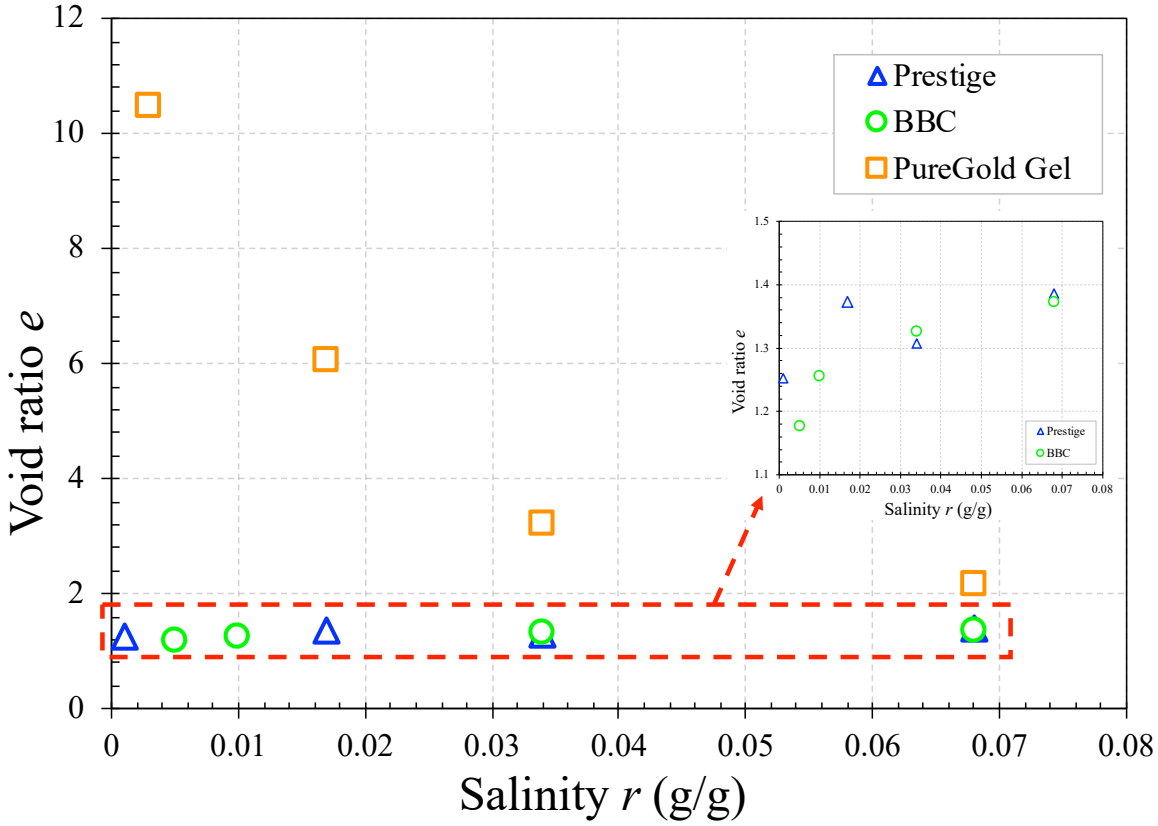

Figure 5.9 Average void ratio of each clay specimens.

CHAPTER 6

INFLUENCES OF CURING TEMPERATURE AND INITIAL WATER CONTENT ON THE THIXOTROPIC BEHAVIOR OF SOFT CLAYS

This paper presents results from an experimental program that investigates the influence of both temperature and initial water content on thixotropic behavior of soft remolded clays. When considering the influence of temperature, all clay specimens were prepared at liquid limit (*LL*). When concerning the effect of initial water content, temperature was maintained at room temperature (i.e., 24 °C). Four soft clays were studied, including two naturally occurring, illite-rich, soft marine clays with moderate salinities and two manufactured, highly purified clays that contain mainly kaolinite and smectite, respectively. The undrained shear strength s_u measurements were conducted using fall cone (FC) at various thixotropic curing times up to 140 days. Results indicate the influence of clay mineralogy besides the two factors on thixotropy. The two natural clays show a higher regain in thixotropic strength than the two manufactured counterparts, most likely due to their higher natural porewater salinity and more diverse clay mineralogy. For montmorillonite clay, both variations in temperature and initial water content did not show a significant change in thixotropic strength ratio (TSR). For kaolinite and illite-rich clays, a higher TSR at a higher temperature indicated that high temperature favors the reorientation or movement of the clay particles. The slope of s_u versus water content curve (flow curve) was found to be constant during thixotropic hardening process for all three clays. These data shed light on analyzing the behavior of surrounding soils of geothermal structures and providing guidance on strength estimation of clays at a specific thixotropic curing time with different natural water content.

6.1 Introduction

Geotechnical engineers have long observed that the strength of natural clays dramatically decreases after considerable disturbance but recovers back to a certain degree with time even if the boundary conditions remain the same (e.g., no change in pressure/stress, temperature, or composition). This time-dependent mechanical hardening phenomenon is called thixotropy, and the term is one of the oldest documented rheological phenomena (Barnes, 1997; Larson and Wei, 2019; Mewis, 1979; Mewis and Wagner, 2009). In geotechnical engineering, initial recognition of the importance of thixotropy started when clay sensitivity was discovered, and many pioneers (e.g., Jacobsson and Pusch, 1972; Mitchell, 1960; Nalezny and Li, 1967; Seed and Chan, 1959; Skempton and Northey, 1952) studied clay thixotropy. It describes a reversible process of sol-gel transition that can be repeated several times without visible changes in the colloidal system. The latest definition of thixotropy specifically for soils is: "Thixotropy is an isothermal, reversible, time-dependent process occurring under conditions of constant composition and volume whereby a material stiffens while at rest and softens or liquefies upon remolding" (Mitchell and Soga, 2005).

Temperature in soils can change seasonally or even daily in some places, and some geothermal structures are subjected to cyclic changes in temperature. Samples obtained during the winter tend to first experience decreases in temperature upon removal from the ground and increase when they arrive in the laboratory unless extra care was taken. The opposite situations happen in summer or hotter climates. Thus, soil samples can be subjected to large temperature changes, and engineers must evaluate the way these changes affect the mechanical behavior of the material. The engineering properties of soils are

generally measured in the laboratory at room temperature. However, these thermal environmental changes can affect some engineering properties of soils such as compressibility, pore water pressure, volume change, strength, and elasticity (Laguros, 1969; Raheem and Vipulanandan, 2019; Svensson and Hansen, 2013). The existing published data indicate that rising temperature can reduce the undrained shear strength of clays because for undrained condition, the thermal expansion of the water increases the pore water pressure and alters the compressibility (Mitchell, 1969; Plum and Esrig, 1969; Xiao et al., 2014). In addition, Mitchell (1969) points out that increasing temperature can also cause a significant decrease in elastic modulus. Thixotropy, which is a fundamental aspect of soil behavior, should be influenced by temperature as well since the temperature shows significant effects on the engineering properties of clays.

Previous studies have shown that various factors, such as water content, plasticity index (*PI*), activity, and clay mineralogy, can affect the thixotropic hardening process. For example, Yang and Andersen (2016) concluded that thixotropy is more significant for clays with higher *PI*, activity, and water content, i.e., the higher the water content and liquidity index, the higher the TSR. Similar experimental results have also been reported in other studies (Lunne and Andersen, 2007; Seng and Tanaka, 2012). However, different results on the effect of water content were also reported by others. Shahriar et al. (2018) presented that clays at a water content 25% lower than their liquid limits exhibit the optimal thixotropic hardening or best thixotropic gain in strength. Therefore, these inconsistent conclusions suggest that some other factors that have not yet been investigated can also affect clay thixotropy to a considerable extent.

However, there are few studies on how temperature affects the thixotropic behavior of clays. Among those studies focusing on the influence of the initial water content, how the flow curve of the clays was affected by thixotropic hardening was not considered. To this end the objective of the study presented in this paper was to investigate the influence of both temperature and initial water content on thixotropic behavior of soft clays. When considering the influence of temperature, all clay specimens were prepared at the *LL*. When concerning the impact of initial water content, temperature was maintained at room temperature (i.e., 24 °C). Thixotropic hardening of each clay specimen was assessed by FC. Data on the evolution of s_u provides a better and systematic understanding of the influence of both temperature and initial water content on this fundamental soil behavior. The results presented can also generate significant practical impacts.

6.2 Materials and Methods

6.2.1 Materials

Four soft clays were studied, including Prestige, PureGold Gel, Boston Blue Clay (BBC), and Onsøy. Detailed description, index properties, and mineralogic compositions of these four clays can be found in Chapter 3.

6.2.2 Influence of Temperature

To study the effect of temperature on the thixotropic hardening process of the above four soft clays, a set of four specimens was prepared for each clay at a water content near their liquid limit (*LL*s) and tested at four different temperatures, i.e., 4, 24 (ambient temperature), 44, and 64 ºC. Therefore, the *LL* of each clay sample at the target temperature

was first determined. For each set of specimens, *DI* water was added to the original clay to bring its water content to the *LL* corresponding to the test temperature, followed by overnight curing in a temperature-controlled water bath set at the corresponding target temperature for equilibrium on both temperature and moisture. The equilibrated samples were again thoroughly mixed prior to the preparation of individual specimens for thixotropy testing.

To maintain the testing temperature as close to the proposed target temperature, a 4 ºC controlled temperature laboratory room was used for the tests at 4 ºC. For experiments at the higher temperatures, such as 44 ºC and 64 ºC, the specimens were heated using a hot plate (Fisher Scientific, Inc.) inside a temperature-controlled chamber set at the target temperature.

6.2.3 Influence of Initial Water Content

Three of the above four clays, including Prestige, PureGold Gel, and BBC, were studied concerning the effect of initial water content on the thixotropic hardening process. For each clay, three sets of clay specimens were prepared at three different initial water contents, i.e., 0.8*LL*, *LL*, and 1.2*LL*. For each set of specimens, *DI* water was first added to the original clay to prepare the clay sample at a water content near or close to the target initial water content, followed by overnight curing for temperature and moisture equilibrium in a sealed plastic bag stored in a temperature-controlled chamber set at 24 °C. The equilibrated samples were again thoroughly mixed prior to the preparation of individual specimens for thixotropy testing. To only focus on the influence of the initial water content, specimens and testing temperatures were stored and maintained at 24 °C.

6.2.4 Fall Cone Testing

Temporal evolution of the undrained shear strength s_u of the soft clay specimens during thixotropic hardening was assessed using fall cone (FC) testing by following the ISO 17892-6 standard method (2017). Specimens were prepared following the same method described in Chapter 3 (section 3.2.3). Each thoroughly remolded clay was carefully filled into a series of jars and, all sealed jars were stored underwater in a temperature-controlled water bath set at the target temperature. Such a series of carefully prepared specimens enabled multiple s_u measurements by following a pre-designed temporal curing schedule of up to 142 days (e.g., 0, 1, 2, …, 64, 128, 142 days). At each specific hardening or curing time, one jar from each studied clay was retrieved from the water bath, and three to five FC measurements were performed at different locations of the specimen surface to avoid mutual interference using a 60° and 60 g cone (ISO 2017), which were averaged and converted to s_u per the ISO (2017).

For quality control, after the above measurements, each tested specimen was again fully remolded and retested to ensure that the fully remolded undrained shear strength s_{ur} was equal to that at time $t = 0$. Additionally, the final water content of the cured specimen was also measured at the end of all these measurements, and then compared with that at $t = 0$. If the final water content deviated from the initial one by 2%, then a new specimen was prepared, and all measurements were repeated. In addition to water content measurements, the void ratio and organic matter measured following ASTM (2014)were also calculated as a quality control if data is available.

6.3 Results and Discussion

6.3.1 Liquid Limit

Figure 6.1 shows the determinations of *LL* for the four clays at different temperatures. PureGold Gel and Onsøy are temperature-dependent. The *LL* of PureGold Gel dramatically increases with increasing temperature, Onsøy slightly decreases, and both Prestige and BBC show little or no change.

6.3.2 Influence of Temperature on Thixotropy

Figure 6.2a to Figure 6.2d summarize the temporal evolution of s_u of the four clays at different temperatures and different thixotropic curing times up to more than 140 days. Overall, all the specimens show thixotropic hardening to various extents and generally have a fast initial increase in s_u in the first few days, accompanied by a slower increase in s_u at prolonged curing durations. The initial fully remolded undrained shear strength s_{u0} is defined as the s_u at time t = 0 day (i.e., the starting point for the thixotropic process). It ranges from 1.8 to 2.0 kPa for Prestige, 1.9 to 2.0 kPa for PureGold Gel, 1.0 to 1.5 kPa for BBC, and 1.4 to 2.0 kPa for Onsøy. To compensate for the difference of s_{u0} values, the normalized thixotropic strength ratio (TSR), s_u/s_{u0}, are also plotted in Figure 6.3a to Figure 6.3d. The TSR of Prestige ranges from 1.6 to 2.6 at t = ~ 140 days, while BBC and Onsøy reach the same range only after around two weeks of curing. Additionally, the two natural clays, BBC and Onsøy, show a relatively higher tendency of thixotropic hardening, especially BBC, which achieved a TSR ranging from 5 to 15 after 140 days of curing. The various extent of thixotropic hardening of each specimen was caused by the differences in temperature and mineralogy.

Figure 6.3d shows that the highest temperature (64 ºC) causes the Onsøy clay to have the fastest initial rate of thixotropic hardening (i.e., the strength increase rate is the fastest at the beginning of the thixotropic process) and the highest ultimate strength. The overall trend shows that TSR increases with increasing temperature for Onsøy. Prestige and BBC up to 44 ºC at which the highest degree of thixotropic hardening and ultimate strength (herein defined as the maximum strength or a plateau observed in the strength-time curves) was measured. For PureGold Gel, Figure 6.3c indicates that the strength regain does not change much with temperature. Generally, the natural clays show higher sensitivities to the temperature, and greater strengths are achieved at prolonged thixotropy.

The dashed lines in Figure 6.2 and Figure 6.3 represent the best fit of s_u and TSR data for all the specimens using modified Burgers' five parameter model (Barnes, 2000). The two-parts thixotropic behavior of all the specimens, including a rapid increase in s_u at the initial phase over a very short time and a slow increase in s_u later over a prolonged time, can be efficiently described by the model. Detailed fitting parameters c_1 to c_5, and the coefficient of determination R^2, are summarized in Table 6.1. As explained in Chapters 3 and 5, fitting parameters, c_3 and c_5, are indications of the degree of viscosity of the clays. The results show they are affected by both the clay mineralogy, temperature, and salinity. In general, low to normal temperature (4 - 24 ºC) increases the rigidity of BBC, whereas imposing the opposite effect on Prestige, PureGold Gel, and Onsøy. Normal to moderate temperature (24 - 44 ºC) tends to reduce the rigidity of BBC and Onsøy but increases it of Prestige and PureGold Gel. Moreover, moderate to high temperature (44 - 64 ºC) increases the rigidity of BBC and Onsøy but lowers it for Prestige and PureGold Gel.

As part of the quality control, the water contents measured after all FC

measurements are shown in Figure 6.4. The water content measurements show little variation at the relatively low temperatures, which verify that these specimens did not experience noticeable water loss during the thixotropic process. However, the higher differences in the data collected at 64 ºC result from the high drying rate and difficulty performing the tests at such a high temperature. Statistics of all specimens' water contents measured after all FC measurements are summarized in Table 6.2, which further indicates the specimens were well prepared and boundary conditions were unchanged.

The surface tension, viscosity, and pore water pressure are all affected by temperature. The pore water pressure was reported to be raised with increasing temperature, which results in a reduction in s_u (Mitchell, 1969). It explains the initial remolded s_{ur} decrease with increasing temperature. Surface tension, which is the property of the surface of a liquid that allows it to resist an external force, decreases with increasing temperature (Cini et al., 1972; Wen et al., 2018). Besides, the viscosity of water remarkably decreases with temperature, and the flow resistance reduces with decreasing viscosity (Korson et al., 1969). The lower viscosity and resistance favor the reorientation or movement of the clay particles, which is one factor that enhances the strength since the clay particles can reorient or move to a more preferred structure to have a stronger strength with time.

6.3.3 Influence of Initial Water Content on Thixotropy

Figure 6.5a to Figure 6.5c summarize the temporal evolution of s_u of the three clays prepared at different initial water contents relative to *LL* curing up to more than 140 days. Generally, all the specimens show thixotropic hardening and two-part thixotropic behavior (i.e., a fast initial increase in s_u in the first few days, accompanied by a slower increase in

s_u at prolonged curing durations). The effect of the initial water content on thixotropic hardening was observed to be influenced by mineralogy as well. The initial fully remolded undrained shear strength s_{u0} is defined as the s_u at time t = 0 day. It ranges from 0.7 to 5.1 kPa for Prestige, 1.2 to 3.1 kPa for PureGold Gel, and 0.6 to 4.7 kPa for BBC, which are reasonable since higher s_u results from lower initial water content at the beginning of thixotropy. To compensate for the difference of s_{u0} values, their normalized TSR, s_u/s_{u0}, are also plotted in Figure 6.6a to Figure 6.6c. The TSR of Prestige ranges from 2.0 to 2.6 at t = ~ 140 days, while BBC can achieve the same range after around a week of curing. Additionally, BBC, which is a natural clay with relatively complex mineralogical composition and porewater salinity, shows a relatively higher tendency of thixotropic hardening at all three different initial water contents. The various extent of thixotropic hardening of each specimen was caused by the differences in initial water contents and mineralogy. Figure 6.6c shows that the regain in strength during thixotropy does not change much with different initial water contents for PureGold Gel. For Prestige and BBC, the highest thixotropic gain in strength can be observed near liquid limit. Overall, the natural clays show higher sensitivities to the initial water content, and greater strengths are achieved at prolonged thixotropy for all three different initial water contents.

The dashed lines in Figure 6.5 and Figure 6.6 represent the best fit of s_u and TSR data for all the specimens using modified Burgers' five parameter model (Barnes, 2000). Detailed fitting parameters c_1 to c_5, and the coefficient of determination R^2, are summarized in Table 6.3. As explained in previous sections and chapters, c_3 and c_5 indicate the degree of viscosity of the clay specimens. The results show they are greatly affected by not only initial water content but also mineralogy. Combining the results from previous chapters,

they are also affected by temperature and salinity. In general, if the initial water content is lower than *LL*, increasing initial water content can improve the rigidity of BBC, whereas imposing the opposite effect on Prestige and PureGold Gel. If the initial water content is greater than *LL*, increasing initial water content tends to increase the rigidity of Prestige and PureGold Gel but reduces it of BBC. More importantly, when plotting the relationship between s_u and water content during thixotropic process, the s_u versus water content curve of each clay at each specific thixotropic curing time was observed to be more or less parallel (Figure 6.7). Each curve was fitted with a linear equation, and the slopes were plotted in Figure 6.8, which indicates the slope of s_u versus water content curve during thixotropic hardening process are constant for all three clays. Therefore, the s_u of each clay at different initial water contents at different curing times during thixotropy can be estimated based on these results.

As part of the quality control, the water contents measured after all FC measurements are shown in Figure 6.9. The water content measurements show little variation at different initial water contents. Statistics of all specimens' water contents measured after all FC measurements are summarized in Table 6.4, which further indicates that the measured water contents have little variation, verifying that these specimens did not experience noticeable alterations in water content during the thixotropic curing period. The void ratio measurements for each set of clay specimens and organic matter calculations for part of specimens are plotted in Figure 6.10 and Figure 6.11. The void ratio calculations further indicate that all specimens were consistently prepared in this study. The averaged void ratio of each clay prepared at different initial water contents, which is shown in Figure 6.12, increases with an increasing amount of water. The organic matter calculations

indicate there is no organic matter growth during thixotropy.

6.4 Conclusions

Macroscopic experimentation was conducted to investigate the influence of temperature on the thixotropic behavior of four soft clays, including two natural marine clays, BBC and Onsøy, and two manufactured clays, Prestige and PureGold Gel. The influence of initial water content on the thixotropic behavior of soft clays was also studied, covering only three clays, including BBC, Prestige, and PureGold Gel. Based on the above results and findings, the following major conclusions can be drawn:

- Thixotropic hardening is observed in all four soft clays at different temperatures and different initial water contents. The two natural clays show a higher regain in thixotropic strength than the two manufactured counterparts, most likely due to their higher natural porewater salinity and more diverse clay mineralogy.
- Both Prestige and BBC at *LL* exhibit the optimal thixotropic hardening or can achieve the highest thixotropic gain in strength.
- The thixotropic gain increases with increasing temperature for Onsøy. Prestige and BBC at the temperature of 44 ºC exhibit the highest degree of thixotropic hardening and ultimate strength.
- Both various temperatures and initial water contents do not change the thixotropic gain of PureGold Gel.
- The slope of s_u versus water content curve (flow curve) during thixotropic hardening process are constant for all three studied clays.

- The lower viscosity and resistance of water results from high temperature favor the reorientation or movement of the clay particles, which is one factor that increase the TSR since the clay particles can easier reorient or move to a more preferred structure to have a stronger strength with time.

6.5 Acknowledgments

This work was supported by the National Science Foundation (NSF) under Award CMMI 1640306. The author wants to thank Yiming Cao, a graduate student in the same group as the author from UMass Amherst, who helped with the experiments concerning the temperature effects, especially performed all tests at the most difficult temperature.

6.6 Declarations of Interest

None.

Table 6.1 Summary of the fitting parameters for the modified Burgers model (temperature)

Sample	Temperature (°C)	Property	c_1	c_2	c_3	c_4	c_5	R^2
BBC	4	s_u (kPa)	1.53	1.71	1.07	1735.20	2.53×10^{-5}	0.97
		s_u/s_{u0}	1.00	1.13	1.07	1147.54	2.52×10^{-5}	0.97
	24	s_u (kPa)	1.41	2.46	1.99	3.05	2.53×10^{-2}	0.99
		s_u/s_{u0}	1.00	1.75	1.96	2.16	2.51×10^{-2}	0.99
	44	s_u (kPa)	1.26	7.47	0.28	323.26	1.43×10^{-4}	0.99
		s_u/s_{u0}	1.00	8.04	0.33	27.18	2.00×10^{-3}	0.99
	64	s_u (kPa)	0.98	4.08	1458326.16	2.89	1.21×10^{-1}	0.94
		s_u/s_{u0}	1.00	4.17	46.40	2.95	1.21×10^{-1}	0.94
PureGold Gel	4	s_u (kPa)	1.99	0.94	2.10	1.49	3.20×10^{-2}	1.00
		s_u/s_{u0}	1.00	0.47	2.12	0.76	3.20×10^{-2}	0.99
	24	s_u (kPa)	2.01	1.80	0.44	2.75	3.00×10^{-3}	0.98
		s_u/s_{u0}	1.00	0.95	0.45	1.44	3.00×10^{-3}	0.98
	44	s_u (kPa)	1.90	1.57	1.59	1.09	2.40×10^{-2}	0.98
		s_u/s_{u0}	1.00	0.83	1.55	0.57	2.40×10^{-2}	0.98
	64	s_u (kPa)	2.01	0.80	1.16	4.83	7.00×10^{-3}	0.99
		s_u/s_{u0}	1.00	0.40	1.26	2.36	8.00×10^{-3}	0.99
Prestige	4	s_u (kPa)	2.00	0.59	12048.73	0.65	3.60×10^{-2}	0.98
		s_u/s_{u0}	1.00	0.29	210.39	0.32	3.70×10^{-2}	0.98
	24	s_u (kPa)	1.93	1.13	0.76	565.14	2.44×10^{-5}	0.99
		s_u/s_{u0}	1.00	0.62	0.48	318.66	2.21×10^{-5}	0.96
	44	s_u (kPa)	2.04	2.43	0.13	0.27	1.33×10^{-1}	0.98
		s_u/s_{u0}	1.00	0.20	3706.05	1.37	1.16×10^{-1}	0.99
	64	s_u (kPa)	1.78	1.22	1.02	1.18	2.10×10^{-2}	0.99
		s_u/s_{u0}	1.00	0.69	1.10	0.67	2.30×10^{-2}	0.99
Onsøy	4	s_u (kPa)	1.99	1.37	46.76	1.95	1.51×10^{-2}	0.99
		s_u/s_{u0}	1.00	0.69	4.74	0.94	1.62×10^{-2}	0.99
	24	s_u (kPa)	1.97	1.27	4.97	1.71	7.41×10^{-2}	0.98
		s_u/s_{u0}	1.00	0.64	4.12	0.86	7.40×10^{-2}	0.98
	44	s_u (kPa)	1.83	3.21	0.69	1839.70	8.74×10^{-6}	0.98
		s_u/s_{u0}	1.00	1.68	0.67	998.57	8.56×10^{-6}	0.98
	64	s_u (kPa)	1.40	4.08	2573.90	7.67	4.19×10^{-2}	0.99
		s_u/s_{u0}	1.00	2.93	52594.85	5.50	4.19×10^{-2}	0.99

Note: R^2 = coefficient of determination

Table 6.2 Water content statistics of all temperature specimens during the FC testing

Specimens	Temperature (ºC)	Average	Standard deviation	Coefficient of variation
BBC	4	45	0.13	0.29
	24	45	0.35	0.78
	44	42	0.46	1.09
	64	43	0.66	1.55
PureGold Gel	4	419	2.69	0.64
	24	418	4.01	0.36
	44	416	2.73	0.65
	64	464	6.91	1.49
Prestige	4	44	0.24	0.56
	24	43	0.57	1.33
	44	43	0.69	1.63
	64	45	1.81	4.05
Onsøy	4	65	0.37	0.57
	24	66	0.54	0.82
	44	65	1.02	1.58
	64	55	1.02	1.87

Table 6.3 Summary of the fitting parameters for the modified Burgers model (initial water content)

Sample	Initial water content (%)	Property	c_1	c_2	c_3	c_4	c_5	R^2
BBC	0.8*LL*	s_u (kPa)	4.74	6.17	1.24	4.63	3.78×10^{-2}	1.00
		s_u/s_{u0}	1.00	1.29	1.22	0.96	3.82×10^{-2}	1.00
	1.0*LL*	s_u (kPa)	1.40	2.50	1.93	3.03	2.42×10^{-2}	0.99
		s_u/s_{u0}	1.00	1.79	1.93	2.17	2.42×10^{-2}	0.99
	1.2*LL*	s_u (kPa)	0.61	0.64	0.68	1.04	1.52×10^{-2}	1.00
		s_u/s_{u0}	1.00	1.02	0.67	1.67	1.53×10^{-2}	1.00
PureGold Gel	0.8*LL*	s_u (kPa)	3.12	1.79	1.12	2.45	3.27×10^{-2}	1.00
		s_u/s_{u0}	1.00	0.58	1.12	0.79	3.32×10^{-2}	1.00
	1.0*LL*	s_u (kPa)	1.91	1.81	0.61	1.43	9.37×10^{-3}	1.00
		s_u/s_{u0}	1.00	0.98	0.62	0.74	9.51×10^{-3}	0.99
	1.2*LL*	s_u (kPa)	1.19	0.98	0.80	1.27	1.10×10^{-2}	1.00
		s_u/s_{u0}	1.00	0.84	0.84	1.08	1.11×10^{-2}	1.00
Prestige	0.8*LL*	s_u (kPa)	5.08	1.30	1.29	5.40	1.70×10^{-2}	1.00
		s_u/s_{u0}	1.00	0.26	1.22	1.08	1.60×10^{-2}	1.00
	0.95*LL*	s_u (kPa)	1.96	1.12	0.74	793.01	1.72×10^{-5}	0.99
		s_u/s_{u0}	1.00	0.59	0.74	425.56	1.65×10^{-5}	0.99
	1.2*LL*	s_u (kPa)	0.69	0.20	3.06	0.50	3.29×10^{-2}	0.99
		s_u/s_{u0}	1.00	0.30	2.95	0.72	3.14×10^{-2}	0.99

Note: R^2 = coefficient of determination

Table 6.4 Water content statistics of all specimens during the FC testing

Specimens	Initial water content (%)	Average	Standard deviation	Coefficient of variation
BBC	0.8*LL*	39	0.50	1.27
	1.0*LL*	45	0.36	0.81
	1.2*LL*	59	0.36	0.62
PureGold Gel	0.8*LL*	337	2.09	0.62
	1.0 *LL*	418	4.01	0.96
	1.2*LL*	503	2.95	0.59
Prestige	0.8*LL*	37	0.58	1.55
	0.95 *LL*	43	0.57	1.33
	1.2*LL*	55	0.32	0.57

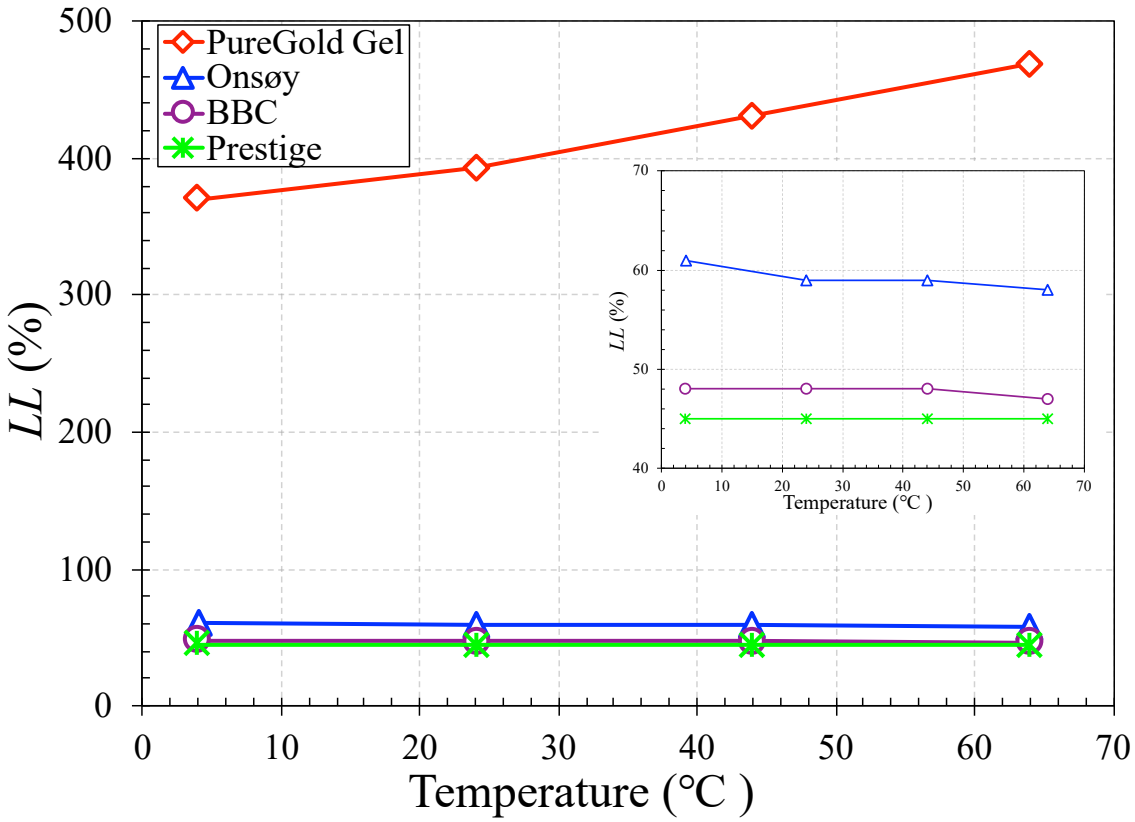

Figure 6.1 Liquid Limits determinations of each clay at different temperatures.

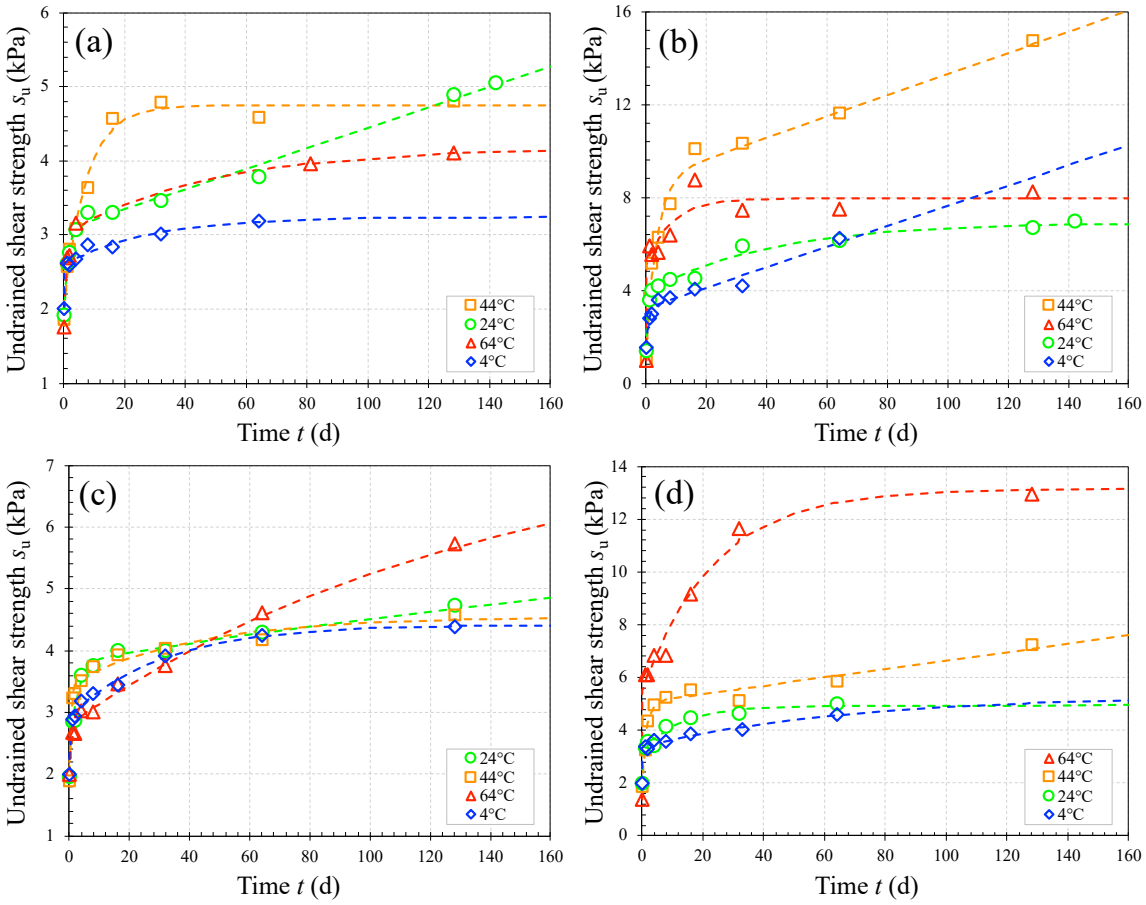

Figure 6.2 Thixotropic evolution of undrained shear strength at different temperatures: s_u vs. time of (a) Prestige; (b) BBC; (c) PureGold Gel; (d) Onsøy.

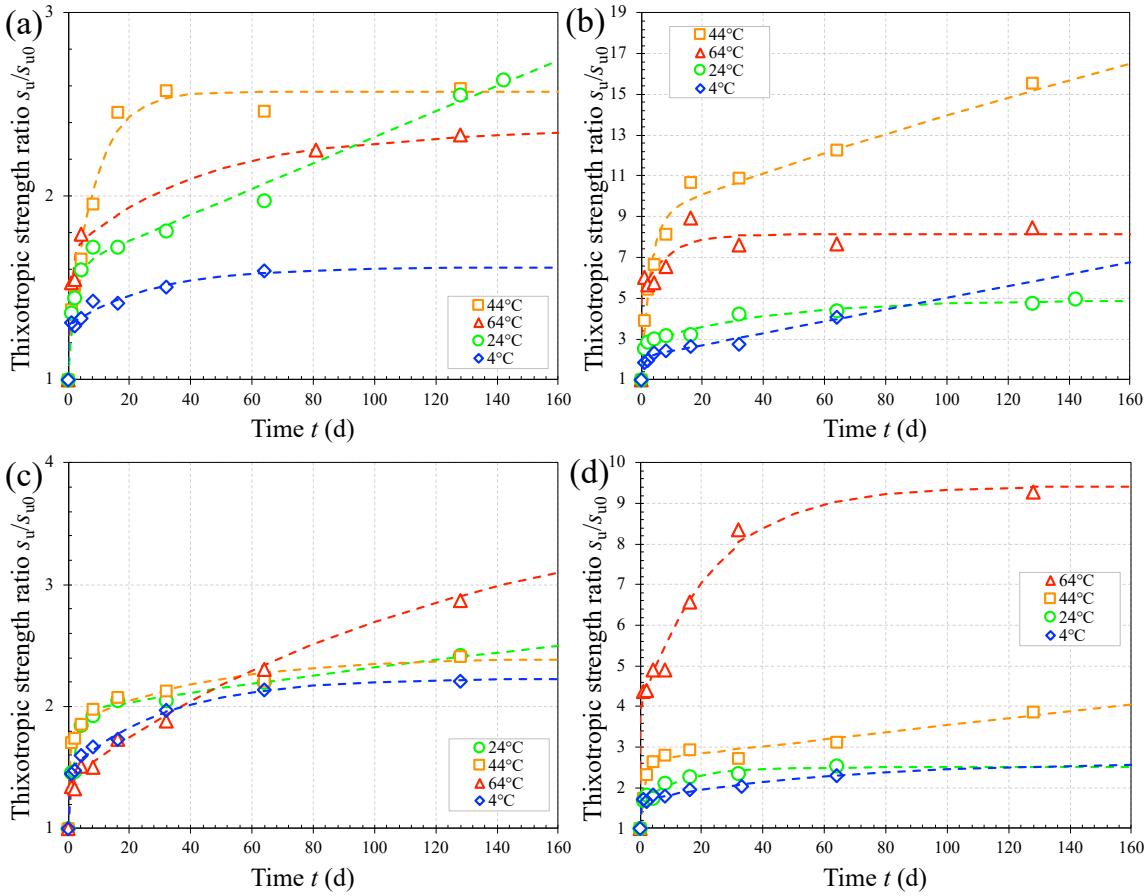

Figure 6.3 Thixotropic evolution of undrained shear strength at different temperatures: TSR vs. time of (a) Prestige; (b) BBC; (c) PureGold Gel; (d) Onsøy.

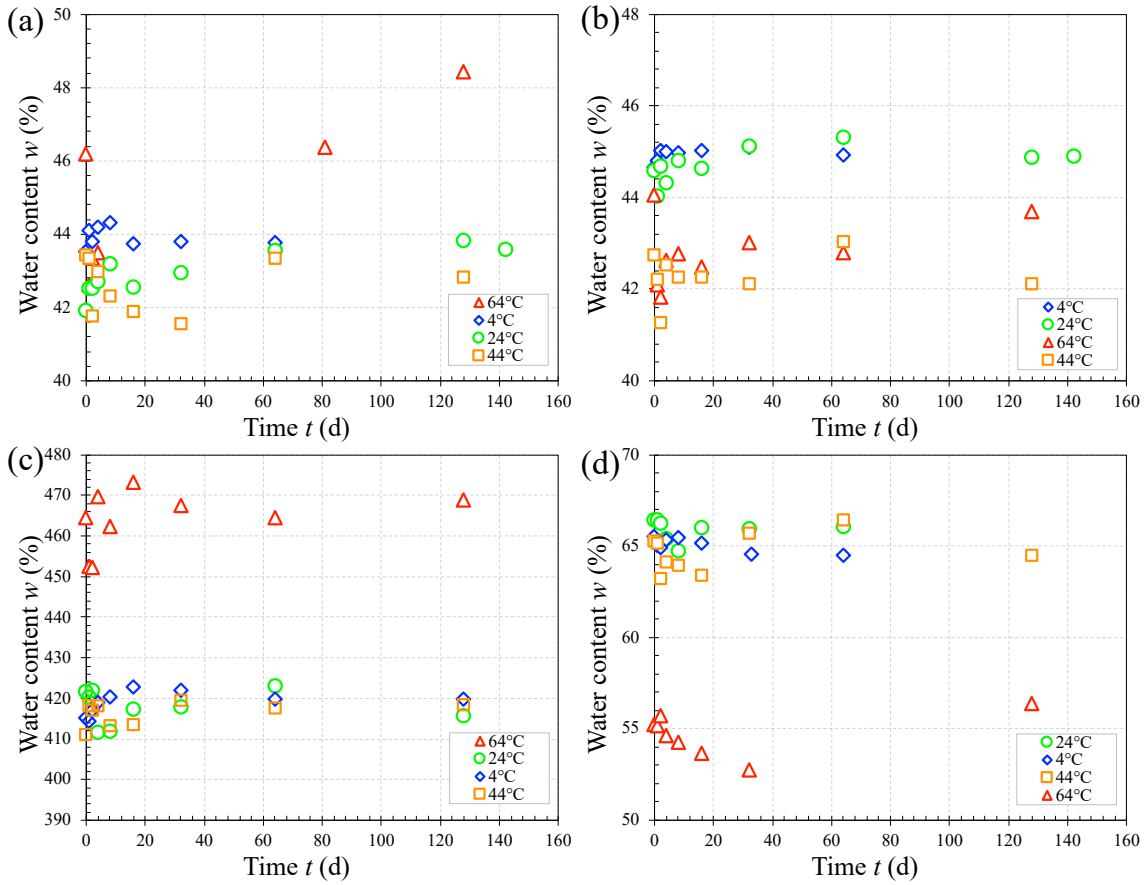

Figure 6.4 Water content measurements of all FC specimens during thixotropy at different temperatures: (a) Prestige; (b) BBC; (c) PureGold Gel; (d) Onsøy.

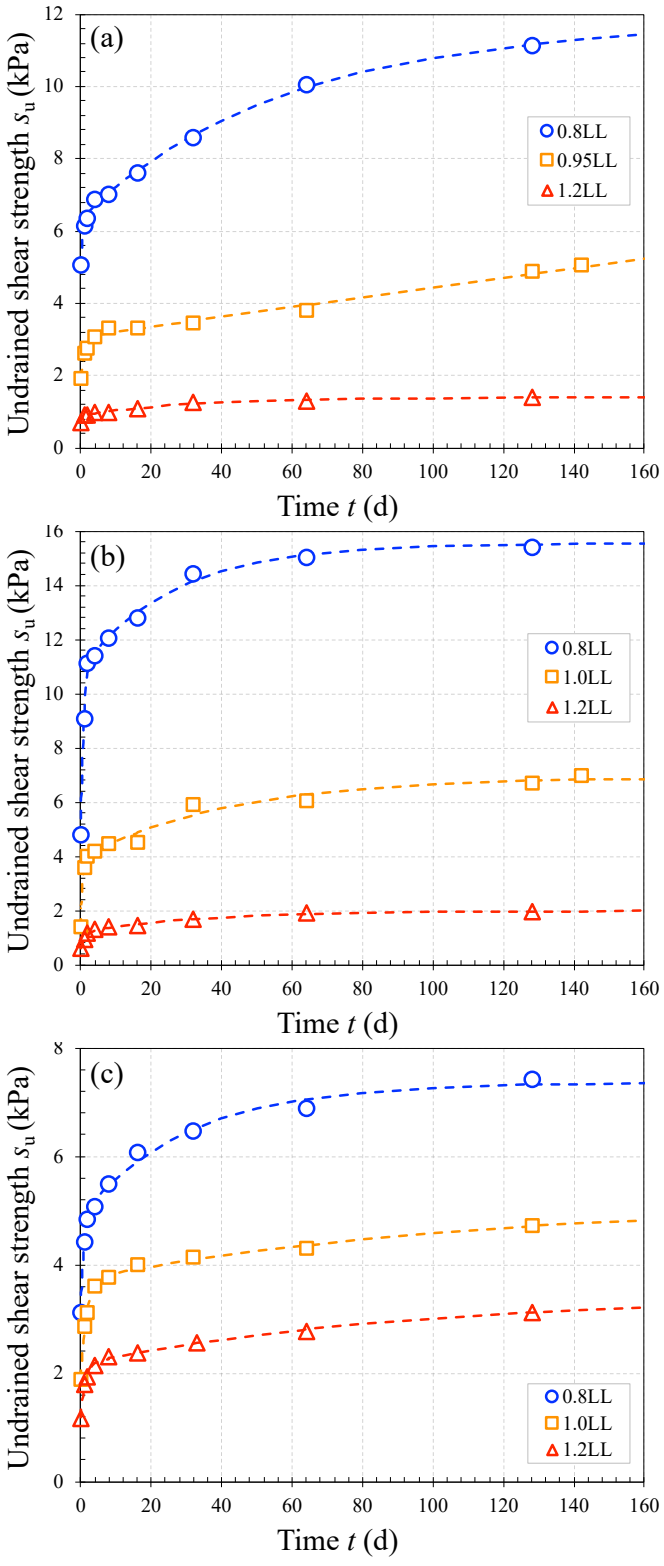

Figure 6.5 Thixotropic evolution of undrained shear strength with different initial water contents: s_u vs. time of (a) Prestige; (b) BBC; (c) PureGold Gel.

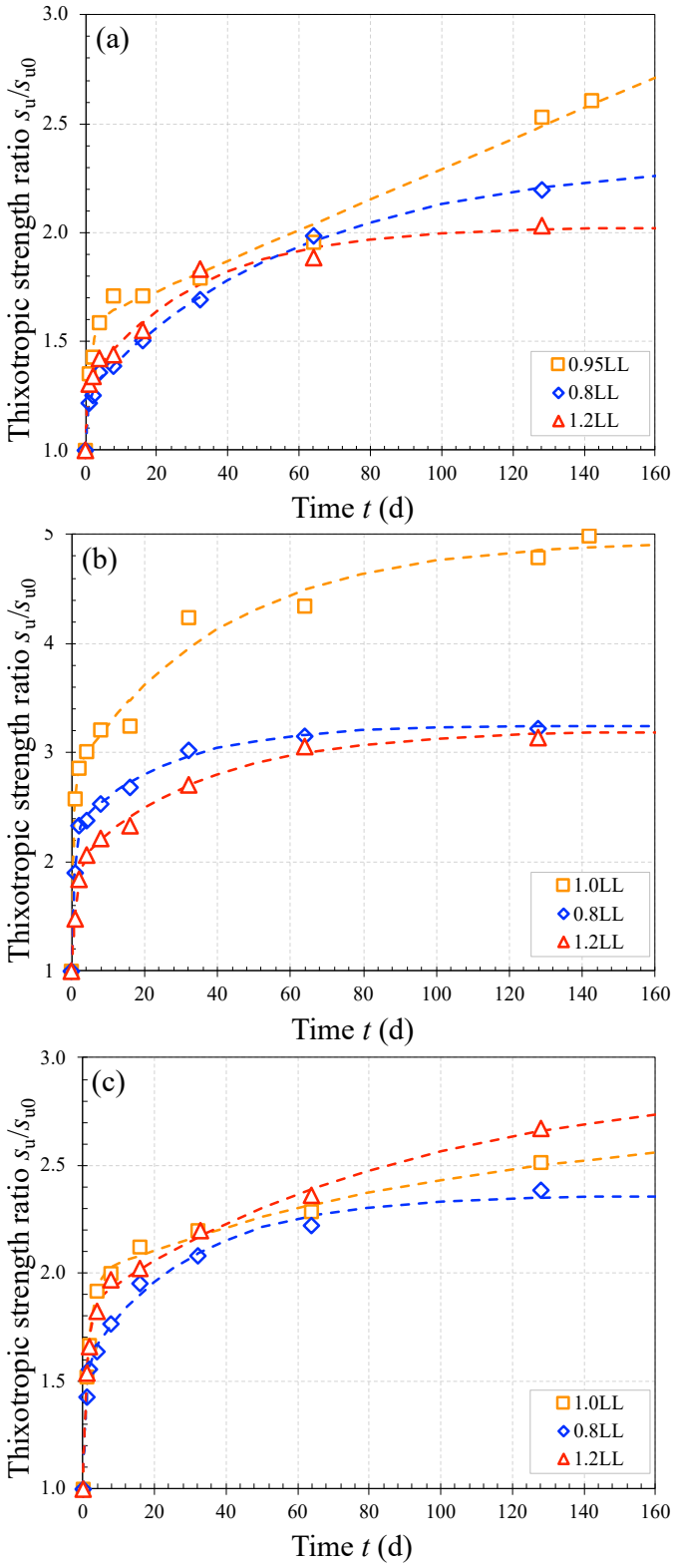

Figure 6.6 Thixotropic evolution of undrained shear strength with different initial water contents: TSR vs. time of (a) Prestige; (b) BBC; (c) PureGold Gel.

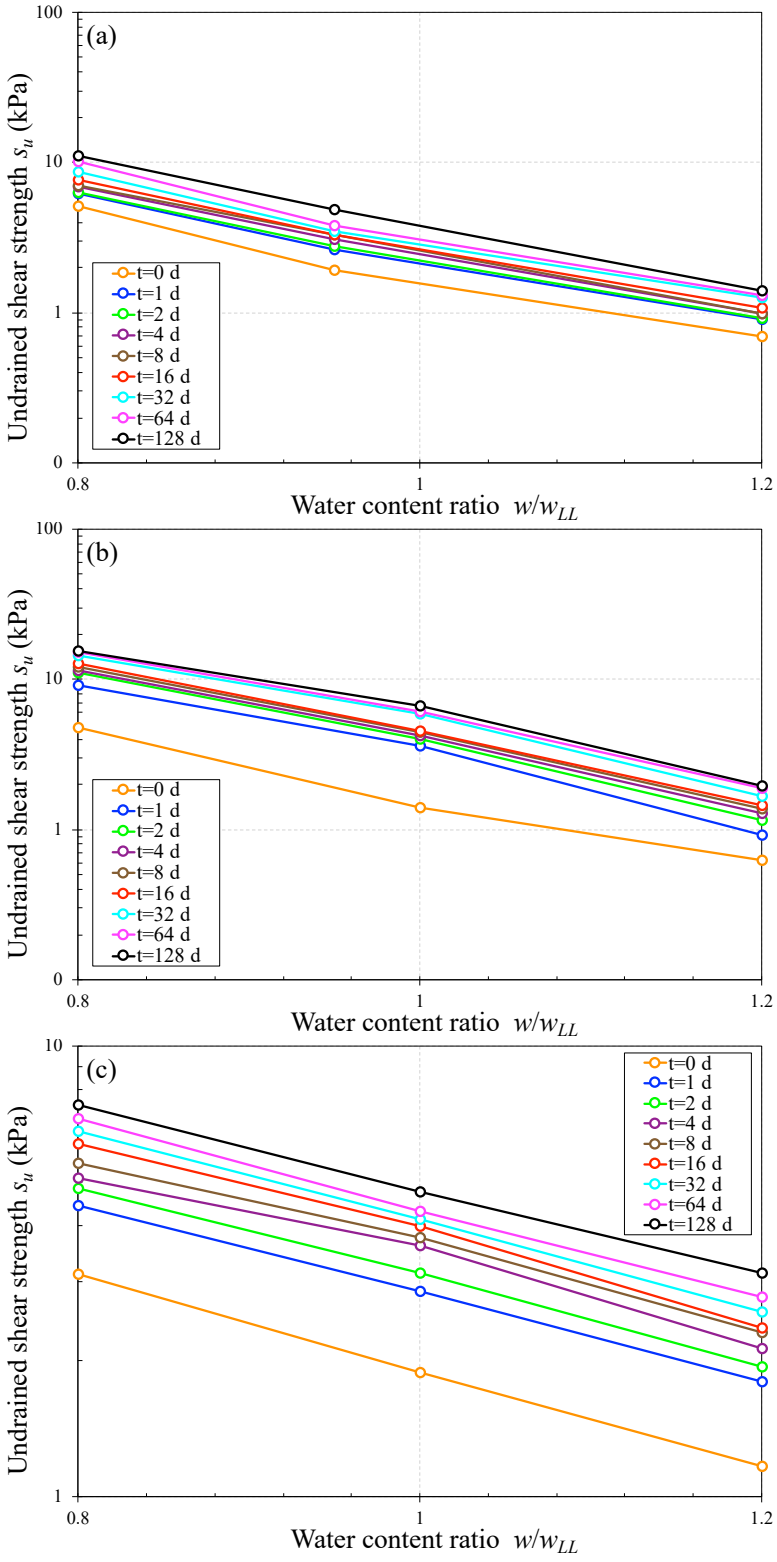

Figure 6.7 Undrained shear strength vs. water content ratio (flow curve): (a) Prestige; (b) BBC; (c) PureGold Gel.

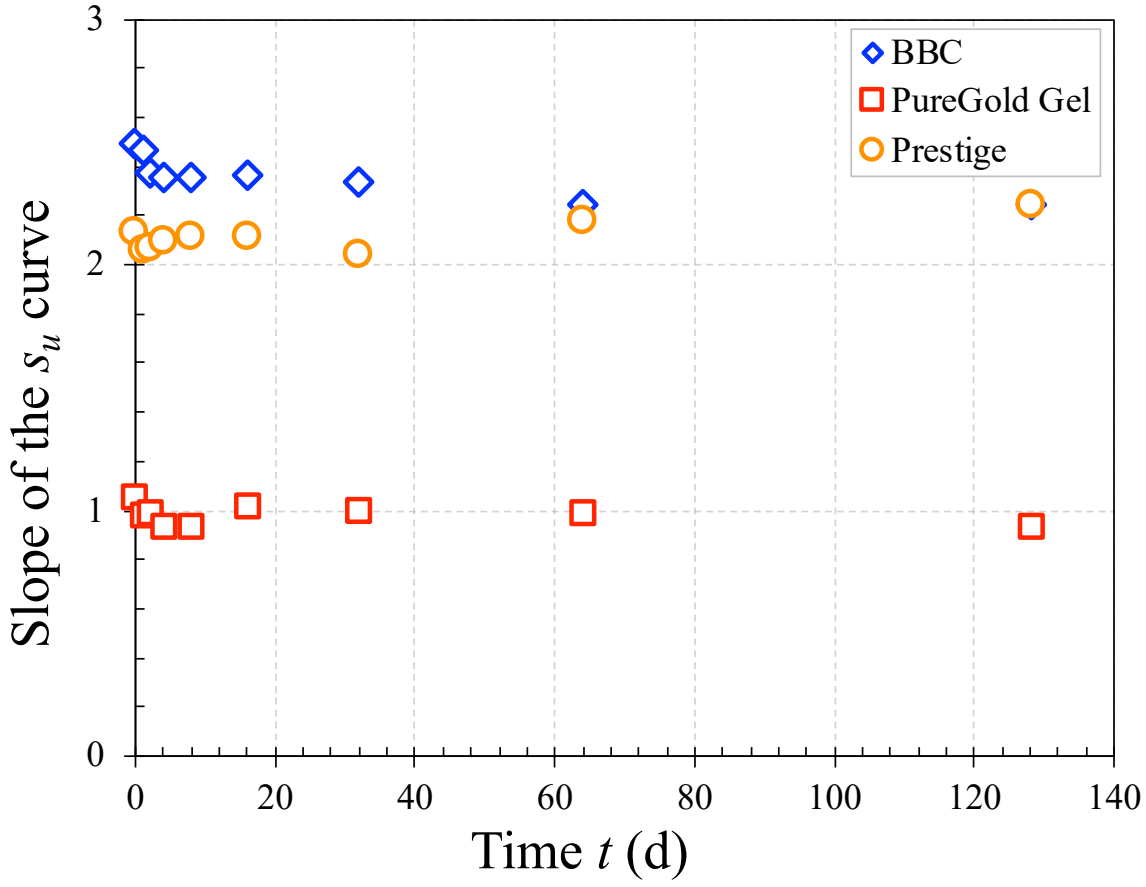

Figure 6.8 Slope of the flow curve during thixotropic hardening: (a) Prestige; (b) BBC; (c) PureGold Gel.

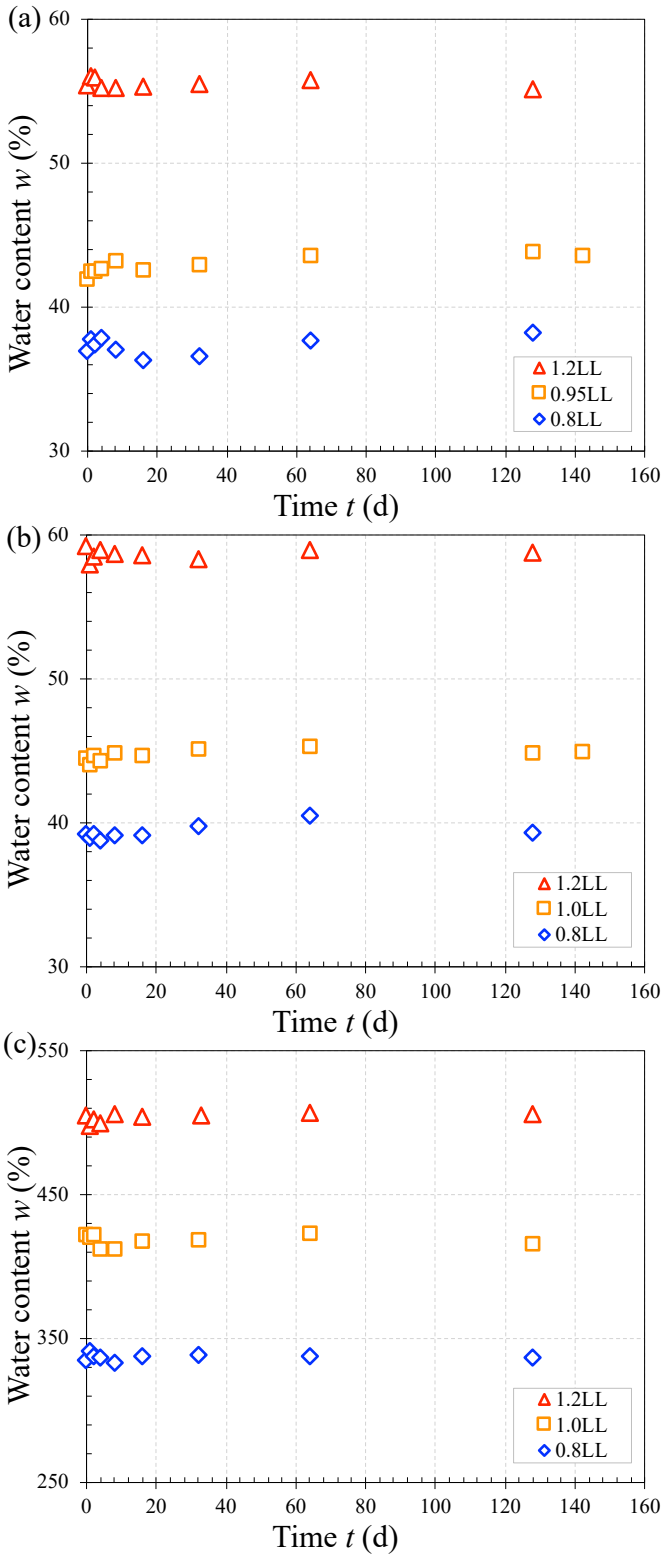

Figure 6.9 Water content measurements of all FC specimens during thixotropy with different initial water contents: (a) Prestige; (b) BBC; (c) PureGold Gel.

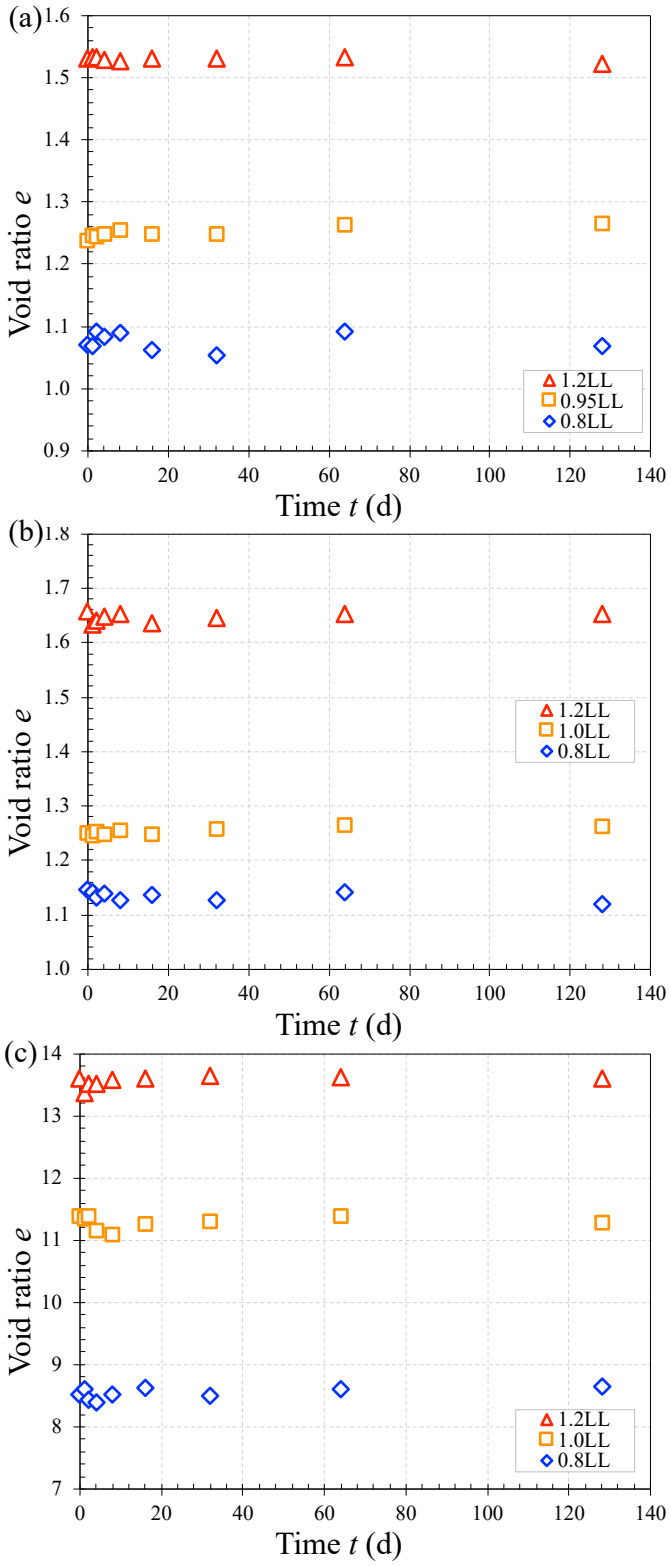

Figure 6.10 Void ratio measurements of all FC specimens during thixotropy with different initial water contents: (a) Prestige; (b) BBC; (c) PureGold Gel.

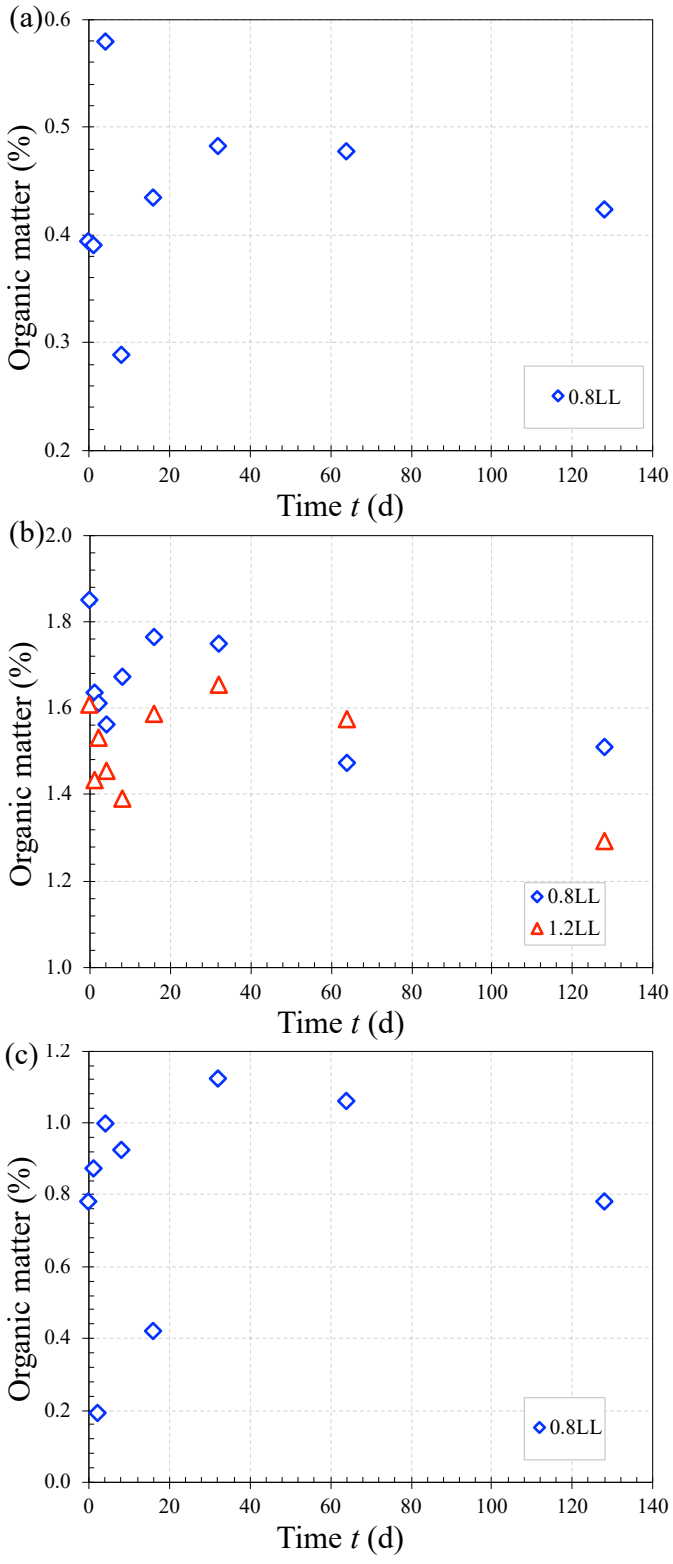

Figure 6.11 Organic matter measurements of part of FC specimens during thixotropy with different initial water contents: (a) Prestige; (b) BBC; (c) PureGold Gel.

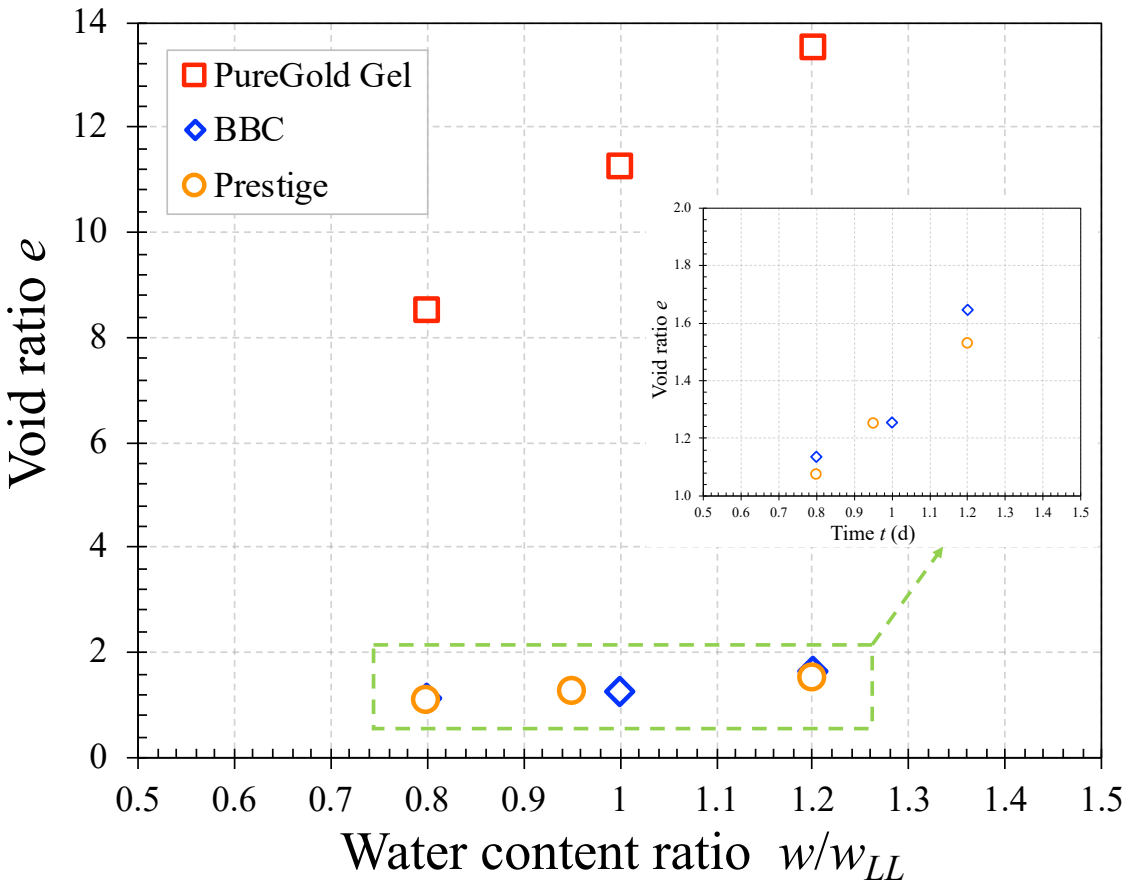

Figure 6.12 Average void ratio of each clay specimens.

CHAPTER 7

CONCLUSIONS AND FUTURE WORK

7.1 Conclusions

The overall objective of this dissertation was to develop a basic understanding of the microstructural and macromechanical mechanisms of thixotropy of soft clays, which can help expand the knowledge base on this time-dependent soil behavior. Multiscale experimentation efforts, including macroscale mechanical testing and microscale soil fabric characterization, were made to achieve this goal. In this section, a summary of the major findings obtained through this multiscale investigation on soft clays during thixotropy is presented as follows:

- In general, all studied soft clays, being either naturally-formed or laboratory-synthetic, possess thixotropic hardening behavior. Both undrained shear strength and maximum shear modulus increase with time. The rigidity index (the ratio of shear modulus to undrained shear strength) could be treated approximately as a constant during the entire thixotropic hardening in typical engineering practice. Additionally, such thixotropic behavior is affected by the porewater salinity, temperature, and initial water content, and their interplay in controlling the thixotropy is rather complex.
- The temporal evolution of the microstructure of soft clays is complex, including reorientation from the high shearing-induced parallel orientation, hydrogen bond, or other interparticle force-induced aggregation to form face-to-face associated particle groups, further flocculation of aggregates, and continuous formation of thicker aggregates.

- Both 1DXRD and 2DXRD are viable techniques for quantitatively characterizing the temporal fabric evolution of wet clays, which provides direct and quantitative evidence for the fundamental microscopic mechanisms governing the thixotropic behavior of soft clays.
- Multiple mechanisms of soft clay thixotropy were unraveled by microscale characterization, including soil fabric evolution (such as clay particle reorientation, aggregation, flocculation), homogenization of prior disturbance, defects/flaws, microstructure (e.g., porosity distribution), and pore pressure, and contact aging. Although these mechanisms may occur simultaneously during the entire duration of thixotropic hardening, the two dissimilar stages identified by macroscopic mechanical testing are controlled by different primary mechanisms. While the 1st stage may be affected by all of the above mechanisms, fabric evolution may play the primary role. However, in the 2nd stage, contact aging may become dominant upon the completion of fabric evolution, occurring primarily in the 1st stage.
- Clay mineralogy and composition, particularly clay minerals with chemically active surfaces (e.g., surface charges, surface-adsorbed cations, electrical double layer), also play an important role in governing the thixotropic behavior, particularly for varying temperature and porewater salinity conditions. Different clay minerals may exhibit different degrees of thixotropic hardening rate and magnitude, and the salinity and temperature at the maximum of the hardening rate and magnitude are also affected by the clay mineralogy.

- All clays at different porewater salinity exhibit thixotropic hardening to various extents, and an optimum porewater salinity exists, varying from clay to clay, at which a soft clay may exhibit the highest TSR. Higher thixotropic gain in strength results from greater microfabric changes. The thickness of EDL reduces with increasing porewater salinity, while surface tension and viscosity of water increase, which contributes to greater resistance to interparticle shearing hence a higher s_u in the beginning but entangle the rearrangements of the clay particles (e.g., reorientation) in difficulty hence lower TSR.
- The slope of s_u versus water content curve (flow curve) during thixotropic hardening process remains constant for all three studied clays.
- The lower viscosity and resistance of water results from high temperature favor the reorientation or movement of the clay particles, which is one factor that increase the TSR since the clay particles can easier reorient or move to a more preferred structure to have a stronger strength with time.
- The different results of each clay indicate that the effect of mineralogy besides the porewater salinity, temperature, and initial water content on thixotropic behavior of soft clays, which warrants further analysis.

7.2 Future Perspectives

The underlying mechanisms of thixotropy of soft clay are complex, and this fundamental soil behavior is influenced by various physical and chemical factors, including temperature, porewater salinity, and water content. Since a range of time-dependent engineering properties of soft clays widely encountered in engineering practice was

governed by thixotropy, more studies should be conducted to broaden the impacts. The microfabric evolution of the clay during thixotropy revealed from microscale experiments conducted in this dissertation is interesting and can be extended further. Besides the microscale experimentation applied in this dissertation, additional mechanical testing can also be utilized to confirm the theories or principles that have been used hundred years in our geotechnical field. The following briefly describes the objectives of some potential research topics to be explored:

(1) According to Terzaghi's effective stress principle, an increase in strength or stiffness should result from an increase in effective stress. Effective stress can be determined if the soil suction can be measured since for the thixotropy tests conducted in this work the total stress is zero.

(2) Clay minerals with chemically active surfaces (e.g., surface charges, surface-adsorbed cations, electrical double layer) were discovered to play an important role in governing the thixotropic behavior. Different pure clay minerals can be studied to understand the influence of clay mineralogy itself.

(3) Pore size distributions of each clay during the thixotropic curing process can be probed by techniques such as computed tomography, mercury porosimetry, and gas adsorption. The results can further confirm and support one of thixotropic mechanisms summarized in this dissertation.

(4) The changes in particle sizes during thixotropy can also be determined from advanced techniques, such as small-angle X-ray scattering, which can further support the "parallel aggregation" mechanism and help better understand the mechanisms of this soil behavior.

BIBLIOGRAPHY

Abend, S., Lagaly, G., 2000. Sol–gel transitions of sodium montmorillonite dispersions. Appl. Clay Sci. 16, 201–227. https://doi.org/10.1016/S0169-1317(99)00040-X

Abu-Farsakh, M., Rosti, F., Souri, A., 2015a. Evaluating pile installation and the following thixotropic and consolidation setup by numerical simulation for full scale pile load tests. Can. Geotech. J. 52, 1734–1746. https://doi.org/10.1139/cgj-2014-0470

Abu-Farsakh, M., Rosti, F., Souri, A., 2015b. Evaluating pile installation and subsequent thixotropic and consolidation effects on setup by numerical simulation for full-scale pile load tests. Can. Geotech. J. 52, 1734–1746. https://doi.org/10.1139/cgj-2014-0470

Almer, J., Lienert, U., Peng, R.L., Schlauer, C., Odén, M., 2003. Strain and texture analysis of coatings using high-energy x-rays. J. Appl. Phys. 94, 697–702. https://doi.org/10.1063/1.1582351

Andersen, K.H., Jostad, H.P., 2004. Shear strength along inside of suction anchor skirt wall in clay, in: Offshore Technology Conference. Offshore Technology Conference, Houston, Texas. https://doi.org/10.4043/16844-MS

Andersen, K.H., Jostad, H.P., 2002. Shear strength along outside wall of suction anchors in clay after installation, in: The Twelfth International Offshore and Polar Engineering Conference. International Society of Offshore and Polar Engineers, Kitakyushu, Japan.

Angelini, R., Zaccarelli, E., de Melo Marques, F.A., Sztucki, M., Fluerasu, A., Ruocco, G., Ruzicka, B., 2014. Glass–glass transition during aging of a colloidal clay. Nat. Commun. 5, 4049. https://doi.org/10.1038/ncomms5049

Arnold, J.E., Goodeve, C.F., 1940. The coefficient of thixotropy of suspensions of carbon black in mineral oil. J. Phys. Chem. 44, 652–670. https://doi.org/10.1021/j150401a013

Arnold, M., 1967. A study of thixotropic action in bentonite clay. University of Adelaide.

Astbury, N.F., Moore, F., 1970. Torsional hysteresis in plastic clay. Rheol. Acta 9, 124–129. https://doi.org/10.1007/BF01984604

ASTM, 2020. Volume 04.08 - Soil and Rock (I): D420 to D5876 and Volume 04.09 - Soil and Rock (II): D5877 to latest.

ASTM, 2014. Standard Test Methods for Moisture, Ash, and Organic Matter of Peat and Other Organic Soils.

Baligh, M.M., Azzouz, A.S., Chin, C., 1987. Disturbances Due to "Ideal" Tube Sampling. J. Geotech. Eng. 113, 739–757. https://doi.org/10.1061/(ASCE)0733-9410(1987)113:7(739)

Barnes, H.A., 2000. A handbook of elementary rheology. Institute of Non-Newtonian Fluid Mechanics, University of Wales, Aberystwyth.

Barnes, H.A., 1997. Thixotropy - A review. J. Nonnewton. Fluid Mech. 70, 1–33. https://doi.org/10.1016/S0377-0257(97)00004-9

Basta, A.H., El-Saied, H., El-Sayad, S.Y., Morsy, F., 1998. The rheological properties of paper coating suspensions and their application. Surf. Coatings Int. 81, 426–434. https://doi.org/10.1007/BF02692972

Berland, S., Launay, B., 1995. Shear softening and thixotropic properties of wheat flour doughs in dynamic testing at high shear strain. Rheol. Acta 34, 622–625. https://doi.org/10.1007/BF00712321

Berthonneau, J., Hoover, C.G., Grauby, O., Baronnet, A., Pellenq, R.J.-M., Ulm, F.-J., 2017. Crystal-chemistry control of the mechanical properties of 2:1 clay minerals. Appl. Clay Sci. 143, 387–398. https://doi.org/10.1016/j.clay.2017.04.010

Bonacci, F., Chateau, X., Furst, E.M., Fusier, J., Goyon, J., Lemaître, A., 2020. Contact and macroscopic ageing in colloidal suspensions. Nat. Mater. 19, 775–780. https://doi.org/10.1038/s41563-020-0624-9

Bontempi, E., Benedetti, D., Zacco, A., Pantos, E., Boniotti, S., Saletti, C., Apostoli, P., Depero, L.E., 2008. Analysis of crystalline phases in airborne particulate matter by two-dimensional X-ray diffraction (XRD^2). J. Environ. Monit. 10, 82–88. https://doi.org/10.1039/B715517D

Boswell, P.G.H., 1948. A preliminary examination of the thixotropy of some sedimentary rocks. Q. J. Geol. Soc. 104, 499–526. https://doi.org/10.1144/GSL.JGS.1948.104.01-04.23

Brindley, G.W., Kurtossy, S.S., 1961. Quantitative determination of kaolinite by x-ray diffraction. Am. Mineral. 46, 1205–1215.

Brown, G.M., Noespirlet, M.R., Busing, W.R., Levy, H.A., 1977. Dodecatungstophosphoric acid hexahydrate, $(H_5O_2^+)_3(PW_{12}O_{40}^{3-})$. The true structure of keggin's "pentahydrate" from single-crystal X-ray and neutron-diffraction data. Acta Crystallogr. Sect. B Struct. Crystallogr. Cryst. Chem. 33, 1038–1046. https://doi.org/10.1107/S0567740877005330

Burt, R., 2014. Kellogg soil survey laboratory methods manual, Version 5. ed. United States Department of Agriculture, Natural Resource Conservation Service.

Bzdek, B.R., Power, R.M., Simpson, S.H., Reid, J.P., Royall, C.P., 2016. Precise, contactless measurements of the surface tension of picolitre aerosol droplets. Chem. Sci. 7, 274–285. https://doi.org/10.1039/C5SC03184B

Casagrande, A., 1948. Classification and identification of soils. Trans. Am. Soc. Civ. Eng.

113, 901–930.

Casagrande, A., 1932. The structure of clay and its importance in foundation engineering. Bost. Soc. Civ. Eng. 72–112.

Chang, C., Nguyen, Q.D., Rønningsen, H.P., 1999. Isothermal start-up of pipeline transporting waxy crude oil. J. Nonnewton. Fluid Mech. 87, 127–154. https://doi.org/10.1016/S0377-0257(99)00059-2

Cini, R., Loglio, G., Ficalbi, A., 1972. Temperature dependence of the surface tension of water by the equilibrium ring method. J. Colloid Interface Sci. 41, 287–297. https://doi.org/https://doi.org/10.1016/0021-9797(72)90113-0

Collins, D.M., Mostafavi, M., Todd, R.I., Connolley, T., Wilkinson, A.J., 2015. A synchrotron X-ray diffraction study of in situ biaxial deformation. Acta Mater. 90, 46–58. https://doi.org/10.1016/J.ACTAMAT.2015.02.009

Coussot, P., Gaulard, F., 2005. Gravity flow instability of viscoplastic materials: The ketchup drip. Phys. Rev. E 72, 31409. https://doi.org/10.1103/PhysRevE.72.031409

Coussot, P., Nguyen, Q.D., Huynh, H.T., Bonn, D., 2002. Viscosity bifurcation in thixotropic, yielding fluids. J. Rheol. (N. Y. N. Y). 46, 573–589. https://doi.org/10.1122/1.1459447

Davis, T.J., Gao, D., Gureyev, T.E., Stevenson, A.W., Wilkins, S.W., 1995. Phase-contrast imaging of weakly absorbing materials using hard X-rays. Nature 373, 595–598. https://doi.org/10.1038/373595a0

de Souza Mendes, P.R., Thompson, R.L., 2012. A critical overview of elasto-viscoplastic thixotropic modeling. J. Nonnewton. Fluid Mech. 187–188, 8–15. https://doi.org/10.1016/J.JNNFM.2012.08.006

Deirieh, A., Chang, I.Y., Whittaker, M.L., Weigand, S., Keane, D., Rix, J., Germaine, J.T., Joester, D., Flemings, P.B., 2018. Particle arrangements in clay slurries: The case against the honeycomb structure. Appl. Clay Sci. 152, 166–172. https://doi.org/10.1016/j.clay.2017.11.010

DeJong, J.T., Randolph, M.F., 2012. Influence of partial consolidation during cone penetration on estimated soil behavior type and pore pressure dissipation measurements. J. Geotech. Geoenvironmental Eng. 138, 777–788. https://doi.org/10.1061/(ASCE)GT.1943-5606.0000646

Di Maio, C., 1996. Exposure of bentonite to salt solution: osmotic and mechanical effects. Géotechnique 46, 695–707. https://doi.org/10.1680/geot.1996.46.4.695

Díaz-Rodríguez, J.A., Santamarina, J.C., 1999. Thixotropy: The case of Mexico city soils, in: XI Panamerican Conference on Soil Mechanics and Geotechnical Engineering. Brazil, pp. 441–448. https://doi.org/10.13140/2.1.3191.4883

Döbelin, N., Kleeberg, R., 2015. Profex: A graphical user interface for the Rietveld refinement program BGMN. J. Appl. Crystallogr. 48, 1573–1580. https://doi.org/10.1107/S1600576715014685

Dohrmann, R., Rüping, K., Kleber, M., Ufer, K., Jahn, R., 2009. Variation of preferred orientation in oriented clay mounts as a result of sample preparation and composition. Clays Clay Miner. 57, 686–694. https://doi.org/10.1346/CCMN.2009.0570602

Dubrovinsky, L.S., Saxena, S.K., Lazor, P., Ahuja, R., Eriksson, O., Wills, J.M., Johansson, B., 1997. Experimental and theoretical identification of a new high-pressure phase of silica. Nature 388, 362–365. https://doi.org/10.1038/41066

Engler, O., Randle, V., 2010. Introduction to texture analysis : Macrotexture, microtexture and orientation mapping, 2nd Editio. ed. CRC Press, Taylor & Francis Group, Boca Raton.

Freundlich, H., Rawitzer, W., 1927. Influence of metals on thixotropic sols and gels. Colloid Polym. Sci. 41, 102–104.

Fugro, E.B., 2004. Pore Fluid Salinity.

Gamble, D.L., 1936. Thixotropy in paints influence on packaging and application properties of flat wall coatings. Ind. Eng. Chem. 28, 1204–1210. https://doi.org/10.1021/ie50322a020

Goldsack, D.E., Franchetto, R., 1977. The viscosity of concentrated electrolyte solutions. I. Concentration dependence at fixed temperature. Can. J. Chem. 55, 1062–1072. https://doi.org/10.1139/v77-148

Goodeve, C.F., 1939. A general theory of thixotropy and viscosity. Trans. Faraday Soc. 35, 342–358. https://doi.org/10.1039/TF9393500342

Gorakhki, M.H., Bareither, C.A., 2015. Salinity effects on sedimentation behavior of kaolin, bentonite, and soda ash mine tailings. Appl. Clay Sci. 114, 593–602. https://doi.org/10.1016/J.CLAY.2015.07.018

Guo, Z., Wang, L.-Z., Yuan, F., 2014. Set-up and pullout mechanism of suction caisson in a soft clay seabed. Mar. Georesources Geotechnol. 32, 135–154. https://doi.org/10.1080/1064119X.2012.716503

Harris, K.D.M., Tremayne, M., Lightfoot, P., Bruce, P.G., 1994. Crystal structure determination from powder diffraction data by Monte Carlo methods. J. Am. Chem. Soc. 116, 3543–3547. https://doi.org/10.1021/ja00087a047

He, B.B., 2009a. Introduction, in: Two-Dimensional X-Ray Diffraction. John Wiley & Sons, Inc., pp. 1–27. https://doi.org/10.1002/9780470502648.ch1

He, B.B., 2009b. Geometry Conventions, in: Two-Dimensional X-Ray Diffraction, Wiley

Online Books. John Wiley & Sons, Inc., pp. 28–50. https://doi.org/10.1002/9780470502648.ch2

He, B.B., 2009c. Two-Dimensional X-Ray Diffraction, 2nd ed. John Wiley & Sons, Inc., New Jersey.

He, B.B., 2009d. Texture analysis, in: John Wiley & Sons, I. (Ed.), Two-dimensional X-ray Diffraction, Wiley Online Books. pp. 235–270. https://doi.org/10.1002/9781119356080.ch8

He, B.B., 2003. Introduction to two-dimensional X-ray diffraction. Powder Diffr. 18, 71–85. https://doi.org/10.1154/1.1577355

He, B.B., Preckwinkel, U., Smith, K.L., 2002. Stress and texture analysis with two-dimensional X-ray diffraction. Mater. Sci. Forum 404–407, 109–114. https://doi.org/10.4028/www.scientific.net/MSF.404-407.109

He, B.B., Preckwinkel, U., Smith, L.K., 2000. Fundamentals of two-dimensional X-ray diffraction (XRD^2). Adv. X-ray Anal. 43, 273–280.

Helming, K., Preckwinkel, U., 2005. Texture analysis with area detectors. Solid State Phenom. 105, 71–76. https://doi.org/10.4028/www.scientific.net/SSP.105.71

Hielscher, R., Schaeben, H., 2008. A novel pole figure inversion method: Specification of the MTEX algorithm. J. Appl. Crystallogr. 41, 1024–1037. https://doi.org/10.1107/S0021889808030112

ISO/TS 17892-12, 2018. Geotechnical investigation and testing - Laboratory testing of soil - Part 12: Determination of Atterberg limits.

ISO/TS 17892-6, 2017. Geotechnical investigation and testing - Laboratory testing of soil - Part 6: Fall cone test.

Jacobsson, A., Pusch, R., 1972. Thixotropic action in remoulded quick clay. Bull. Int. Assoc. Eng. Geol. 5, 105–110. https://doi.org/10.1007/BF02634659

Jaswal, B.B.S., Rai, P.K., Singh, T., Zorba, V., Singh, V.K., 2019. Detection and quantification of heavy metal elements in gallstones using X-ray fluorescence spectrometry. X-Ray Spectrom. 48, 178–187. https://doi.org/10.1002/xrs.3010

Jeanjean, P., 2006. Setup characteristics of suction anchors for soft gulf of Mexico clays: Experience from field installation and retrieval, in: Offshore Technology Conference. Offshore Technology Conference, Houston, Texas, USA. https://doi.org/10.4043/18005-MS

Jeong, S.W., Locat, J., Leroueil, S., 2012. The effects of salinity and shear history on the rheological characteristics of illite-rich and Na-montmorillonite-rich clays. Clays Clay Miner. 60, 108–120. https://doi.org/10.1346/CCMN.2012.0600202

Jeong, S.W., Locat, J., Torrance, J.K., Leroueil, S., 2015. Thixotropic and anti-thixotropic behaviors of fine-grained soils in various flocculated systems. Eng. Geol. 196, 119–125. https://doi.org/10.1016/j.enggeo.2015.07.014

Joshi, Y.M., Reddy, G.R.K., Kulkarni, A.L., Kumar, N., Chhabra, R.P., 2008. Rheological behaviour of aqueous suspensions of laponite: New insights into the ageing phenomena, in: Proceedings of the Royal Society A: Mathematical, Physical and Engineering Sciences. Royal Society, pp. 469–489. https://doi.org/10.1098/rspa.2007.0250

Kanitpanyacharoen, W., Wenk, H., Kets, F., Lehr, C., Wirth, R., 2011. Texture and anisotropy analysis of Qusaiba shales. Geophys. Prospect. 59, 536–556. https://doi.org/10.1111/j.1365-2478.2010.00942.x

Kassem, M.A., Kassem, A.A., Salama, H.A., 1970. Studies on wool wax II: Investigation of the phenomenon of thixotropy. Fette, Seifen, Anstrichm. 72, 366–370. https://doi.org/10.1002/lipi.19700720503

Keaveny, J.M., Mitchell, J.K., 1986. Strength of fine-grained soils using the piezocone, in: Use of In Situ Tests in Geotechnical Engineering. ASCE, Reston, Virginia, pp. 668–685.

Kelessidis, V.C., 2008. Investigations on the thixotropy of bentonite suspensions. Energy Sources, Part A Recover. Util. Environ. Eff. 30, 1729–1746. https://doi.org/10.1080/15567030701456261

Korson, L., Drost-Hansen, W., Millero, F.J., 1969. Viscosity of water at various temperatures. J. Phys. Chem. 73, 34–39. https://doi.org/10.1021/j100721a006

Krage, C.P., Broussard, N.S., DeJong, J.T., 2014. Estimating rigidity index based on CPT measurements, in: Third International Symposium on Cone Penetration Testing. Las Vegas, Nevada, USA, pp. 727–735.

Labanda, J., Llorens, J., 2008. Effect of aging time on the rheology of Laponite dispersions. Colloids Surfaces A Physicochem. Eng. Asp. 329, 1–6. https://doi.org/10.1016/J.COLSURFA.2008.06.035

Ladd, C.C., DeGroot, D.J., 2003. Recommended practice for soft ground site characterization: Arthur Casagrande Lecture, in: 12th Panamerican Conference on Soil Mechanics and Geotechnical Engineering. Boston, MA, pp. 3–57.

Laguros, J.G., 1969. Effect of temperature on some engineering properties of clay soils. Highw. Res. Board Spec. Rep.

Lambe, T.W., 1953. The structure of inorganic soil, in: Proceedings of the American Society of Civil Engineers. pp. 1–49.

Landon, M.M., DeGroot, D.J., Sheahan, T.C., 2007. Nondestructive sample quality

assessment of a soft clay using shear wave velocity. J. Geotech. Geoenvironmental Eng. 133, 424–432. https://doi.org/10.1061/(ASCE)1090-0241(2007)133:4(424)

Lange, K., Rowe, R.K., Jamieson, H., Flemming, R.L., Lanzirotti, A., 2010. Characterization of geosynthetic clay liner bentonite using micro-analytical methods. Appl. Geochemistry 25, 1056–1069. https://doi.org/10.1016/J.APGEOCHEM.2010.04.011

Lanzirotti, A., Tappero, R., Schulze, D.G., 2010. Practical application of synchrotron-based hard X-ray microprobes in soil sciences. Dev. Soil Sci. 34, 27–72. https://doi.org/10.1016/S0166-2481(10)34002-5

Larson, R.G., Wei, Y., 2019. A review of thixotropy and its rheological modeling. J. Rheol. (N. Y. N. Y). 63, 477–501. https://doi.org/10.1122/1.5055031

Lessard, G., Mitchell, J.K., 1985. The causes and effects of aging in quick clays. Can. Geotech. J. 22, 335–346. https://doi.org/10.1139/t85-046

Lide, D.R. (Ed.), 2005. CRC handbook of chemistry and physics, 86th ed. CRC Press., Boca Raton (FL). https://doi.org/10.1021/ja059868l

Liebling, R.S., Kerr, P.F., 1965. Observations on quick clay. Geol. Soc. Am. Bull. 76, 853–878. https://doi.org/10.1130/0016-7606(1965)76[853:OOQC]2.0.CO;2

Lin, C.-Y., 2020. Alternative form of standard linear solid model for characterizing stress relaxation and creep: Including a novel parameter for quantifying the ratio of fluids to solids of a viscoelastic solid. Front. Mater. 7, 11. https://doi.org/10.3389/fmats.2020.00011

Liu, Q., Su, X., Lei, D., Qin, Y., Wen, J., Guo, F., Wu, Y.A., Rong, Y., Kou, R., Xiao, X., Aguesse, F., Bareño, J., Ren, Y., Lu, W., Li, Y., 2018. Approaching the capacity limit of lithium cobalt oxide in lithium ion batteries via lanthanum and aluminium doping. Nat. Energy 3, 936–943. https://doi.org/10.1038/s41560-018-0180-6

Lonardelli, I., Wenk, H.-R., Lutterotti, L., Goodwin, M.B., 2005. Texture analysis from synchrotron diffraction images with the rietveld method: Dinosaur tendon and salmon scale. J. Synchrotron Radiat. 12, 354–360. https://doi.org/10.1107/S090904950500138X

Low, H.E., Lunne, T., Andersen, K.H., Sjursen, M.A., Li, X., Randolph, M.F., 2010. Estimation of intact and remoulded undrained shear strengths from penetration tests in soft clays. Géotechnique 60, 843–859. https://doi.org/10.1680/geot.9.P.017

Lunne, T., Andersen, K.H., 2007. Soft clay shear strength parameters for deepwater geotechnical design, in: Proceedings of the 6th International Offshore Site Investigation and Geotechnics Conference: Confronting New Challenges and Sharing Knowledge. London. UK.

Luo, S., Lu, Y., Wu, Y., Song, J., DeGroot, D.J., Jin, Y., Zhang, G., 2020. Cross-scale characterization of the elasticity of shales: Statistical nanoindentation and data analytics. J. Mech. Phys. Solids 140, 103945. https://doi.org/10.1016/j.jmps.2020.103945

Lutterotti, L., Vasin, R., Wenk, H.-R., 2014. Rietveld texture analysis from synchrotron diffraction images. I. Calibration and basic analysis. Powder Diffr. 29, 76–84. https://doi.org/10.1017/S0885715613001346

Ma, S., Qian, Y., Kawashima, S., 2018. Experimental and modeling study on the non-linear structural build-up of fresh cement pastes incorporating viscosity modifying admixtures. Cem. Concr. Res. 108, 1–9. https://doi.org/10.1016/J.CEMCONRES.2018.02.022

Malmgren, S., Ciosek, K., Hahlin, M., Gustafsson, T., Gorgoi, M., Rensmo, H., Edstrom, K., 2013. Comparing anode and cathode electrode/electrolyte interface composition and morphology using soft and hard X-ray photoelectron spectroscopy. Electrochim. Acta 97, 23–32. https://doi.org/10.1016/j.electacta.2013.03.010

Martin, C., Pignon, F., Piau, J.-M., Magnin, A., Lindner, P., Cabane, B., 2002. Dissociation of thixotropic clay gels. Phys. Rev. E 66, 21401. https://doi.org/10.1103/PhysRevE.66.021401

Martin, R.T., 1966. Quantitative fabric of wet kaolinite. Clays Clay Miner. 14, 271–287. https://doi.org/10.1346/CCMN.1966.0140124

Mas, R., Magnin, A., 1994. Rheology of colloidal suspensions: Case of lubricating greases. J. Rheol. (N. Y. N. Y). 38, 889–908. https://doi.org/10.1122/1.550598

Matthies, S., Wenk, H.-R., Vinel, G.W., 1988. Some basic concepts of texture analysis and comparison of three methods to calculate orientation distributions from pole figures. J. Appl. Crystallogr. 21, 285–304. https://doi.org/10.1107/S0021889888000275

Mayne, P.W., 2007. Cone penetration testing state-of-practice. NCHRP Proj. 20–05.

Meng, B., Wu, J., Li, Y., Lou, L., 2008. Aging process of the bond between colloidal particles measured using laser tweezers. Colloids Surfaces A Physicochem. Eng. Asp. 322, 253–255. https://doi.org/10.1016/j.colsurfa.2008.02.018

Mercer, H.A., Weymann, H.D., 1974. Structure of thixotropic suspensions in shear flow. III. Time-dependent behavior. Trans. Soc. Rheol. 18, 199–218. https://doi.org/10.1122/1.549356

Mewis, J., 1979. Thixotropy - A general review. J. Nonnewton. Fluid Mech. 6, 1–20. https://doi.org/10.1016/0377-0257(79)87001-9

Mewis, J., Wagner, N.J., 2009. Thixotropy. Adv. Colloid Interface Sci. 147–148, 214–227. https://doi.org/10.1016/j.cis.2008.09.005

Mitchell, J.K., 1969. Temperature effects on the engineering properties and behavior of soils. Highw. Res. Board Spec. Rep. 9–28.

Mitchell, J.K., 1960. Fundamental aspects of thixotropy in soils. Soil Mech. Found. Div. 86, 19–52.

Mitchell, J.K., Soga, K., 2005. Fundamentals of soil behavior, John Wiley & Sons Inc. Hoboken, NJ. https://doi.org/10.1016/j.jhazmat.2005.06.004

Moretto, O., 1948. Effect of natural hardening on the unconfined compression strength of remolded clays, in: Proceedings of the 2nd International Conference on Soil Mechanics and Foundation Engineering. Rotterdam, pp. 137–144.

Nalezny, C.L., Li, M.C., 1967. Effect of soil structure and thixotropic hardening on swelling behavior of compacted clay soils. Highw. Res. Rec. 1–22.

Neumann, B.S., Sansom, K.G., 1970. The study of gel formation and flocculation in aqueous clay dispersions by optical and rheological methods. Isr. J. Chem. 8, 315–324. https://doi.org/10.1002/ijch.197000038

Nishiyama, Y., Langan, P., Chanzy, H., 2002. Crystal structure and hydrogen-bonding system in cellulose 1β from synchrotron X-ray and neutron fiber diffraction. J. Am. Chem. Soc. 124, 9074–9082. https://doi.org/10.1021/ja0257319

O'Brien, D.K., Wenk, H., Ratschbacher, L., You, Z., 1987. Preferred orientation of phyllosilicates in phyllonites and ultramylonites. J. Struct. Geol. 9, 719–730. https://doi.org/10.1016/0191-8141(87)90155-6

O'Brien, N.R., 1971. Fabric of kaolinite and illite floccules. Clays Clay Miner. 19, 353–359. https://doi.org/10.1346/CCMN.1971.0190603

O'Day, P.A., Rivera, N., Root, R., Carroll, S.A., 2004. X-ray absorption spectroscopic study of Fe reference compounds for the analysis of natural sediments. Am. Mineral. 89, 572–585. https://doi.org/10.2138/am-2004-0412

Osipov, V.I., Nikolaeva, S.K., Sokolov, V.N., 1984. Microstructural changes associated with thixotropic phenomena in clay soils. Géotechnique 34, 293–303. https://doi.org/10.1680/geot.1984.34.3.293

Osterman, J., 1963. Studies on the properties and formation of quick clays. Clays Clay Miner. 12, 87–108. https://doi.org/10.1346/CCMN.1963.0120112

Ozdemir, O., Karakashev, S.I., Nguyen, A. V., Miller, J.D., 2009. Adsorption and surface tension analysis of concentrated alkali halide brine solutions. Miner. Eng. 22, 263–271. https://doi.org/10.1016/j.mineng.2008.08.001

Pecharsky, V.K., Zavalij, P.Y., 2009. Solving crystal structure from powder diffraction data, in: Pecharsky, V.K., Zavalij, P.Y. (Eds.), Fundamentals of Powder Diffraction

and Structural Characterization of Materials. Springer US, Boston, MA, pp. 497–545. https://doi.org/10.1007/978-0-387-09579-0_15

Peng, J., DeGroot, D.J., Cao, Y., Zhang, G., 2020. Rigidity index of soft remolded clays during thixotropic hardening, in: 4th International Symposium on Frontiers in Offshore Geotechnics. Austin, Texas.

Peng, J., Luo, S., Wang, D., Cao, Y., DeGroot, D.J., Zhang, G., 2021a. Multiple thixotropisms of liquid limit-consistency clays unraveled by multiscale experimentation. J. Geotech. Geoenvironmental Eng. in press.

Peng, J., Luo, S., Wang, D., Ren, Y., Fan, L., DeGroot, D.J., Zhang, G., 2021b. Quantitative evaluation of thixotropy-governed microfabric evolution in soft clays. Appl. Clay Sci. 210, 106157. https://doi.org/10.1016/j.clay.2021.106157

Peterfi, T., 1927. Arch entwicklungsmech. Organ 112, 680.

Petrellis, N.C., Flumerfelt, R.W., 1973. Rheological behavior of shear degradable oils: Kinetic and equilibrium properties. Can. J. Chem. Eng. 51, 291–301. https://doi.org/10.1002/cjce.5450510305

Philippe, B., Dedryvère, R., Allouche, J., Lindgren, F., Gorgoi, M., Rensmo, H., Gonbeau, D., Edström, K., 2012. Nanosilicon electrodes for lithium-ion batteries: Interfacial mechanisms studied by hard and soft X-ray photoelectron spectroscopy. Chem. Mater. 24, 1107–1115. https://doi.org/10.1021/cm2034195

Pignon, F., Magnin, A., Piau, J.-M., 1998. Thixotropic behavior of clay dispersions: Combinations of scattering and rheometric techniques. J. Rheol. (N. Y. N. Y). 42, 1349–1373. https://doi.org/10.1122/1.550964

Pineda, J.A., Kelly, R., Bates, L., Sheng, D., Sloan, S., 2013. Effects of pore fluid salinity on the shear strength of a soft clay, in: Fifth Biot Conference on Poromechanic, Proceedings. pp. 1460–1469. https://doi.org/10.1061/9780784412992.174

Plum, R.L., Esrig, M.I., 1969. Some temperature effects on soil compressibility and pore water pressure. Spec. Report-highw. Res. Board 231.

Poojary, D.M., Clearfield, A., 1997. Application of X-ray powder diffraction techniques to the solution of unknown crystal structures. Acc. Chem. Res. 30, 414–422. https://doi.org/10.1021/ar960143j

Popmintchev, T., Chen, M.-C., Bahabad, A., Gerrity, M., Sidorenko, P., Cohen, O., Christov, I.P., Murnane, M.M., Kapteyn, H.C., 2009. Phase matching of high harmonic generation in the soft and hard X-ray regions of the spectrum, in: Proceedings of the National Academy of Sciences. NATL ACAD SCIENCES, 2101 CONSTITUTION AVE NW, WASHINGTON, DC 20418 USA, pp. 10516–10521. https://doi.org/10.1073/pnas.0903748106

Pusch, R., 1968. A technique for investigation of clay microstructure. Swedish Geotechnical Institute.

Pusch, R., 1966. Investigation of clay microstructure by using ultra-thin sections. Swedish Geotech. Inst.

Pusch, R., 1962. Clay particles, their size, shape and arrangement in relation to some important physical properties of clays. Statens rad for Byggnadsforskning.

Rack, A., Zabler, S., Müller, B.R., Riesemeier, H., Weidemann, G., Lange, A., Goebbels, J., Hentschel, M., Görner, W., 2008. High resolution synchrotron-based radiography and tomography using hard X-rays at the BAMline (BESSY II). Nucl. Instruments Methods Phys. Res. Sect. A Accel. Spectrometers, Detect. Assoc. Equip. 586, 327–344. https://doi.org/10.1016/j.nima.2007.11.020

Raheem, A.M., Vipulanandan, C., 2019. Salt contamination and temperature impacts on the rheological and electrical resistivity behaviors of water based drilling mud. Energy Sources, Part A Recover. Util. Environ. Eff. 1–21. https://doi.org/10.1080/15567036.2019.1587080

Ramirez-Rico, J., Lee, S.-Y., Ling, J.J., Noyan, I.C., 2016. Stress measurement using area detectors: A theoretical and experimental comparison of different methods in ferritic steel using a portable X-ray apparatus. J. Mater. Sci. 51, 5343–5355. https://doi.org/10.1007/s10853-016-9837-3

Randolph, M.F., Cassidy, M., Gourvenec, S., Erbrich, C.J., 2005. Challenges of offshore geotechnical engineering, State of the Art Paper, in: Organising, C.O.T.I. (Ed.), Challenges of Offshore Geotechnical Engineering. Millpress Science Publishers, The Netherlands, pp. 123–176.

Rodriguez-Navarro, C., Kudlacz, K., Ruiz-Agudo, E., 2012. The mechanism of thermal decomposition of dolomite: New insights from 2D-XRD and TEM analyses. Am. Mineral. 97, 38–51. https://doi.org/10.2138/am.2011.3813

Rosenqvist, I.T., 1953. Considerations on the sensitivity of Norwegian quick-clays. Géotechnique 3, 195–200. https://doi.org/10.1680/geot.1953.3.5.195

Ross, R.A., Weymann, H.D., Chuang, M.C., 1973. Structure of thixotropic suspensions in shear flow: II. Optical properties. Phys. Fluids 16, 784–789. https://doi.org/10.1063/1.1694428

Roussel, N., Ovarlez, G., Garrault, S., Brumaud, C., 2012. The origins of thixotropy of fresh cement pastes. Cem. Concr. Res. 42, 148–157. https://doi.org/10.1016/j.cemconres.2011.09.004

Salazar, S., Coffman, R., 2014. Design and fabrication of end platens for acquisition of small-strain piezoelectric measurements during large-strain triaxial extension and triaxial compression testing. Geotech. Test. J. 37, 948–958.

https://doi.org/10.1520/GTJ20140057

Sas, W., Gabryś, K., Szymański, A., 2014. Comparison of resonant column and bender elements tests on selected cohesive soil from warsaw. Electron. J. Polish Agric. Univ. 17.

Seed, H.B., Chan, C.K., 1959. Thixotropic characteristics of compacted clays. Trans. Am. Soc. Civ. Eng. 124, 894–916.

Seng, S., Tanaka, H., 2012. Properties of very soft clays: A study of thixotropic hardening and behavior under low consolidation pressure. Soils Found. 52, 335–345. https://doi.org/10.1016/J.SANDF.2012.02.010

Shahriar, A.R., Abedin, M.Z., Jadid, R., 2018. Thixotropic aging and its effect on 1-D compression behavior of soft reconstituted clays. Appl. Clay Sci. 153, 217–227. https://doi.org/10.1016/J.CLAY.2017.12.029

Shein, E. V, Verkhovtseva, N. V, Bykova, G.S., Suslenkova, M.M., 2019. Formation of microaggregates in kaolinite suspension inoculated by Bacillus velezensis (SEM-investigations). IOP Conf. Ser. Earth Environ. Sci. 368, 12043. https://doi.org/10.1088/1755-1315/368/1/012043

Shen, S.-L., Han, J., Du, Y.-J., 2008. Deep mixing induced property changes in surrounding sensitive marine clays. J. Geotech. Geoenvironmental Eng. 134, 845–854. https://doi.org/10.1061/(ASCE)1090-0241(2008)134:6(845)

Skempton, A.W., Northey, R.D., 1952. The sensitivity of clays. Geotechnique 3, 30–53. https://doi.org/10.1680/geot.1952.3.1.30

Speziale, S., Lonardelli, I., Miyagi, L., Pehl, J., Tommaseo, C.E., Wenk, H., 2006. Deformation experiments in the diamond-anvil cell: texture in copper to 30 GPa. J. Phys. Condens. Matter 18, S1007–S1020. https://doi.org/10.1088/0953-8984/18/25/s08

Środoń, J., Drits, V.A., McCarty, D.K., Hsieh, J.C.C., Eberl, D.D., 2001. Quantitative X-ray diffraction analysis of clay-bearing rocks from random preparations. Clays Clay Miner. 49, 514–528. https://doi.org/10.1346/CCMN.2001.0490604

Svensson, P.D., Hansen, S., 2013. Combined salt and temperature impact on montmorilloite hydration. Clays Clay Miner. 61, 328–341. https://doi.org/10.1346/CCMN.2013.0610412

Svergun, D.I., Richard, S., Koch, M.H.J., Sayers, Z., Kuprin, S., Zaccai, G., 1998. Protein hydration in solution: Experimental observation by x-ray and neutron scattering, in: Proceedings of the National Academy of Sciences. NATL ACAD SCIENCES, 2101 CONSTITUTION AVE NW, WASHINGTON, DC 20418 USA, pp. 2267–2272. https://doi.org/10.1073/pnas.95.5.2267

Tan, X., Hu, L., Reed, A.H., Furukawa, Y., Zhang, G., 2014. Flocculation and particle size analysis of expansive clay sediments affected by biological, chemical, and hydrodynamic factors. Ocean Dyn. 64, 143–157. https://doi.org/10.1007/s10236-013-0664-7

Tan, X., Liu, F., Hu, L., Reed, A.H., Furukawa, Y., Zhang, G., 2017. Evaluation of the particle sizes of four clay minerals. Appl. Clay Sci. 135, 313–324. https://doi.org/10.1016/j.clay.2016.10.012

Tang, C.C., MacLean, E.J., Roberts, M.A., Clarke, D.T., Pantos, E., Prag, A.J.N.W., 2001. The study of attic black gloss sherds using synchrotron X-ray diffraction. J. Archaeol. Sci. 28, 1015–1024. https://doi.org/10.1006/JASC.2000.0608

Teh, C.I., Houlsby, G.T., 1991. An analytical study of the cone penetration test in clay. Géotechnique 41, 17–34. https://doi.org/10.1680/geot.1991.41.1.17

Teich-McGoldrick, S.L., Greathouse, J.A., Jové-Colón, C.F., Cygan, R.T., 2015. Swelling properties of montmorillonite and beidellite clay minerals from molecular simulation: Comparison of temperature, interlayer cation, and charge location effects. J. Phys. Chem. C 119, 20880–20891. https://doi.org/10.1021/acs.jpcc.5b03253

Toby, B.H., 2006. R factors in Rietveld analysis: How good is good enough? Powder Diffr. 21, 67–70. https://doi.org/10.1154/1.2179804

Toorman, E.A., 1997. Modelling the thixotropic behaviour of dense cohesive sediment suspensions. Rheol. Acta 36, 56–65. https://doi.org/10.1007/BF00366724

Turner, A.J., Rodewald, C.W., 1949. An experimental study of thixotropy in bentonite suspensions. J. Colloid Sci. 4, 283–298. https://doi.org/10.1016/0095-8522(49)90010-0

Twining, B.S., Baines, S.B., Fisher, N.S., Maser, J., Vogt, S., Jacobsen, C., Tovar-Sanchez, A., Sanudo-Wilhelmy, S.A., 2003. Quantifying trace elements in individual aquatic protist cells with a synchrotron X-ray fluorescence microprobe. Anal. Chem. 75, 3806–3816. https://doi.org/10.1021/ac034227z

Van Houtte, P., 1980. A method of orientation distribution function analysis from incomplete pole figures normalized by an iterative method. Mater. Sci. Eng. 43, 7–11. https://doi.org/10.1016/0025-5416(80)90201-3

van Olphen, H., 1963. An introduction to clay colloid chemistry. Interscience Publishers, New York.

van Paassen, L.A., Gareau, L.F., 2004. Effect of pore fluid salinity on compressibility and shear strength development of clayey soils, in: Hack, R., Azzam, R., Charlier, R. (Eds.), Engineering Geology for Infrastructure Planning in Europe. Springer, Berlin, Heidelberg, pp. 327–340. https://doi.org/10.1007/978-3-540-39918-6_39

Vesic, A.S., 1972. Expansion of cavities in infinite soil mass. Soil Mech. Found. Div. 98, 265–290.

Wang, Z., Zhang, Q., Konno, M., Saito, S., 1994. Sol–gel transition of alginate solution by the addition of various divalent cations: A rheological study. Biopolymers 34, 737–746. https://doi.org/10.1002/bip.360340606

Wei, Y., Lin, Y., Xie, R., Xu, Y., Yao, J., Zhang, J., 2015. The flow behavior, thixotropy and dynamical viscoelasticity of fenugreek gum. J. Food Eng. 166, 21–28. https://doi.org/10.1016/J.JFOODENG.2015.05.015

Wen, J., Shi, K., Sun, Q., Sun, Z., Gu, H., 2018. Measurement for surface tension of aqueous inorganic salt. Front. Energy Res. 6. https://doi.org/10.3389/fenrg.2018.00012

Wenk, H.-R., Grigull, S., 2003. Synchrotron texture analysis with area detectors. J. Appl. Crystallogr. 36, 1040–1049. https://doi.org/10.1107/S0021889803010136

Wenk, H.-R., Kanitpanyacharoen, W., Voltolini, M., 2010. Preferred orientation of phyllosilicates: Comparison of fault gouge, shale and schist. J. Struct. Geol. 32, 478–489. https://doi.org/10.1016/j.jsg.2010.02.003

Wenk, H.-R., Lutterotti, L., Kaercher, P., Kanitpanyacharoen, W., Miyagi, L., Vasin, R., 2014. Rietveld texture analysis from synchrotron diffraction images. II. Complex multiphase materials and diamond anvil cell experiments. Powder Diffr. 29, 220–232. https://doi.org/10.1017/S0885715614000360

Weymann, H.D., Chuang, M.C., Ross, R.A., 1973. Structure of thixotropic suspensions in shear flow: I. Mechanical properties. Phys. Fluids 16, 775–783. https://doi.org/10.1063/1.1694427

Widjonarko, N.E., 2016. Introduction to advanced X-ray diffraction techniques for polymeric thin films. Coatings 6. https://doi.org/10.3390/coatings6040054

Xiao, S., Suleiman, M.T., McCartney, J.S., 2014. Shear behavior of silty soil and soil-structure interface under temperature effects. Geo-characterization Model. Sustain. GSP No 234, 4105–4114.

Yamashita, S., Kawaguchi, T., Nakata, Y., Mikami, T., Fujiwara, T., Shibuya, S., 2009. Interpretation of international parallel test on the measurement of Gmax using bender elements. Soils Found. 49, 631–650. https://doi.org/10.3208/sandf.49.631

Yang, S., Andersen, K.H., 2016. Thixotropy of marine clays. Geotech. Test. J. 39. https://doi.org/10.1520/GTJ20150020

Ye, S., Yang, Z., Xu, J., Shang, Z., Xie, J., 2019. Clay–graphene oxide liquid crystals and their aerogels: Synthesis, characterization and properties. R. Soc. Open Sci. 6, 181439. https://doi.org/10.1098/rsos.181439

Yukselen-Aksoy, Y., Kaya, A., Ören, A.H., 2008. Seawater effect on consistency limits and compressibility characteristics of clays. Eng. Geol. 102, 54–61. https://doi.org/10.1016/J.ENGGEO.2008.07.005

Zakeri, A., Liedtke, E., Clukey, E.C., Jeanjean, P., 2014. Long-term axial capacity of deepwater jetted piles. Géotechnique 64, 966–980. https://doi.org/10.1680/geot.14.P.014

Zhang, G., 2002. Laboratory characterization of a highly weathered old alluvium in San Juan, Puerto Rico. Massachusetts Institute of Technology.

Zhang, G., Germaine, J., Whitttle, A., 2005. An evaluation of the mechanical and chemical dispersion methods for a tropical old alluvium. Geotech. Test. J. 28, 123–132. https://doi.org/10.1520/GTJ12248

Zhang, G., Germaine, J.T., Whittle, A.J., Ladd, C.C., 2004a. Soil structure of a highly weathered old alluvium. Géotechnique 54, 453–466. https://doi.org/10.1680/geot.2004.54.7.453

Zhang, G., Germaine, J.T., Whittle, A.J., Ladd, C.C., 2004b. Index properties of a highly weathered old alluvium. Géotechnique 54, 441–451. https://doi.org/10.1680/geot.2004.54.7.441

Zhang, G., Whittle, A.J., Germaine, J.T., Martin, R.T., 2003. A simple sample-mounting method for random powder X-ray diffraction. Clays Clay Miner. 51, 218–225. https://doi.org/10.1346/CCMN.2003.0510212

Zhang, G., Yin, H., DeGroot, D.J., 2013a. Thixotropism of micron-sized saltwater clay flocs. Géotechnique Lett. 3, 162–165. https://doi.org/10.1680/geolett.13.00049

Zhang, G., Yin, H., Lei, Z., Reed, A.H., Furukawa, Y., 2013b. Effects of exopolymers on particle size distributions of suspended cohesive sediments. J. Geophys. Res. Ocean. 118, 3473–3489. https://doi.org/10.1002/jgrc.20263

Zhang, X.W., Kong, L.W., Yang, A.W., Sayem, H.M., 2017. Thixotropic mechanism of clay: A microstructural investigation. Soils Found. 57, 23–35. https://doi.org/10.1016/j.sandf.2017.01.002